

MoDOT

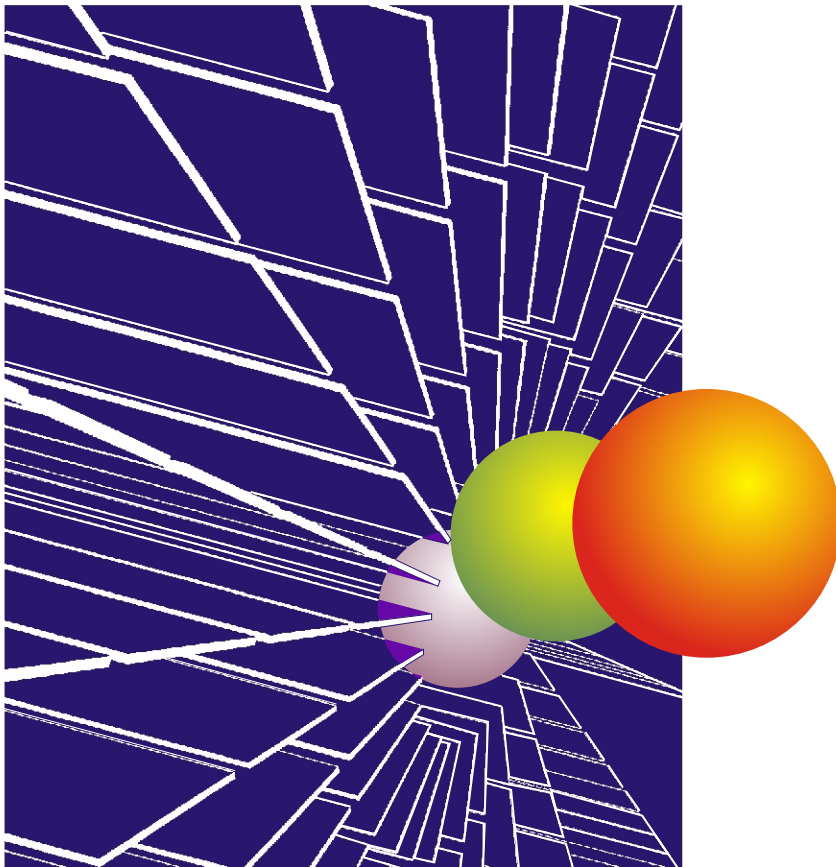
Research, Development and Technology

University of Missouri-Rolla

RDT 04-017

Design, Fabrication and Testing of Low Profile Composite Bypass Road Panel: Phase 1

RI 02-016



June, 2004

Technical Report Documentation Page

1. Report No. RDT 04-017	2. Government Accession No.	3. Recipient's Catalog No.	
4. Title and Subtitle Design, Fabrication, and Testing of Low – Profile Composite Bypass Road Panel: Phase I		5. Report Date June 2004	
		6. Performing Organization Code UMR	
7. Author/s S. Rocca and A. Nanni		8. Performing Organization Report No. RI02 – 016 / RDT 04-017	
9. Performing Organization Name and Address Center for Infrastructure Engineering Studies, University of Missouri – Rolla 223 Engineering Research Lab. Rolla, MO 65409		10. Work Unit No.	
		11. Contract or Grant No.	
12. Sponsoring Organization Name and Address MODOT 105 West Capital Av., Jefferson City, MO 65102 UTC 223 Engineering Research Lab., Rolla, MO 65409		13. Type of report and period covered Technical Report; 6/2002 – 12/2003	
		14. Sponsoring Agency Code MoDOT	
15. Supplementary Notes			
16. Abstract <p>The objective of this research project was to demonstrate the feasibility of Glass Fiber Reinforced Polymer (GFRP) systems for low – profile bypass roadways, in particular, sandwich panels comprised of GFRP facings and an innovative Fiber Reinforced Foam (FRF) core.</p> <p>In order to investigate the performance of the sandwich construction, an experimental program including static and dynamic fatigue tests was performed. In particular, the static tests included two different characterizations: compression and flexure. The same type of specimens tested under static loading, were cyclically conditioned in order to analyze the behavior of the material and determine its residual strength. In both situations the specimens were conditioned to 500,000; 1,000,000; 1,500,000 and 2,000,000 cycles. The specimens utilized in the experimental program were collected from different sandwich panels with the purpose of verifying homogeneity in the mechanical properties of the material.</p> <p>The investigation focused on the ultimate bearing capacity and stiffness (compressive and flexural) of the sandwich structure, as well as its residual strength and rigidity after fatigue conditioning. The mechanical properties determined in this study constitute the base for a complement extension of this research: the development of a schematic solution for site implementation. This project may have significant repercussions in the construction and repair of existing structures.</p>			
17. Key Words bypass roadway, deflection, flexural stiffness, GFRP, sandwich panel,		18. Distribution Statement No restrictions. This document is available to the public through NTIC, Springfield, VA 22161	
19. Security Classification (of this report) Unclassified	20. Security Classification (of this page) Unclassified	21. No. of pages 59 w/o Appendices	22. Price

Final Report for Contract RI02 – 016

DESIGN, FABRICATION, AND TESTING OF LOW – PROFILE COMPOSITE

BYPASS ROAD PANEL: PHASE I

Final Report

Prepared for

Missouri Department of Transportation

By

Silvia Rocca

Dr. Antonio Nanni

Center for Infrastructure Engineering Studies

University of Missouri – Rolla

June 2004

EXECUTIVE SUMMARY

The objective of this research project was to demonstrate the feasibility of Glass Fiber Reinforced Polymer (GFRP) systems for low-profile bypass roadways, in particular, sandwich panels comprised of GFRP facings and an innovative Fiber Reinforced Foam (FRF) core were investigated. The most relevant feature of this technology is the core, which is reinforced by continuous webs in the transverse direction and lattices of angled stitches in the longitudinal direction, both of them GFRP materials. Due to manufacturing process limitations, the sandwich panels of an overall thickness of 3.5 in (89 mm), presented internal joints in the longitudinal and transverse directions. It will be later seen that this characteristic greatly influences the mode of failure under flexural loading.

In order to investigate the performance of the sandwich construction, an experimental program including static and dynamic fatigue tests was performed. In particular, the static tests included two different characterizations: compression and flexure. The same type of specimens tested under static loading, were cyclically conditioned in order to analyze the behavior of the material and determine its residual strength. In both cases, the specimens were conditioned to 500,000; 1,000,000; 1,500,000 and 2,000,000 cycles. The specimens utilized in the experimental program were collected from different sandwich panels with the purpose of verifying homogeneity in the mechanical properties of the material. Cubic specimens of 4 in (102 mm) by 4 in (102 mm) and 3.5 in (89 mm) thick, and two types of beams (longitudinally-cut and transversally-cut) 8 in (203 mm) wide and 58 in (1.47 m) long were utilized in the compressive and flexural tests, respectively. The investigation focused on the ultimate capacity and stiffness (compressive and flexural) of the sandwich structure, as well as its residual strength and rigidity after fatigue conditioning.

Among the most remarkable conclusions drawn from the compression laboratory testing of cubic GFRP sandwich specimens is the following: the residual compressive strength after two million cycles is approximately 869 psi (6 MPa), which is considerably higher than the peak surface pressure resulting from a HS25-44 truck wheel equal to 100 psi (6.9 kPa). The parameters obtained in the flexural experiments were complemented by an analysis which considered two possible cases when deploying the panel system (field application): panel laid over an opening and panel fully supported. For the first case, a panel of 3.5 in (89 mm) thick and 2.8 ft (85.34 cm) length is recommended. For the latter, a panel of 3.5 in (89 mm) thick and 8 ft (2.44 m) is considered appropriate. The analysis was carried out taking into account a design load corresponding to a HS25-44 truck, as well as serviceability and strength criteria.

The mechanical properties resulting from the performed compressive and flexural experiments on virgin and fatigue-conditioned samples, constitute the basis for the assessment and validation of the material system for the intended application. This material system may also have significant repercussions in the repair of existing structures.

ACKNOWLEDGEMENTS

The researchers would like to express their appreciation to the Missouri Department of Transportation (MoDOT) for funding this research project, as well as WebCore Technologies, Inc. for providing the sandwich panels; their support is much appreciated.

Additionally, acknowledgments also go to Rolla Technical Institute (RTI) and the laboratory technicians at the University of Missouri-Rolla for their valuable assistance in the realization of the experiments.

The University Transportation Center on Advanced Materials and NDT Technologies based at the University of Missouri – Rolla is also acknowledged for its financial support.

TABLE OF CONTENTS

EXECUTIVE SUMMARY	iii
ACKNOWLEDGEMENTS	iv
TABLE OF CONTENTS	v
LIST OF FIGURES	vii
LIST OF TABLES	xi
NOMENCLATURE	xii
1. INTRODUCTION	1
1.1. BACKGROUND	1
1.1.1. FRP Sandwich Panel	1
1.1.2. Material Description	1
1.1.2.1 Hybrid Stitched/Webbed FRF Core	2
1.1.2.2 Panel Faces	3
1.1.3. Sandwich Panel Manufacturing	3
1.2. SCOPE AND OBJECTIVE	3
1.3. PREVIOUS RESEARCH	3
1.4. OUTLINE OF THE REPORT	5
2. COMPRESSIVE TEST	7
2.1. STATIC COMPRESSIVE TEST	7
2.1.1. Test Set Up	7
2.1.2. Experimental Results	9
2.1.2.1 Panel A	9
2.1.2.2 Panel B	11
2.2. FATIGUE COMPRESSIVE TEST	12
2.2.1. Test Set Up	13
2.2.1.1 Conditioning Load Level 1	16
2.2.1.2 Conditioning Load Level 2	18
2.2.1.3 Conditioning Load Level 3	18
2.2.1.4 Conditioning Load Level 4	19
2.2.2. Experimental Results	20
2.2.2.1 Conditioning Load Level 1	20
2.2.2.2 Conditioning Load Level 2	23
2.2.2.3 Conditioning Load Level 3	24
2.2.2.4 Conditioning Load Level 4	25
3. FLEXURAL TEST	29
3.1. ORDINARY BEAM THEORY	29
3.2. STATIC FLEXURAL TEST	31
3.2.1. Test Set Up	31
3.2.1.1 Test 1	32
3.2.1.2 Test 2	33
3.2.2. Experimental Results	35
3.2.2.1 Test 1	35
3.2.2.2 Test 2	38
3.3. FATIGUE FLEXURAL TEST	41
3.3.1. Test Setup	41

3.3.2. Experimental Results.....	43
4. DISCUSSION OF RESULTS.....	49
4.1. COMPRESSIVE TESTS.....	49
4.2. FLEXURAL TESTS.....	49
4.2.1. Panel over an opening.....	50
4.2.2. Fully supported panel.....	51
5. CONCLUSIONS.....	55
6. RECOMMENDATIONS FOR POSSIBLE SITE IMPLEMENTATION.....	56
6.1. AIRFIELD MATTING.....	57
APPENDICES.....	60
A: LITERATURE REVIEW.....	60
B: COMPRESSIVE FATIGUE PERFORMANCE – PANEL A.....	73
C: COMPRESSIVE FATIGUE PERFORMANCE – PANEL B.....	76
D: FLEXURAL BEHAVIOR.....	80
E: NON DESTRUCTIVE EVALUATION.....	118
F: SYSTEM PERFORMANCE SPECIFICATION FOR THE RAPID PARKING RAMP EXPANSION (RPRE).....	123
LIST OF REFERENCES.....	134

LIST OF FIGURES

Figure	Page
1.1 FRF Core - 3 in (76 mm)	2
1.2 Hybrid FRF Panel Section	2
2.1 Sandwich Panel Cubic Specimen.....	7
2.2 Potentiometer attached to the cubic specimen.....	8
2.3 Load vs. Displacement - Static Compressive Test - Panel A	10
2.4 Load vs. Displacement - Static Compressive Test - Panel B.....	11
2.5 Failure Mode - Compressive Test.....	12
2.6 Bottom Steel Plate.....	14
2.7 Test Setup - Fatigue Compressive Test	14
2.8 Test Setup Schematic - Fatigue Compressive Test.....	15
2.9 Bottom Steel Plate Schematic - Fatigue Compressive Test.....	16
2.10 Conditioning Level 1 - Panel B – After 583,374 cycles.....	22
2.11 Conditioning Load Level 2 - Panel B	23
2.12 Conditioning Load Level 3 - Panel B	25
2.13 Failure - Conditioning Load Level 4 – Panel A.....	26
2.14 Residual Ultimate Compressive Strength	27
2.15 Residual Ultimate Compressive Modulus E.....	27
2.16 Conditioning Load S vs. Number of cycles N	28
3.1 Sandwich Beam and Cross Section.....	29
3.2 FRF Core Schematic.....	32
3.3 Static Flexural Test Setup Schematic	32
3.4 Flexural Test Setup - Static Test 1	33
3.5 Load Spreading - Static Test 2.....	33
3.6 Flexural Test Setup - Static Test 2.....	34
3.7 Modes of Failure (Longitudinally-cut; Static Test 1)	37
3.8 Modes of Failure (Transversally-cut; Static Test 1)	37
3.9 Representative Load vs. Loading Point Deflection Curves – Static Test 1	38
3.10 Mode of Failure (Longitudinally-cut; Static Test 2).....	39
3.11 Modes of Failure (Transversally-cut; Static Test 2)	40
3.12 Representative Load vs. Midspan Deflection - Static Test 2.....	40
3.13 Fatigue Flexural Test Setup Schematic.....	42
3.14 Fatigue Flexural Test Setup	42
3.15 Load Spreading Details.....	43
3.16 Load vs. Midspan Deflection (Longitudinally-cut; Fatigue Flexural Test).....	45
3.17 Load vs. Midspan Deflection (Transversally-cut; Fatigue Flexural Test).....	45
3.18 Modes of Failure (Longitudinally-cut; Fatigue Flexural Test).....	46
3.19 Modes of Failure (Transversally-cut; Fatigue Flexural Test).....	46
3.20 Residual Ultimate Load - Flexure.....	47
3.21 Residual Bending Stiffness (Longitudinally-cut; Flexure).....	48
3.22 Residual Bending Stiffness (Transversally-cut; Flexure).....	48
4.1 Truck Wheel Footprint and Effective Area Schematic - Plane View	50
4.2 Fully Supported Panel Schematic	52
4.3 Midspan Deflection vs. Soil Elastic Modulus.....	53

4.4 Bending Stress vs. Soil Elastic Modulus	54
6.1 Foam block wound with glass fiber reinforcement (Webcore Technologies).....	58
6.2 Composite Structure - foam removed (Webcore Technologies)	58
6.3 Connector Details.....	59
6.4 Matting Array.....	59
A 1 Sandwich Panel Structure Idealization (One Ocean Kayacs – Composite Sandwich Core) .	62
A 2 Types of Sandwich Constructions (Vinson J. The Behavior of Sandwich Structures of Isotropic and Composite Materials, 1999).....	63
A 3 Yielding of Fracture of the Facing (Zenkert D. The Handbook of Sandwich Construction)	67
A 4 Face Wrinkling (Zenkert D. The Handbook of Sandwich Construction).....	67
A 5 General Buckling (Zenkert D. The Handbook of Sandwich Construction).....	67
A 6 Core Shear Failure (Zenkert D. The Handbook of Sandwich Construction).....	68
A 7 Core or Panel Indentation (Zenkert D. The Handbook of Sandwich Construction).....	68
A 8 Shear Crimping (Zenkert D. The Handbook of Sandwich Construction).....	69
A 9 Face Dimpling (Zenkert D. The Handbook of Sandwich Construction)	69
B 1 Load versus Displacement - 0.5 Million Cycles - Panel A	74
B 2 Load versus Displacement - 1 Million Cycles - Panel A	74
B 3 Load versus Displacement - 1.5 Million Cycles - Panel A	75
B 4 Load versus Displacement - 2 Million Cycles - Panel A	75
C 1 Load vs. Displacement - 0.5 Million Cycles - 37%Pu - Panel B	77
C 2 Load vs. Displacement - 2.1 Million Cycles – 37.1% Pu - Panel B	77
C 3 Load vs. Displacement - 66 Thousand Cycles – 43.3% Pu - Panel B.....	78
C 4 Load vs. Displacement - 2.1 Million Cycles – 43.3% Pu - Panel B	78
C 5 Load vs. Displacement - 65 Thousand Cycles – 49.5% Pu - Panel B.....	79
D 1 Load vs. Loading Point Deflection L2 - Static Test 1	81
D 2 Load vs. Loading Point Deflection - Beam L3 – Static Test 1	81
D 3 Load vs. Loading Point Deflection - Beam L4 - Static Test 1	82
D 4 Load vs. Loading Point Deflection – Beam L5 - Static Test 1	82
D 5 Load vs. Loading Point Deflection – Beam L6 - Static Test 2	83
D 6 Load vs. Midspan Deflection - Beam L6 - Static Test 2.....	83
D 7 Load vs. Loading Point Deflection - Beam L7 - Static Test 2.....	84
D 8 Load vs. Midspan Deflection -Beam L7 - Static Test 2.....	84
D 9 Load vs. Loading Point Deflection - Beam T1 - Static Test 1	85
D 10 Load vs. Loading Point Deflection - Beam T2 - Static Test 1	85
D 11 Load vs. Loading Point Deflection - Beam L3 - Static Test 1	86
D 12 Load vs. Loading Point Deflection - Beam T4 - Static Test 1	86
D 13 Load vs. Loading Point Deflection - Beam T5 - Static Test 1	87
D 14 Load vs. Loading Point Deflection - Beam T6 - Static Test 2.....	87
D 15 Load vs. Midspan Deflection - Beam T6 - Static Test 2.....	88
D 16 Load vs. Loading Point Deflection - Beam T7 - Static Test 2.....	88
D 17 Load vs. Midspan Deflection - Beam T7 - Static Test 2.....	89
D 18 Load vs. Loading Pt. Deflection - Beam 1L - Fatigue Test.....	89
D 19 Load vs. Midspan Deflection - Beam 1L - Fatigue Test.....	90
D 20 Load vs. Loading Pt. Deflection - Beam 2L - Fatigue Test.....	90
D 21 Load vs. Midspan Deflection - Beam 2L - Fatigue Test.....	91
D 22 Load vs. Loading Pt. Deflection - Beam 4L - Fatigue Test.....	91

D 23 Load vs. Midspan Deflection - 4L - Fatigue Test.....	92
D 24 Load vs. Loading Pt. Deflection - Beam 1T - Fatigue Test.....	92
D 25 Load vs. Midspan Deflection - Beam 1T - Fatigue Test.....	93
D 26 Load vs. Loading Pt. Deflection - Beam 2T - Fatigue Test.....	93
D 27 Load vs. Midspan Deflection - Beam 2T - Fatigue Test.....	94
D 28 Load vs. Loading Pt. Deflection - Beam 3T - Fatigue Test.....	94
D 29 Load vs. Midspan Deflection - Beam 3T - Fatigue Test.....	95
D 30 Load vs. Loading Pt. Deflection - Beam 4T - Fatigue Test.....	95
D 31 Load vs. Midspan Deflection - Beam 4T - Fatigue Test.....	96
D 32 Bending Stiffness D1 - Beam L2 – Static Test 1.....	96
D 33 Bending Stiffness D1 - Beam L3 - Static Test 1.....	97
D 34 Bending Stiffness D1 - Beam L4 - Static Test 1.....	97
D 35 Bending Stiffness D1 - Beam L5 - Static Test 1.....	98
D 36 Bending Stiffness D1 - Beam L6 - Static Test 2.....	98
D 37 Bending Stiffness D2 - Beam L6 - Static Test 2.....	99
D 38 Bending Stiffness D3 - Beam L6 - Static Test 2.....	99
D 39 Bending Stiffness D1 - Beam L7 - Static Test 2.....	100
D 40 Bending Stiffness D2 - Beam L7 - Static Test 2.....	100
D 41 Bending Stiffness D3 - Beam L7 - Static Test 2.....	101
D 42 Bending Stiffness D1 - Beam T1 - Static Test 1.....	101
D 43 Bending Stiffness D1 - Beam T2 - Static Test 1.....	102
D 44 Bending Stiffness D1 - Beam T3 - Static Test 1.....	102
D 45 Bending Stiffness D1 - Beam T4 - Static Test 1.....	103
D 46 Bending Stiffness D1 - Beam T5 - Static Test 1.....	103
D 47 Bending Stiffness D1 - Beam T6 - Static Test 2.....	104
D 48 Bending Stiffness D2 - Beam T6 - Static Test 2.....	104
D 49 Bending Stiffness D3 - Beam T6 - Static Test 2.....	105
D 50 Bending Stiffness D1 - Beam T7 - Static Test 2.....	105
D 51 Bending Stiffness D2 - Beam T7 - Static Test 2.....	106
D 52 Bending Stiffness D3 - Beam T7 - Static Test 2.....	106
D 53 Residual Bending Stiffness D1 - Beam 1L.....	107
D 54 Residual Bending Stiffness D2 - Beam 1L.....	107
D 55 Residual Bending Stiffness D3 - Beam 1L.....	108
D 56 Residual Bending Stiffness D1 - Beam 2L.....	108
D 57 Residual Bending Stiffness D2 - Beam 2L.....	109
D 58 Residual Bending Stiffness D3 - Beam 2L.....	109
D 59 Residual Bending Stiffness D1 - Beam 4L.....	110
D 60 Residual Bending Stiffness D2 - Beam 4L.....	110
D 61 Residual Bending Stiffness D3 - Beam 4L.....	111
D 62 Residual Bending Stiffness D1 - Beam 1T.....	111
D 63 Residual Bending Stiffness D2 - Beam 1T.....	112
D 64 Residual Bending Stiffness D3 - Beam 1T.....	112
D 65 Residual Bending Stiffness D1 - Beam 2T.....	113
D 66 Residual Bending Stiffness D2 - Beam 2T.....	113
D 67 Residual Bending Stiffness D3 - Beam 2T.....	114
D 68 Residual Bending Stiffness D1 - Beam 3T.....	114

D 69 Residual Bending Stiffness D2 - Beam 3T	115
D 70 Residual Bending Stiffness D3 - Beam 3T	115
D 71 Residual Bending Stiffness D1 - Beam 4T	116
D 72 Residual Bending Stiffness D2 - Beam 4T	116
D 73 Residual Bending Stiffness D3 - Beam 4T	117
E 1 Microwave Non-Destructive Technique Images.....	117

LIST OF TABLES

Table	Page
2.1 Specimens Physical Characteristic - Panel A	7
2.2 Specimens Physical Characteristic - Panel B.....	8
2.3 Static Compressive Test Results - Panel A.....	10
2.4 Static Compressive Test Results - Panel B.....	11
2.5 Levels of Load - Fatigue Compressive Test	13
2.6 Equivalent Levels of Load - Panel A & Panel B	13
2.7 Physical Characteristics - Conditioning Load Level 1 - Panel A	17
2.8 Physical Characteristics - Conditioning Load Level 1 - Panel B.....	17
2.9 Physical Characteristics - Conditioning Load Level 2 - Panel B.....	18
2.10 Physical Characteristics - Conditioning Load Level 3 - Panel B.....	19
2.11 Physical Characteristics - Conditioning Load Level 4 - Panel A	20
2.12 Residual Mechanical Properties - Conditioning Load Level 1 - Panel A.....	21
2.13 Residual Mechanical Properties - Conditioning Load Level 1 - Panel B.....	22
2.14 Residual Mechanical Properties - Conditioning Load Level 2 - Panel B.....	24
2.15 Residual Mechanical Properties - Conditioning Load Level 3 - Panel B.....	25
3.1 Mechanical Properties (Longitudinally-cut; Static Test 1).....	35
3.2 Mechanical Properties (Transversally-cut; Static Test 1).....	36
3.3 Mechanical Properties (Longitudinally-cut; Static Test 2).....	39
3.4 Mechanical Properties (Transversally-cut; Static Test 2).....	39
3.5 Fatigue Conditioning Load Values	41
3.6 Residual Mechanical Properties (Longitudinally-cut; Flexure).....	43
3.7 Residual Mechanical Properties (Transversally-cut; Flexure).....	44
4.1 Bending Stiffness and Elastic Modulus - Flexure.....	50
4.2 Bending Stress Average Values.....	51
4.3 Soil Elastic Modulus K.....	54
A 1 Core Characteristic - Sandwich Property (D. Zenkert, The Handbook of Sandwich Construction, 1997).....	65
F 1 C-130 COMPATIBILITY	132

NOMENCLATURE

A	cross sectional area, in ² (Equation 1)
AG	core shear stiffness, lb
b	width of the sandwich beam, in
c	thickness of the core, in (Equation 4)
d	distance between the center lines of facings, in (Equation 4)
D	bending stiffness of a composite beam, lb.in ² (Equation 1.3)
D1	bending stiffness as a function of the applied load and the deflection at the loading point, (lb.in ²)
D2	bending stiffness as a function of the applied load and the shear modulus, lb.in ²
D3	bending stiffness as a function of the applied load and the deflection at midspan, lb.in ²
E	compressive modulus, psi (Equation 2)
E _c	modulus of elasticity of the core, psi
E _f	modulus of elasticity of the facings, psi
G	core shear modulus, psi
h	depth of the sandwich beam, in (Equation 7)
I	overall centroidal moment of inertia, in ⁴
k	b x K ₀ , lb/in ² (Equation 21)
K ₀	soil elastic modulus, lb/in ³
L	length of the beam, in
M	bending moment, lb.in
(M ₀) _{L=8ft}	maximum bending moment in a fully supported sandwich beam, kip.ft
P	applied load, lb
P _U	ultimate load, lb
q	uniform distributed load, lb/in
Q	shear force, lb
S	slope of the initial linear portion of load versus displacement curve, lb/in (Equation 2)
t	core thickness, in (Equation 2)
t	thickness of an individual sandwich facing, in (Equation 4)
u	displacement of the loading block
w ₂	vertical displacement due to shear, in (Equation 1.16)
(y ₀) _{finite length}	midspan deflection for a finite length sandwich beam, in (Equation 20)
(y ₀) _{infinite length}	midspan deflection for an infinite length sandwich beam, in (Equation 21)
z	distance from the neutral axis to a certain point along the depth of the cross section sandwich beam, in
R	curvature radius at an specific point of the elastic curve (1/R is called curvature), in
Δ _{Loading Point}	deflection at the loading point due to bending, in

Δ_{Midspan}	deflection at the midspan due to bending, in
Δ_U	ultimate displacement, in
γ	core shear strain
λ	fully supported beam deflection parameter, 1/in (Equation 22)
σ	compressive strength, psi (Equation 1)
$(\sigma_f)_{\text{max}}$	maximum bending stress in the facing, psi
$(\sigma_c)_{\text{max}}$	maximum bending stress in the core, psi
σ^{facing}	facing bending stress, psi
σ_U^{facing}	ultimate facing bending stress, psi
σ_U	ultimate compressive strength, ksi
τ	shear stress, psi
τ_U	ultimate core shear stress, psi

1. INTRODUCTION

1.1. BACKGROUND

The American Society of Testing and Materials (ASTM C274-99) defines a sandwich structure as follows: A structural sandwich is a special form of a laminated composite comprising of a combination of different materials that are bonded to each other so as to utilize the properties of each separate component to the structural advantage of the whole assembly.

Ever since sandwich constructions appeared in 1940s, the primary applications have been in the aircraft, missile and spacecraft structures industries, not to mention their suitability for boat bulkheads (weight reduction), auto racing cars and sports items such as water and snow skis, kayaks, canoes, among others.

The sandwich structure is composed of two faces and a core. Usually the faces are identical in material and thickness, unless a variation is necessary by the type of application. The variety of types of sandwich constructions basically depends upon the configuration of the core, not to mention the material constituents. The most common types of core are: foam, honeycomb and web core truss (Vinson, 1999).

The faces that must be stiff, strong and thin; are separated and bonded to a light, weaker and thick core. The adhesion of both materials is very important for the load transferring and therefore the functioning of the sandwich as a whole.

Regarding the behavior of a sandwich structures, an analogy with an I cross section is appropriate. In this efficient type of section, as much as possible of the material is placed in the flanges situated farthest from the neutral axis (center of bending), and enough material is left in the web to make the flanges work together and to resist shear and buckling. Likewise, in a sandwich, the faces act as the flanges and the core takes the place of the web, in other words, the faces carry in – plane and bending loads, while the core resist transverse shear forces and keeps the facings in place (Vinson, 1999).

Compared to a single laminate structure, by using the sandwich concept, the flexural rigidity and flexural strength can be significantly increased.

The properties of primary interest of the facings are summarized as follows:

- High stiffness providing high flexural rigidity
- High tensile and compressive strength
- Impact resistance
- Surface finish
- Environmental resistance
- Wear resistance

1.1.1. FRP Sandwich Panel. For structural applications in civil engineering, low cost sandwich panels can be used. The combination of a Fiber-Reinforced Foam (FRF) with glass fiber polymer composites facings allows the construction of a low cost composite structure (Stoll et al. 2001).

The description, fabrication method, constituents, and properties of the material, which were provided by WebCore Technologies (Ohio), are now presented.

1.1.2. Material Description. This sandwich structure is characterized by a new type of core referred to as FRF. It is composed of closed-cell foam combined with dry fibers. The foam keeps in position different structural fiber forms that at the end becomes Fiber-Reinforced

Polymer (FRP) members once infused with resin during molding. These members take the form of angled struts oriented in truss or flat continuous webs (Stoll et al. 2001).

This type of foam has been fabricated in thickness varying from ½ in (12.7 mm) to 3 in (76.2 mm), and glass reinforcement have been used. There are two variants of FRF cores developed by WebCore, and they are described as follows:

- Stitched FRF Core
- Hybrid Stitched/Webbed FRF Core

Since the latter is the type of core composing the sandwich structure matter of this investigation, it is now described in detail.

1.1.2.1 Hybrid Stitched/Webbed FRF Core. This version is characterized by stitching in the x-direction (longitudinal) and by continuous webs in the y-direction (transverse). The continuous fibers are composed of fabric forming $\pm 58^\circ$ fiber angles. The webs are created by applying fabric to one side of a foam board, sawing the board into strips, and then stacking the strips together with the fabric on one side of a strip sandwiched against the next strip. The spacing of the webs is determined by the thickness of the starting foam, and the cutting width of the foam strips determines the height of the core. The stacked strips are then packed together and stitched in the x-direction. The material constituent of the stitches and the webs is Glass Fiber Reinforced Polymer (GFRP).

Generally a pre-attached GFRP fabric is applied to the top and bottom before stitching to provide integrity to the core. The size of this lamina is limited by the width of the stitching machine; therefore this fabric can not be continuous in large panels. A section of hybrid FRF core is shown in Figure 1.1 and Figure 1.2.



Figure 1.1 FRF Core - 3 in (76 mm)

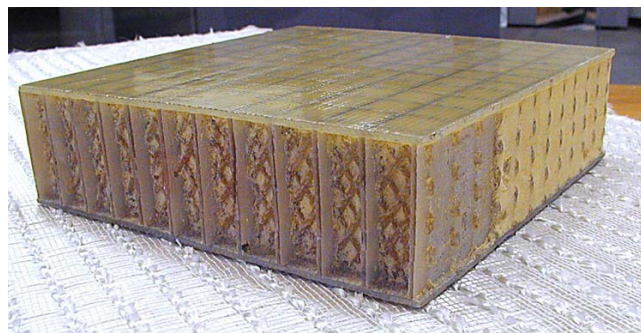


Figure 1.2 Hybrid FRF Panel Section

The engineering properties are affected by several factors such as: the stitch advance, stitch row spacing, stitch/tow weight, web fabric weight and web fabric spacing. The greater the amount of fiber reinforcement, the larger the quantity of resin absorbed during processing, so is the weight and cost of the panel. Therefore, there is an exchange of the engineering properties and the weight and the cost of the structure.

1.1.2.2 Panel Faces. The skin reinforcement consists of the pre-attached GFRP fabric plus several layers of bidirectional E-glass fabrics added during molding.

The sandwich panel characterized in this research was composed of GFRP facings of 0.25 in (6.35 mm) thick and hybrid stitched/webbed FRF core of 3 in (76.2 mm) depth.

1.1.3. Sandwich Panel Manufacturing. Using FRF core and the vacuum-assisted resin transfer molding technique (VARTM), the production of sandwich panels is carried out. The great number of flow paths through the foam provided by the roving and the fabric allow infusion into all the parts of the panel including corners, and excellent wet out of the facings (Stoll et al. 2001).

Using this method, a 190 ft² (17.7 m²) sandwich panel with a 3 in (76.2 mm) thick core fully infused with 700 lb (3.11 kN) of resin in approximately 10 minutes. The panel is left on a table under vacuum overnight. Following curing, the demolding of the panel and installation of lifting bolts requires approximately 1 to 2 hours (Stoll et al. 2002). Regarding the weight of the sandwich panel, it is about 8 lb/ft² (383.6 kN/m²).

In addition to the previous information, a literature survey on the subject of sandwich panels is offered in the Appendix A. This is to allow the reader to become more familiar with sandwich structures, which are not very common in civil engineering.

1.2. SCOPE AND OBJECTIVE

In the last few years, the availability of lightweight FRP sandwich panels, not only for bridge decks, but also for temporary bypass roadways, has been identified as a very interesting alternative to traditional methods of construction. For this reason, an investigation whose starting point is the mechanical characterization of a sandwich panel structure comprised of a FRF core was conducted. The determination of a sandwich mechanical properties as well as its performance under different load conditions provide part of the information necessary to decide whether the material is suitable or not for construction use.

1.3. PREVIOUS RESEARCH

Extensive work in the area of sandwich panel theory application was developed by Allen (1969) and Vinson (1999). In the area of civil engineering, the most remarkable features regarding projects in the United States where FRP panels have been utilized as bridge decks are presented herein.

Since 1996, the application of FRP sandwich panels in the United States has been identified as an alternative solution for either bridge construction or rehabilitation, which has become more popular and accepted. The following FRP sandwich panel bridges show how geographically well distributed the bridges are within the country. These projects are considered as demonstrations of one of the several potential applications of FRP sandwich panels in the civil engineering arena. Further investigation of this type of structure is necessary in order for it to become a commercially-viable product. Regarding published laboratory test results from

experiments conducted in the GFRP sandwich panels manufactured by Webcore Technologies, there is limited availability (Stoll et al. 2002).

No-Name Creek Bridge – On November 1996 over No-Name Creek, the nation's first all composite, fiber reinforced polymer (FRP) bridge, was installed in Russell, Kansas. This short-span bridge demonstrates the viability of the structural panel concept. The bridge is 23 ft (7.01 m) long and is capable of supporting an AASHTO HS20-44 truck. It was built with fiber-reinforced honeycomb lightweight, heavy-duty structural sandwich panels, manufactured by Kansas Structural Composites. Details about this project have been summarized by Gill and Plunkett (2000).

Salem Avenue Bridge – The Salem Avenue bridge is located in Dayton, Ohio. The overall bridge length is 679 ft (207 m) with span lengths of 130 ft (39.6 m), 137 ft (41.8 m), 145 ft (44.2 m), 137 ft (41.8 m) and 130 ft (39.6 m). The bridge is comprised of FRP deck panels supported by steel girders spaced 8.75 ft (2.7 m) on center. The FRP materials were provided by Composite Deck Solutions, Creative Pultrusions, Inc., Hardcore Composites, Inc., and Infrastructure Composites International. The purpose was to evaluate different FRP panel technologies in a single project. More information about this project is outlined by Henderson (2000) and Reising et al. (2001).

Crawford County Bridge – The Kansas Department of Transportation (KDOT) installed two FRP composite bridge decks on Kansas State Highway 126 (west of Pittsburg, Kansas), one in October 1999 and the other one in November 1999. Each 45 ft. long and 32 ft. wide decks meet AASHTO HS-25 requirements. The old bridge decks were deteriorated and needed to be widened. The panels were manufactured by Kansas Structural Composites.

Bently's Bridge – The Bently's bridge is a truss bridge rehabilitated with long span composite decks. It is located in Chemung, New York, and it was installed in 1999. The simple – span through truss bridge is 140 ft (42.7 m) in length. It consists of FRP deck panels supported by steel truss beams spaced at 14 ft (4.3 m) on center. The FRP materials were provided by Hardcore Composites. Before rehabilitation the bridge had a reinforced concrete deck. The composite deck reduced the dead load of the structure by 265 tons (530 kips). The NYDOT saved over one million dollars as a result of rehabilitating the bridge versus the demolition and the consequent new construction. Details about the project were outlined by Wagh (2001).

St. Johns Street, Jay Street and St. Francis Street Bridges – As part of an investigation conducted in the University of Missouri-Rolla, FRP panels were utilized in these three bridges located in Missouri. Two bridges had panels being supported by steel girders and the other one is only comprised of FRP deck panels. The type of sandwich constructions that was utilized was honeycomb sandwich panels, manufactured and installed by Kansas Structural Composites, Inc. The bridges were designed to carry a standard HS20-44 (approximately 180 kN) truck load. They were tested in-situ having an illustration of the overall behavior of the panel performance. Also more load tests have been conducted in the bridges, so in that way it is possible the observation of the structure under real environmental conditions with the time.

Hebble Creek Bridge – This bridge is located at Wright Patterson AFB, Dayton, Ohio. Stoll et al. (2002) detailed the design, fabrication, testing and installation of low-profile composite bridge deck carried out by WebCore. A stone and reinforced concrete bridge across Hebble Creek was replaced due to the degradation of the structure. The deck of the bridge was comprised of sandwich composite material with fiber glass skins and FRF core, and it was designed to be mounted on steel I-beams stringers. The installation of the new structure itself

was completed in one day. Additional four days were necessary for ultimate details such as filling up of gaps, installation of sidewalk and guard railings, and finally the paving process.

INEEL Bridge – This bridge was constructed in 1997 and is located in Idaho Falls, Idaho. The total length of this single span structure is 30 ft (9.1 m). The bridge consists of FRP deck panels. The FRP materials were provided by Martin Marietta Composites.

Tech21 Bridge – The Tech21 bridge is located on Smith Road in Butler County, Ohio. The total span length (single span) is 33 ft (10.1 m). This bridge is composed of FRP box beams and deck panels. The FRP materials were also supplied by Martin Marietta Composites. The bridge was built in 1997. Details about this project are outlined by Zoghi et al. (2002).

Bennet's Creek – The Bennet's Creek bridge is located in Steuben County, New York. The overall length of the structure is 23 ft (7 m). The deck of the structure is composed of FRP panels, they were provided by Hardcore Composites. More information regarding this bridge can be found in the papers Allampalli et al. (2000) and Allampalli et al. (2001).

Laurel Run Bridge – The Laurel Run bridge is located in Somerset County, Pennsylvania. The total length of this single span structure is 25 ft (7.62 m). This bridge consists on FRP deck panels mounted in steel girders spaced 2.9 ft (0.9 m) on center. The panels were supplied by Creative Pultrusions, Inc. Details about this bridge were outlined by Shekar et al. (2002).

Muddy Run Bridge – This bridge is located on I-351 in Glasgow, Delaware. The overall bridge length (single span structure) is 32 ft (9.7 m), and the deck consists on FRP panels, which were provided by Hardcore Composites. The corresponding details were outlined by Chajes et al. (2000).

Bridge I-92 – It is located in New Castle, Delaware. Its total span length (single span) is 35 ft (10.7 m). The structure consists of FRP bridge panels supported by steel girders spaced 2.8 ft (0.9 m) on center. The FRP materials were provided by Hardcore Composites.

1.4. OUTLINE OF THE REPORT

The work presented in this report is organized as follows:

Section 2 deals with the performance of two sandwich panels with FRF core, under both static and fatigue compressive conditions. The corresponding results and pertinent discussions for both panels A and B (defective), as well as the failure mode are presented.

Section 3 details the static and cyclic flexural testing of two directional different sandwich beams (longitudinally-cut and transversally-cut). Along with the outcomes, the mode of failure and corresponding results are shown.

In Section 4, the experimental results from the compressive and the flexure tests are discussed. The related conclusions are outlined in Section 5.

As a complement for an envisioned second complementary phase to this research project, in Section 6 recommendations for a possible site implementation of a bypass road panel are presented.

Appendix A presents a FRP sandwich structure literature survey, in order to provide the reader with the most remarkable features of this type of composite and its multiple applications since its appearance in the 1940s.

Appendices B and C show the plots corresponding to the compressive fatigue performance of panel A, and panel B, respectively.

Appendix D shows the flexural behavior of the control and fatigue conditioned sandwich beams, including plots of applied load versus deflection (at loading point and at midspan), and plots of bending stiffness versus applied load.

Appendix E presents the evaluation of sandwich panel cubic samples, conducted through microwave Non-Destructive Technique (NDT) inspection. The primary goal of this assessment was to detect possible delamination in the interface foam (core)-facing, in a fatigue conditioned specimen. The NDT technique showed not to be applicable for this type of sandwich structure. The images that were obtained in the evaluation are presented herein.

In Appendix F, additional information is presented, which consists of the March 7th document issued by the Department of the Air Force, for the development of the airfield matting.

2. COMPRESSIVE TEST

In order to observe and analyze the performance of the FRF sandwich structure, testing of nominal cubic specimens under both static and cyclic loading was conducted in the laboratory, and mechanical properties such as ultimate compressive capacity, compressive strength and compressive modulus were determined.

2.1. STATIC COMPRESSIVE TEST.

2.1.1. Test Set Up. This test was accomplished according to ASTM C365 “Standard Test Method for Flatwise Compressive Properties of Sandwich Cores” (2000). The corresponding calculations to obtain the aforementioned mechanical properties are presented. According to the standard, cubic nominal specimens of 4 in (102 mm) were cut out of panel A. See Figure 2.1. The real dimensions of the specimens were the same of the panel thickness: 3.5 in (89 mm).

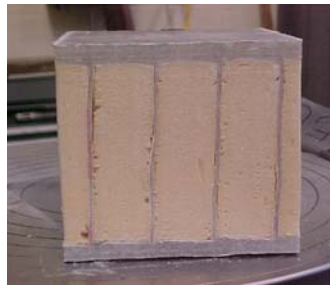


Figure 2.1 Sandwich Panel Cubic Specimen

Table 2.1 and Table 2.2 summarize the geometrical properties of the specimens utilized in this test, they were cut out of panel A and panel B, respectively. Their dimensions and weight were measured to the nearest 0.01 in (0.25 mm) and 0.01 lb (0.044 N), in that order.

Table 2.1 Specimens Physical Characteristic - Panel A

Specimen	Length (in)	Width (in)	Core Thickness (in)	Weight (lb)
A1	3.88	3.88	3.00	1.03
A2	4.06	3.88	2.93	1.08
A3	3.94	3.56	2.93	1.02
A4	3.94	3.88	3.00	1.05
A5	3.88	3.88	2.97	1.06
A6	3.94	3.94	2.97	1.07

Note: 1 in = 25.4 mm, 1 lb = 4.45 N

Table 2.2 Specimens Physical Characteristic - Panel B

Specimen	Length (in)	Width (in)	Core Thickness (in)	Weight (lb)
B1	3.96	4.03	2.98	1.01
B2	4.05	4.08	2.96	1.05
B3	3.93	3.99	2.95	0.98
B4	4.05	4.07	2.95	1.03
B5	4.04	4.06	2.97	1.04
B6	4.02	3.96	2.94	1.02

Note: 1 in = 25.4 mm, 1 lb = 4.45 N

The equipment utilized for this test was a MTS880 universal testing machine, and the data was acquired using a personal computer with the suitable software. Regarding the instrumentation, since the core of the sandwich specimens is composed of foam, it was not possible to fix an extensometer to it and obtain vertical displacement readings; instead, a potentiometer was attached to the side corresponding to the longitudinal direction of the panel on the specimens, otherwise the widening in the transversal direction would have avoided accurate readings. Some silicon was placed between the foam and potentiometer (see Figure 2.2).

**Figure 2.2 Potentiometer attached to the cubic specimen**

For the actual test, the specimen was centered under the load plate to ensure a correct pressure distribution. The crosshead displacement was set up at first at the loading rate suggested in the ASTM standard: 0.02 in/min (0.50 mm/min), but this rating was not suitable to attain the time to failure between 3 and 6 minutes suggested in the standard. Therefore, the loading rate used was 0.0043 in/min (0.1075 mm/min) and the individual average time to failure of the specimens was 5.45 minutes.

The MTS880 was set up in such manner that the acquired data consisted in the load applied (lb), the stroke (loading block displacement) and the vertical deformation measured by the potentiometer (in). Hence, having the MTS880 set up on ramp to failure, and on the proper displays (monitoring), the load was applied through a suspended loading block over the entire surface of the sandwich cube, at the above mentioned rate.

2.1.2. Experimental Results

The compressive strength is determined as follows:

$$\sigma = \frac{P}{A} \quad (1)$$

Where:

σ = Compressive strength, psi (MPa)

P = Ultimate load, lb (N)

A = Cross sectional area: in² (mm²)

The compressive modulus can be computed using the following expression:

$$E = \frac{St}{A} \quad (2)$$

Where:

E = Compressive Modulus, psi (MPa)

S = $\Delta P/\Delta u$ slope of the initial linear portion of load versus displacement curve, lb/in (N/mm)

u = Displacement of the loading block

t = Core thickness, in (mm)

With the available data, it was possible to plot load versus displacement curves for each specimen, and in order to calculate the parameter ‘S’ necessary for the computation of the compressive modulus in equation 2, the initial linear portion of those curves was taken in between 5000 lb (22.25 kN) and 10,000 lb (44.50 kN), this load interval was considered appropriate based on the average value of the control specimens.

2.1.2.1 Panel A. The average value of the control specimens indicates that the ultimate compressive capacity was 18.94 kips (84.28 kN), the compressive strength corresponding to the ultimate load was 1.26 ksi (8.68 MPa) and the compressive modulus was 82.57 ksi (568.9 MPa). Their standard deviations were: 0.821 kips (3.65 kN), 0.071 ksi (0.49 MPa) and 6.038 ksi (41.6 MPa), respectively (see Table 2.3). Figure 2.3 shows the load applied versus displacement curve for the five specimens as well as the interval considered as the initial linear portion necessary for the computation of the compressive modulus E.

Table 2.3 Static Compressive Test Results - Panel A

Specimens	P_U (kip)	Δ_U (in)	σ_U (ksi)	E (ksi)
A1	18.32	0.060	1.22	88.16
A2	18.75	0.064	1.19	78.15
A3	18.48	0.060	1.32	90.37
A4	19.72	0.063	1.29	74.31
A5	20.18	0.057	1.34	83.26
A6	18.17	0.058	1.17	81.16
Mean Value	18.94	0.060	1.26	82.57
Standard Deviation	0.82	0.003	0.07	6.04
Coefficient of Variation	4.33%	4.53%	5.64%	7.31%

Note: 1 in = 25.4 mm, 1 kip = 4.4497 kN, 1 ksi = 6.89MPa

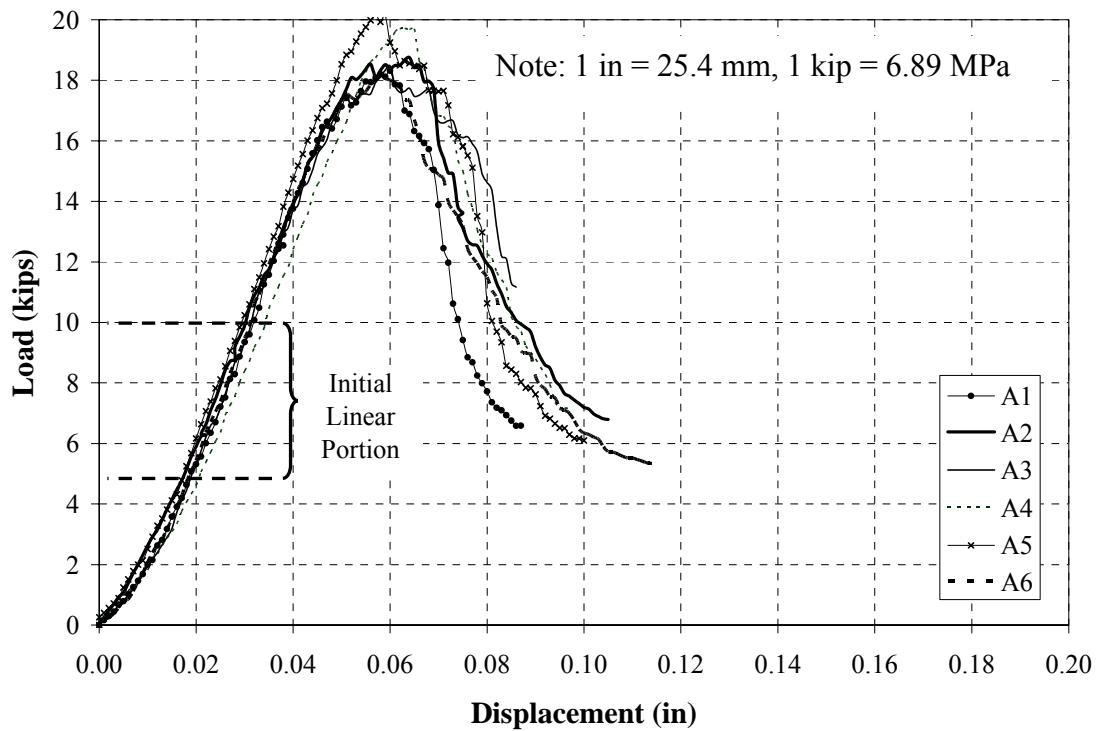


Figure 2.3 Load vs. Displacement - Static Compressive Test - Panel A

2.1.2.2 Panel B. Same nominal cubic specimens were cut out of panel B and tested up to failure, and the corresponding results are presented in Table 2.4. The ultimate load of sample B3 was approximately three standard deviations away from the average value, in other words, the probability of getting a value such as B3's in a set of six specimens is very low: 1.8 percent. Therefore, according to Chauvenet's criterion (Taylor, 1982), specimen B3 was drawn out of the computations. The corresponding load versus displacement curves are presented in Figure 2.4.

Table 2.4 Static Compressive Test Results - Panel B

Specimens	P_U (kip)	Δ_U (in)	σ_U (ksi)	E (ksi)
B1	15.26	0.055	0.96	60.54
B2	16.26	0.053	0.99	66.88
B3*	9.90	0.042	0.63	54.14
B4	14.41	0.059	0.87	63.29
B5	17.57	0.051	1.07	73.27
B6	13.02	0.059	0.82	66.57
Mean	15.30	0.055	0.94	66.11
Standard Deviation	1.74	0.004	0.10	4.77
Coefficient of Variation	11.35%	6.46%	10.53%	7.22%

*Specimen not included in the computations

Note: 1 in = 25.4 mm, 1 kip = 4.4497 kN, 1 ksi = 6.89MPa

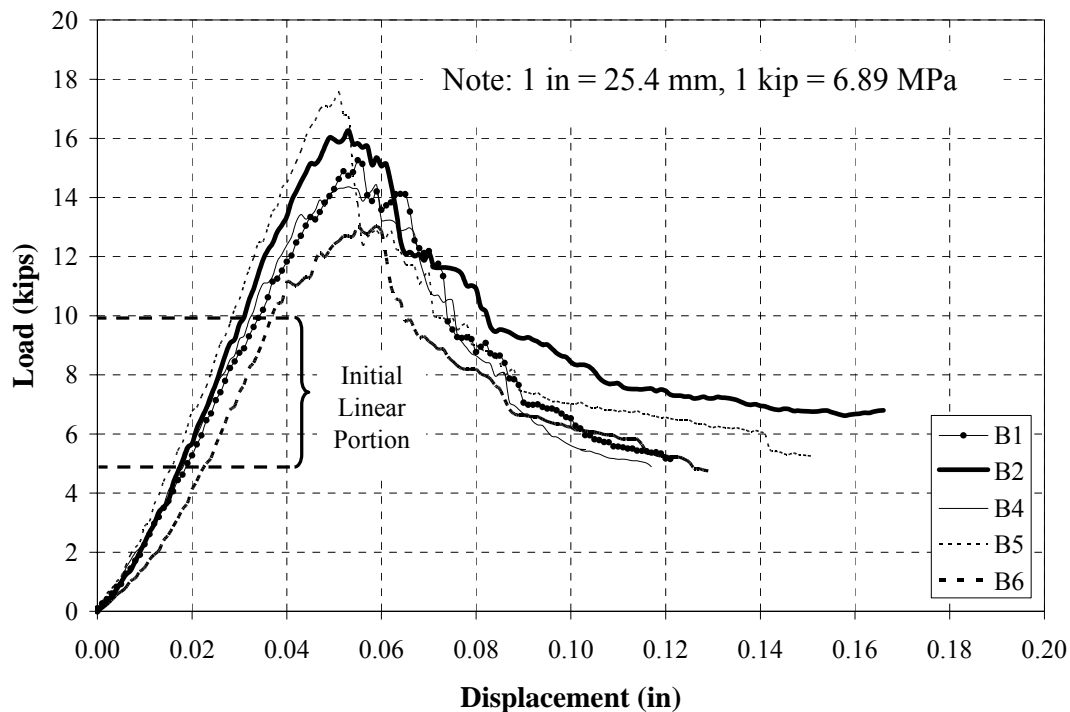


Figure 2.4 Load vs. Displacement - Static Compressive Test - Panel B

According to the results presented in Table 2.3 and Table 2.4, the average ultimate load capacity and compressive modulus from Panel B corresponds to approximately 80 percent of panel A's, while the strength is equivalent to 75 percent.

Concerning the mode of failure, it was observed in all the specimens (Panel A and B), buckling of the continuous webs and the subsequent creation of gaps in between the foam and the webs. Due to the longitudinal configuration of the stitches, the specimens popped out in that direction generating horizontal cracks in the foam (see Figure 2.5).

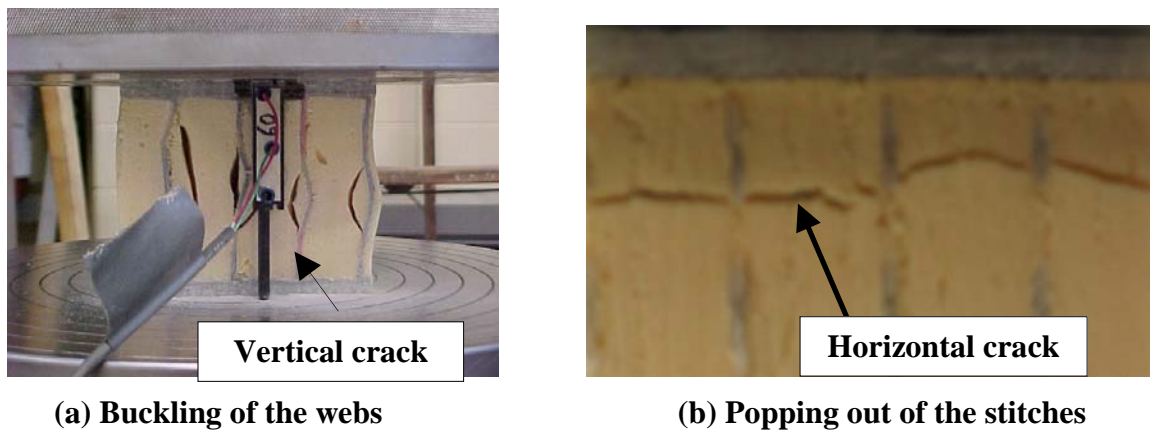


Figure 2.5 Failure Mode - Compressive Test

Under compressive vertical stress, the continuous webs buckle originating vertical cracks or gaps and bending of the foam in the transverse direction, and since the foam has negligible tensile resistance, the appearance of a horizontal crack is the consequence. This crack development is also influenced by the fact that the lattice created by the stitches does experience deformation in its longitudinal direction. Contrary to the vertical cracks, the horizontal crack was not expected under compression, but it is the result of the configuration of the material that affects the mode of failure.

The static performance of panel A is better than panel B's, this is based in the fact that for a set of six specimens for both panels, the results obtained from A showed higher consistency (less variation) than the ones obtained from panel B, not only for the ultimate load, also for the strength and modulus.

2.2. FATIGUE COMPRESSIVE TEST

The purpose of this test was to determine the performance of the sandwich panel under repeated loading. After conditioning of the specimens to 500,000; 1,000,000; 1,500,000 and 2,000,000 cycles at preset load levels and the subsequent monotonic compressive test to failure, it was possible to study the behavior of the material comparing it to the one observed in the Static Compressive Test for both panels A and B.

Four different levels of load were imposed in this test. For the minimum level (Load Level 1) it was decided to take the value of 30 percent, which is above the "Sustained plus Cyclic Stress Limit" for Glass FRP suggested by ACI 440(2R-02): 20 percent. The maximum level (Load Level 4) corresponds to 60 percent of the ultimate compressive capacity. The levels of load shown in the following table were calculated based on the ultimate compressive capacity

of Panel A. In Table 2.5, the different levels are presented in the ranges of the imposed loads. A minimum of 5 percent of the ultimate compressive capacity was considered suitable to maintain the stability of the specimens and equipment during the conditioning.

Table 2.5 Levels of Load - Fatigue Compressive Test

Load Values	Load Level 1 30% P_U (kip)	Load Level 2 35% P_U (kip)	Load Level 3 40% P_U (kip)	Load Level 4 60% P_U (kip)
Minimum	0.95	0.95	0.95	0.95
Maximum	5.68	6.63	7.58	11.36

Note: 1 kip = 4.4497 kN

Samples from panel A were statically tested and the levels of load for the fatigue test were based on the ultimate compressive capacity of this panel. After this static experiment, the conditioning under Load Level 1 (30 percent) and Load Level 4 (60 percent) were accomplished with specimens also from panel A. Later on, to carry out the test under the two remaining load levels (40 percent and 35 percent) and also a repetition of the first load level (30 percent), cubic samples were cut out of panel B.

The reduction in the compressive capacity of panel B with respect to panel A had a direct effect in the fatigue experiments that were conducted with specimens cut out of panel B. The actual percentages were obviously much higher as it can be seen in Table 2.6 below.

Table 2.6 Equivalent Levels of Load - Panel A & Panel B

	Panel A $P_U = 18.94$ kips	Panel B $P_U = 15.30$ kips
Load Level 1	30%	37.1%
Load Level 2	35%	43.3%
Load Level 3	40%	49.5%
Load Level 4*	60%	—

*Panel B was not tested under this load level.

Note: 1 kip = 4.4497 kN

2.2.1. Test Set Up. Same nominal cubic specimens as for the static test were utilized for the four load levels experiments, and the samples were also first measured, and weighed.

The MTS880 universal testing machine was also suitable for the conduction of the cyclic test, since it is capable of applying a defined amplitude loading, and in addition to a set up oscilloscope, it is possible to monitor the variation of the load during conditioning. The load levels showed in Table 2.5 correspond to the maximum values applied to the specimens, and a value of 5 percent of the ultimate load was adopted as a minimum value. With a frequency of 5 Hz, the duration of the test for each imposed level of load was approximately five days, due to the fact that the four series of four specimens were stacked and it was removed one series at the time after each 500, 000 cycles until the last series accumulated 2 million cycles.

For safety reasons, avoidance of horizontal displacement of the specimens, and to guarantee a uniform load distribution from the crosshead over each sample during conditioning,

a steel frame was built and placed in the MTS880 machine. This frame was composed of four 12 in (304.8 mm) by 12 in (304.8 mm) plates and one bottom plate of 14 in (355.6 mm) by 14 in (355.6 mm), all of them of a thickness of 1 in (25.4 mm). The biggest plate was properly fixed to the bottom plate of the machine and the rest of them were stacked aligned. Square tubes of a length of 2 in (50.8 mm) and 1 in (25.4 mm) by 1 in (25.4 mm) cross section, were welded in each plate in the proper layout (uniform load distribution over the samples), to constrain the displacement of the specimens during cycling (see Figure 2.6 and Figure 2.7). In addition to that, circular holes were drilled at a distance of 2.5 in (63.5 mm) from the sides in each corner in every steel plate, and steel rods were placed through them to prevent horizontal relative displacements of the plates (see Figure 2.8 and Figure 2.9).



Figure 2.6 Bottom Steel Plate

The specimens were set up on the plates in four series of four. Since the faces of the specimens were not completely smooth, it was considered convenient to place high resistance rubber pads in between the specimen face and each steel plate (top and bottom), therefore there was a better distribution of the load over the samples.



Figure 2.7 Test Setup - Fatigue Compressive Test

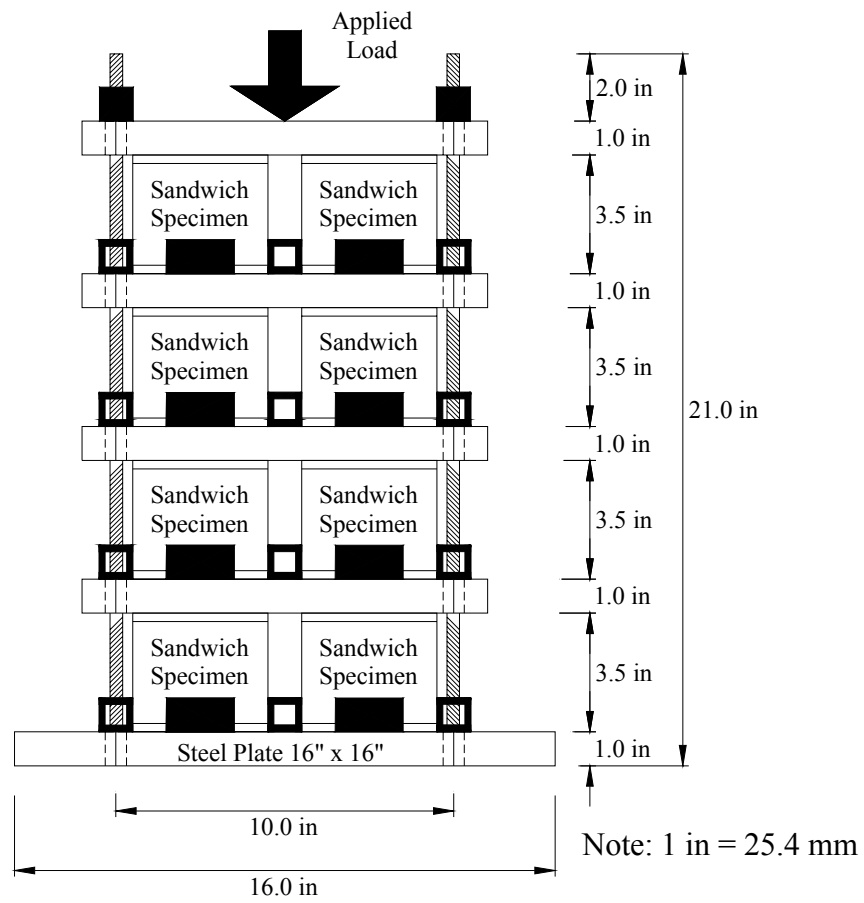


Figure 2.8 Test Setup Schematic - Fatigue Compressive Test

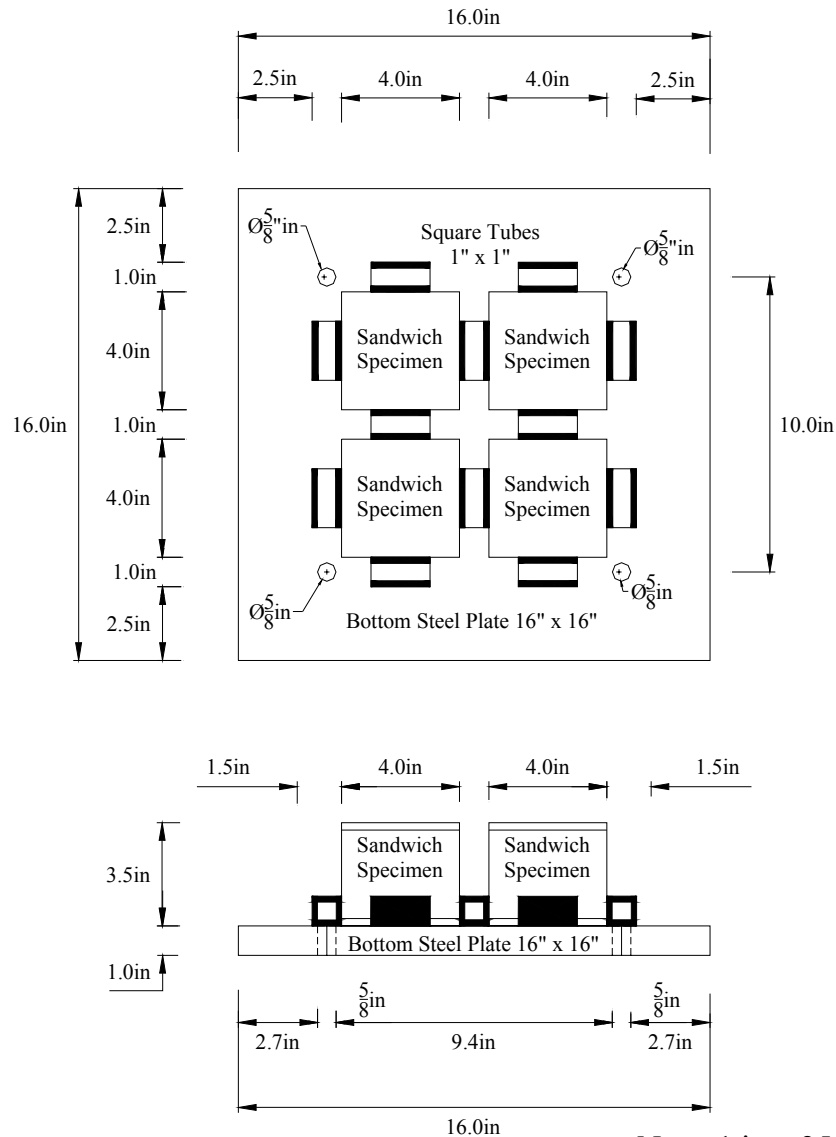


Figure 2.9 Bottom Steel Plate Schematic - Fatigue Compressive Test

2.2.1.1 Conditioning Load Level 1. The fatigue conditioning under a load level of 30 percent of the compressive capacity of panel A was conducted separately for specimens from this same panel, and later on also for samples cut out of panel B. As it was detailed in Table 2.5, the maximum applied load per specimen was 5.68 kips (25.27 kN). Therefore, for the four samples set by each layer, the total maximum load carried out through the crosshead of the machine was 22.72 kips (101.1 kN) and a minimum of 3.8 kips (16.91 kN). Table 2.7 and Table 2.8 present the physical characteristics of the specimens from panel A and panel B, respectively.

Table 2.7 Physical Characteristics - Conditioning Load Level 1 - Panel A

Specimen	Number of cycles (millions)	Length (in)	Width (in)	Core Thickness (in)	Weight (lb)
1A	0.5	4.05	3.99	2.93	1.08
1B		3.88	3.92	2.93	1.03
1C		3.85	3.93	2.93	1.05
1D		4.10	3.92	3.08	1.09
2A	1.0	3.89	3.92	2.94	1.02
2B		3.91	3.91	2.95	1.05
2C		3.90	3.91	2.94	1.03
2D		4.05	3.92	2.93	1.04
3A	1.5	3.92	3.92	2.94	1.03
3B		3.91	3.93	2.92	1.03
3C		3.91	3.92	2.92	1.05
3D		3.89	3.94	2.93	1.04
4A	2.0	3.89	3.91	2.93	1.03
4B		3.92	3.93	2.92	1.05
4C		3.89	3.89	2.94	1.04
4D		3.88	3.89	2.93	1.02

Note: 1 in = 25.4 mm, 1 lb = 4.45 N

Table 2.8 Physical Characteristics - Conditioning Load Level 1 - Panel B

Specimen	Number of cycles (millions)	Length (in)	Width (in)	Core Thickness (in)	Weight (lb)
1A	0.5	4.03	3.96	2.95	1.02
1B		3.83	3.89	2.94	0.98
1C		4.02	3.84	2.96	0.99
1D		3.86	3.95	2.95	0.97
2A	1.0	3.95	4.04	2.95	1.02
2B		3.99	4.07	2.96	1.06
2C		4.05	3.98	2.94	0.95
2D		3.99	3.84	2.96	1.00
3A	1.5	4.01	4.06	2.97	1.05
3B		3.97	4.01	2.98	0.98
3C		4.00	4.00	2.96	1.02
3D		4.00	4.02	2.97	1.02
4A	2.0	3.99	4.02	2.98	1.04
4B		3.99	3.99	2.98	1.03
4C		4.03	3.98	2.94	1.04
4D		4.00	3.99	2.96	1.02

Note: 1 in = 25.4 mm, 1 lb = 4.4497 N

2.2.1.2 Conditioning Load Level 2. The load range considered for this experiment (35 percent of the ultimate) corresponded to 0.95 kips (4.23 kN) to 6.63 kips (29.5 kN) per specimen, according to Table 2.5. Hence, the total maximum load applied in the four specimens set by series was 26.52 kips (118 kN).

Since the utilized samples were cut out of Panel B, the imposed load corresponded to actually 43 percent of its real ultimate compressive capacity, not to 35 percent as it was assumed at the beginning. The physical characteristics of the samples are shown in Table 2.9.

Table 2.9 Physical Characteristics - Conditioning Load Level 2 - Panel B

Specimen	Number of cycles (millions)	Length (in)	Width (in)	Core Thickness (in)	Weight (lb)
1A	0.5	4.11	4.07	2.96	1.07
1B		4.02	3.99	2.97	1.04
1C		4.04	4.06	2.97	1.00
1D		4.06	3.93	2.95	1.01
2A	1.0	4.03	4.06	2.96	1.06
2B		4.04	4.10	2.97	0.99
2C		4.10	3.98	2.99	1.02
2D		4.04	4.07	2.96	1.04
3A	1.5	4.02	4.09	2.95	1.05
3B		4.02	4.10	2.99	1.05
3C		4.03	4.10	2.96	1.05
3D		4.01	4.11	2.97	1.04
4A	2.0	4.02	4.04	2.99	1.02
4B		3.98	4.10	2.99	1.04
4C		3.89	3.99	2.98	1.01
4D		4.02	4.03	2.98	1.03

Note: 1 in = 25.4 mm, 1 lb = 4.45 N

2.2.1.3 Conditioning Load Level 3. The maximum imposed compressive load was 7.58 kips (33.73 kN) per specimen (40 percent). Therefore, for the four cubic samples set by each layer, the maximum total load applied through the crosshead was 30.32 kips (135 kN). The specimens were prepared in the same manner as for the previous fatigue experiments. Table 2.10 presents the physical characteristics of the samples.

Table 2.10 Physical Characteristics - Conditioning Load Level 3 - Panel B

Specimen	Number of cycles (millions)	Length (in)	Width (in)	Core Thickness (in)	Weight (lb)
1A	0.5	4.07	3.93	2.99	1.00
1B		3.96	4.03	2.98	1.02
1C		3.97	4.03	2.99	1.02
1D		4.01	4.02	2.98	1.07
2A	1.0	3.99	4.04	2.99	1.02
2B		4.02	4.04	2.99	1.02
2C		4.14	4.02	2.98	1.02
2D		4.03	4.03	2.98	1.00
3A	1.5	4.04	4.12	2.99	1.04
3B		4.05	4.05	2.96	1.05
3C		3.97	4.03	2.98	1.01
3D		4.06	3.98	2.96	0.94
4A	2.0	4.02	3.95	2.99	1.01
4B		4.03	4.10	2.99	1.04
4C		4.05	4.01	2.97	1.04
4D		4.06	4.04	2.95	1.04

Note: 1 in = 25.4 mm, 1 lb = 4.45 N

2.2.1.4 Conditioning Load Level 4. Each layer of four specimens was conditioned at a maximum load of 45.44 kips (202.2 kN) and a minimum of 3.8 kips (16.91 kN). The physical characteristics of the samples are presented in Table 2.11.

Table 2.11 Physical Characteristics - Conditioning Load Level 4 - Panel A

Specimen	Number of cycles (millions)	Length (in)	Width (in)	Core Thickness (in)	Weight (lb)
1A	0.5	3.86	3.95	2.95	1.03
1B		3.87	3.90	2.97	1.11
1C		3.70	3.80	2.98	1.00
1D		3.88	3.90	2.97	1.03
2A	1.0	3.90	3.93	2.96	1.13
2B		4.07	3.95	2.98	1.10
2C		3.89	3.91	2.98	1.07
2D		3.96	3.90	2.94	1.14
3A	1.5	3.82	3.89	2.95	1.03
3B		3.89	3.94	2.98	1.14
3C		3.84	3.93	2.95	0.99
3D		3.88	3.94	2.93	1.05
4A	2.0	4.18	3.83	2.97	1.11
4B		4.10	3.93	2.98	1.07
4C		3.89	3.86	2.95	1.02
4D		4.03	3.86	2.94	1.11

Note: 1 in = 25.4 mm, 1 lb = 4.45 N

2.2.2. Experimental Results. After the fatigue conditioning, a potentiometer was attached to the specimen in the same way as for the static test described in Section 3.1, to be individually tested to failure. The computation of the residual mechanical properties was completed as for the static test.

2.2.2.1 Conditioning Load Level 1. Table 2.12 presents the results obtained for the samples from panel A. The specimens 1C, 2A and 3B were not considered due to the high percentage difference among the samples in the corresponding series, in both the residual ultimate load and the residual modulus E. For the case of specimen 4D, its value of residual ultimate load is much lower than the average value of the rest of the samples in the same series. The corresponding load versus displacement curves can be found in Appendix B.

Table 2.12 Residual Mechanical Properties - Conditioning Load Level 1 - Panel A

Specimens	P_U (kips)	Δ_U (in)	σ_U (ksi)	E (ksi)
500,000 Cycles				
1A	17.20	0.057	1.06	64.95
1C*	7.68	0.037	0.51	46.42
1B	16.08	0.061	1.06	69.26
1D	15.61	0.048	0.97	70.48
Mean	16.29	0.055	1.03	68.23
Standard Deviation	0.820	0.007	0.052	2.907
Coefficient of Variation	5.03%	12.03%	5.03%	4.26%
1,000,000 Cycles				
2A*	13.24	0.053	0.87	61.03
2B	17.70	0.055	1.16	75.02
2C	17.00	0.055	1.12	84.84
2D	17.19	0.051	1.08	80.74
Mean	17.30	0.054	1.12	80.20
Standard Deviation	0.362	0.002	0.038	4.929
Coefficient of Variation	2.09%	4.30%	3.36%	6.15%
1,500,000 Cycles				
3A	13.54	0.054	0.88	83.20
3B*	13.00	0.084	0.85	37.43
3C	16.87	0.054	1.10	80.16
3D	16.72	0.045	1.10	78.78
Mean	15.71	0.051	1.03	80.71
Standard Deviation	1.88	0.005	0.13	2.26
Coefficient of Variation	11.97%	10.19%	12.37%	2.80%
2,000,000 Cycles				
4A	16.89	0.052	1.11	74.86
4B	16.19	0.049	1.05	72.31
4C	16.45	0.051	1.09	77.19
4D*	11.58	0.031	0.77	75.66
Mean	16.51	0.051	1.08	74.79
Standard Deviation	0.356	0.002	0.030	2.437
Coefficient of Variation	2.15%	3.01%	2.80%	3.26%

*Specimen not included in the computations.

Note: 1 in = 25.4 mm, 1 kip = 4.4497 kN, 1 ksi = 6.89MPa

Regarding the performance of the samples from panel B, all the cubic specimens survived the first 0.5 million cycles, so the top series was removed and the three remaining were left to continue the conditioning. After 83374 cycles (total of 583,374) the top two series failed (see Figure 2.10). One specimen in the top layer crushed and therefore the rest could not bear the

imposed load and also failed. The steel plate in between both layers tilted causing also crashing of the specimens in the next series. The samples in the bottom layer were apparently not damaged, so that cycling was continued. This last series was able to resist 2,083,374 cycles without failure. The results for this panel after the fatigue conditioning are shown in Table 2.13.

Table 2.13 Residual Mechanical Properties - Conditioning Load Level 1 - Panel B

Specimens	P_U (kips)	Δ_U (in)	σ_U (ksi)	E (ksi)
500,000 cycles				
1A	14.72	0.059	0.92	63.30
1B	15.37	0.064	1.03	66.72
1C	15.32	0.048	0.99	77.76
1D	12.58	0.046	0.83	68.78
Mean	14.50	0.054	0.94	69.14
Standard Deviation	1.313	0.009	0.091	6.175
Coefficient of Variation	9.05%	15.95%	9.66%	8.93%
2,083,374 cycles				
4A	17.33	0.069	1079	69877
4B	14.56	0.064	914	52969
4C	16.31	0.076	1018	66830
4D	14.72	0.067	922	70265
Mean	15.73	0.069	0.98	64.99
Standard Deviation	1.327	0.005	0.082	8.156
Coefficient of Variation	8.44%	7.39%	8.33%	12.55%

Note: 1 in = 25.4 mm, 1 kip = 4.4497 kN, 1 ksi = 6.89 kPa



Figure 2.10 Conditioning Level 1 - Panel B – After 583,374 cycles

2.2.2.2 Conditioning Load Level 2. After 66,263 cycles the top two layers of specimens from only panel B failed. From the two remaining series, one was removed and one was left to continue the cycling, the latter reached 2,066,263 cycles without any visible damage (see Figure 2.11).



(a) Setup after 66,263 cycles



(b) Setup after 2,066,263 cycles

Figure 2.11 Conditioning Load Level 2 - Panel B

For the up to failure test, a potentiometer was attached to each of the samples of the two layers that resisted the aforementioned number of cycles. The results of the static test conducted in the conditioned samples are presented in Table 2.14.

Table 2.14 Residual Mechanical Properties - Conditioning Load Level 2 - Panel B

Specimens	P_U (kips)	Δ_U (in)	σ_U (ksi)	E (ksi)
66 263 cycles				
3A	16.16	0.059	0.98	69.31
3B	13.95	0.044	0.85	66.81
3C	18.93	0.067	1.15	72.30
3D	17.44	0.062	1.06	65.37
Mean	16.62	0.058	1.01	68.45
Standard Deviation	2.11	0.010	0.13	3.042
Coefficient of Variation	12.70%	17.07%	12.61%	4.44%
2 066 263 cycles				
4A	14.51	0.052	0.89	68.48
4B*	17.59	0.057	1.08	79.05
4C	13.77	0.056	0.89	62.39
4D	14.28	0.068	0.88	64.72
Mean	14.19	0.059	0.89	65.20
Standard Deviation	0.381	0.008	0.006	3.073
Coefficient of Variation	2.68%	14.19%	0.69%	4.71%

* Specimens not considered in the calculations.

Note: 1 in = 25.4 mm, 1 kip = 4.45 kN, 1 ksi = 6.89 MPa

2.2.2.3 Conditioning Load Level 3. The fatigue conditioning of specimens cut out of panel B was started without inconvenient, but after 65340 cycles, the third series starting from the top failed. The top layer was removed and the two remaining series continued the cycling. There is no record of the exact number of cycles at which these two last layers crashed. The MTS880 was set up for 500,000 cycles, but since no limits were set up in the stroke, the machine continued the cycling until it reached the present count (see Figure 2.12). The results of the specimens statically tested after conditioning to 65340 cycles are presented in Table 2.15.



(a) Setup after 65340 cycles



(b) Failure of two last layers

Figure 2.12 Conditioning Load Level 3 - Panel B**Table 2.15 Residual Mechanical Properties - Conditioning Load Level 3 - Panel B**

Specimens	P_U (kips)	Δ_U (in)	σ_U (ksi)	E (ksi)
65 340 cycles				
1A*	11.23	0.051	0.70	48.76
1B	16.07	0.053	1.01	70.05
1C	16.15	0.060	1.01	65.93
1D	12.66	0.053	0.79	52.31
Mean	14.96	0.055	0.93	62.77
Standard Deviation	2.00	0.004	0.129	9.285
Coefficient of Variation	13.34%	7.30%	13.79%	14.79%

Note: *Specimen not considered in the calculations.

1 in = 25.4 mm, 1 kip = 4.45 kN, 1 ksi = 2.89 MPa

Panel B under the three different levels of load: 30, 35 and 40 percent (based on the ultimate compressive capacity of panel A), was subjected to actually 37.1, 43.3 and 49.5 percent of its real compressive capacity. The load versus displacement curves for all the specimens from panel B are displayed in Appendix C.

2.2.2.4 Conditioning Load Level 4. The set up was prepared in the same way as it was described for the previous levels of load and only specimens from panel A were placed. During the definition of the load range, after less than 100 cycles, the second layer of specimens starting from the bottom, failed. For this premature failure to occur, it was only necessary that one of the specimens in the layer had crashed first, hence the load being applied was redistributed and the remaining three specimens were not able to withstand it. See Figure 2.13. No static test was performed in the remaining samples.



Figure 2.13 Failure - Conditioning Load Level 4 – Panel A

In the following two figures, the residual ultimate compressive strength as well as the residual compressive modulus E are presented as a function of the number of cycles at which the different sets of specimens were subjected to. Figure 2.14 and Figure 2.15 showed that there is not appreciable reduction in the compressive capacity of the material. The minimum measured residual ultimate compressive strength corresponds to 80 percent of its ultimate value, fatigue conditioned to 2,066,263 cycles. The minimum measured residual compressive modulus E is 86 percent of the virgin sample after 2,083,374 cycles.

Figure 2.16 presents a summary of the data in the form of a S-N diagram, where S is the conditioning load and N is the number of cycles in millions. The letter in the label of each point designates the panel they belong to, and the number references the conditioning load level. The points with an arrow indicate the set of specimens that did not fail during the conditioning, therefore for certain number of cycles it was determine their residual strength (hollow points). The colored dots without an arrow represent the series of samples that failed during the fatigue conditioning. Additionally, the points are labeled according to the panel where they were obtained from (A or B), and the levels of load at which they were conditioned to (1, 2 and 3).

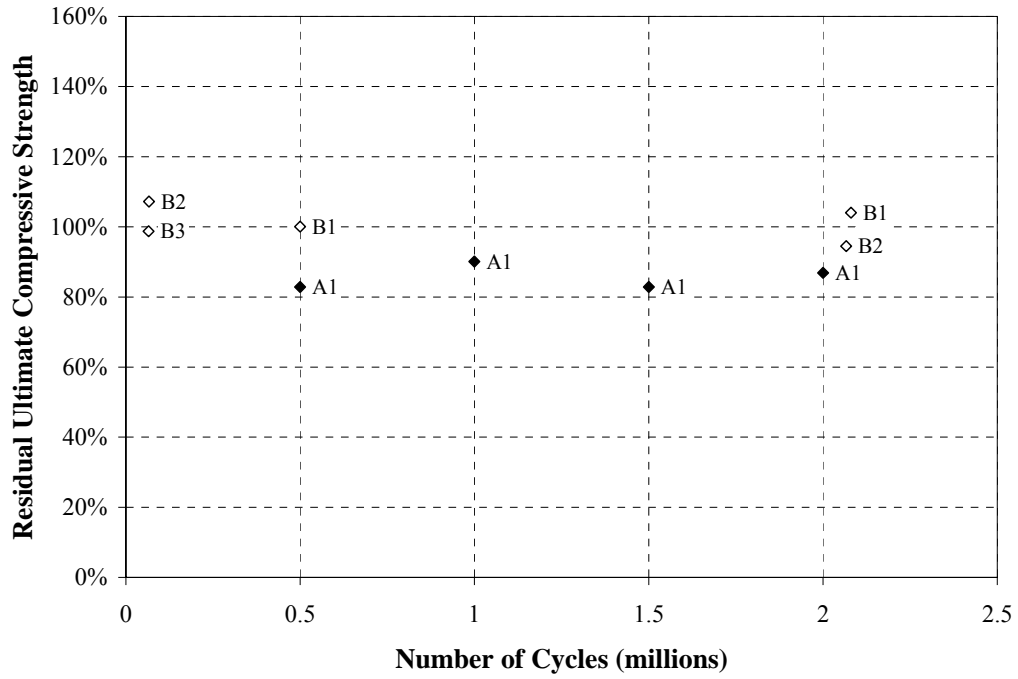


Figure 2.14 Residual Ultimate Compressive Strength

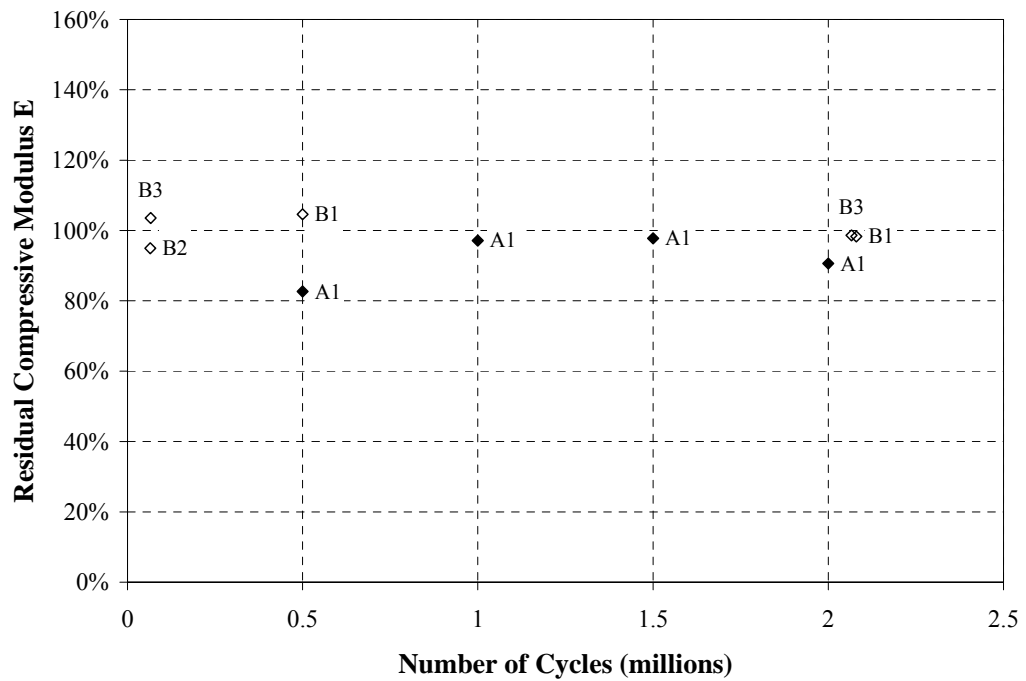


Figure 2.15 Residual Ultimate Compressive Modulus E

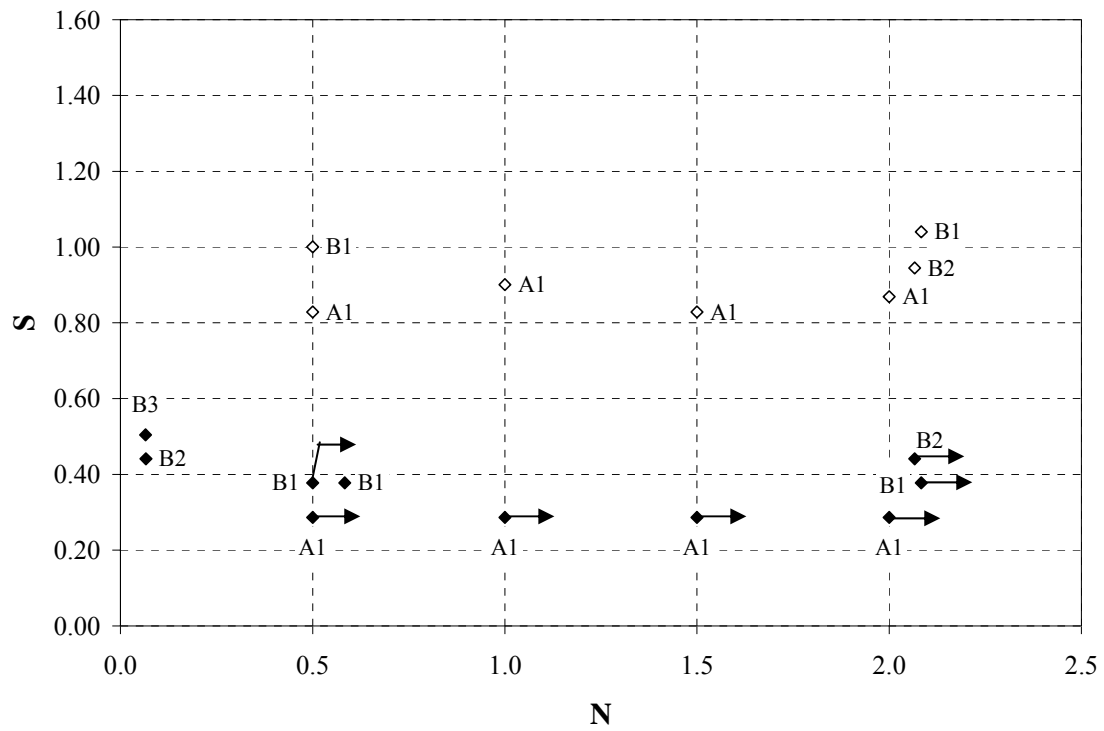


Figure 2.16 Conditioning Load S vs. Number of cycles N

3. FLEXURAL TEST

Testing of sandwich beams of 8 in (20.32 cm) wide and 58 in (147.32 cm) long, was conducted under static and cyclic load condition. The computations of the mechanical properties such as facing stress, sandwich bending stiffness and core shear strength are presented. The significance of the influence of the core shear modulus and its contribution to the overall deflection of a member subjected to bending moment is analyzed. The evaluation of the experimental results is accomplished through the application of ordinary beam theory (Allen, 1970).

3.1. ORDINARY BEAM THEORY

Figure 3.1 shows a sandwich beam composed of two thin faces each of thickness t and a thick layer (core) of thickness c . The depth of the beam is h and the width is b . For the purpose of the analysis, it is assumed that both the faces and the core material are isotropic materials.

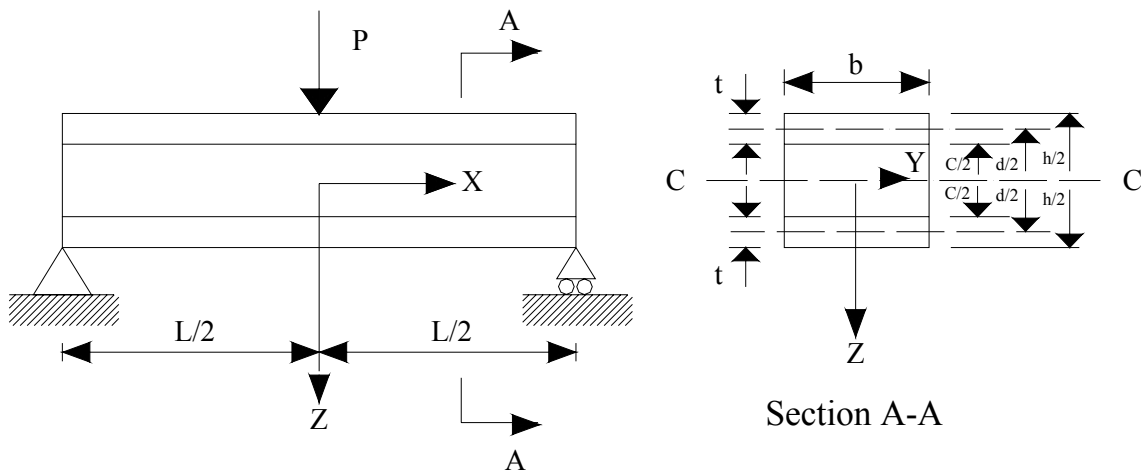


Figure 3.1 Sandwich Beam and Cross Section

The ordinary beam theory is also based upon the assumption that cross sections remain plain and perpendicular to the longitudinal axis before and after bending, therefore the following relationship will be utilized:

$$\frac{M}{EI} = \frac{1}{R} \quad (3)$$

Where EI is the flexural stiffness, but since the beam matter of this analysis is a composite beam, the flexural stiffness will be the summation of the flexural rigidities of the two different materials (faces and core). For convenience in the calculations, the flexural stiffness EI will be denoted by D .

$$D = \underbrace{E_f \frac{bt^3}{6} + E_f \frac{btd^2}{2}}_{\text{Stiffness of the faces}} + \underbrace{E_c \frac{bc^3}{12}}_{\text{Stiffness of the core}} \quad (4)$$

Where:

- E_f = Modulus of Elasticity of the facings, psi
 E_c = Modulus of Elasticity of the core, psi
 b = Width of the beam, 8 in (20.32 cm)
 t = Thickness of a single facing, 0.25 in (6.35 mm)
 c = Thickness of the core, 3 in (76.2 mm)
 d = Distance between the center lines of both faces, 3.25 in (82.55 mm)

The first term becomes 1 percent of the second one when:

$$3\left(\frac{d}{t}\right)^2 > 100 \quad (5)$$

Following the ordinary beam theory, the stresses in the faces and core can be determined. The strain at a distance z from the neutral axis, it is: Mz/D and multiply by the corresponding modulus of elasticity yields to the bending stress at position z . Thus:

$$\sigma_f = \frac{Mz}{D} E_f \Rightarrow \left(\frac{c}{2} \leq z \leq \frac{h}{2}; -\frac{h}{2} \leq z \leq -\frac{c}{2} \right) \quad (6)$$

$$\sigma_c = \frac{Mz}{D} E_c \Rightarrow \left(-\frac{c}{2} \leq z \leq \frac{c}{2} \right)$$

The maximum stresses for the facing and core are obtained when z is $\pm h/2$ and $\pm c/2$, respectively:

$$(\sigma_f)_{\max} = \pm \frac{ME_f}{D} \frac{h}{2} \quad (7)$$

$$(\sigma_c)_{\max} = \pm \frac{ME_c}{D} \frac{c}{2}$$

Equation 8 represents the shear stress τ . This expression results from the assumption of a core weak enough ($E_c = 0$) to provide significant contribution to the flexural stiffness of a sandwich beam, and consequently the shear stress could be assumed to be constant throughout the depth of the core.

$$\tau = \frac{Q E_f t d}{D 2} \quad (8)$$

Where Q is the shear force acting at the given cross section, and the remaining parameters have already been stated. Since it is assumed not significant contribution of the elastic modulus of the core in the flexural stiffness of the composite, then the third term in Equation 4 can be negligible. Additionally, if the condition stated in Equation 5 is fulfilled ($507 > 100$), then the expression for the flexural rigidity is:

$$D = E_f \frac{b t d^2}{2} \quad (9)$$

Substituting Equation 9 in Equation 8, the expression of the shear stress in the core is reduced to the following:

$$\tau = \frac{Q}{b d} \quad (10)$$

The shear stress is related to the shear strain as follows: $\gamma = \frac{Q}{G b d}$; where G is the shear modulus of the core material. According to Allen (1970), no shear strains are assumed in the

facings of the sandwich beam, and the shear contribution in the overall deflection for a simply supported beam, four point bending and third point loading is $\frac{PL}{6AG}$, where A is the area of the cross section and the term AG is called shear stiffness. Therefore, the overall deflection considering both the contribution of the bending and shear at the loading point and at midspan for a beam of are as follows:

$$\Delta_{\text{loading pt}} = \underbrace{\frac{5PL^3}{324D}}_{\text{Bending}} + \underbrace{\frac{PL}{6AG}}_{\text{Shear}} \quad (11)$$

$$\Delta_{\text{midspan}} = \underbrace{\frac{23PL^3}{1296D}}_{\text{Bending}} + \underbrace{\frac{PL}{6AG}}_{\text{Shear}} \quad (12)$$

Where:

P = Applied load, lb (N).

L = Span length, in (mm).

D = Bending stiffness, lb.in² (N.m²).

Regarding the facing bending stress at the constant moment region of $\frac{PL}{6}$, from Equation 7 can be derived the following expression:

$$\sigma^{\text{facing}} = \frac{ME_f}{D} \frac{h}{2} = \frac{PLh}{6btd^2} \quad (13)$$

3.2. STATIC FLEXURAL TEST

3.2.1. Test Set Up. This test was performed according to ASTM C393 “Standard Test Method for Flexural Properties of Sandwich Constructions” (2000). The objective was to determine in the sandwich construction: the flexural stiffness, core shear strength and core shear modulus, and the facings strength. The calculations to obtain the mechanical properties of the sandwich panel, as well as the comparison of the results are presented herein. Additionally, it will also be discussed the degree of sensitivity reached during the experiments that considerably affected the determination of the aforementioned properties, will be discussed.

The evaluated specimens can be described as a rectangular cross section, with a depth equal to the thickness of the sandwich panel: 3.5 in (89 mm); a width of 8 in (203.2 mm) and a length of 58 in (1.47 m). Due to the anisotropy of the material, two types of specimens were considered for testing: transversally-cut (y-direction) and longitudinally-cut (x-direction). In Figure 3.2 it is shown the layout of the core of the sandwich panel according to Stoll et al. (2001).

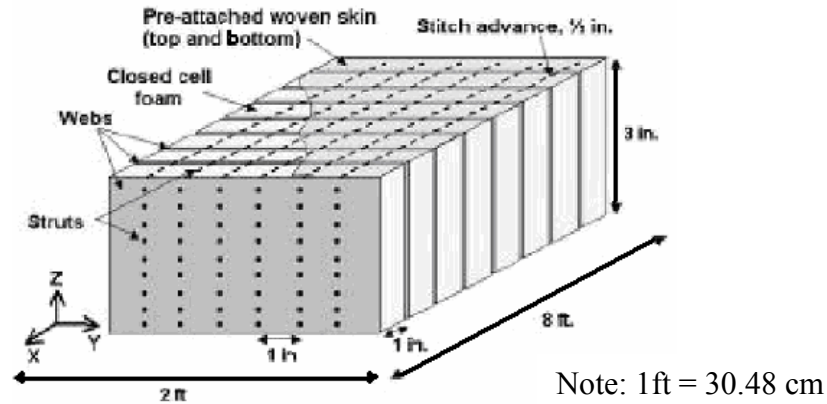


Figure 3.2 FRF Core Schematic

The flexural test was conducted under four point bending configuration. The sandwich beam specimens were tested over a clear span of 54 in (1.4 m) with equal loads applied at 18 in (0.46 m) from each support, leaving a constant moment region in the middle of also 18 in (0.46 m) long (see Figure 3.3).

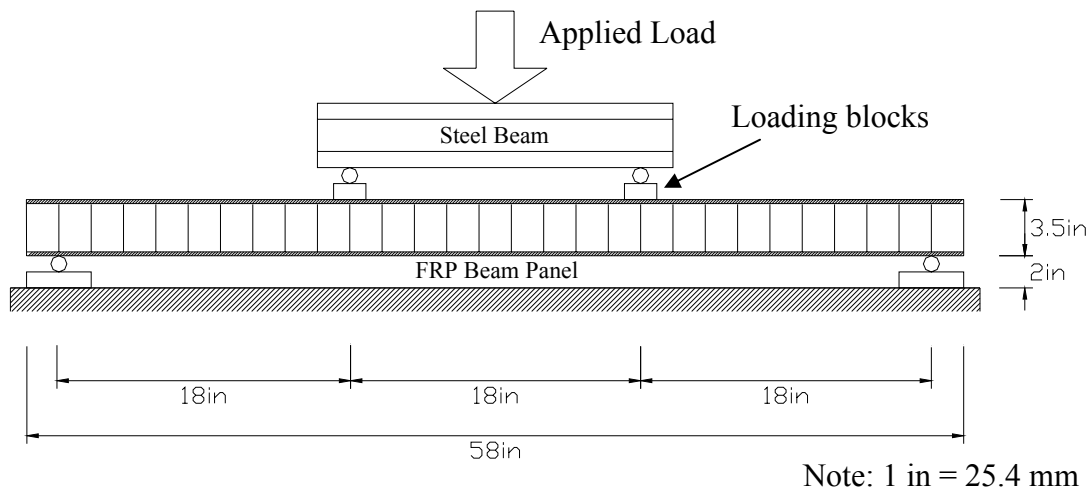


Figure 3.3 Static Flexural Test Setup Schematic

A variation in the manner of application of the load (Test 1 and Test 2) was considered to investigate the influence of localized loads, and how they affect the mode of failure.

3.2.1.1 Test 1. It was conducted in an Instron machine and a total of ten specimens, five of each type (longitudinally-cut and transversally-cut), were tested. Every sandwich beam was set up according to the four point bending configuration. The load was applied through the crosshead of the machine at a rate of 0.3 in/min (7.62 mm/min), which showed to be suitable to attain failure in 5 to 6 minutes. Two 1 in (25.4 mm) diameter steel rods were used to transfer the load to the sandwich beam, and in between them and the top facing of the beam, no spreader material was placed (see Figure 3.4).



Figure 3.4 Flexural Test Setup - Static Test 1

No instrumentation was attached to the beams. The data later utilized was provided by the machine itself: applied load (lb) and stroke (loading block displacement). The latter corresponds to the vertical deflection of the beam at the loading points.

The absence of spreader material at the supports and at the loading points, as well as the measuring instrumentation given by the testing machine, made the difference with respect to the performance of Test 2.

3.2.1.2 Test 2. A MTS880 Universal Testing Machine was utilized in this experiment. Two sandwich beams per each type according to the direction of the panel (longitudinally-cut and transversally-cut) were evaluated. The four point bending configuration was used. In this occasion, the load spreading was accomplished through the use of 1 in (25.4 mm) steel rods welded to steel plates of 8 in (203 mm) long and 2 in (50.8 mm) wide and cement putty (spreader material). In between the supports and the bottom facing of the sandwich beam was placed high resistance rubber pads (see Figure 3.5).

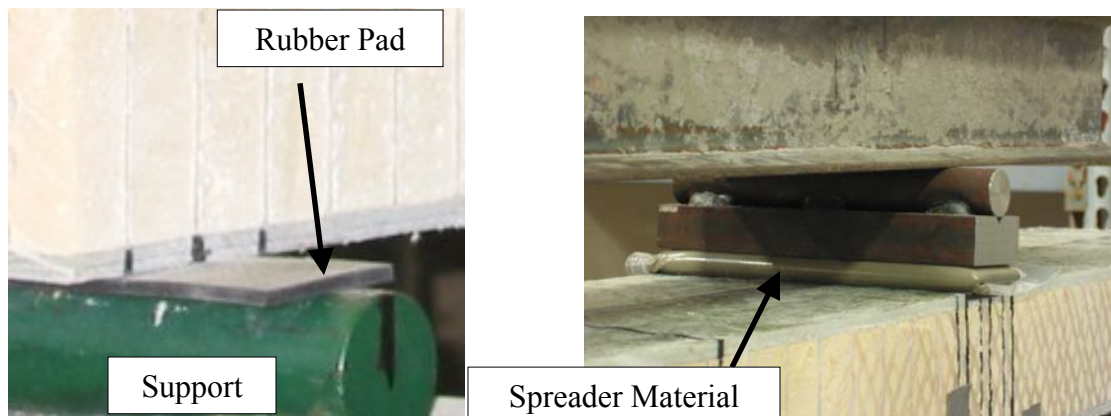


Figure 3.5 Load Spreading - Static Test 2

The instrumentation utilized in this test consisted of two Linear Variable Differential Transformers (LVDT) transducers placed at each support point of the beam (top faces), five string transducers, two of them located at midspan in both sides of the beam, and the rest at the loading points (see Figure 3.6).

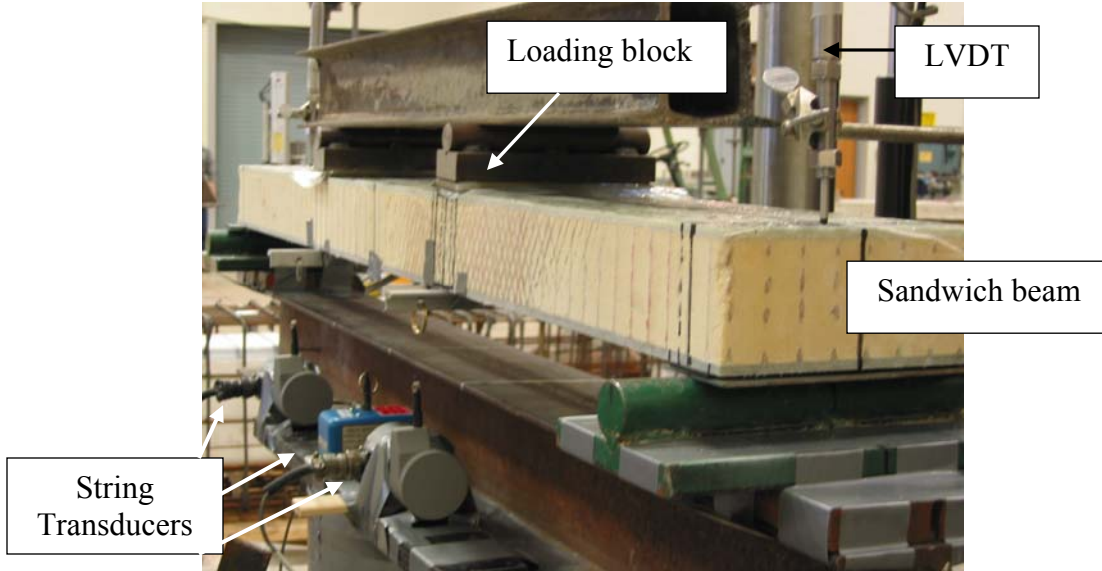


Figure 3.6 Flexural Test Setup - Static Test 2

The bending stiffness of the sandwich beams was computed in three ways, which were the inclusion of the deformation linked to shear effects, or either the measured deflection at either midspan or at the loading point of the sandwich beam. This was considered in order to investigate the influence of the shear deformation and consequently the shear modulus in the overall deflection of a sandwich beam. In Test 1, it is assumed that the experimental deflection is solely due to flexure and taking into account the data available (load applied and deflection at the loading point), Equation 14 provides the values for bending stiffness D1. From the experiments conducted in Test 2, since data concerning deflections not only at the loading point, but also at midspan of the beam are available, three bending rigidities were computed, D1, D2 and D3. For the computation of the bending stiffness D2, contribution of the flexure and shear in the total measured deflection were considered (Equation 16). The computation of D3 is similar to D1, with the difference that the measured deflection data is at midspan (Equation 15).

$$\Delta_{\text{loading pt}} = \frac{5PL^3}{324D1} \Rightarrow D1 = \frac{5PL^3}{324\Delta_{\text{loading pt}}} \quad (14)$$

$$\Delta_{\text{midspan}} = \frac{23PL^3}{1296D3} \Rightarrow D3 = \frac{23PL^3}{1296\Delta_{\text{midspan}}} \quad (15)$$

$$\left. \begin{aligned} \Delta_{\text{midspan}} &= \frac{23PL^3}{1296D2} + \frac{PL}{169G} \\ \Delta_{\text{loading pt}} &= \frac{5PL^3}{324D2} + \frac{PL}{169G} \end{aligned} \right\} D2 = \frac{\frac{23PL^3}{1296} - \frac{5PL^3}{324}}{\Delta_{\text{midspan}} - \Delta_{\text{loading pt}}} \quad (16)$$

$$G = \frac{PL}{169 \left(\Delta_{\text{midspan}} - \frac{23PL^3}{1296D2} \right)} \quad (17)$$

3.2.2. Experimental Results. The experimental mechanical properties for the longitudinally-cut and transversally – cut beams in test 1 and test 2 are presented herein.

3.2.2.1 Test 1. The results obtained for both type of specimens as well as their corresponding average value, standard deviation and coefficient of variation values are presented in Table 3.1 and Table 3.2. Among the longitudinally-cut beams, the specimen L1 is not considered according to Chauvenet’s criterion (Taylor, 1982), by which the data of ultimate load provided by the aforementioned beam is more than two standard deviations away from the average value of ultimate load.

Table 3.1 Mechanical Properties (Longitudinally-cut; Static Test 1)

Specimen	P_U (kip)	σ_U^{facing} (ksi)	$D1$ (kips.in)	τ_U (ksi)	Mode of failure
L1*	25.68	38.29	3888	0.49	Indentation of top facing Compression
L2	19.35	28.85	3842	0.37	Indentation of top facing Compression
L3	17.79	26.53	3802	0.34	Delamination
L4	18.00	26.84	3841	0.35	Delamination
L5	17.83	26.59	3712	0.34	Indentation of top facing Compression
Mean	18.24	27.20	3800	0.35	
Standard Deviation	0.74	1.11	61	0.01	
Coefficient of Variation	4.08%	4.08%	1.61%	4.07%	

*Beam not considered in the computations.

Note: 1 in = 25.4 mm, 1 kip = 4.4497 kN, 1 ksi = 6.89 MPa, 1 kip.in = 113 N.m

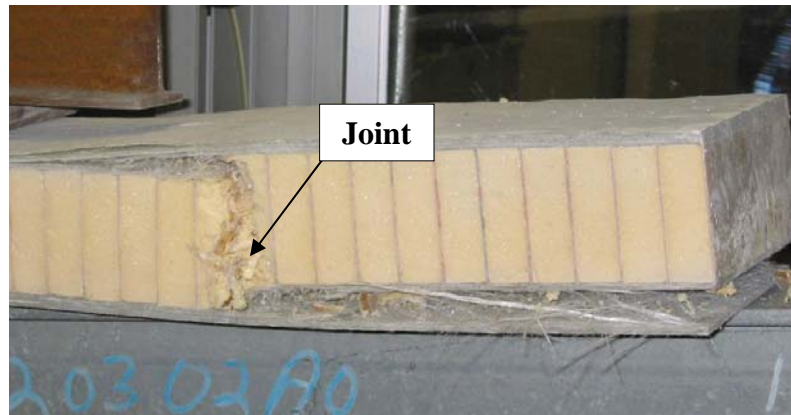
Table 3.2 Mechanical Properties (Transversally-cut; Static Test 1)

Specimen	P_U (kips)	σ_U^{facing} (ksi)	Dl (kips.in)	τ_U (ksi)	Mode of failure
T1	13.71	20.44	3431	0.26	Delamination
T2	13.89	20.70	3467	0.27	Delamination
T3	13.02	19.41	3447	0.25	Wrinkling
T4	14.47	21.58	3570	0.28	Delamination
T5	13.27	19.79	3325	0.26	Wrinkling
Mean	13.67	20.38	3448	0.26	
Standard Deviation	0.56	0.84	88	0.01	
Coefficient of Variation	4.13%	4.13%	2.54%	4.15%	

Note: 1 kip = 4.4497 kN, 1 ksi = 6.89 MPa, 1 kip.in = 113 N.m

The last column in Table 3.1 indicates the mode of failure for each of the longitudinally-cut beams. The beams whose failure was due to compressive forces and indentation of the top facings (L1, L2 and L5) presented crushing at the loading points. Delamination starting in a transversal joint present on one side of the specimen was the observed type of failure in the remaining two beams (L3 and L4) (see Figure 3.7).

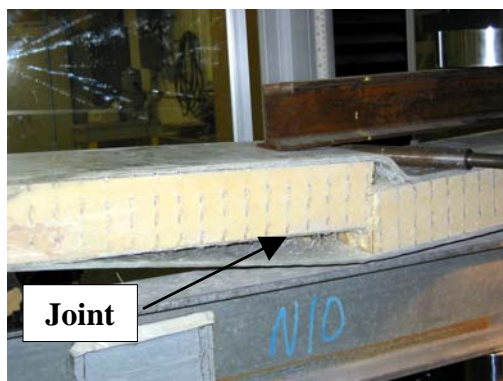
**(a) Indentation and Compression****(b) Indentation**



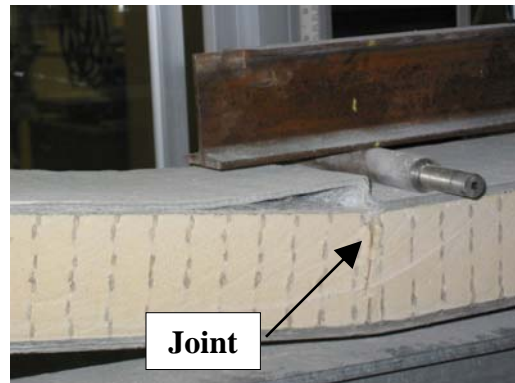
(c) Delamination

Figure 3.7 Modes of Failure (Longitudinally-cut; Static Test 1)

Regarding the mode of failure of the transversally-cut specimens, three beams (T1, T2 and T4) collapsed due to delamination of the top and bottom facings, and only two specimens (T3 and T5) presented wrinkling of the top face near the loading point (see Figure 3.8).



(a) Delamination



(b) Wrinkling

Figure 3.8 Modes of Failure (Transversally-cut; Static Test 1)

Figures illustrating the Load versus Loading Point Deflection as well as Load versus Bending Stiffness for each beam from test 1 are presented in Appendix D. A representative Load versus Loading Point Deflection graph of two beams L3 and T2, is presented in the following figure:

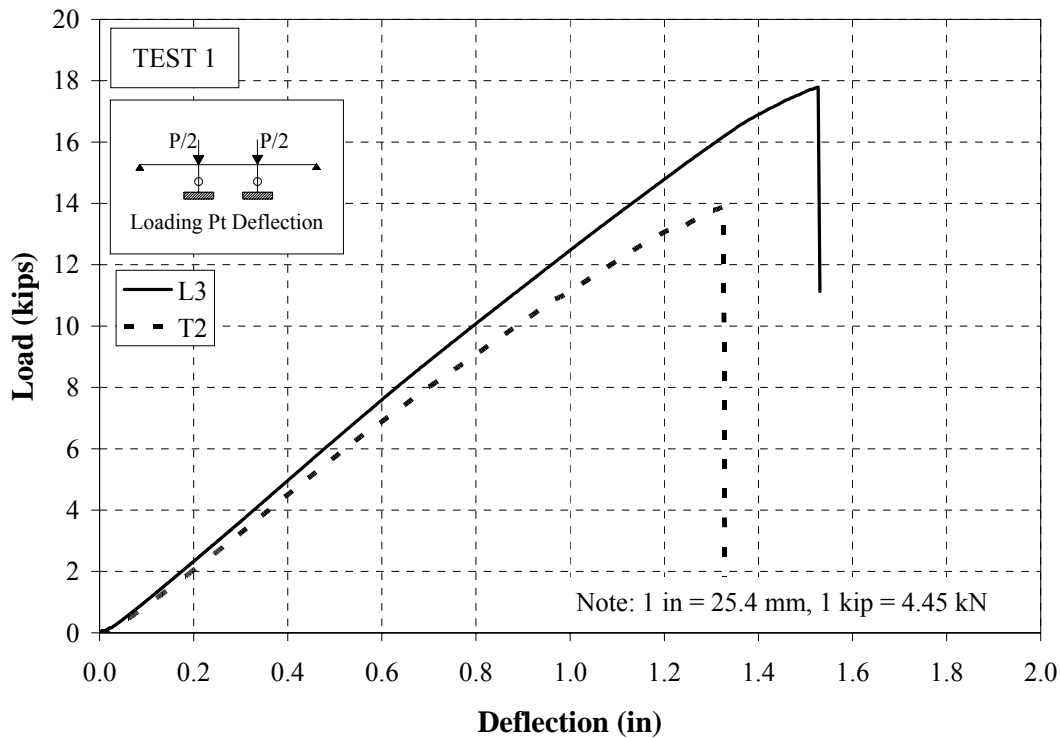


Figure 3.9 Representative Load vs. Loading Point Deflection Curves – Static Test 1

3.2.2.2 Test 2. The results that are obtained for bending stiffness D_1 , D_2 and D_3 as well as the ultimate load, facing bending stresses, and core shear strengths for both types of beams (longitudinally-cut and transversally-cut) are presented in Table 3.3 and Table 3.4. The values of core shear modulus G for each beam are not reported in the corresponding tables since the sensitivity of the test setup, instrumentation, and the equipment did not allow the assessment of values that could be useful for technical purposes. The values of bending stiffness D_2 for specimen T6 will not be considered for technical purposes for the same reason, even though they are reported. The Load versus Deflection (midspan and at loading point) curves, and the Load versus Bending Stiffness (D_1 , D_2 and D_3) for all the beams statically tested are presented in Appendix D.

Table 3.3 Mechanical Properties (Longitudinally-cut; Static Test 2)

Specimen	P_U (kips)	$D1$ (kips.in)	$D2$ (kips.in)	$D3$ (kips.in)	σ_U^{facing} (ksi)	τ_U (ksi)
L6	14.54	3874	3685	3848	21.68	0.28
L7	17.13	3872	3920	4335	28.63	0.33
Mean	15.83	3873	3802	4092	25.15	0.30
Standard Deviation	1.83	1.41	166	345	4.91	0.03
Coefficient of Variation	11.58%	0.04%	4.37%	8.42%	19.53%	11.48%

1 kip = 4.4497 kN, 1 ksi = 6.89 MPa, 1 kip.in = 113 N.m

Table 3.4 Mechanical Properties (Transversally-cut; Static Test 2)

Specimen	P_U (kips)	$D1$ (kips.in)	$D2$ (kips.in)	$D3$ (kips.in)	σ_U^{facing} (ksi)	τ_U (ksi)
T6	13.66	4144	6219	4322	20.37	0.26
T7	13.80	3976	4194	4003	20.57	0.27
Mean	13.73	4060	5207	4162	34066	0.26
Standard Deviation	0.10	119	1431	226	722	0.00
Coefficient of Variation	0.71%	2.93%	27.49%	5.42%	2.12%	0.54%

1 kip = 4.4497 kN, 1 ksi = 6.89 MPa, 1 kip.in = 113 N.m

Concerning the failure mode observed in this second test, both specimens cut out in the longitudinal direction of the panel, failed due to compression. The wrinkling phenomenon occurred at a joint present almost at midspan in the beams. No delamination was observed in these specimens (see Figure 3.10).

**Figure 3.10 Mode of Failure (Longitudinally-cut; Static Test 2)**

The two tested transversally-cut beams experienced delamination of the facings, which also started at the joints. The mode of failure caused by compressive stresses known as wrinkling occurred in beam T6, followed by delamination of the top facing. A joint present at midspan of specimen T7 had considerable influence in its collapse; the delamination started at this weak point (see Figure 3.11).

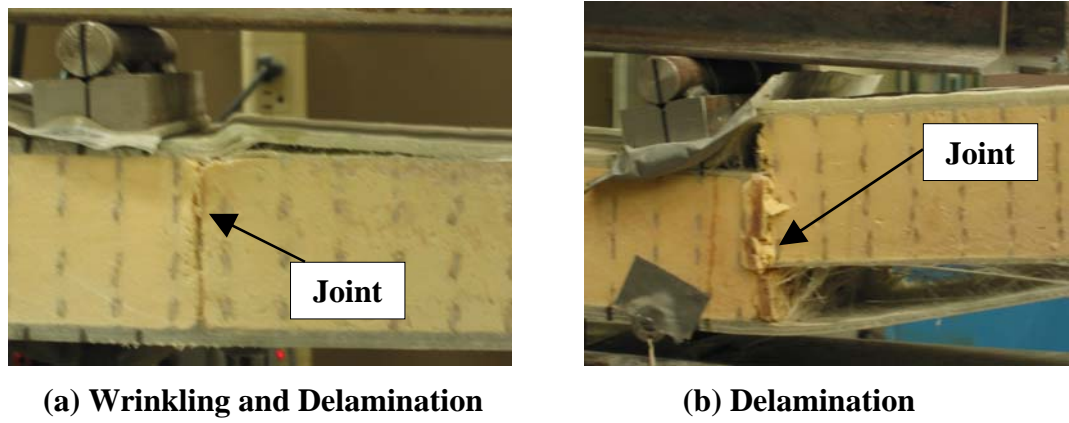


Figure 3.11 Modes of Failure (Transversally-cut; Static Test 2)

A representative Load versus Midspan Deflection graph from beams L6 and T7 is presented in the following figure:

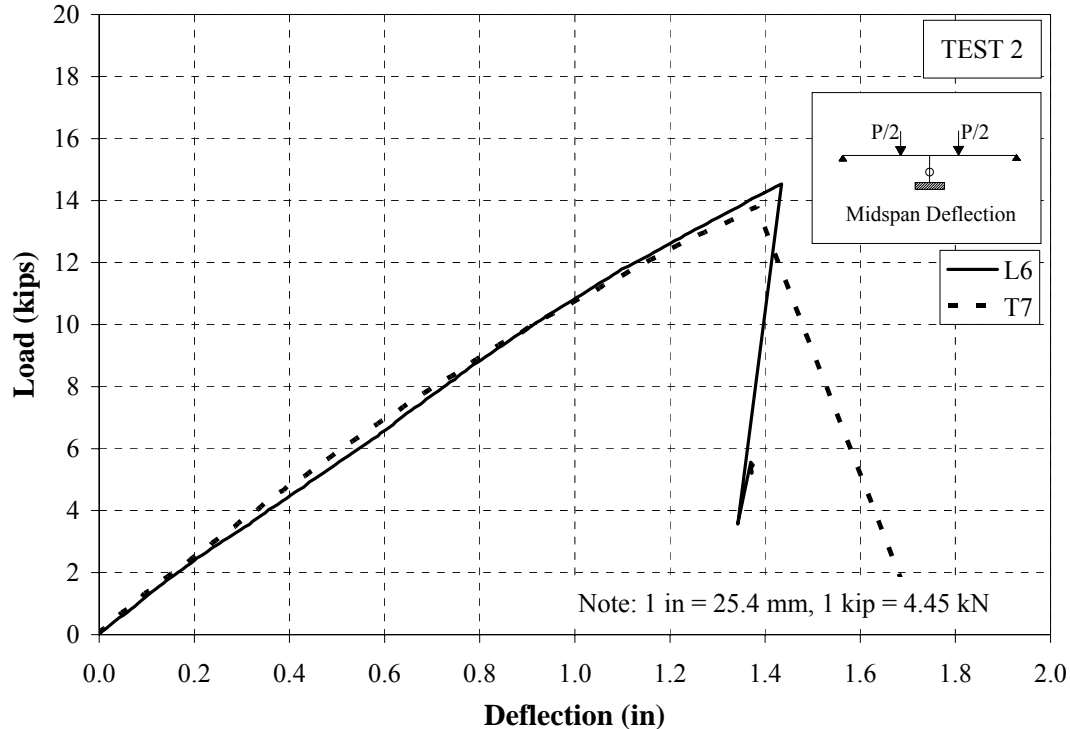


Figure 3.12 Representative Load vs. Midspan Deflection - Static Test 2

3.3. FATIGUE FLEXURAL TEST

The analysis of the performance of GFRP sandwich beams cut out of the panel in two different directions (longitudinally-cut and transversally-cut) under continuous loading and to a certain number of cycles, was the primary purpose of this experiment. The specimens were fatigue conditioned to 500,000; 1,000,000; 1,500,000 and 2,000,000 cycles at a single load level of 20 percent of the ultimate compressive capacity (P_U) corresponding to each type of beam. A minimum level of applied load equivalent to 5 percent of P_U , was considered suitable to preserve the stability of the specimen and equipment during the conditioning. The following table indicates the values of load at which both types of specimens were subjected to.

Table 3.5 Fatigue Conditioning Load Values

	Longitudinally – cut Specimens $P_U = 17$ kips	Transversally – cut Specimens $P_U = 14$ kips
Minimum (5%)	0.85 kips	0.70 kips
Maximum (20%)	3.40 kips	2.80 kips

Note: 1 kip = 4.4497 kN

3.3.1. Test Setup. Same sized beam specimens were utilized in this experiment. The test was conducted in a MTS880 Universal Testing Machine, capable of applying a determinate load range and it also permits the monitoring of the variation of the load during conditioning. Regarding the duration of the experiment, it was defined by an imposed frequency of 3 Hz, and for each half a million of cycles the test lasted approximately 2 days.

A total of eight beams were fatigue conditioned, four specimens per type (longitudinally-cut and four transversally-cut), one specimen per each aforementioned number of cycles (500,000; 1,000,000; 1,500,000 and 2,000,000).

For the test itself, same loading configuration as for the static flexural test was kept (four point bending). It was also considered the possible displacement of either the beam specimen or the loading blocks; therefore, a steel frame was built and mounted in the MTS880. It consisted in two components, the spreader beams and the beam base. The loading was performed through a steel piece grabbed from the top by the MTS superior grip, and it was composed of two steel I – beams S4 x 9.5 of a length of 20 in (508 mm) laterally welded and properly placed on the steel loading blocks resting on the sandwich beam at 18 in (457.2 mm) from each support. With respect to the beam base, it consisted of a steel I-beam W6 x 20 fixed to the bottom plate of the MTS880, two supports spaced 54 in (1.37 m) were welded to it and also four steel angles were vertically joined to each corner of the steel beam in order to prevent longitudinal or transversal displacement of the beam specimen. The schematic of the test setup is presented in Figure 3.13. Figure 3.14 illustrates the actual setup of the test. Regarding the load spreading, it was accomplished through high resistance rubber pads of 8 in (203.2 mm) x 2 in (50.8 mm) attached to the bottom of each steel loading block. Each of these latter was made out of one bar of 8 in (203.2 mm) long and 1 in (25.4 mm) diameter welded to a rectangular piece of 8 in (203.2 mm) long, 2 in (50.8 mm) wide and 1 in (25.4 mm) thick. A rubber pad was also placed in the interface of the beam specimen and each of the supports (see Figure 3.15).

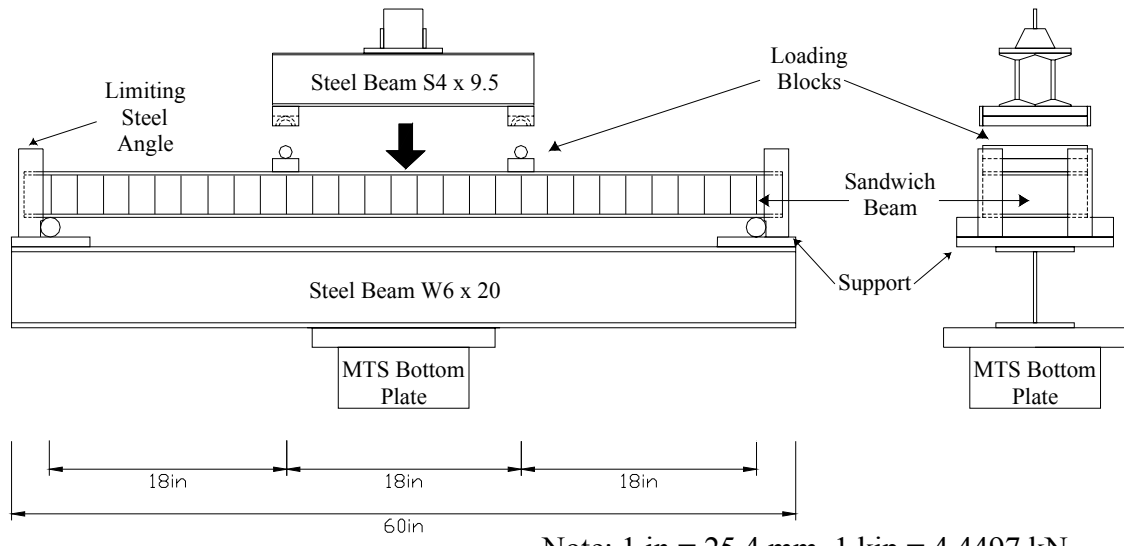


Figure 3.13 Fatigue Flexural Test Setup Schematic



Figure 3.14 Fatigue Flexural Test Setup

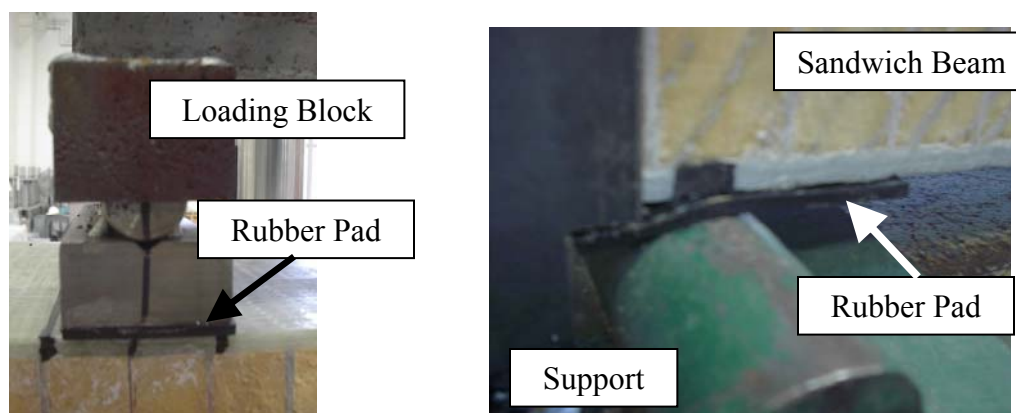


Figure 3.15 Load Spreading Details

After reaching the preset numbers of cycles, each sandwich beam was statically tested to failure. The load was applied in displacement control at a rate of 0.25 in/min (6.35 in/min), which permitted to attain a time of failure in between five to six minutes. The instrumentation consisted in four Linear Variable Differential Transformers (LVDT) transducers, they were located at midspan, at the loading point, at the support of the sandwich beam (top face) and a fourth LVDT was attached to the steel beam to also measure its deformation. The data acquired was composed of the applied load and the vertical displacements at the location of the previously mentioned LVDTs.

3.3.2. Experimental Results. Contrary to the compressive experiment, where for certain levels of load there was failure of specimens during the cycling, no collapse of the sample beams occurred during this flexural fatigue conditioning. The computations of the bending stiffness D1, D2 and D3 were carried out utilizing Equations 14, 16 and 15, respectively, as it was previously mentioned. Each of the values presented herein for these rigidities for each specimen corresponds to the average value in a load interval from 5 kips (22.25 kN) to 10 kips (44.5 kN). Expression 10 was applied to obtain the core shear stress τ_U , and the one corresponding to Equation 13, for the facing bending stress σ_U . The results corresponding to the longitudinally-cut beams and transversally-cut beams are presented in Table 3.6 and Table 3.7, in that order:

Table 3.6 Residual Mechanical Properties (Longitudinally-cut; Flexure)

Number of cycles (millions)	Specimen	P_U (kips)	D1 (kip.in)	D2 (kip.in)	D3 (kip.in)	σ_U^{facing} (ksi)	τ_U (ksi)
0.5	1L	15.63	4912	5214	4948	23.31	0.30
1.0	2L	15.83	4459	5548	4575	23.61	0.31
2.0	4L	20.64	4950	3831	4765	30.77	0.40

1 kip = 4.4497 kN, 1 ksi = 6.89 MPa, 1 kip.in = 113 N.m

Due to a problem with the data acquisition system, the data concerning the longitudinally-cut specimen subjected to 1.5 million of cycles was lost, and therefore is not

shown in the table above. The values of D1 and D3 of 1L, 2L and 4L, vary among each other in a maximum of 3.89 percent. Rigidity D2 shows a higher variation of almost 22.83 percent with respect to the corresponding average value of D1 and D3. The greater ultimate load, and the ultimate stresses are directly related to the facing stress and shear strength, they correspond to specimen 4L.

Table 3.7 Residual Mechanical Properties (Transversally-cut; Flexure)

Number of cycles (millions)	Specimen	P_U (kips)	D1 (kip.in)	D2 (kip.in)	D3 (kip.in)	σ_U^{facing} (ksi)	τ_U (ksi)
0.5	1T	14.86	4292	4300	4292	22.16	0.29
1.0	2T	19.47	4731	5300	4797	29.03	0.37
1.5	3T	17.07	5165	5315	5184	25.45	0.33
2.0	4T	15.09	4651	7766	4907	22.50	0.29

1 kip = 4.4497 kN, 1 ksi = 6.89 MPa, 1 kip.in = 113 N.m

The values of D1 and D3 differ among themselves for each specimen in a maximum of 5.5 percent. It is worth to mention that just for the case of 1T, the variation of D2 with respect to D1 and D3 is very small (0.01 percent). The highest ultimate load which corresponds to specimen 2T is of 19.47 kips.

Load versus midspan deflection for each type of fatigue conditioned specimens are combined in the following figure. Individual load versus deflection curves (at midspan and at the loading points), as well as bending stiffness (D1, D2 and D3) versus load curves for each fatigue conditioned beam are presented in Appendix D.

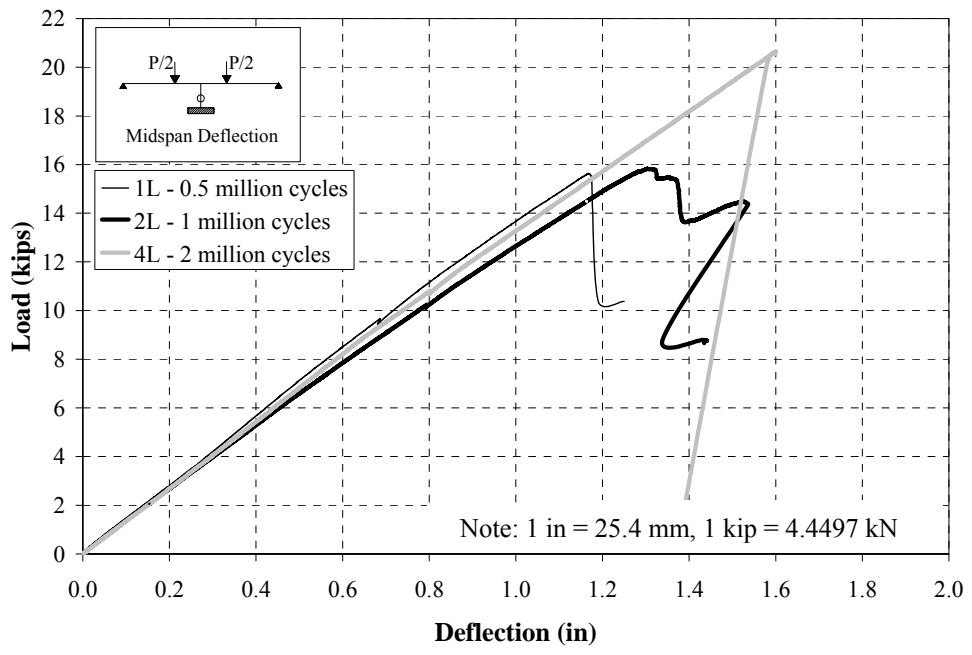


Figure 3.16 Load vs. Midspan Deflection (Longitudinally-cut; Fatigue Flexural Test)

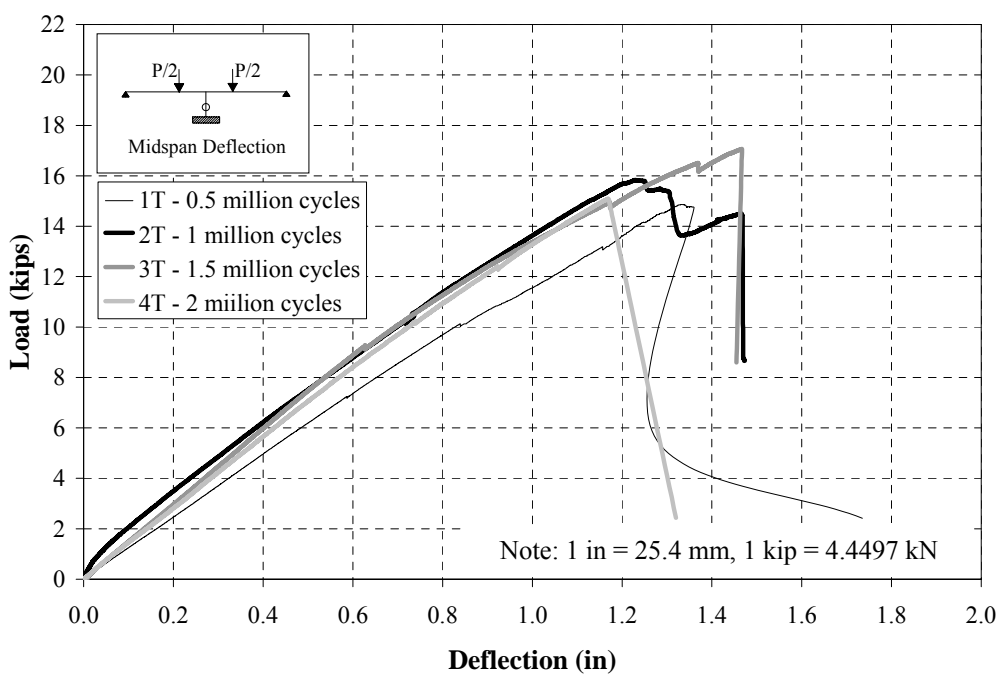


Figure 3.17 Load vs. Midspan Deflection (Transversally-cut; Fatigue Flexural Test)

With regards to the mode of failure, the shear failure in specimens 1L and 2L generated gaps in the interface facing and foam, only sample 4L showed wrinkling of the top face next to one of the loading points. It is worth to note that none of these three beams presented joints in

the core resulting from the manufacturing process. Illustrations for the modes of collapse are shown in Figure 3.18.



(a) Shear Failure



(b) Delamination and Shear Failure



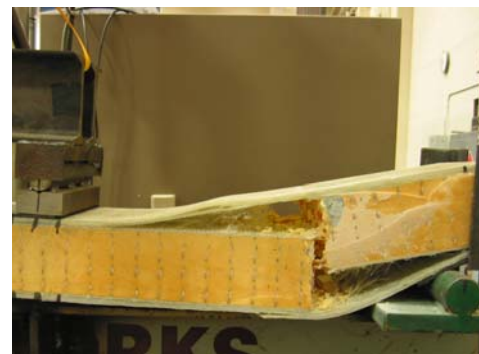
(c) Wrinkling

Figure 3.18 Modes of Failure (Longitudinally-cut; Fatigue Flexural Test)

The modes of failure of the transversally-cut specimens, after the fatigue conditioning and consequently testing to failure, are presented in the illustrated Figure 3.19. The failure of the beam subjected to half a million cycles (1T) was occasioned by delamination mainly in the top face. With respect to the rest of the beams (2T, 3T and 4T), the delamination of their corresponding top and bottom facings were affected by the presence of the transversal joint (starting point of delamination).



(a) Wrinkling and Delamination



(b) Delamination and Shear Failure

Figure 3.19 Modes of Failure (Transversally-cut; Fatigue Flexural Test)

Figure 3.20 presents the residual ultimate load of both types of specimens. Figure 3.21 and Figure 3.22 show the residual bending stiffness (D1 and D3) for the longitudinally-cut and the transversally-cut specimens, respectively. The flexural rigidity D2 is not presented in the plots due to its great variability with respect to the values of D1 and D3. The plots corresponding to the residual facing stress and residual shear strength for both types of specimens are presented in Appendix D. The residual rigidities are presented in percentages with respect to the base values from the control specimen average (static test) versus the number of cycles. In Figure 3.21 and Figure 3.22, the increment of the residual bending stiffness, especially for the beam specimens, fatigue conditioned the most, this phenomenon in this particular composite material could be symbolically explained as a simple chain composed by links. Once the links are straighten up the composite material allows appropriate load transfer and interconnection. When the sandwich beam is fatigue cycled, the various polymer micro-links composing of the material will align or reorder themselves inducing minor effects in the performance and mechanical properties.

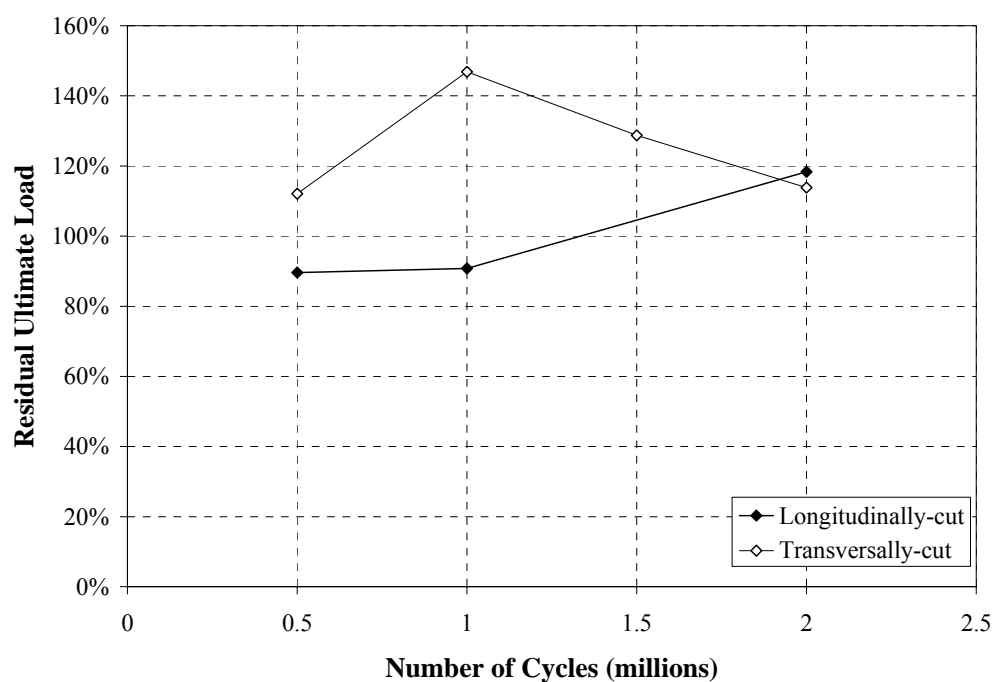


Figure 3.20 Residual Ultimate Load - Flexure

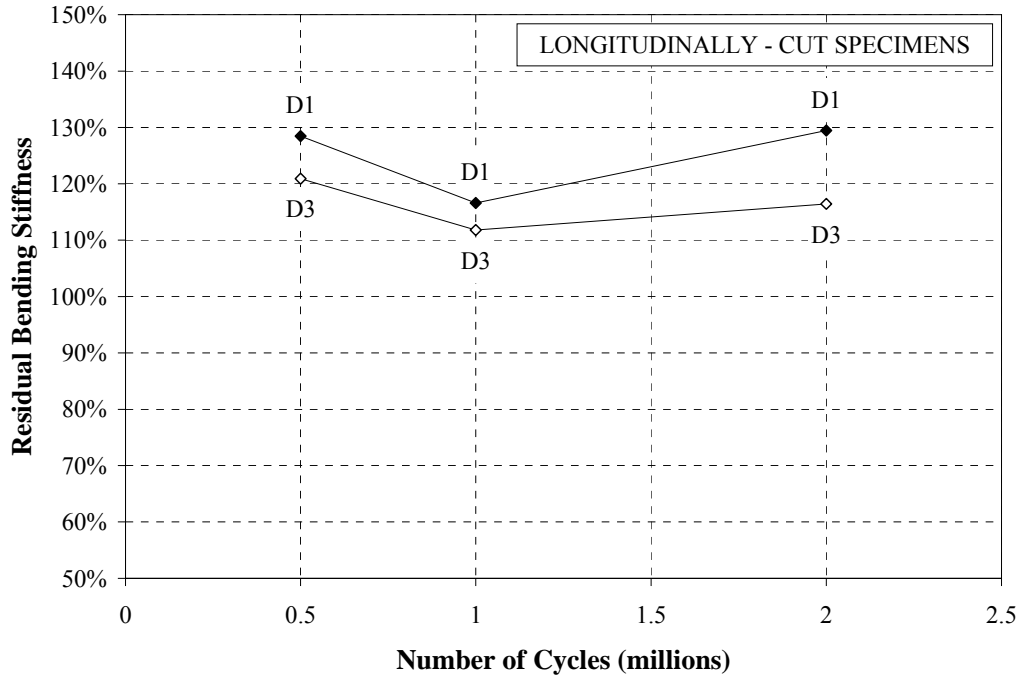


Figure 3.21 Residual Bending Stiffness (Longitudinally-cut; Flexure)

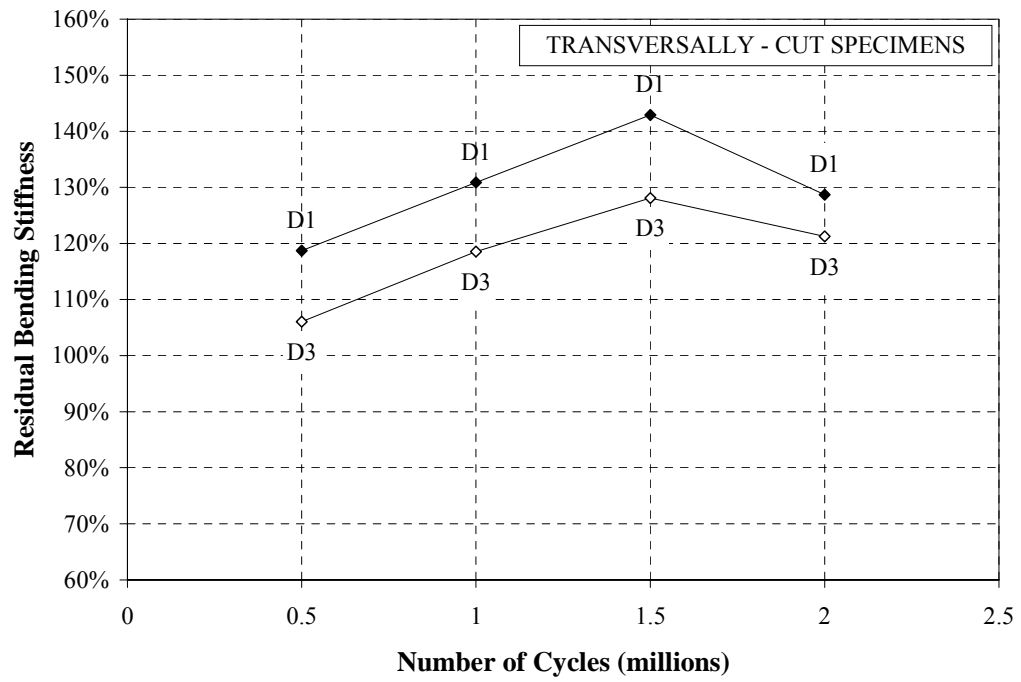


Figure 3.22 Residual Bending Stiffness (Transversally-cut; Flexure)

4. DISCUSSION OF RESULTS

4.1. COMPRESSIVE TESTS

Based on the results of the compressive tests conducted on cubic specimens from two different panels (A and B), it is concluded that the quality of the manufacturing process affected the results of the virgin and the fatigue conditioned samples.

The residual compressive strength after two million cycles was found to be 869 psi (6 MPa) for the lower quality panel (B). Considering a wheel load of 15 kips (67 kN) for a HS25-44 truck and including an impact factor of 1.3, the peak wheel load is 19.5 kips (87 kN). With a double wheel footprint having dimensions of 10 in (25.4 cm) in the traffic direction and 20 in (50.8 cm) in the cross-traffic direction for a total area of 200 in² (1290 cm²), it is found that the peak surface pressure is approximately 100 psi (6.9 kPa). Comparing this value to the residual compressive strength, a safety factor equal to 8 is found.

4.2. FLEXURAL TESTS

When deploying the panel system, different boundary conditions can be found depending upon the site where it is executed. In general, from the structural point of view, two cases can be considered:

- a) Panel laid over an opening
- b) Panel fully supported

These possible situations lead to the flexural experiments conducted on the beam samples under static and cyclic loading. The first case could result from cavities originated between the sub-grade and the panel system due to drainage, or if the matting is laid over an opening like a culvert.

Table 5.1 summarizes the average values of elastic modulus and flexural stiffness of the sandwich construction. Even though the internal reinforcement in the core of the panel (webs in the transversal direction and a lattice of stitches in the longitudinal direction) contributes to the bending stiffness and consequently in the determination of the elastic modulus, a conservative approach takes the facings of the sandwich panel as the sole carriers of bending stress. If for design reasons, the need of approximating the cross section of the sandwich beam to the cross section of an I-beam rises, an elastic modulus E of 3.61 msi (24.87 GPa) could be assumed.

The bending stiffnesses designated as $D1$ and $D3$, to represent two values of the flexural rigidity computed with the applied load and measured deflections of the experiments, are expressed as follows (Equation 14 and Equation 15):

$$D1 = \frac{5PL^3}{324\Delta_{\text{loading point}}}$$

$$D3 = \frac{23PL^3}{1296\Delta_{\text{midspan}}}$$

With regards to the results presented in Table 5.1, average values of $D1$ and $D3$ for fatigue conditioned beams are: 4768 kip.in (538.8 kN.m) and 4823 kip.in (545 kN.m), for the longitudinally-cut and transversally-cut specimens, respectively. Since both values are sufficiently close, for technical purposes a bending stiffness of 4796 kip.in (542 kN.m) can be assumed as representative of this material.

Table 4.1 Bending Stiffness and Elastic Modulus - Flexure

Specimen			D1 (kip.in)	E1 (msi)	D3 (kip.in)	E3 (msi)
Longitudinally-cut	Control	Average	3824	2.90	4092	3.10
		Standard Deviation	61	0.05	345	0.26
		Coef. of Variation	1.59%	1.59%	8.42%	8.42%
	Fatigue Conditioned	Average	4773	3.62	4762	3.61
		Standard Deviation	273	0.21	186	0.14
		Coef. of Variation	5.72%	5.72%	3.92%	3.92%
Transversally-cut	Control	Average	3587	2.72	4258	3.23
		Standard Deviation	249	0.19	90	0.07
		Coef. of Variation	6.95%	6.95%	2.12%	2.12%
	Fatigue Conditioned	Average	4710	3.57	4936	3.74
		Standard Deviation	359	0.27	469	0.35
		Coef. of Variation	7.62%	7.62%	9.49%	9.49%

Note: 1 msi = 6.89 GPa; 1 kip.in = 113 N.m

4.2.1. Panel over an opening

In order to determine the maximum opening length for which the performance of the sandwich panel is appropriate, not only considering strength but also serviceability (deflections), the following situation is assumed: a panel placed over a culvert, fixed at both ends due to the connection system. The worst-case loading condition for the HS25-44 loading truck, corresponds to one wheel of the rear axle located at midspan. This load is uniformly distributed over a surface area of 10 in (25.4 cm) by 20 in (50.8 cm) as it was noted in Section 5.1. When considering 12 in (30.48 cm) wide panel strip in the direction of the traffic for design purposes, the load over an effective area of 10 in (25.4 cm) by 12 in (30.48 cm) is 12 kip (53.4 kN) (see Figure 5.1). The remaining portion of the load is carried by the adjacent strips. The maximum vertical deflection and maximum bending moment based on simple beam theory are expressed by Equation 18 and Equation 19, respectively.

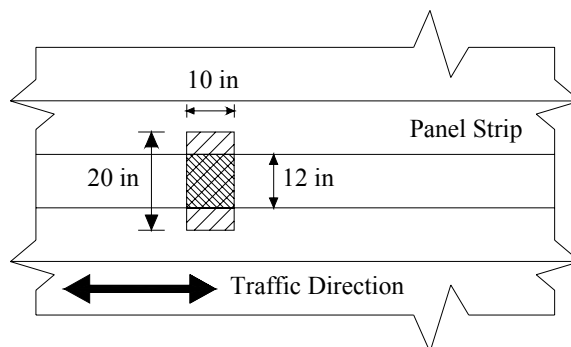


Figure 4.1 Truck Wheel Footprint and Effective Area Schematic - Plane View

$$\Delta_{\max} = \frac{PL^3}{192D} \quad (18)$$

$$M_{\max} = \frac{PL}{8} \quad (19)$$

Where:

P = Effective applied load, 12 kips

L = Span length, in

D = Bending stiffness of the panel, 4796 kip.in

The deflection limit recommended by AASHTO (1996) for concrete slabs of the ratio of the span length over 800 (L/800), is considered appropriate for this application (Stone, 2002). The maximum opening length resulting from Equation 18 is 2.8 ft (85.34 cm), and the corresponding maximum flexural moment (Equation 19) is 4.2 kip.ft (5.7 kN.m). The maximum moment is related to the bending stress according to Equation 7, previously introduced in Section 3.1:

$$\sigma_f = \frac{ME_f h}{D 2}$$

Where the elastic modulus of the panel E_f is 3610 ksi (24.87 GPa) and h is the overall depth of the sandwich panel: 3.5 in (88.9 mm). The resulting maximum bending stress is 5.53 ksi (38.13 MPa), which compared to the guaranteed value (see Table 4.2) of 9.5 ksi (82.34 MPa) obtained from the experimental program, allows to estimate a factor of safety of 1.7.

Table 4.2 Bending Stress Average Values

Specimen		Bending Stress (ksi)
Longitudinally-cut	Average	17.26
	Standard Deviation	2.82
	Coefficient of Variation	16.33%
Transversally-cut	Average	16.52
	Standard Deviation	2.13
	Coefficient of Variation	12.88%

Note: 1 ksi = 6.89 MPa

4.2.2. Fully supported panel

In this section it is aimed to provide recommendations concerning the appropriate length of the panel considering its full support by a substrate with certain bearing capacity. The maximum settlement that the FRP panel can safely withstand is influenced by the condition of the soil (substrate) as well as the length of the panel. In order to analyze this condition, the fully supported panel is idealized as a panel on an elastic foundation or supported by a spring bed (see Figure 5.2). The analysis presented herein is carried out considering a similar loading condition as for the previous case (panel over an opening), as well as sandwich panel strips or beams of 12 in (30.48 cm) for the computations; the only difference is the uniformly distributed load of 1200 lb/in (210.24 kN/m) over a distance of 10 in (25.4 cm) in the direction of the traffic, instead of a concentrated load.

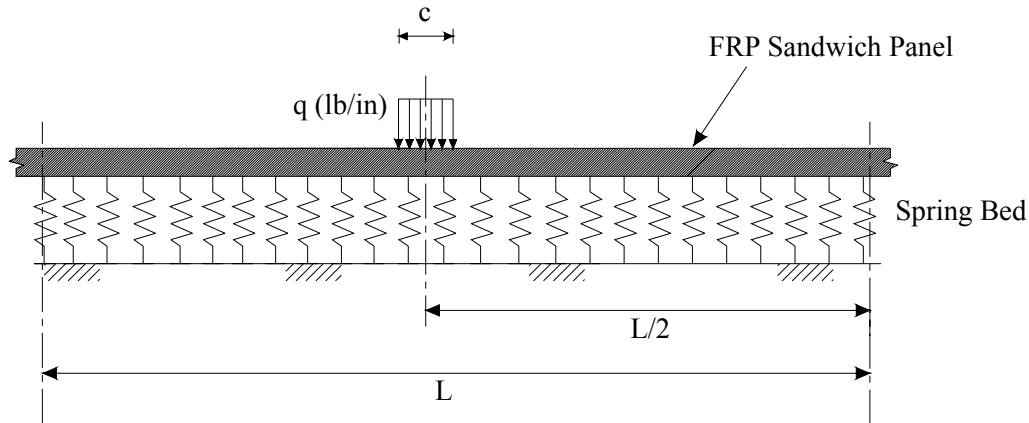


Figure 4.2 Fully Supported Panel Schematic

The following analysis is based on the Theory of Beams on Elastic Foundation (Hetényi, 1967), and it considers the maximum deflection of the sandwich strip and the maximum stress generated by the bending moment as well. Two cases are considered: a beam of finite length and a beam of unlimited length; the vertical deformation for each case individually at midspan (first case) or at a point located at mid-distance c according to Figure 5.2 (second case) is given by the following formulas:

$$(y_0)_{\text{finite length}} = \frac{q}{k} \left[1 - \frac{2 \left(\sinh \left(\lambda \frac{c}{2} \right) \cos(\lambda c) \cosh \left(\frac{\lambda L}{2} \right) + \sin \left(\lambda \frac{c}{2} \right) \cosh(\lambda c) \cos \left(\frac{\lambda L}{2} \right) \right)}{\sinh(\lambda L) + \sin(\lambda L)} \right] \quad (20)$$

$$(y_0)_{\text{unlimited length}} = \frac{q}{2k} \left(2 - e^{-\lambda \frac{c}{2}} \cos \left(\lambda \frac{c}{2} \right) - e^{-\lambda \frac{c}{2}} \cos \left(\lambda \frac{c}{2} \right) \right) \quad (21)$$

Where:

q = Uniform Distributed Load, 1200 lb/in

c = Length over which uniform load is distributed, 10 in

$k = b \times K_0$, lb/in²

b = Width of the panel strip, 12 in

K_0 = Soil Elastic Modulus, lb/in³

D = Bending Stiffness, 4796 kip.in

The parameter λ is given by Equation 22:

$$\lambda = \sqrt[4]{\frac{k}{4D}}, \text{ 1/in} \quad (22)$$

Figure 5.3 shows a family of four curves representing the midspan deflection of different length sandwich beams as a function of the soil modulus K . The sandwich beams show significant similarity among the plots corresponding to the 8 ft (2.44 m), 12 ft (3.66 m) and an infinite length beam. A 4 ft long beam or shorter does not meet the design requirement considered for this application ($L/800$), therefore it is not recommended. On the other side, a sandwich beam of 8 ft long seems to be more appropriate for the intended application.

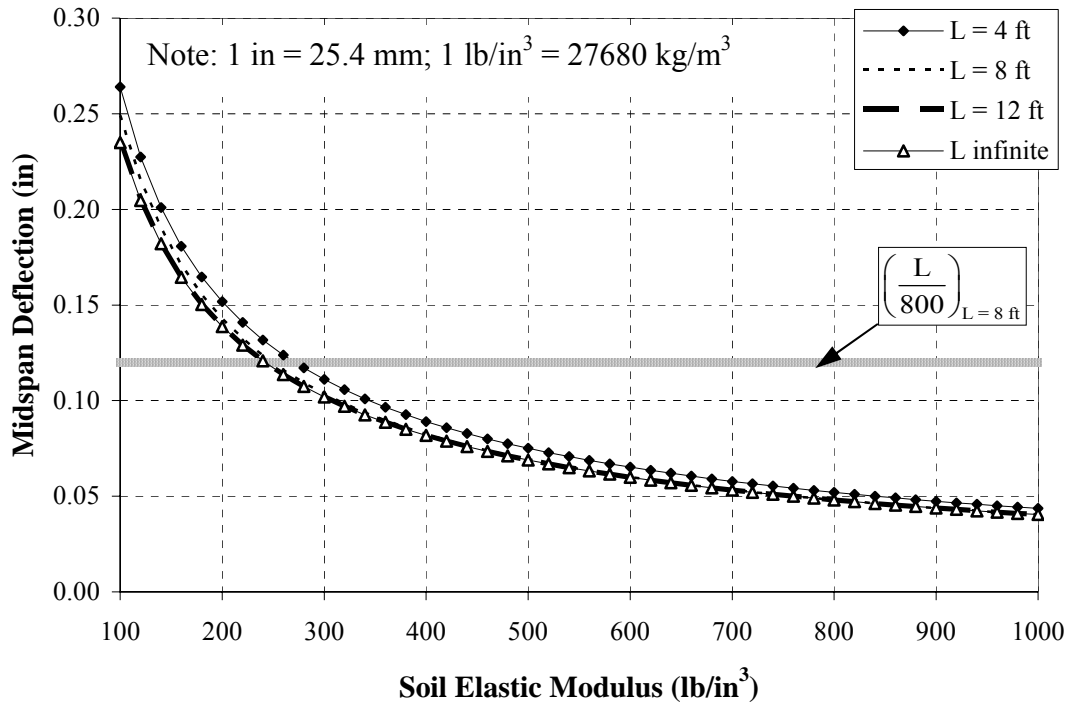


Figure 4.3 Midspan Deflection vs. Soil Elastic Modulus

In addition to the analysis regarding the allowable settlements, it is also important to address the moments generated in the 8 ft (2.44 m) panel strip, and consequently the bending stress. The maximum moment in the panel strip at midspan is expressed by Equation 23 and is shown in Figure 5.4 as a function of the soil elastic modulus. The guaranteed strength value of 9.5 ksi (82.34 MPa) exceeds any of the resulting values of bending stress.

$$(M_0)_{L=8\text{ft}} = \frac{q}{\lambda^2} \frac{\sin\left(\lambda \frac{c}{2}\right) \sinh\left(\lambda \frac{L}{2}\right) \sinh\left(\lambda \frac{c}{2}\right) + \sinh\left(\lambda \frac{c}{2}\right) \sin\left(\lambda \frac{L}{2}\right) \sin\left(\lambda \frac{c}{2}\right)}{\sinh(\lambda L) + \sin(\lambda L)} \quad (23)$$

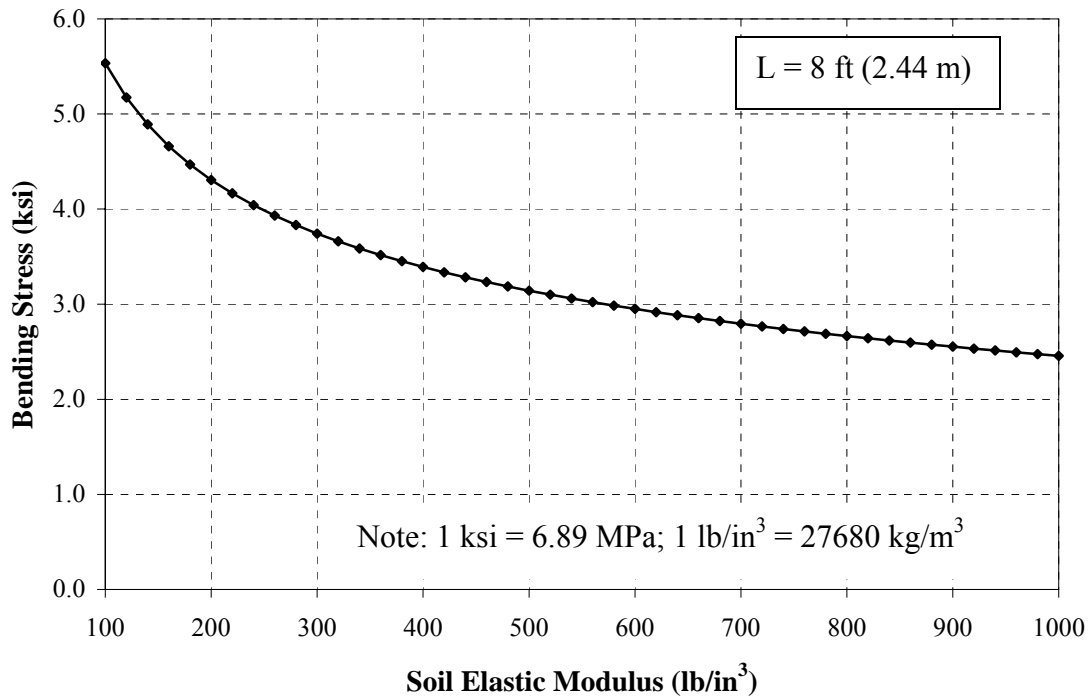


Figure 4.4 Bending Stress vs. Soil Elastic Modulus

Since the soil elastic modulus of the substrate has an important role in the selection of the suitable panel length accounting for both limiting settlements and bending stresses, for further reference, some typical values of the modulus K are listed in Table 5.3 (Das, 1998).

Table 4.3 Soil Elastic Modulus K

Soil Type		(lb/in ³)
Sand (dry or moist)	Loose	29 – 92
	Medium	91 – 460
	Dense	460 – 1380
Sand (Saturated)	Loose	38 – 55
	Medium	128 – 147
	Dense	478 – 552
Clay	Stiff	44 – 92
	Very Stiff	92 – 184
	Hard	> 184

Note: 1 lb/in³ = 275.86 kN/m³

5. CONCLUSIONS

The information gathered as background in addition to the mechanical properties resulting from the performed compressive and flexural experiments on virgin and fatigue conditioned samples, constitute the base for the assessment and validation of the material system for the intended application. Conclusions based on the compressive laboratory testing of cubic GFRP sandwich specimens can be summarized as follows:

- The variation in the mechanical properties of two different panels demonstrated the importance of the quality control of the material, in order to guarantee its homogeneity and performance.
- The residual compressive strength after two million cycles is approximately 869 psi (6 MPa) for the lower quality panel (B), which is considerably higher than the peak surface pressure resulting from a HS25-44 truck wheel of 100 psi (6.9 kPa) over a 200 in² (1290 cm²) area. From the difference of the experimental strength with respect to the demand truck load, a factor of safety equal to 8 is attained.

With regards to the flexural evaluation of two different types of sandwich beams (longitudinal and transversal direction), the following concluding remarks can be drawn:

- The experiments performed according to ASTM C393 have demonstrated their suitability for the determination of flexural mechanical properties, but not for the shear properties, as it is mentioned in the standard.
- The consistency in the values of the bending stiffness D1 and D3, resulting not only from the fatigue test but also from the static experiments, reveals the predominance of the deflection associated with bending. This implies that the input of the deflection linked to the shear in the total deflection can be considered as negligible. For technical purposes, a value of the bending stiffness of 4796 kip-in (542 kN-m) can be assumed.
- The span length of 2.8 ft (85.34 cm) was found as the maximum opening dimension the sandwich panel could be placed over and safely withstand a design load corresponding to a HS25-44 loading truck. The analysis was carried out taking into consideration both the strength criterion and the serviceability (deflection) criterion. The recommended allowable deflection of L/800 was considered suitable for the proposed application.
- For the case of a not connected panel fully-supported by a substrate with certain bearing capacity (elastic foundation), 4 ft (1.22 m) and shorter lengths are not recommended since the midspan deflection is a critical issue, not to mention the implicit demand for a stronger substrate (higher soil elastic modulus). The length of 8 ft (2.44 m) for this situation is considered appropriate, not only for inferring permissible deflections for reasonable soil modulus, but also for satisfying bending strength requirement.
- It is evident that the composition of the material in terms of uniformity, which not only involves the physical characteristics such as the presence of joints or areas of the panel where the facings are thicker, but also individual properties of the constituents

of the sandwich structure, have a direct effect in the overall performance. In other words, it is in the manufacturing process, especially the quality control where great attention should be focused.

6. RECOMMENDATIONS FOR POSSIBLE SITE IMPLEMENTATION

The application of GFRP sandwich panels for temporary reusable bypass roadways to replace traditional construction methods has been recognized as a high-interest option by MODOT.

The development of the GFRP sandwich panels for bypass roadways should be based upon previous experiences, mechanical properties obtained in the laboratory testing, consultation with MODOT personnel, and contribution of industry (for example Webcore Technologies that has been working in a similar field application in the recent past), along with other organizations (for example, the National Composite Center, Kettering, OH). The following requirements are proposed based upon necessities listed in the System Performance Specification for the Rapid Parking Ramp Expansion (Appendix F), issued in March 7, 2003 by the Department of the Air Force for the development of the airfield matting:

a) Performance. The system should be suitable for use as bypass roadways. The properties of the material to be utilized will have direct influence in the performance of the system for the intended use. The system shall be an improvement over the traditional construction, especially in the installation and operating time.

b) Weight. The system should be composed of a light weight material. The threshold for this aspect is to be established depending upon the available equipment for its transportation, deployment and installation. Additionally, the shipping volume must be also considered a variable for which a limit should be suggested.

c) Traffic Loads. The design wheel load, for a low-profile composite bridge deck could be 15 kips (66.75 kN), which corresponds to an AASHTO HS25 truck wheel. The matting should be able to withstand shear stresses resulting from braking and turning of the vehicles.

d) Environmental Performance. The system shall be able to operate in ambient air temperatures from -25°F to 125°F. The matting shall be able to withstand long durations up to 10 years of exposure to sunshine and ultraviolet effects without degradation or failure. Before any weather condition, the system shall provide a non-skid surface and minimize slipping.

Regarding chemicals, the system should not be damaged after exposure or direct contact for an extended period of time with chemicals and liquids, such as: engine oils, fuel, hydraulic fluids, cleaning agents, etc.

e) Substrate Conditions and Preparation. Grading of the substrate, leveling and consolidation of the soil is recommended. A minimum of 4 in (101.6 mm) compacted granular base should be placed on the soil. In absence of a granular base, the panels could be placed on a firmed surface with an appropriate elastic modulus in order to guarantee adequate serviceability (see Section 4.2.2)

f) Personnel. Characteristics beyond grade, aptitude, skill level and physical qualifications of the personnel who operate and maintain the current systems shall not be required.

g) Safety of the System. The system shall not have conditions, materials, or functions that are hazardous for the operation and maintenance personnel. It should be safe to transport, handle, install, disassemble, and store by personnel using the pertinent equipment and tools. Warning devices and safety labels shall be included in the system to help prevent injury during the operation of the system.

h) System Installation. The system installation should be easy and quick to deploy. For this purpose, an appropriate assembly system should be incorporated. The critical components of the bypass roadway are the panel connections and the joints that are formed. Special consideration should be given to them in order to ensure adequate load transfer. In order to avoid lateral displacements resulting from the wheel loads, turning and braking forces, the anchoring system of the panel is also critical. The equipment for installation and maintenance shall be identified as such. An installation rate of at least 300 ft²/man-hour (28 m²/man-hour) is desirable.

i) Maintenance and Repair. The required preventive maintenance checks and services need to be scheduled in order to guarantee the appropriate performance of the system. The repair time should be such that it would not cause a great interruption or disturbance in the traffic flow. The system should be able to permit the replacement of an interior component within minimum necessary period of time. The matting should allow the cleaning of debris such as snow or dirt by plowing and sweeping using conventional equipment, without inducing substantial damage.

j) Panel Replacement. The panels that form the system shall be removable and/or replaceable in the need to substitute a damaged panel or to allow for maintenance of the sub-grade below.

6.1. AIRFIELD MATTING

The proposed recommendations for the airfield matting are based upon the prior similar bypass roadway experiences. Since the use of the airfield matting has similarities with the temporary bypass roadway, a summary of this technology is presented here.

This system has been under development for the last year at Webcore Technologies. The overall objective of this program was to design a robust airfield mat that weighs less and is easier and quicker to deploy than the AM-2 aluminum matting currently used by the Air Force.

The most critical goals to achieve were a maximum panel weight of 4 lb/ft² (0.19 kN/m²), a thickness no greater than 2 in (50.8 mm) and the ability to withstand a repeated rolling wheel of 30,000 lb (133.4 kN) from a simulated F-15 aircraft wheel under soft, 6 CBR (Californian Bearing Ratio), soil conditions. Also, the installation rate target was 450 ft²/hr (42 m²/hr). All the previously mentioned goals were met, only the latter was not tested, but thought to be achievable.

The architecture of the sandwich panel developed for this airfield matting application is different from the material characterized for the bypass roadway project. The difference is in the reinforcement of the core; in the first one, the foam struts are wound with dry rovings or tows in a helical pattern, to be later placed together to achieve the reinforcement in the z-direction of the

panel (Figure 4.1 and Figure 4.2). The second material features a bi-directional reinforcement (x and y directions), made of struts and webs (stitches in the longitudinal direction).

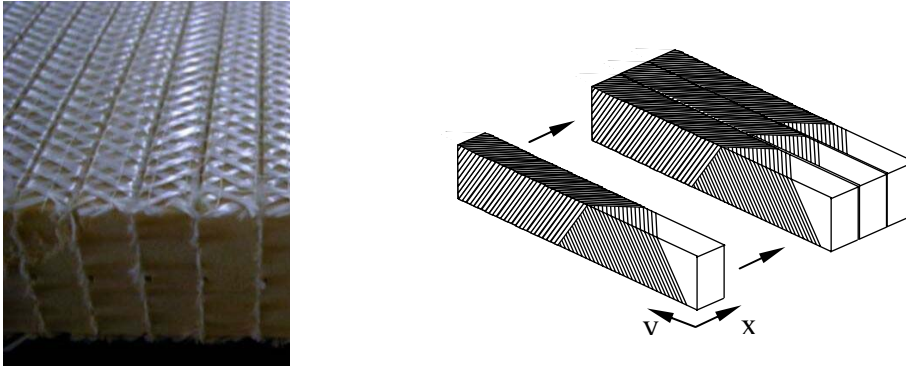


Figure 6.1 Foam block wound with glass fiber reinforcement (Webcore Technologies)

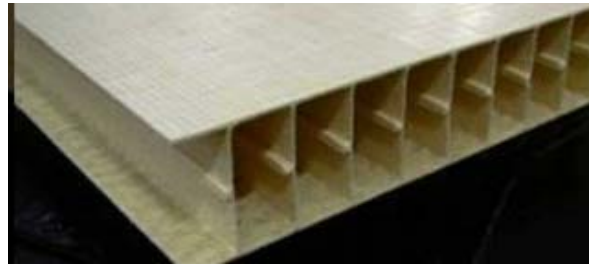


Figure 6.2 Composite Structure - foam removed (Webcore Technologies)

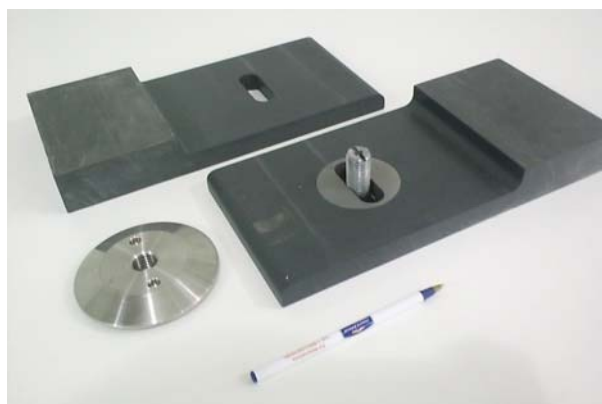
Regarding the assembly of the panels to form the matting, the joints formed of the panel to panel connection are the critical issue. In the prototype developed, a three piece cam lock connector (see Figure 4.3) and an overlapping joint were used in order to facilitate the load transfer. This type of connector not only allows easy installation, but also rapid removal of the boards for replacement or sub grade repairs. The prototype of the FRP airfield matting system is presented in Figure 4.4.



(a) Top view of the connector



(b) Bottom view of the connector



(c) View of unassembled connector and joint

Figure 6.3 Connector Details



Figure 6.4 Matting Array

APPENDIX A
LITERATURE REVIEW

This compilation is based on the following sources:

Atlantic Research Corporation: http://www.atlanticresearchcorp.com/docs/adv_3d.shtml

Hardcore Composites: <http://www.hardcorecomposites.com>

Kansas Structural Composites: <http://www.ksci.com>

National Composite Center: <http://www.compositecenter.org/index1.php>

One Ocean Kayaks-Composite Sandwich Core:

<http://www.oneoceankayaks.com/Sandcore.htm>

Reeve, Scott R. *FRP Composite Bridge Decks: Barriers to Market Development*. National Composite Center, Kettering, OH.

Reinforced Plastics. Volume 47 Number 4. Elsevier, April 2003.

Reinforced Plastics: <http://www.reinforcedplastics.com>

Stoll, F., Banerjee, R., Campbell, S., Day, S. *Manufacture of Fiber-Reinforced-Foam Composite Sandwich Structures*. Blacksburg, VA: ASC 16th Annual Technical Conference, September 2001.

Stoll, F., Klosterman D., Gregory M., Banerjee R., Campbell S., Day S. *Design, Fabrication, Testing and Installation of Low-Profile Composite Bridge Deck*. Long Beach, CA: SAMPE, May 2002.

United States Department of Transportation: www.fhwa.dot.gov

Vinson, Jack R. *The Behavior of Sandwich Structures of Isotropic and Composite Materials*. Pennsylvania: Technomic Publishing Company, Inc, 1999.

WebCore Technologies, Inc: <http://webcoreonline.com>

Zenkert D. *The Handbook of Sandwich Construction*. London, United Kingdom: Chameleon Press, 1997.

The following text does not report the specific reference with exception of the figures and tables.

Sandwich construction is relatively new. It was during World War II (1943) when this concept was originated. An aircraft fuselage was design and fabricated using fiberglass reinforced polyester as faces, and both glass-fabric honeycomb and balsa-wood as core.

The first research paper regarding sandwich construction was published in 1944, and it dealt with in-plane compressive loads. Later on, more studies have been developed upon sandwich panels, such as the failure modes, structural optimization, effects of shear deformations on deflections, theoretical work for different loading modes.

The use of sandwich structures is growing very fast around the world. In Europe, they have been used since the late 1980s, especially in navy ships, but in the United States, airlines manufacturers and military aircraft systems have been the primary use. Its several advantages, the development of new techniques and materials, and the need for high performance, low-weight structures assure that sandwich constructions will continue to be in demand.

A structural sandwich panel consists of two thin, stiff, strong sheets of dense identical material (faces) separated by a thick layer of low density material which may be less stiff and strong (core). The low weight with exceptionally high stiffness and strength makes it ideal for a very wide range of applications where weight is critical. Developments in new cores continue to be of primary interest, such as the new cores manufactured by Webcore Technologies (Ohio).

Foam or solids cores are relatively inexpensive, they can consist of balsa wood, and a wide variety of foam/plastic materials with different densities and shear modulus. Since World

War II, honeycomb-core structures have been widely used, either in the hexagonally or the square shell structure.

The separation of the skins or faces by a low density core increases the moment of inertia of the beam or panel, with a little increment in the weight producing an efficient structure.

Mechanics of a Composite Sandwich Panel

The mechanical properties of a sandwich panel depend upon the core and the face materials, their thickness as well as their configuration. The design process is essentially one of optimization where the weight or the stiffness/unit-weight is minimized.

The best way to visualize the structure of a sandwich core panel is to use the analogy of a simple I beam (see Figure A 1).

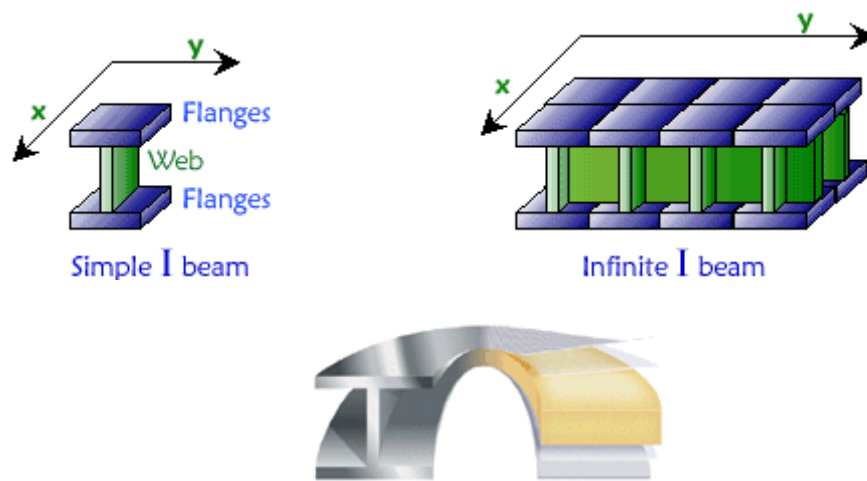


Figure A 1 Sandwich Panel Structure Idealization (One Ocean Kayacs – Composite Sandwich Core)

Like the “I” beam, a sandwich panel consists of strong skins (flanges) bonded to a core (web). The skins are subjected to tension/compression and are the most responsible for the sandwich strength. The core, as it was mentioned before, supports the thin faces so they do not buckle, and stay fixed to each other (like the web does in a “I” beam). It experiences the shear stresses as well as vertical compression and tension stresses.

Unlike the “I” beam, which is designed to withstand stresses along the horizontal axis and bending about the vertical axis, the sandwich construction can be stressed along and about any axis that lay in the X-Y plane. Also an “I” beam is subjected to several local stresses, but a sandwich structure absorbs the load and distributes the stresses over a much larger area. The result is a structure of uniform strength with no weak points.

If a solid laminate is split down the middle and then separated with a core material, the result is a sandwich panel. The new panel weighs little more than the laminate, but its flexural and dynamic strength is much greater. If the thickness of the core material is doubled, the difference is even more remarkable.

The core

The core is the material sandwiched and adhesively bonded to the facings to provide load transfer between components, and it should not be sufficiently flexible to permit significant relative displacements of the faces and core, but it must be stiff for the following reasons:

- To keep the faces parallel to each other at the correct perpendicular distance.
- Stiff enough in shear to guarantee that when the panel is bent the faces do not slide with respect to each other. If this condition is not fulfilled, then the faces behave independently and the sandwich panel effect is lost.

Therefore, if the core has the adequate stiffness, it may make a useful contribution to the bending stiffness of the panel as a whole.

The type of core can be classified into four types (see Figure A2):

- Foam or solid core
- Honeycomb core
- Web core
- A corrugated or truss core

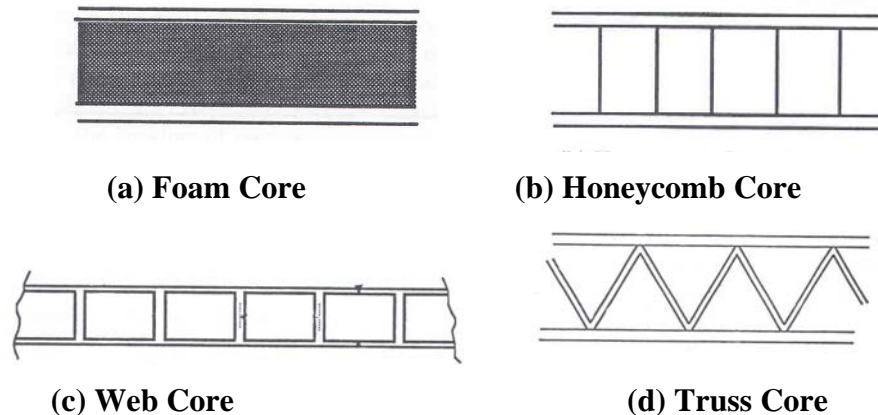


Figure A 2 Types of Sandwich Constructions (Vinson J. The Behavior of Sandwich Structures of Isotropic and Composite Materials, 1999)

The core materials can be classified as follows:

Balsa Wood. End grain balsa's closed-cell structure consists of elongated prismatic cells with a length that is approximately sixteen times the diameter. The densities vary between 6-16 lb/ft³ (96.11 – 256.3 kg/m³). The stiffness and bond strength is excellent.

Cross-linked PVC Foam. Polyvinyl chloride foams are manufactured by combining polyvinyl copolymer with stabilizers, plasticizers, cross-linking, compounds, and blowing agents. They offer a good combination of strength and weight with densities ranging in between 4 - 30 lb/ft³ (64.1 – 480.6 kg/m³).

Thermoplastic foam. It is a very light material; its density is about 2 lb/ft³ (32 kg/m³). It offers very low mechanical properties and the polystyrene (one of its components) would be attacked and dissolved by polyester resin. It has floatable applications and not structural.

Polyurethane foam. It has a wide range of densities, 2 lb/ft³ (32 kg/m³) to 20 lb/ft³ (320.4 kg/m³), but it does not offer the necessary characteristics to be used in structural applications.

Syntactic foam. It is made by mixing hollow micro spheres in resin. It is a thick mixture that can be applied by hand or sprayed. It is sometimes used as a barrier coat.

Linear PVC foam. It is produced mainly for the marine industry. It allows significant deflections before failure. Comparing to the cross-linked PVC, this one shows less favorable static properties and better impact absorption capability.

Honeycomb. This type of cores has been used extensively in the aerospace and transportation industry. Constituent materials include paper, aluminum, phenolic resin, fiberglass, polypropylene and aramid fiber phenolic treated paper. Its densities vary in between 1-6 lb/ft³ (16-96.1 kg/m³). The biggest advantage of this core is that very lightweight panels can be manufactured. The mechanical properties depend upon the materials used.

PMI Foam. Polymethacrylimide (PMI) foam is generally used in advanced composites construction because of its ability to withstand curing temperatures above 350°F (176.7°C).

Plywood. Regarding the moisture absorption, this is a poor material of outdoor exposure. Also, depending on the type of wood, poor bonding of the laminate is a problem.

Since the sandwich constructions have variety of applications, as it will be seen later, the core has to be designed according to the necessity. The following table shows the required properties of the sandwich and the corresponding core characteristics:

Table A 1 Core Characteristic - Sandwich Property (D. Zenkert, *The Handbook of Sandwich Construction, 1997*)

Required Property	Core Characteristic
Weight optimization	Wide density range
Capability to carry transverse loads	High shear modulus
Low out-of-plane deformation	High shear modulus
Prevent panel buckling	High shear modulus
Prevent local buckling of the skin	High tensile and compressive modulus
Fatigue properties	High shear strength, shear strain and fracture toughness
Impact properties	High compressive, shear strength and energy
Tolerance to stress concentrations	High shear strain
Damage tolerance	High fracture toughness and high shear strain. Ductile behavior at high strain rates.
Creep properties	High compressive strength, modulus of elasticity and temperature resistance.
Insulation capacity	Low thermal conductivity and water absorption.
Moisture absorption	Low water absorption and water vapor permeability.
Temperature resistance	High glass transition temperature (T _g)
Process ability	Good adhesion properties, possibility to machine and form, temperature and solvent resistance and dimension stability.

The faces

A sandwich has to have two layers at the top and the bottom. These two facings are the ones that primarily resist the in-plane and lateral (bending) loads. They can either have identical or different thickness and material properties. However, in some special cases, the faces could differ, because perhaps one face is the primary load carrier, subjected to low temperature, while the other face must withstand and elevated temperature, corrosive environment, etc...

The faces can be made out of aramid, glass fiber, carbon fiber, stainless steel and aluminum, giving a durable surface to the structure. The required properties for the facings are:

- High stiffness
- High tensile and compressive strength
- Impact resistance
- Environmental resistance
- Wear resistance

Adhesives

The requirements of the adhesives are usually described as “the bond line must have at least the same tensile and shear strength as the core material”.

The characteristics of the material used as a bonder of adhesive are very important in the performance of a sandwich construction, due to the fact that faces and core must perform as a whole, as a unity. It also has to be taken into account the compatibility among the materials with the core and face, aging, environmental and temperature resistance.

Advantages of Sandwich Structures

Sandwich constructions are playing an increasingly important role in structures because of its exceptional high flexural stiffness-weight ratio compared to other structural elements. It is important to develop optimization of the sandwich construction methods in order to:

- Determine the minimum weight for a given structural geometry, loading and material system
- Compare the best sandwich construction with alternative structural configurations
- Select the best face and core materials to minimize the structural weight
- Select the best lamina orientation sequence for faces composed of laminates
- Compare the optimum construction weight to weights required when there are some restrictions, such as cost, material availability, etc...

In general, foam and honeycomb cores do not carry any appreciable in-plane or bending loads to which the structure is subjected to. Their primary purpose is to ensure the spacing between the faces and to carry the transverse shear loads.

It is also important to note that sandwich structures have two main areas of weakness: the edges and the local inserts. The first ones can be fragile due to peeling stresses and in-plane shocks, which might occur if the panel is not protected. The local stress that will be developed after drilling holes into a sandwich panel to later be screwed to become part of a larger structure, are problems that generally the panel by itself is not strong enough to support. Therefore at the edges and void filling compounds can be used to add strength to weak areas such as those. Another risk is the moisture absorption by the core material; its physical properties can be affected.

Strength of Sandwich Structures

As it was mentioned before, the main advantage of a sandwich construction is that it is stiff and light at the same time. However, stiffness by itself is not enough; the structure must also be strong.

Regarding the strength, there are different modes of failure than can be considered, depending upon the geometry of the sandwich panel and the loading configuration. The structure will fail at whatever mode occurs at the lowest load. The failure modes that could occur are the following:

Yielding or fracture of the face in tension or compression. It will be considered the face or the core to have failed either if yielding occurs or if the component has actually fractured. Therefore for every material used, there will be a maximum allowable stress, which it can be a yield or a fracture stress. The fracture criterion is when the maximum stress reaches this permissible value. For most loading situations, the normal stresses in the faces are usually greater than the shear stresses in the core and faces.



Figure A 3 Yielding of Fracture of the Facing (Zenkert D. The Handbook of Sandwich Construction)

Face Wrinkling. It can either take place when a sandwich is subjected to and in-plane compressive buckling or in the compressive face during bending, or in a combination of both of them. The actual failure can occur in two ways: Wrinkling that becomes unstable causing an indentation in the core if the compressive strength of the core is lower than its tensile strength and the adhesive joint; and the wrinkling causing a tensile fracture if the tensile strength of the core or the adhesive joint is lower than the compressive strength of the core. Definitely the quality of the adhesive joint will affect the wrinkling stress in the composite.

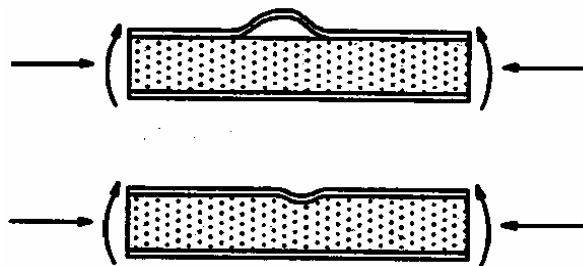


Figure A 4 Face Wrinkling (Zenkert D. The Handbook of Sandwich Construction)

General Buckling. This phenomenon must be avoided since a structure that has buckled may have lost its capability of fulfilling its purpose. The buckling load may also be the ultimate load that the structure can support, because in its buckled shape it may not stand any more load.

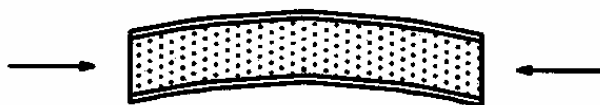


Figure A 5 General Buckling (Zenkert D. The Handbook of Sandwich Construction)

Core Shear Failure. The core material is mainly subjected to shear since it carries almost the entire transverse force. Generally the shear stresses in the core are large compared with the normal stresses; therefore failure will occur when the maximum shear stress exceeds the yield strength of the core. This yield strength depends of the foam density.



Figure A 6 Core Shear Failure (Zenkert D. The Handbook of Sandwich Construction)

Delamination. The failure of the bond between the face and the core is called delamination and is due to overloading. The shear stress in the bond line is almost as high as in the middle of the core, and if the adhesive joint has less strength than the core it will fail before the core. This should be avoided by choosing the proper adhesive and manufacturing methods.

The bond will be also subjected to high stresses if there is high temperature acting on the face, for example sunshine. The core is usually a very good thermal insulator, but the face is not, especially if it is metal.

The adhesive joint would also fail due to fatigue, impact or aging. The main problem with adhesive joint failure is that they are embedded; they can start growing and reach critical sizes before being detected.

Core or Panel Indentation. The possible indentation of the faces and core at the loading points is due to the stress concentrations induced when loads are highly localized. When a load is applied directly, there is also the possibility that the face bend where the load is being located, bends independently from the opposite face, and if the deformation and the stress induced is higher than the compressive stress in the core, the core will fail. It can be avoided by applying the load in over a sufficiently large area.

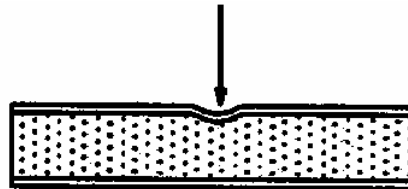


Figure A 7 Core or Panel Indentation (Zenkert D. The Handbook of Sandwich Construction)

Shear Crimping. The shear crimping failure is actually the same as the buckling mode considering thin faces, for example when the critical load equals the shear stiffness. Shear crimping is a shear instability failure. A failure of this kind occurs as a result of large transverse forces induced by large out-of plane deformations. The failure will appear where this transverse force has a maximum value.

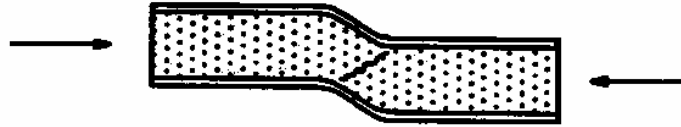


Figure A 8 Shear Crimping (Zenkert D. The Handbook of Sandwich Construction)

Face Dimpling. It is also known as inter-cellular buckling. This instability phenomenon may occur in sandwich structures with honeycomb or corrugated cores.



Figure A 9 Face Dimpling (Zenkert D. The Handbook of Sandwich Construction)

Vibration. In some cases there are restrictions on the minimum allowed natural frequency. In moving structures there is often an imposed movement within a given frequency range, therefore it is better to avoid having a natural frequency of vibration for the structural member lying within the range.

Fatigue. Fatigue is generally said to cause more than 90 percent of all structural failures. For materials such fiber composites, where there is a lack of data available, a conservative way is to use a fatigue limit under which the material can go through a certain number of cycles without exhibit any considerable damage.

Impact damage. An impact may cause visible damage like making a dent in the face of the panel, or it may not leave any visible mark at all. Damage is not always in the direct proximity of the impact, but it can cause debonding, core fracture, delamination or wrinkling damage far away from the actual point of impact. The resistance to the impact depends upon the face material, the core, geometry of the structure, and of course on the size and speed of the impact.

Uses of sandwich construction

Sandwich construction has been used mainly in the aircraft industry since 1940s, and later the use was extended to missile and spacecraft structures. Through the years, the honeycomb-core sandwich construction became widely used on both commercial and military aircraft.

Europe leads the way in the use of sandwich constructions for lightweight railcars, while in the U. S. some of the rapid transit trains use honeycomb sandwich. The U.S. Navy is using honeycomb-sandwich to reduce the ship weight. Sailboats, racing boats, and auto racing cars are all using sandwich construction.

Honeycomb-sandwich construction is also excellent for absorbing mechanical and sound energy. It has a high-crush-strength to weight-ratio. It can also be used to transmit heat or to be an insulator.

In boat hulls, the fiberglass sandwich construction has become very useful, because the foam increases the chance of flotation in emergency situations. The hulls were designed to

withstand underwater explosions, and the fiberglass eliminates the attraction of the hulls to the mines, as well as avoiding salt water corrosion.

In 1995 it was reported the use of honeycomb sandwich structures for an ultra-light-weight sailing ship, with a weight reduction of 70 percent of more conventional graphite composite construction. In the same year, it was also reported the use of sandwich constructions used in roof panels and intermediate floor panels in ground transportation vehicles such as double-decker buses. More recently, sandwich construction is being used in civil engineering rehabilitation projects such as bridge decks.

Applications

For many years conventional materials in different industries and applications have shown their limitations, especially in construction, such as: wood rots, aluminum and steel corrode, concrete abrasion, etc ... Many bridges have to be rebuilt, and lots of buildings have to be restored and so on.

Composites technology has demonstrated its superiority to traditional methods, but not only in construction, there are other several applications, such as:

Boat Building. Not only a sandwich composite vessel is much easier to maintain than steel parts, but the high-strength to weight ratio can be translated into fuel savings. Also the reduction of weight improves stability. The insulation properties are important too, because it is eliminated the need of non-structural insulating materials, reducing refrigeration costs.

Transportation Industry. It's applicable to truck bodies and vans, refrigeration trailers, horse trailers, etc... Buses, that also have to fulfill fire safety requirements, can also have sandwich structures.

Industrial Parts. The honeycomb materials are especially used in the productions of parts such as: molds, tanks for food or chemical products, platforms for special uses, cowling (engine cover) or wind power engines, spray booths, etc.

Composite bridge deck. The Federal Highway Administration Studies shows that 30 to 40 percent of US bridges (over 112,000 bridges) are structural deficient or functionally obsolete and that those percentages are increasing. The main reason for deterioration is corrosion of reinforcement in concrete decks, and greater loads than the design ones when the bridges were built 40 or 50 years ago. The result of these is the weakening of the decks and the increment of the maintenance costs.

The alternative that has been taken position in the last few years is the use of FRP composite decks for bridges rehabilitation. This technology has already been used on approximately 40 bridges nationwide; over half of them are in the states of Ohio, West Virginia and New York, where the use of salt during the winter time had caused premature deterioration in many structures.

FRP materials are significantly greater than conventional bridge materials such as concrete and steel, but the savings in the reduced weight, fast construction, lower maintenance and increased life, compensate this higher cost. Having an overview of a typical deck system, most of them today utilizes glass-reinforcing fibers set in a polyester or vinyl-ester resin matrix. Other FRP material systems that use carbon or aramid fibers and epoxy resins offer superior structural performance characteristics.

Nowadays, the typical deck systems available on the market consists of two main types: pultruded tubes bonded together with adhesive, and honeycomb or sandwich core systems that

use vacuum assisted resin transfer molding techniques. They are pre-engineered and pre-fabricated in a shop, then assembled and installed at a bridge site.

All deck systems required an overlay to prevent slip and also protection of the FRP material. This cover can consist of a conventional latex concrete, micro-silica concrete or high-density concrete. The compatibility of the overlay materials with the composite deck materials is important in order to prevent debonding, cracking of the overlay or damage of the composite.

Hot-applied asphalt has been used as an overlay for FRP decks, but the temperature of the asphalt usually exceeds the glass transition temperature (T_g) of the resin, being not suitable for this purpose, unless the corresponding effect and behavior were first analyzed and tested prior to use. FRP Deck presents the following advantages:

- **Light weight.** FRP decks weight about 10 to 20 percent of a traditional reinforced concrete deck. Using a FRP deck to replace a concrete one reduces significantly the dead load, which is translated in savings in all the structure (member's size, foundations, etc)
- **Corrosion resistance.** The issue for deterioration of reinforced concrete bridges is the corrosion of steel. The road salt that is used against winter weather effects aggravates this problem, because accelerates the corrosion. The consequence is that the life time of a structure is much less than the design life time. An FRP deck is expected to provide a long lasting life with little maintenance.
- **Quick installation time.** Since the FRP decks are fabricated in a factory, the quality control can be closely monitored. Once the superstructure is prepared, prefabricated deck panels can be shipped and installed quickly, comparing to all the time that takes to put up the forms, place the reinforcement steel, pour and cure the concrete, and remove the forms to construct a traditional concrete deck.
- **High strength.** Since the stiffness is very important in the design of an FRP deck, high safety factors must be maintained for the FRP deck. The strength of a FRP composite deck depends upon several factors such as: fiber type and volume, fiber orientation, resin type, manufacturing method, and both the bonding materials in the sandwich composite and in the final assemblage of the deck as a whole structure.
- **Lower life cycle cost.** The life cycle cost savings are more than the compensation related to the high initial cost of the FRP deck compared to the traditional material. Since the materials are chosen based in the engineer's experience and judgment, many agencies and industries prefer to minimize the initial construction cost and do not "see" the benefit of long range durability savings.
- Resistance to de-icing salts and other chemicals

Along with advantages the use of FRP as a bridge deck also presents some drawbacks, such as:

- Higher initial cost compared to a traditional concrete deck. This issue can be compensated by other savings such as maintenance.
- The low modulus of elasticity of the FRP does not allow the designers to optimize the design in terms of the strength.
- There are no standard manufacturing processes.

- Special considerations have to be taken regarding thermal issues. The reaction of FRP in the presence of thermal changes is different than for concrete and steel, especially when it is used on concrete or steel superstructures.
- As any other material, FRP strength and stiffness properties naturally degrade with time, therefore the effect of creep must be considered in the design to guarantee appropriate performance over the life of the structure.
- There are not standards and conventions for material characterization.

In general, FRP deck systems are a beneficial alternative to traditional decks because of the lightweight, fast placement, and long-term durability qualities. But further research is needed in order to optimize FRP decks to gain more acceptances in the industry. Standard design and specifications are also necessary to give engineers and contractors the pertinent information for an adequate and confident design and building of a FRP deck.

It is true that based upon the first cost, FRP decks are not very competitive with traditional materials, therefore it is fundamental to take into account the change in the approach of quantifying costs and making decisions regarding the use of specific structures in certain conditions.

APPENDIX B
COMPRESSIVE FATIGUE PERFORMANCE – PANEL A

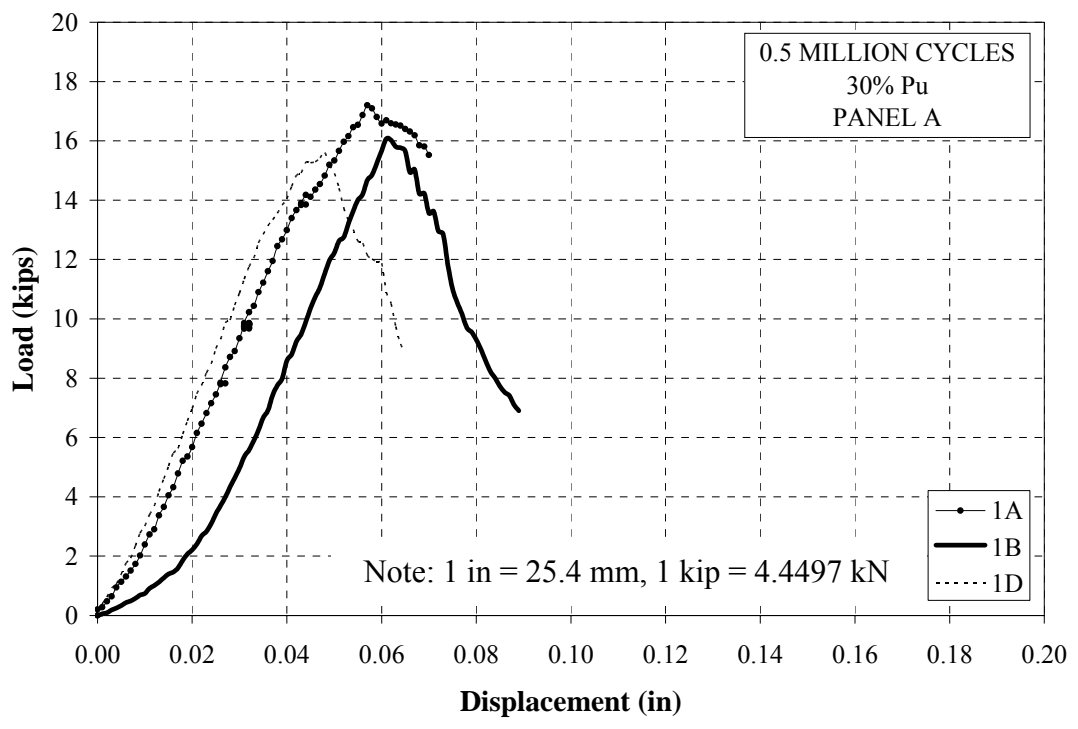


Figure B 1 Load versus Displacement - 0.5 Million Cycles - Panel A

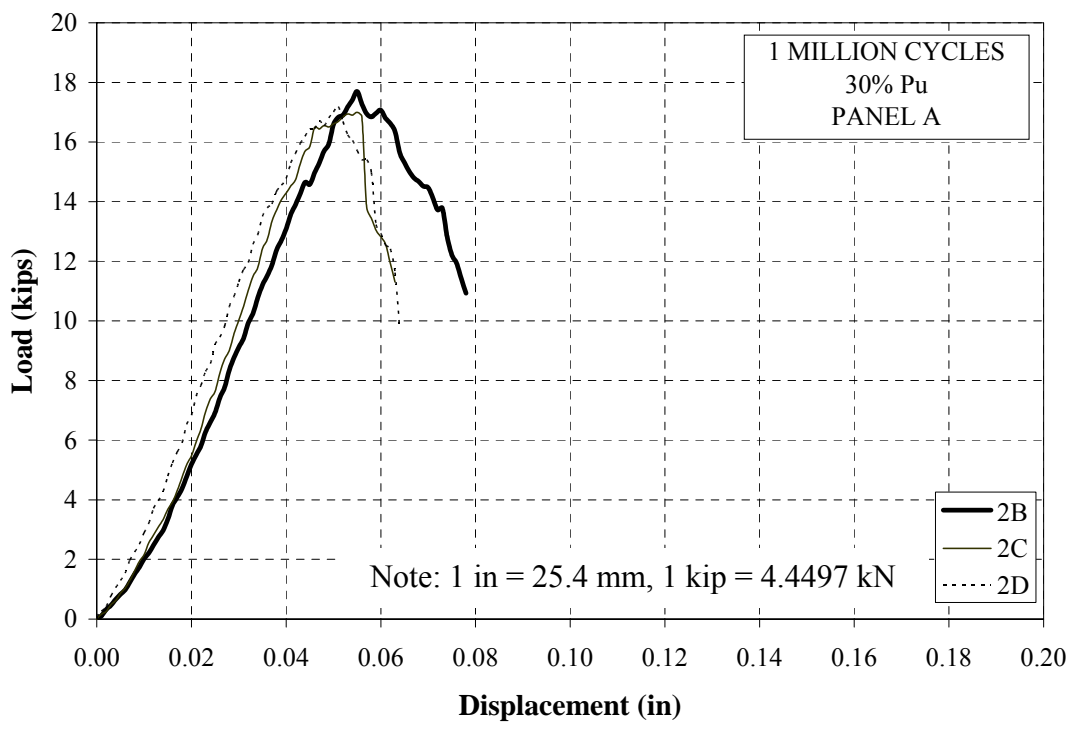


Figure B 2 Load versus Displacement - 1 Million Cycles - Panel A

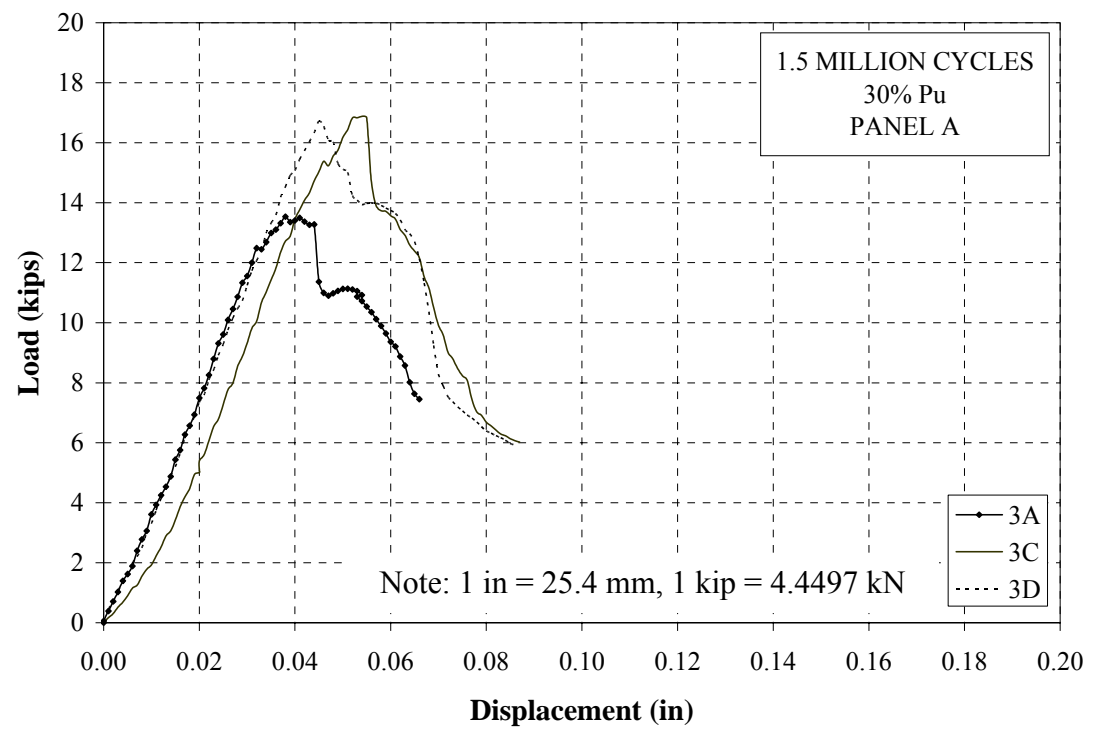


Figure B 3 Load versus Displacement - 1.5 Million Cycles - Panel A

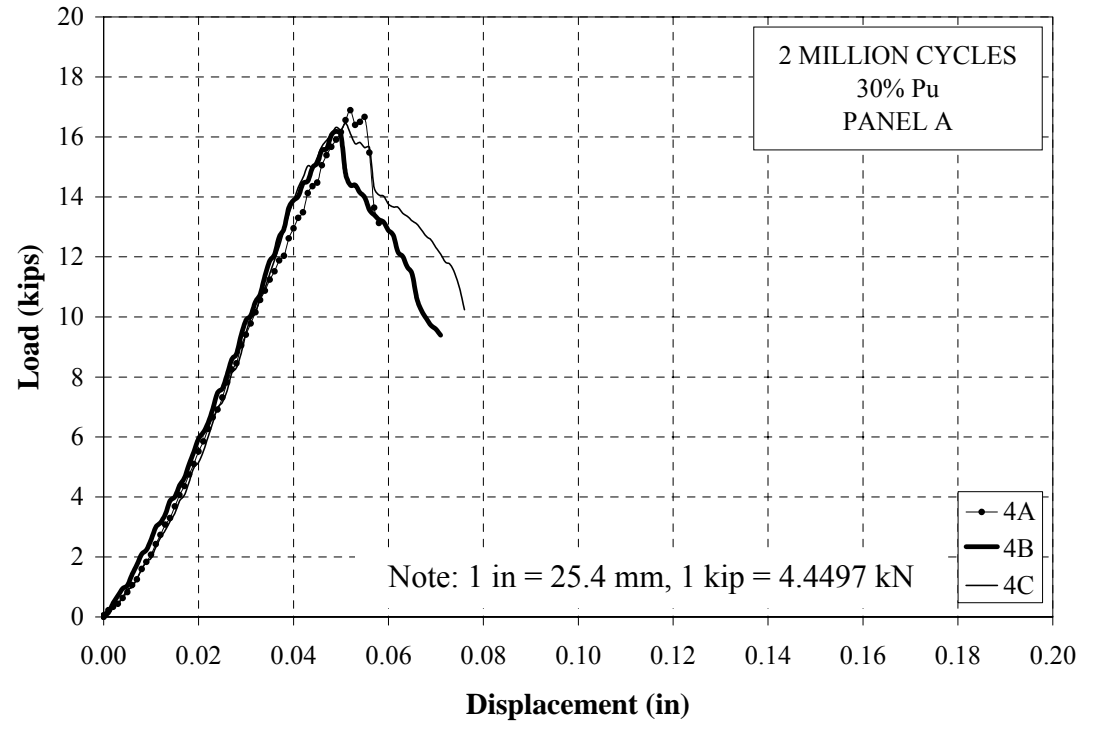


Figure B 4 Load versus Displacement - 2 Million Cycles - Panel A

APPENDIX C

COMPRESSIVE FATIGUE PERFORMANCE – PANEL B

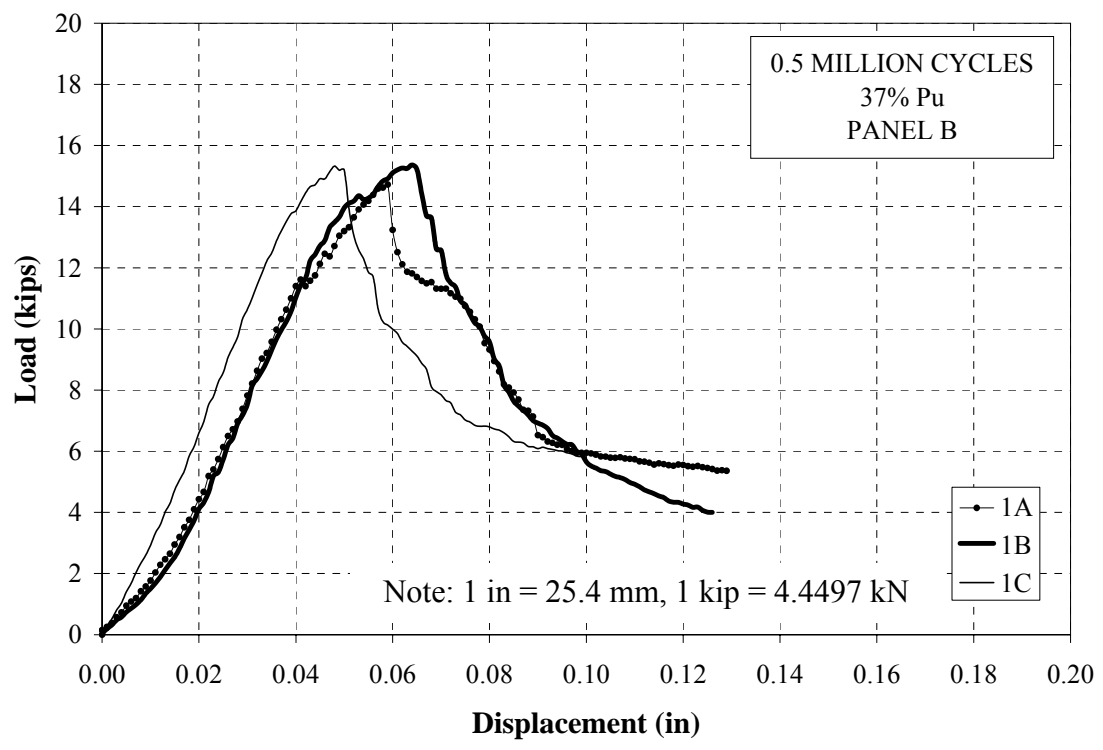


Figure C 1 Load vs. Displacement - 0.5 Million Cycles - 37%Pu - Panel B

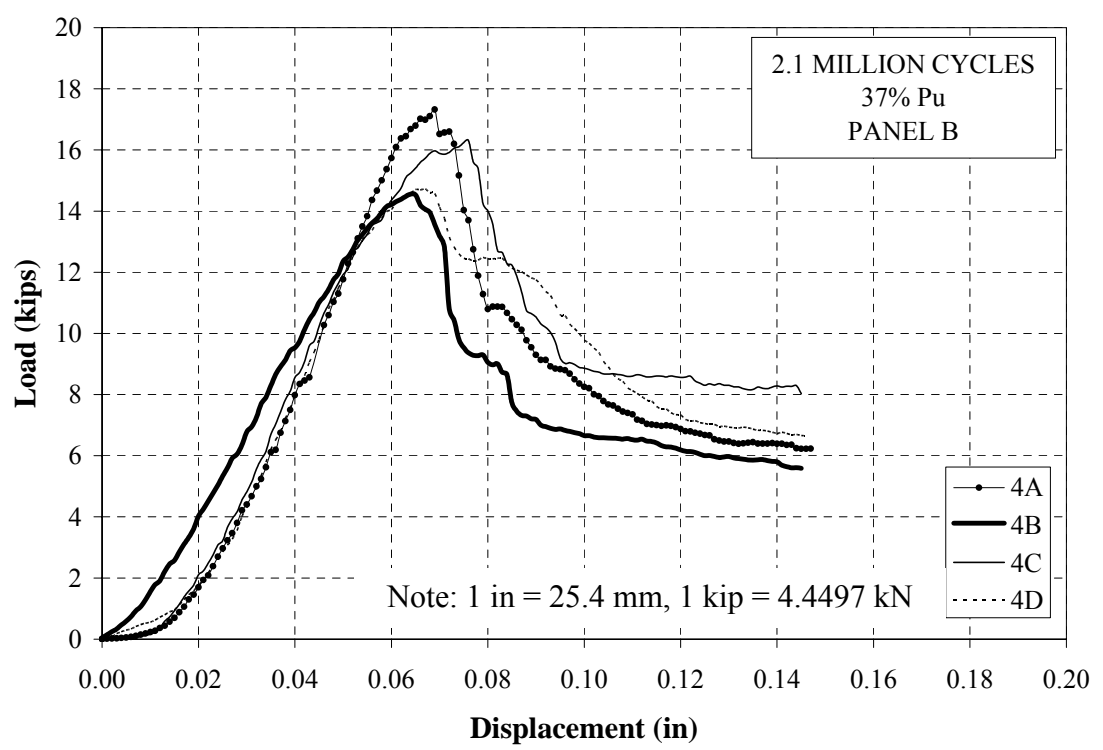


Figure C 2 Load vs. Displacement - 2.1 Million Cycles - 37.1% Pu - Panel B

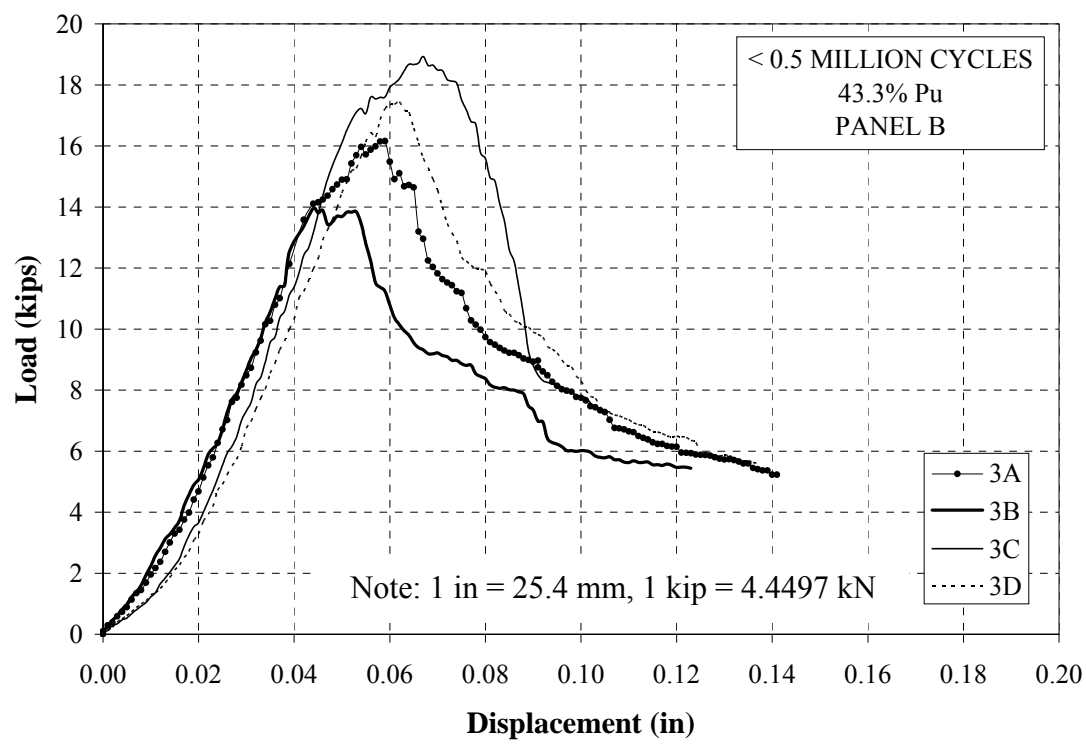


Figure C 3 Load vs. Displacement - 66 Thousand Cycles – 43.3% Pu - Panel B

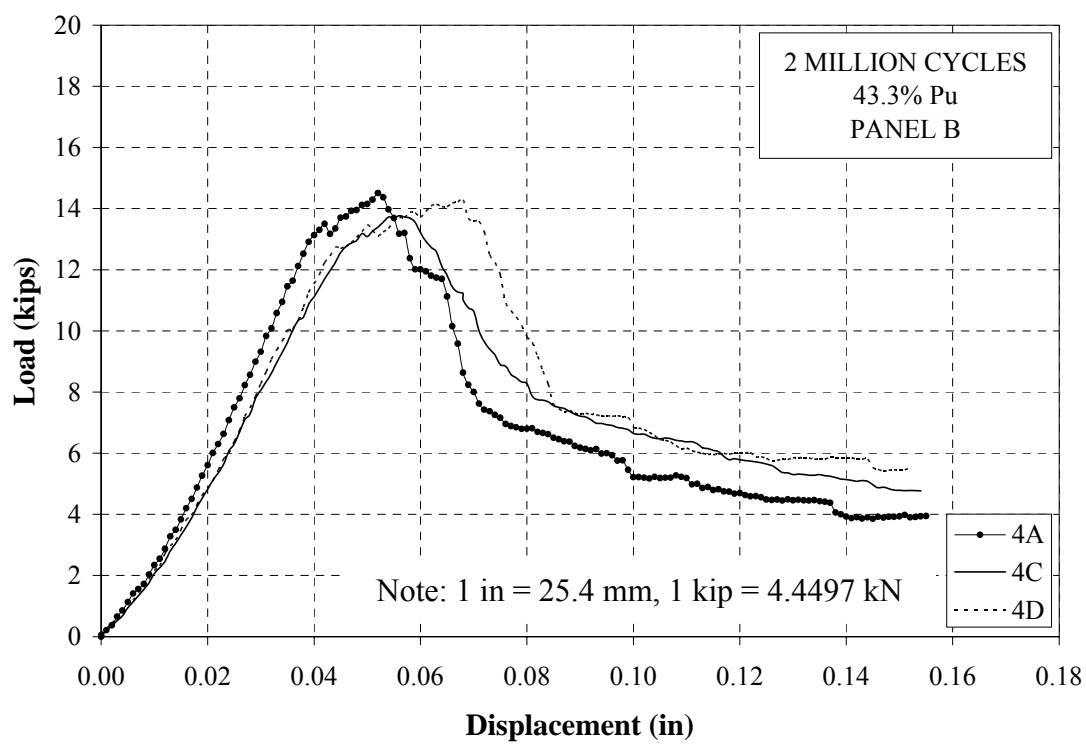


Figure C 4 Load vs. Displacement - 2.1 Million Cycles – 43.3% Pu - Panel B

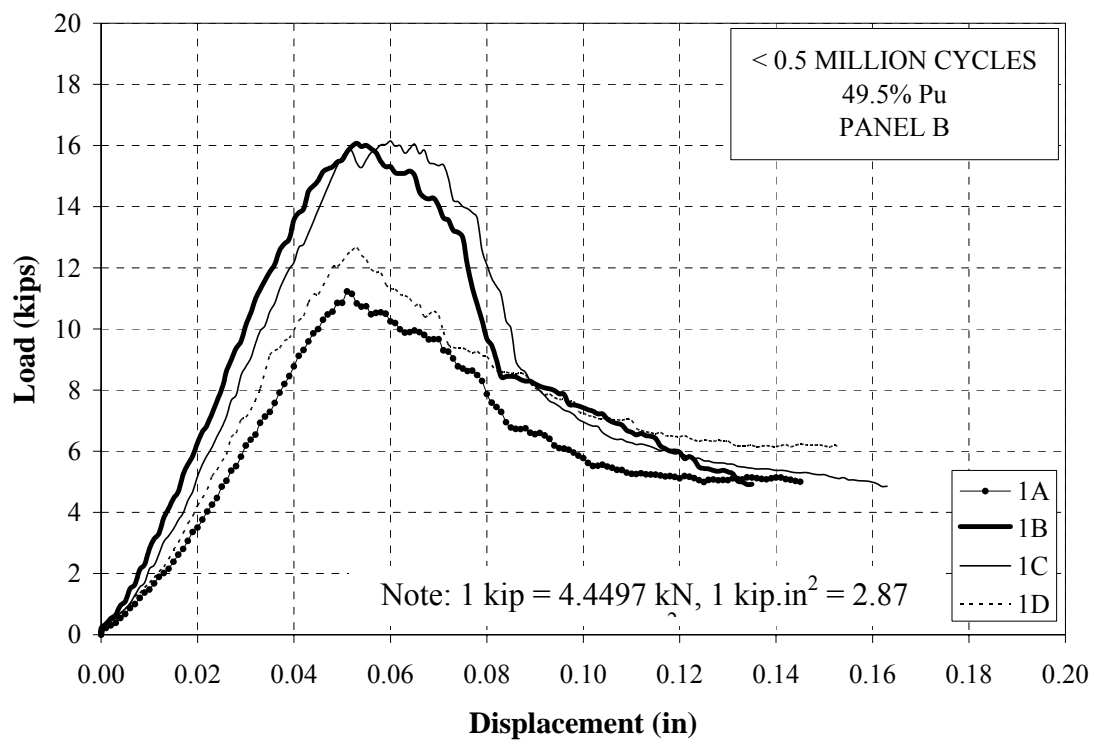


Figure C 5 Load vs. Displacement - 65 Thousand Cycles – 49.5% Pu - Panel B

APPENDIX D
FLEXURAL BEHAVIOR

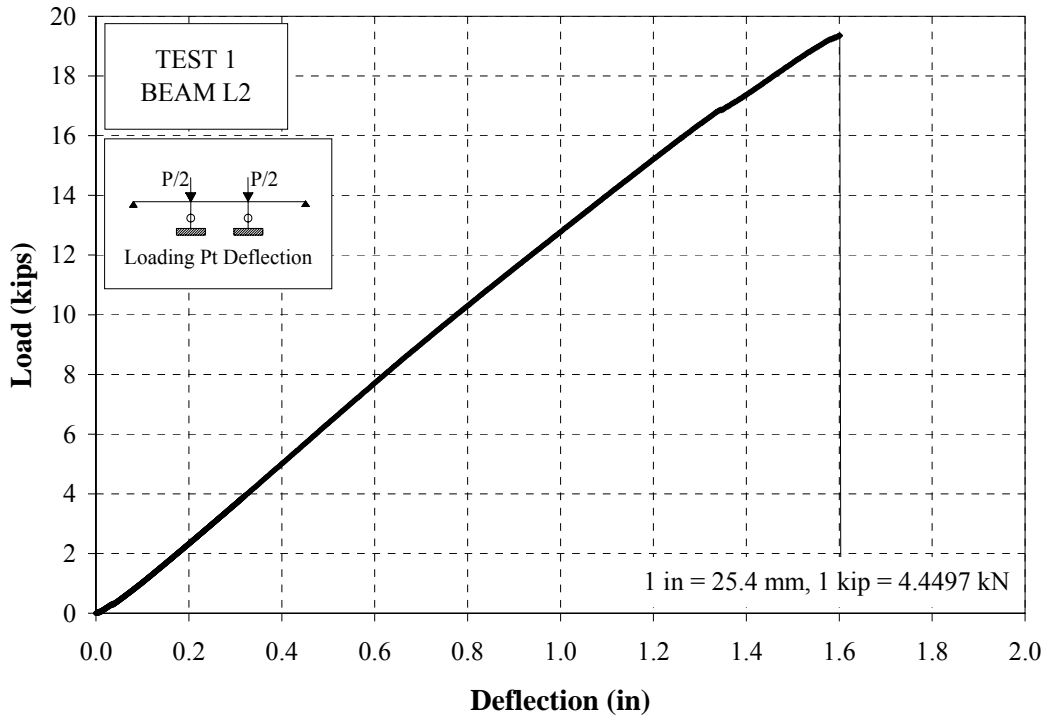


Figure D 1 Load vs. Loading Point Deflection L2 - Static Test 1

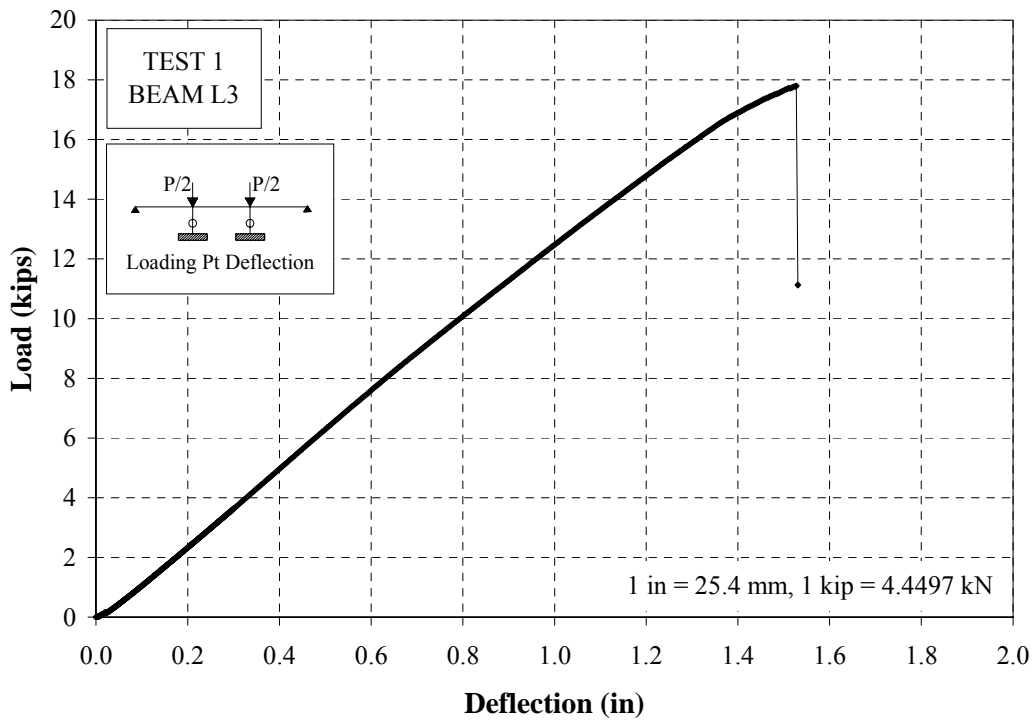


Figure D 2 Load vs. Loading Point Deflection - Beam L3 – Static Test 1

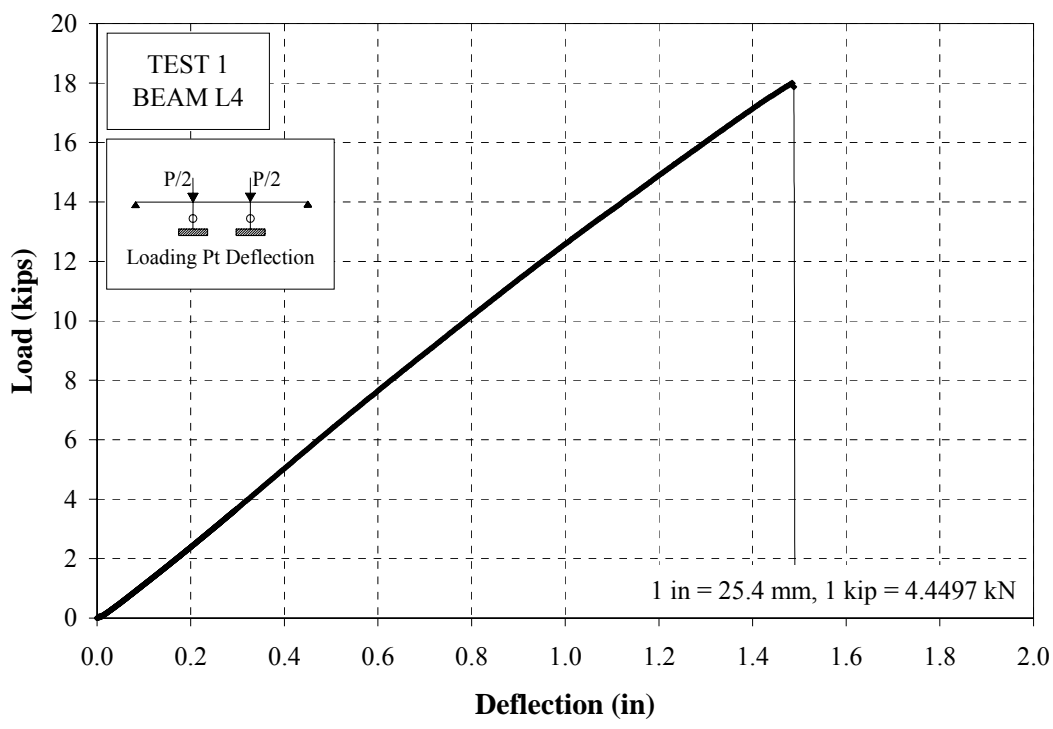


Figure D 3 Load vs. Loading Point Deflection - Beam L4 - Static Test 1

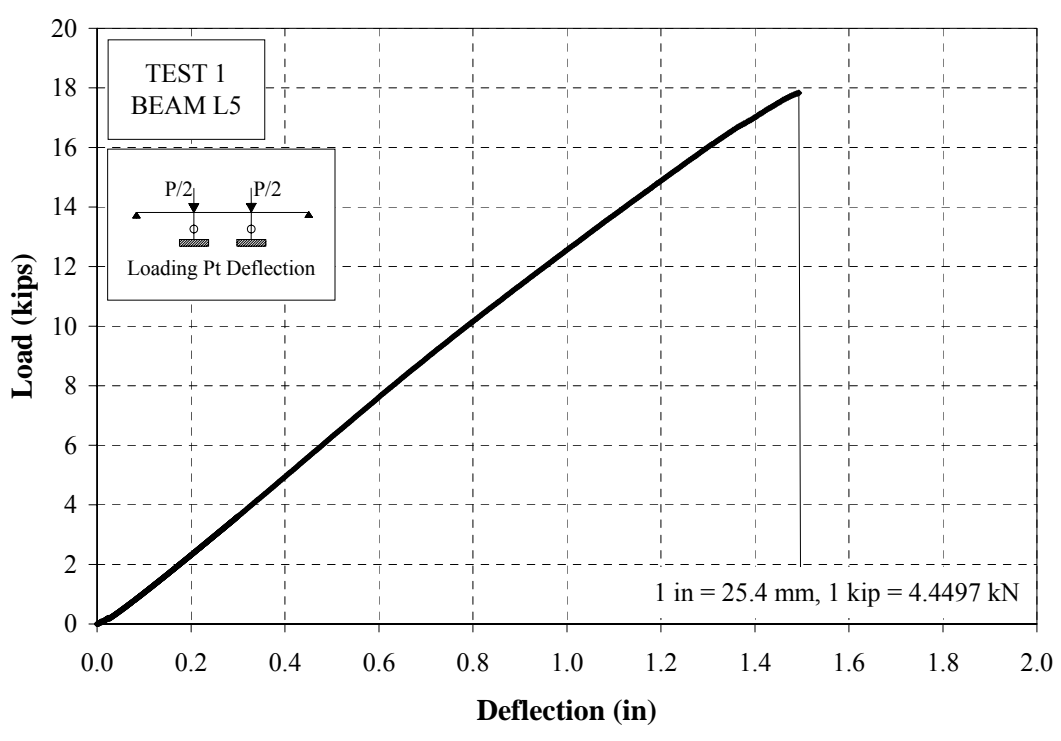


Figure D 4 Load vs. Loading Point Deflection - Beam L5 - Static Test 1

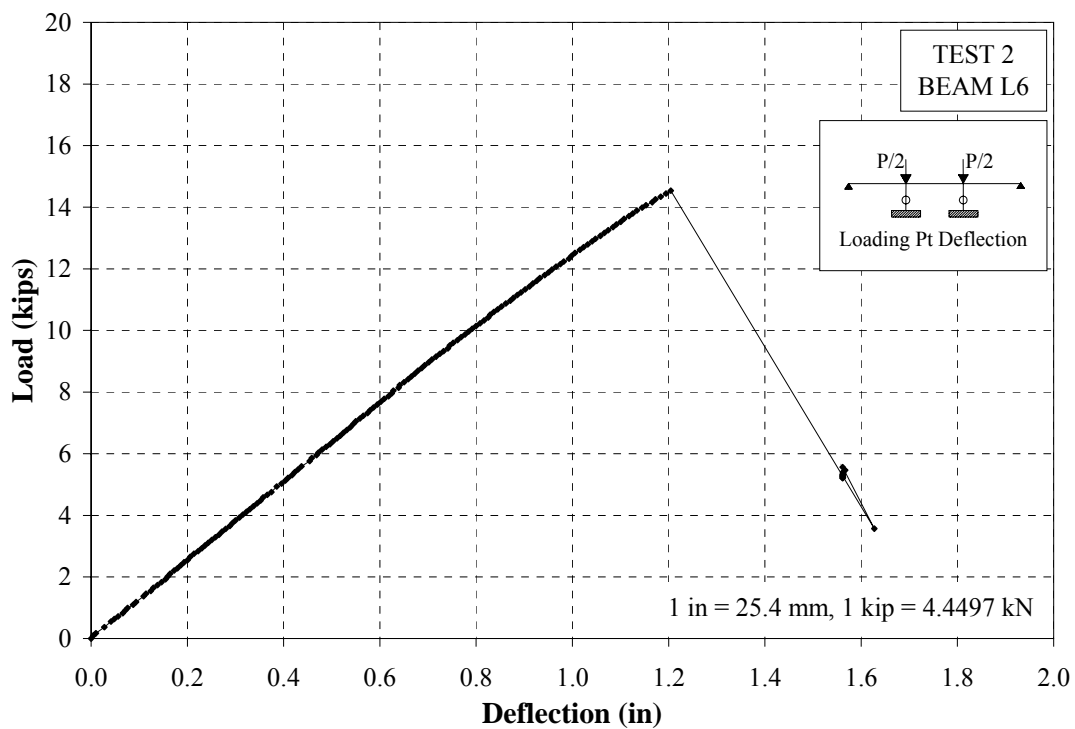


Figure D 5 Load vs. Loading Point Deflection – Beam L6 - Static Test 2

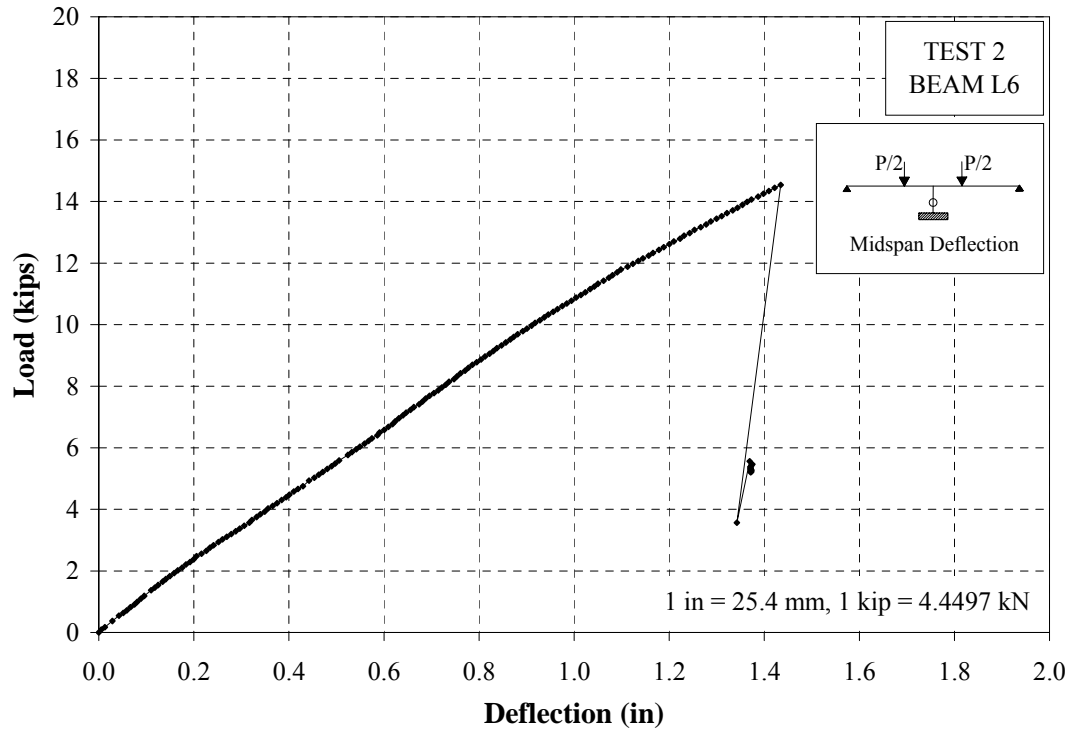


Figure D 6 Load vs. Midspan Deflection - Beam L6 - Static Test 2

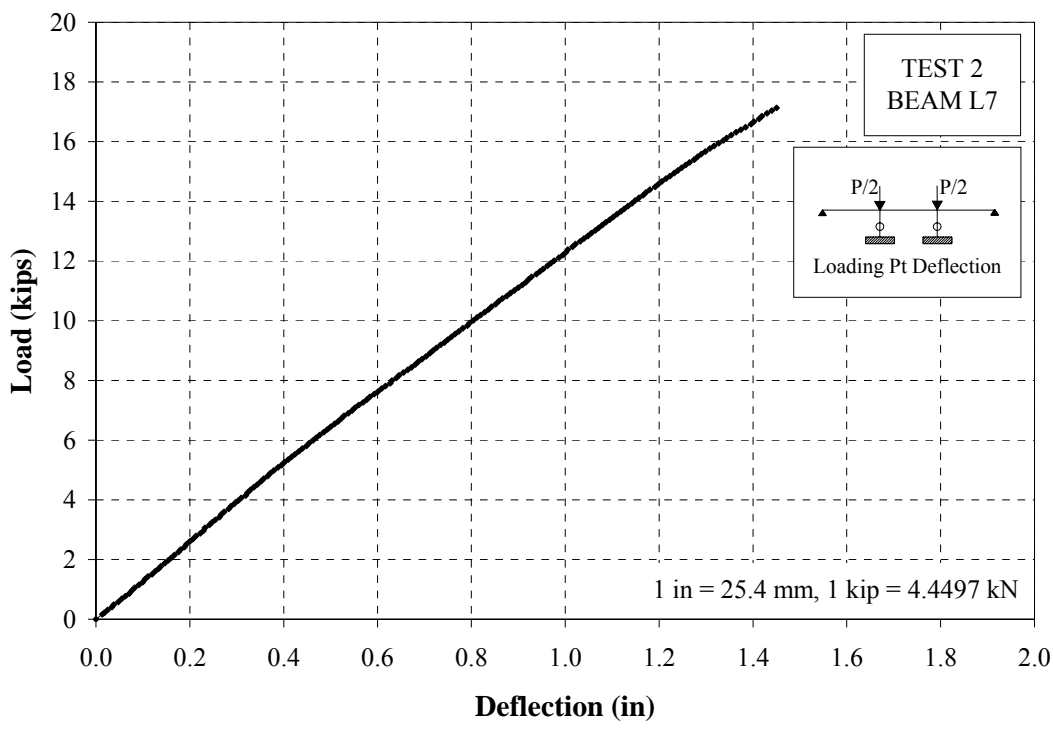


Figure D 7 Load vs. Loading Point Deflection - Beam L7 - Static Test 2

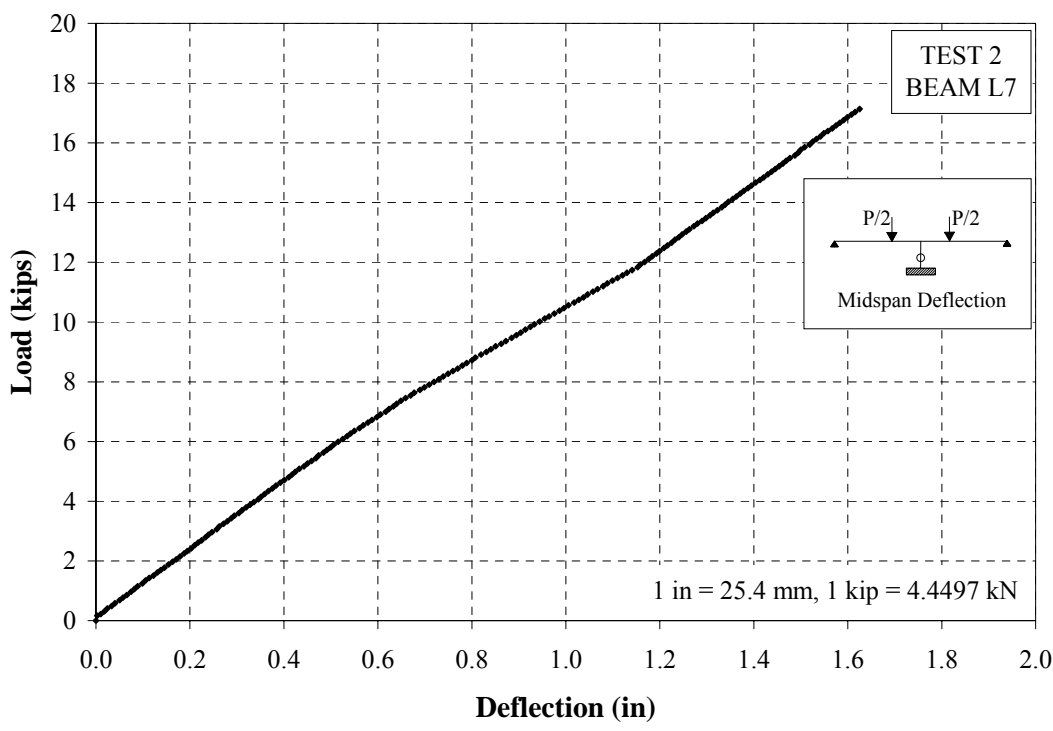


Figure D 8 Load vs. Midspan Deflection -Beam L7 - Static Test 2

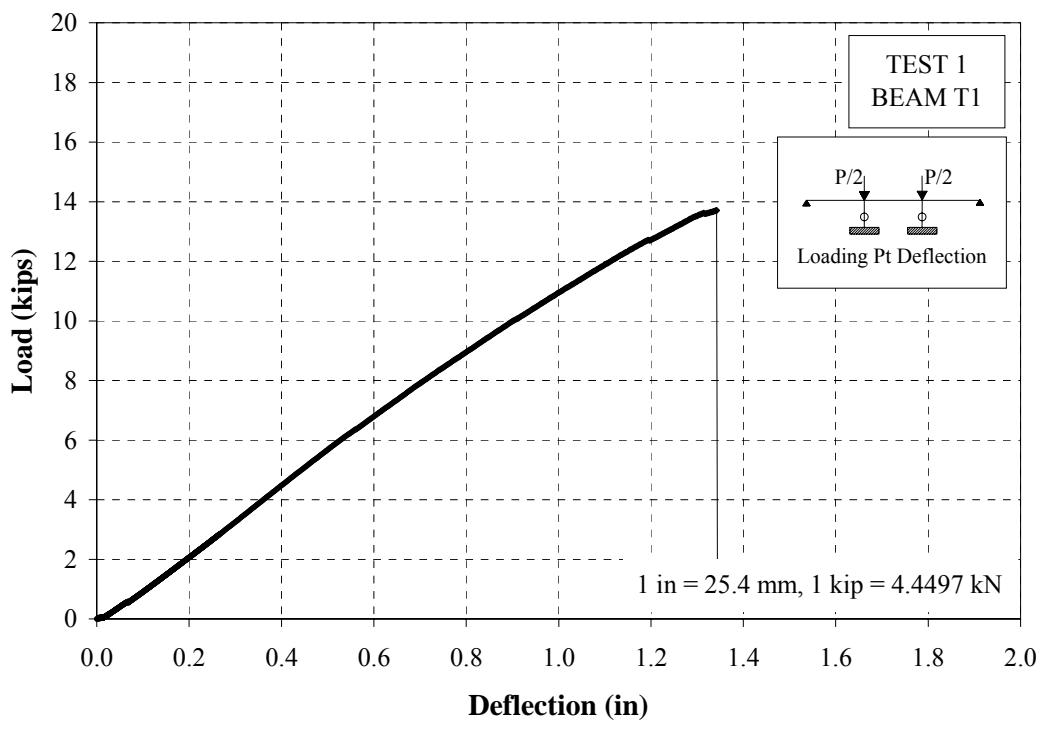


Figure D 9 Load vs. Loading Point Deflection - Beam T1 - Static Test 1

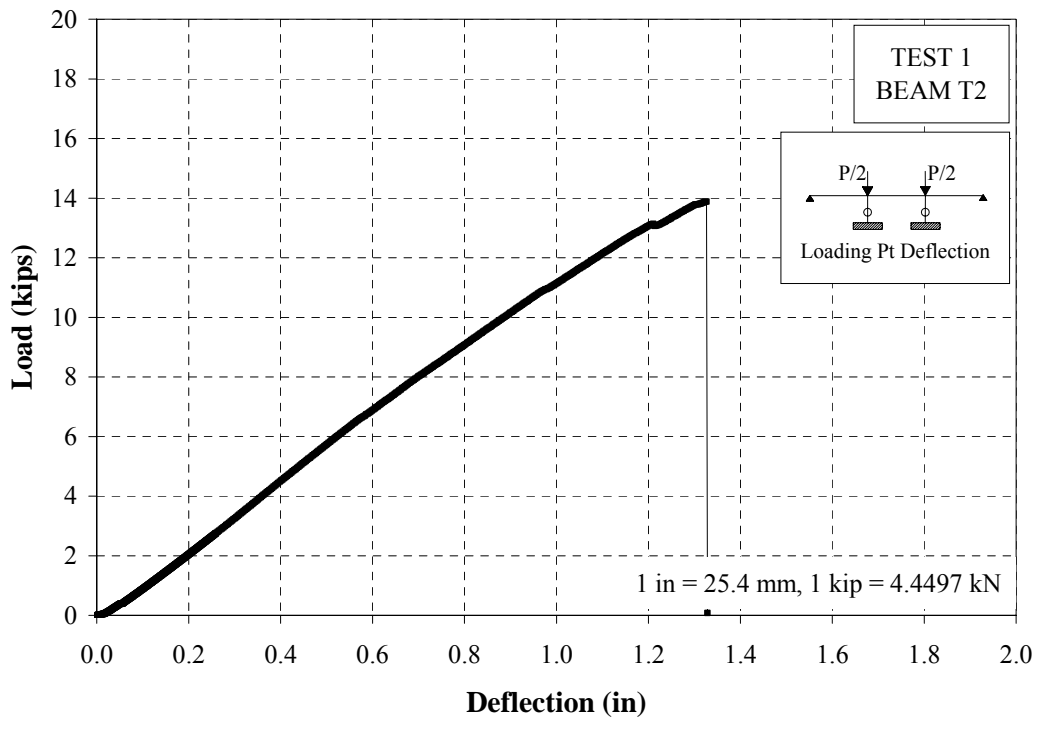


Figure D 10 Load vs. Loading Point Deflection - Beam T2 - Static Test 1

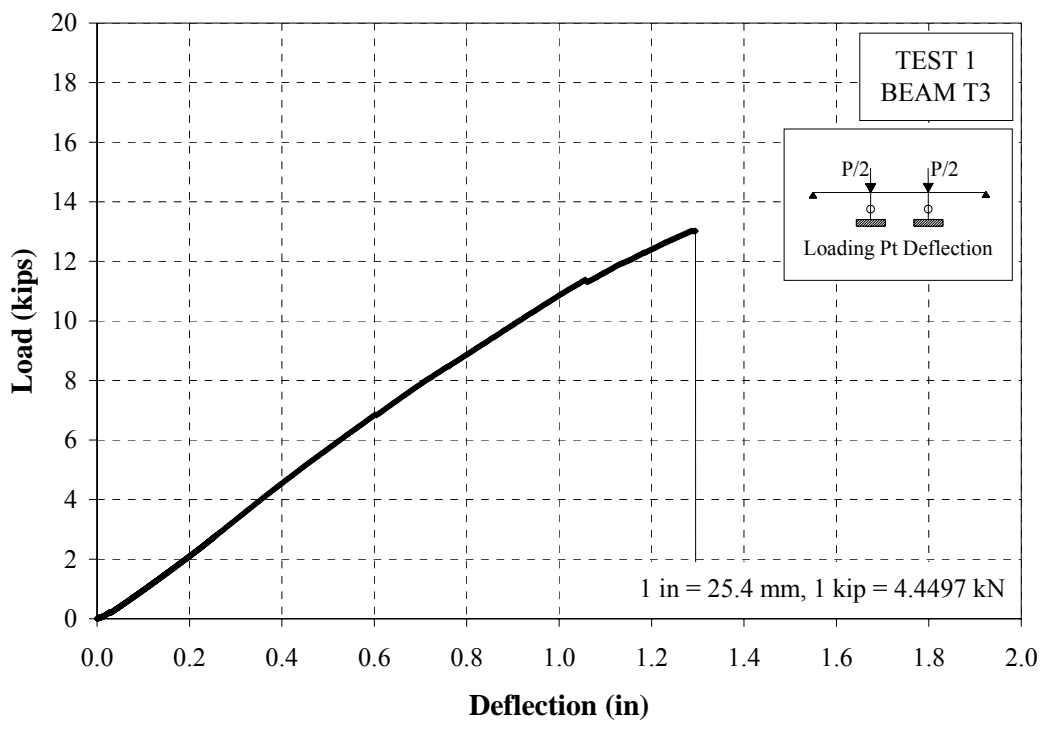


Figure D 11 Load vs. Loading Point Deflection - Beam L3 - Static Test 1

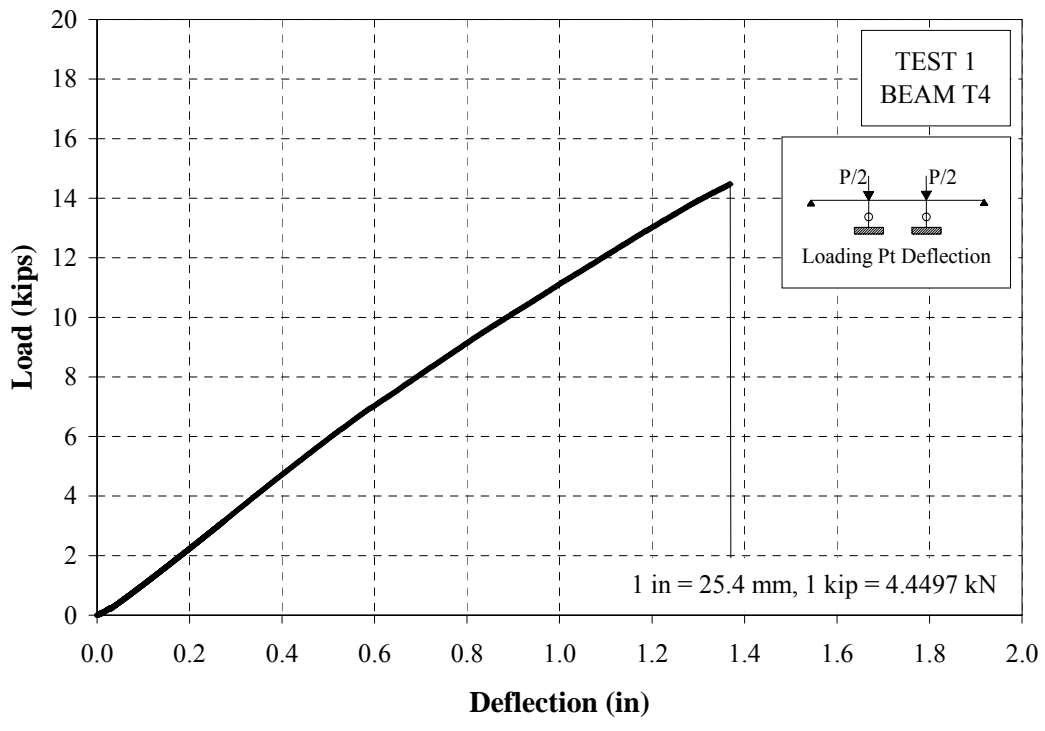


Figure D 12 Load vs. Loading Point Deflection - Beam T4 - Static Test 1

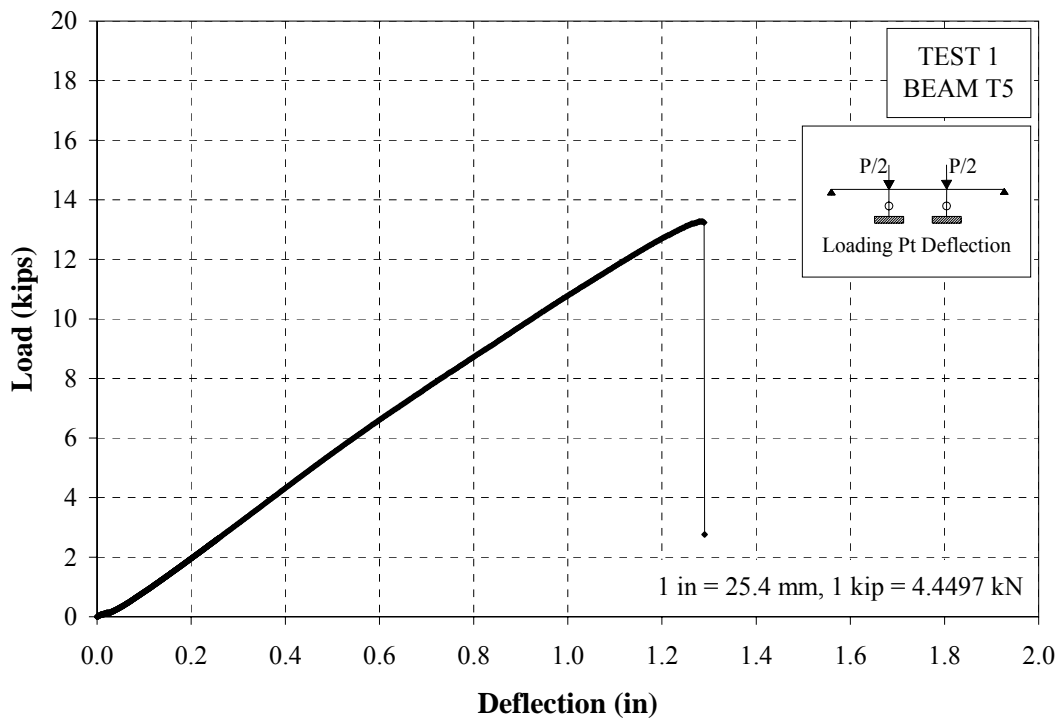


Figure D 13 Load vs. Loading Point Deflection - Beam T5 - Static Test 1

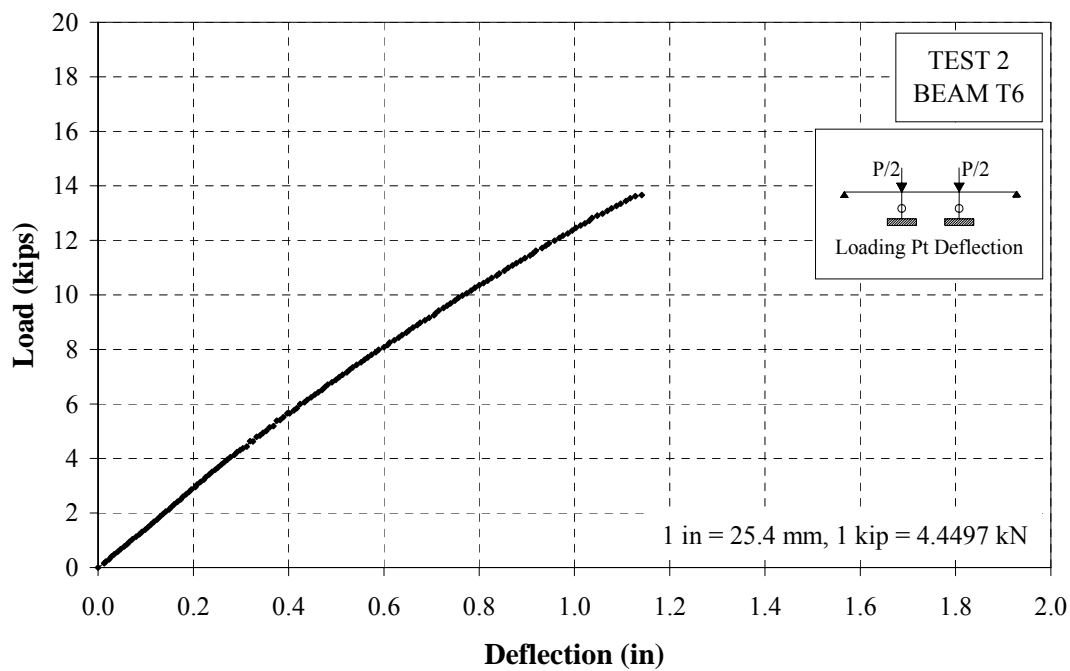


Figure D 14 Load vs. Loading Point Deflection - Beam T6 - Static Test 2

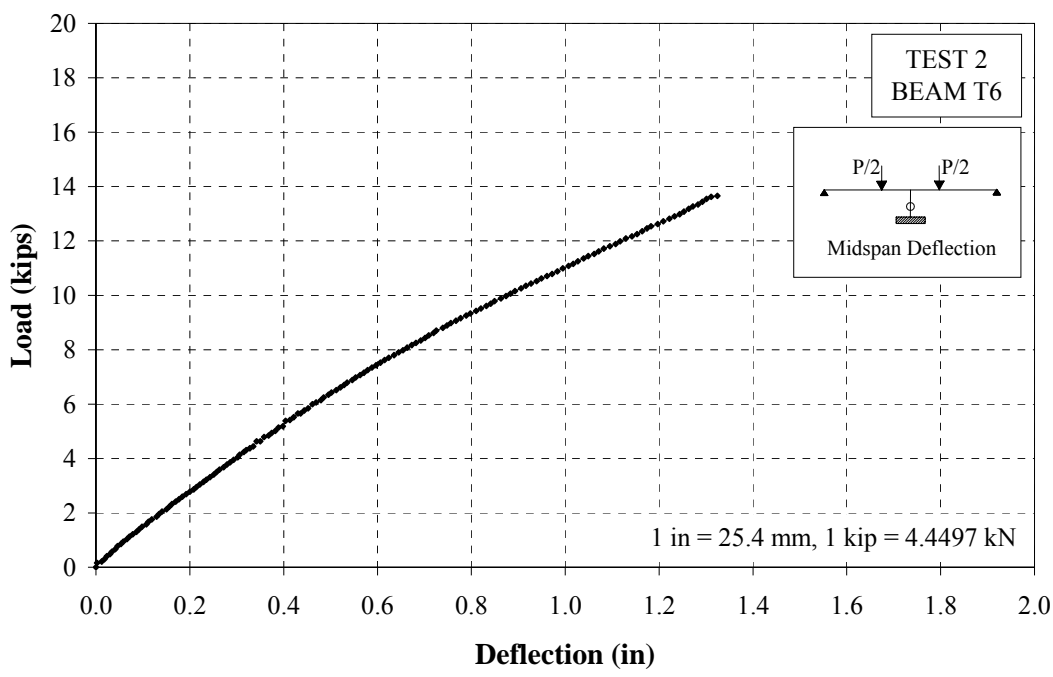


Figure D 15 Load vs. Midspan Deflection - Beam T6 - Static Test 2

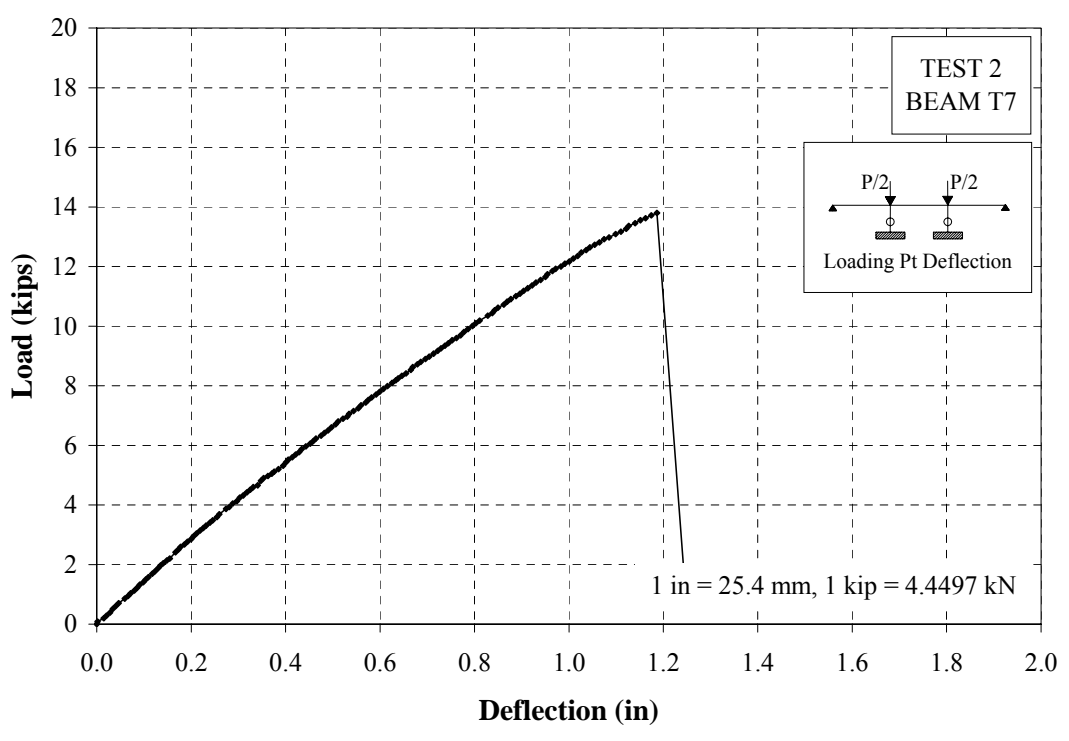


Figure D 16 Load vs. Loading Point Deflection - Beam T7 - Static Test 2

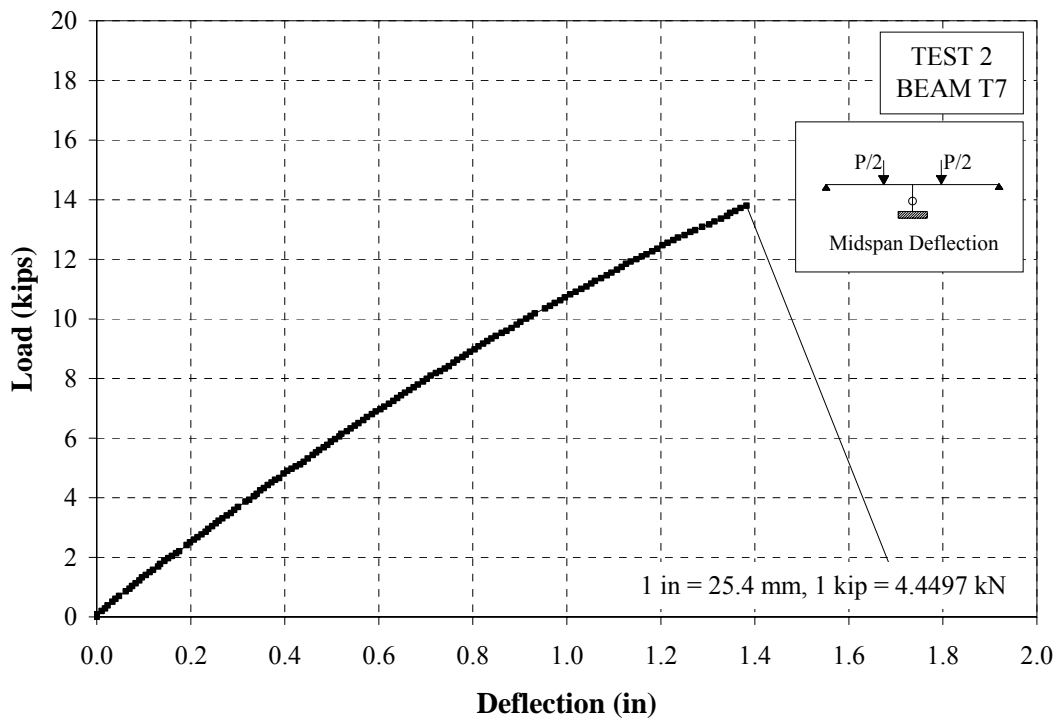


Figure D 17 Load vs. Midspan Deflection - Beam T7 - Static Test 2

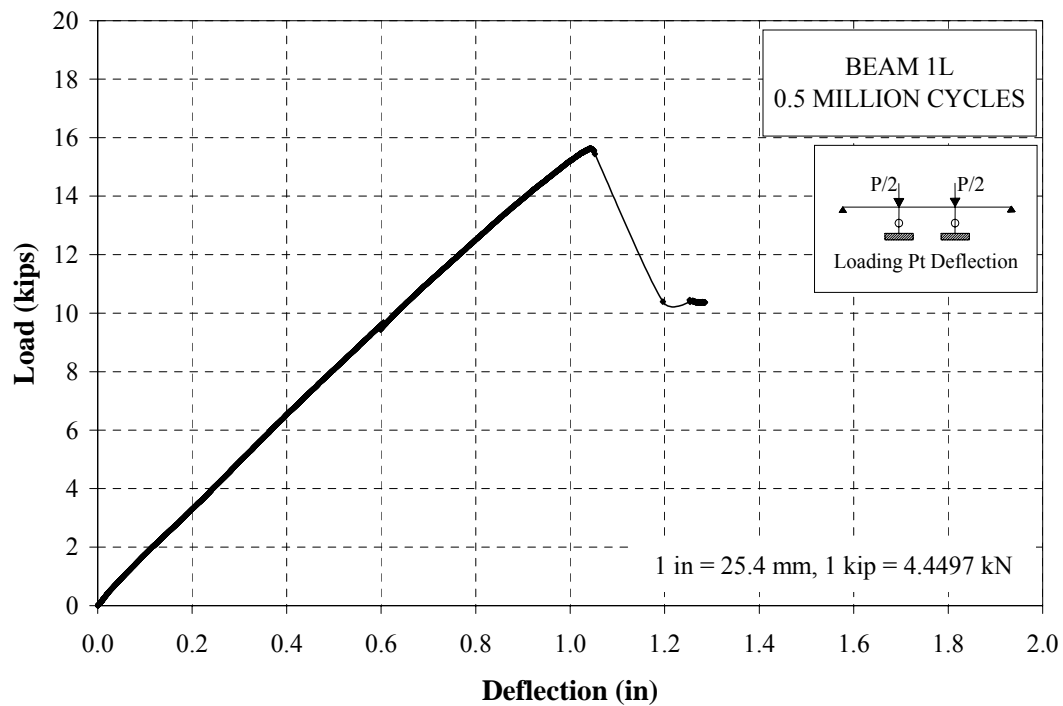


Figure D 18 Load vs. Loading Pt. Deflection - Beam 1L - Fatigue Test

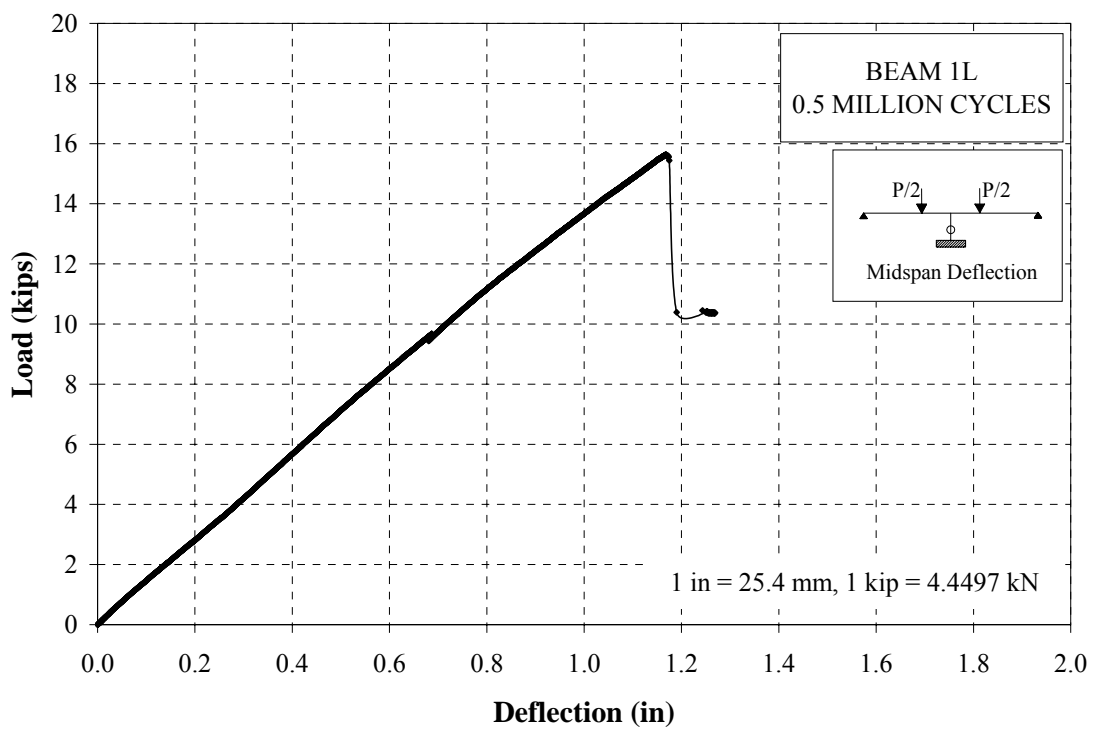


Figure D 19 Load vs. Midspan Deflection - Beam 1L - Fatigue Test

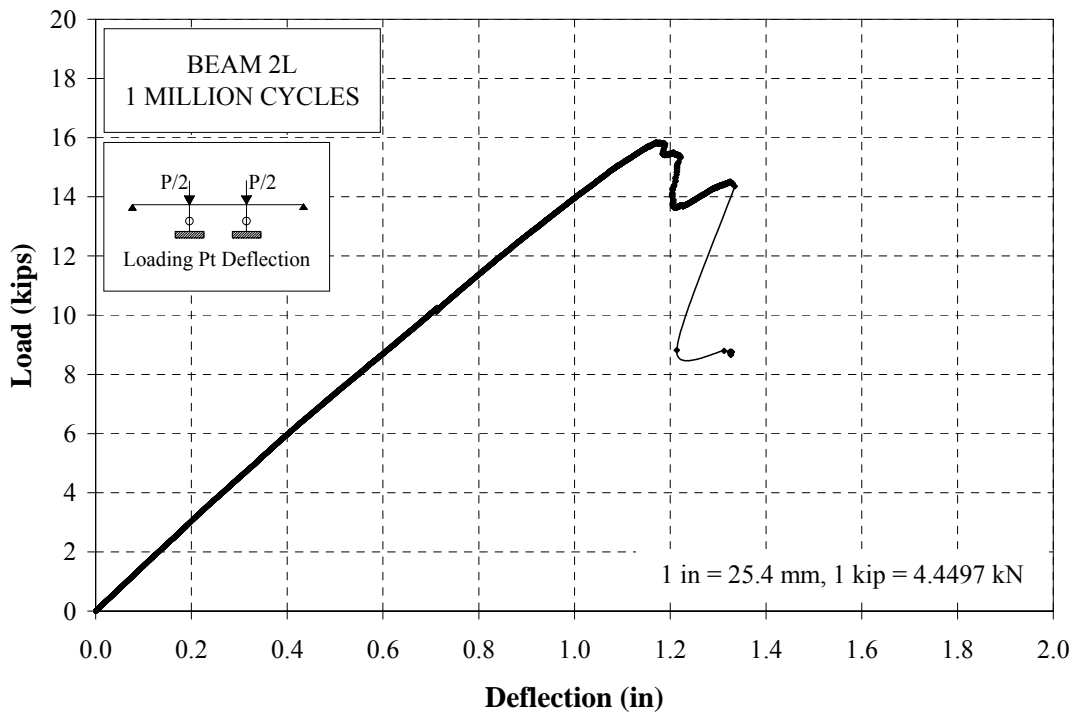


Figure D 20 Load vs. Loading Pt. Deflection - Beam 2L - Fatigue Test

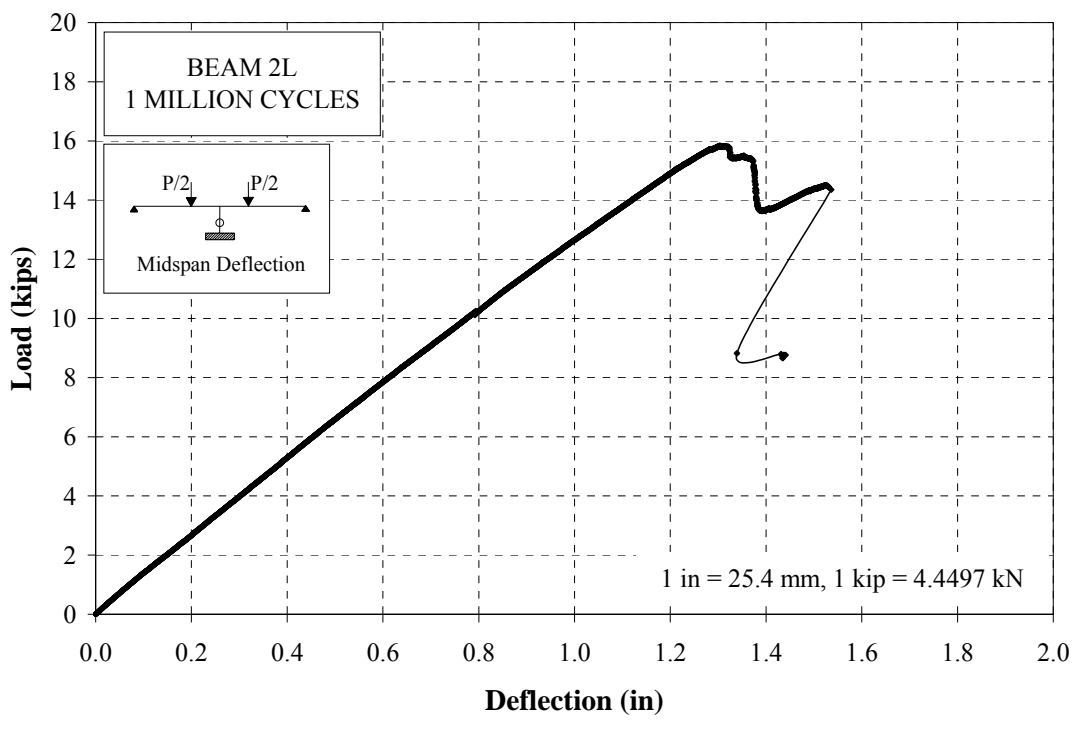


Figure D 21 Load vs. Midspan Deflection - Beam 2L - Fatigue Test

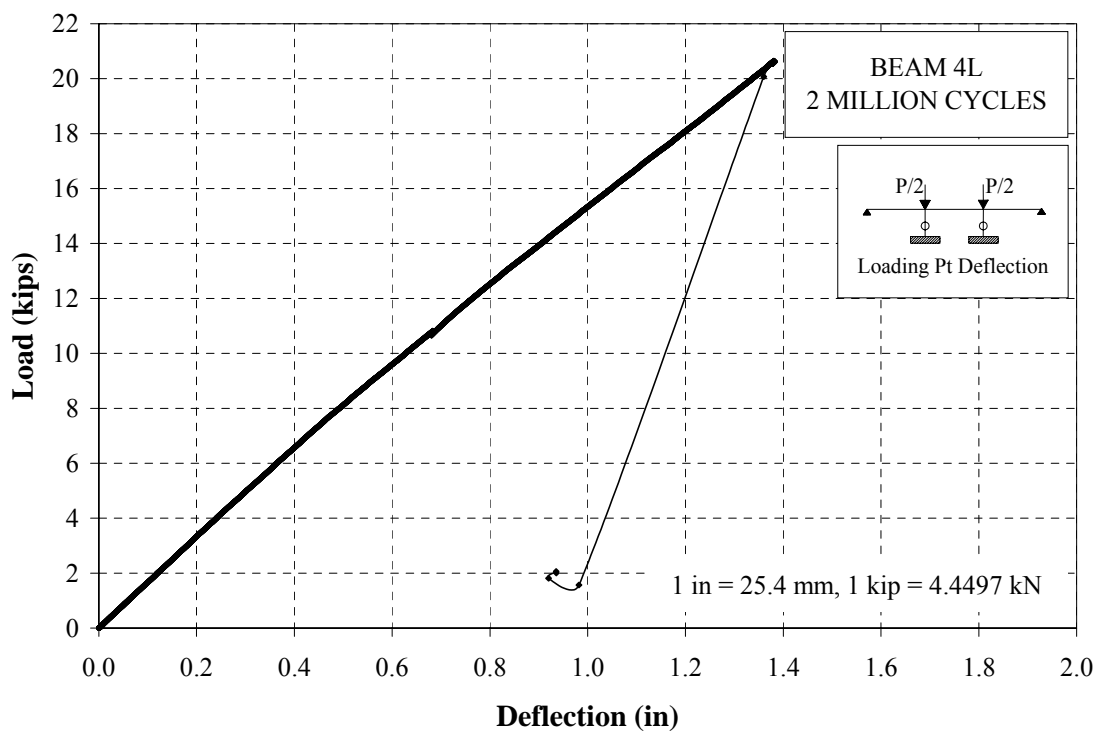


Figure D 22 Load vs. Loading Pt. Deflection - Beam 4L - Fatigue Test

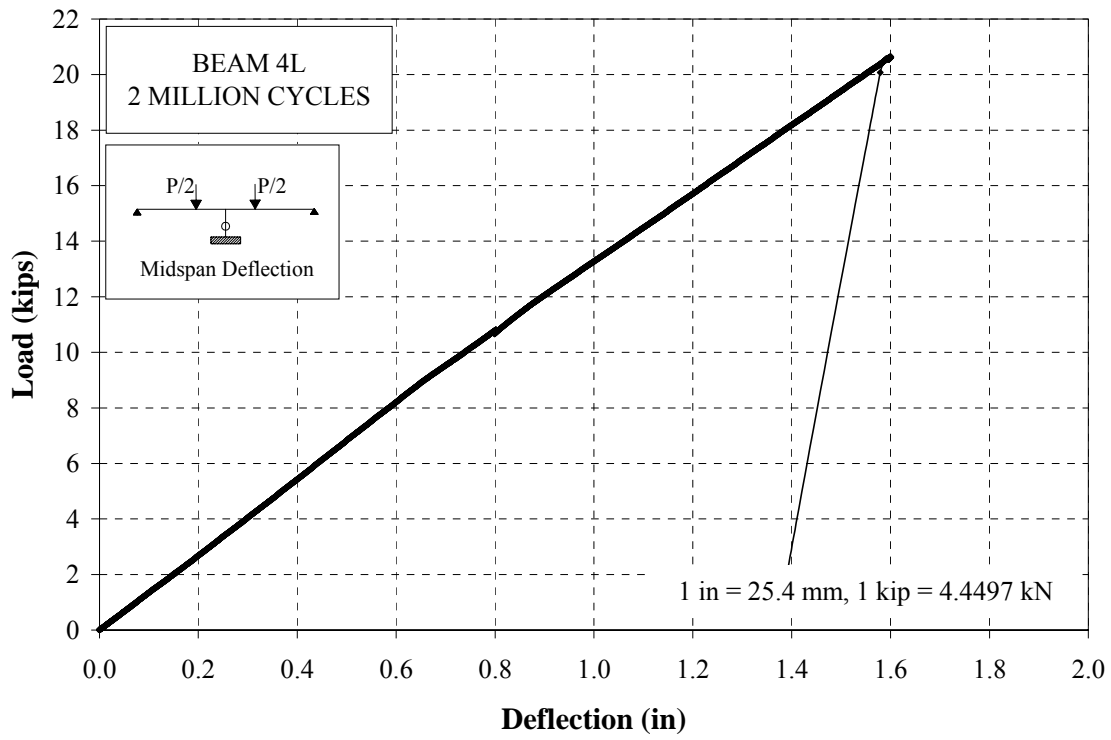


Figure D 23 Load vs. Midspan Deflection - 4L - Fatigue Test

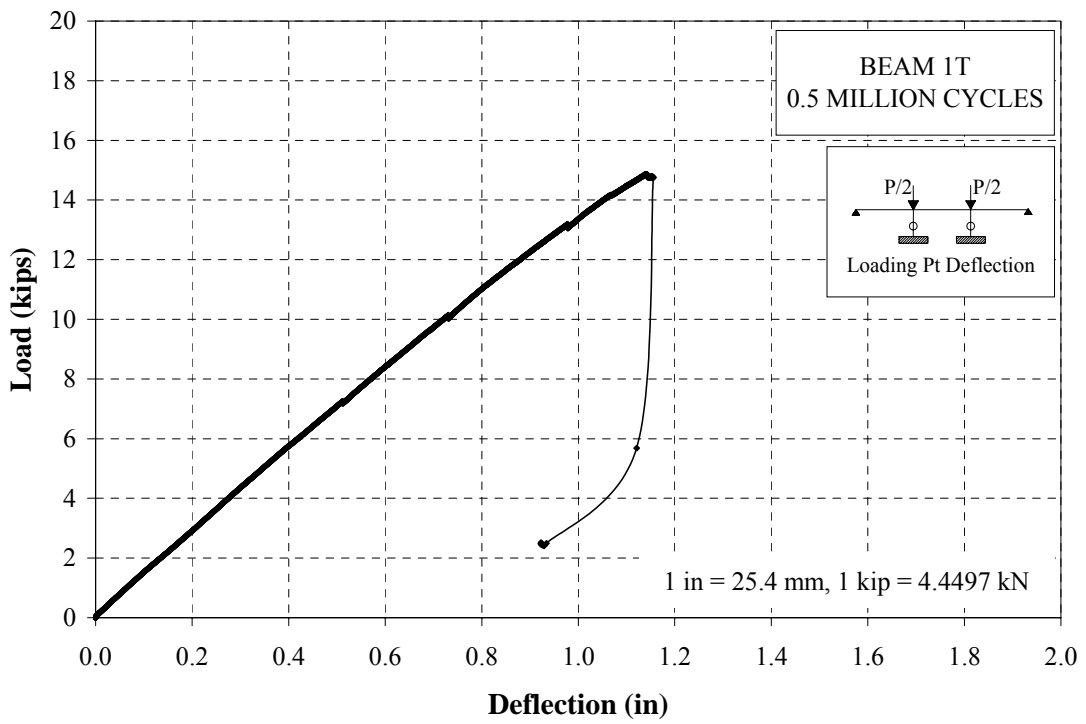


Figure D 24 Load vs. Loading Pt. Deflection - Beam 1T - Fatigue Test

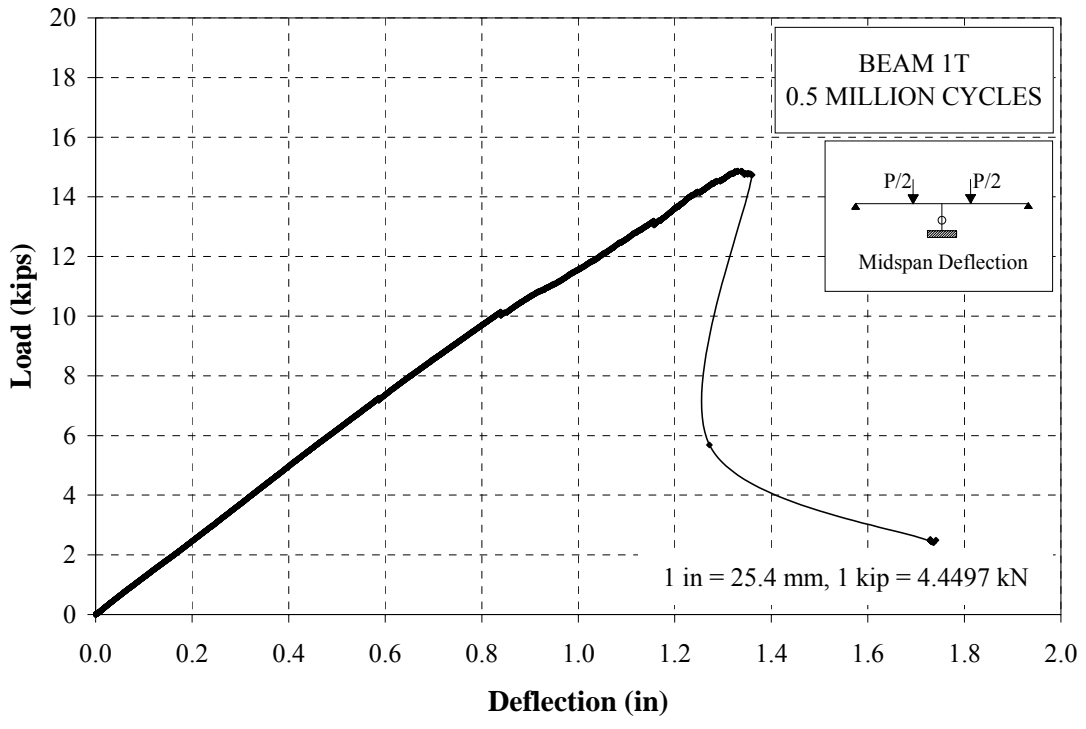


Figure D 25 Load vs. Midspan Deflection - Beam 1T - Fatigue Test

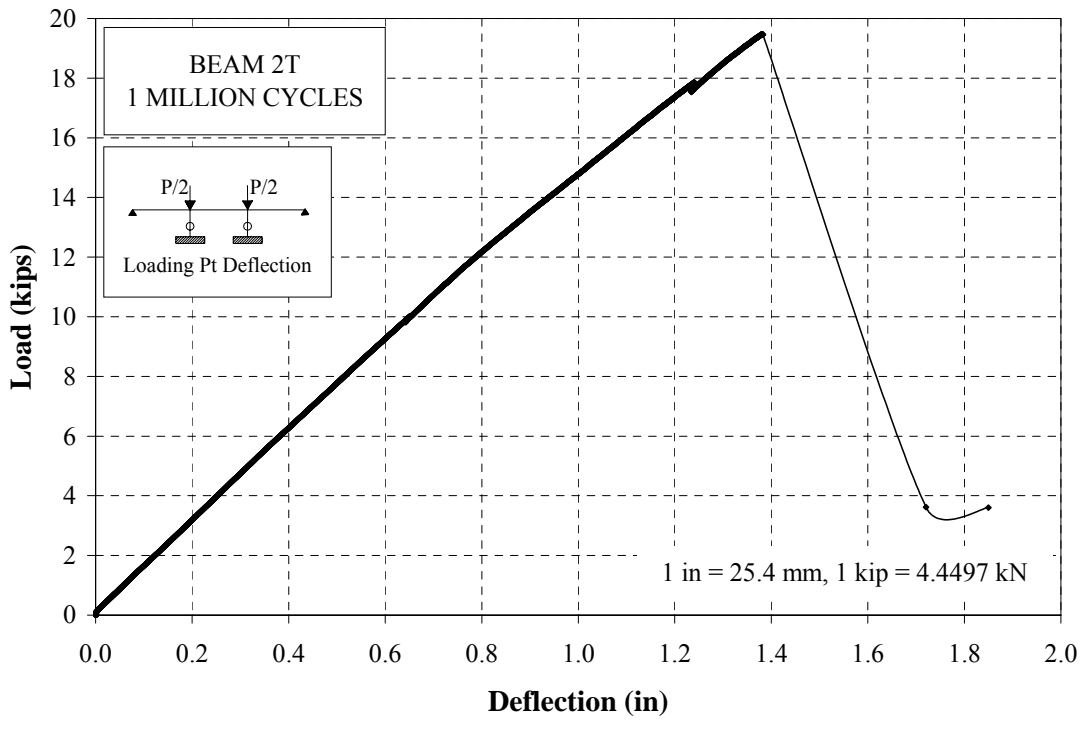


Figure D 26 Load vs. Loading Pt. Deflection - Beam 2T - Fatigue Test

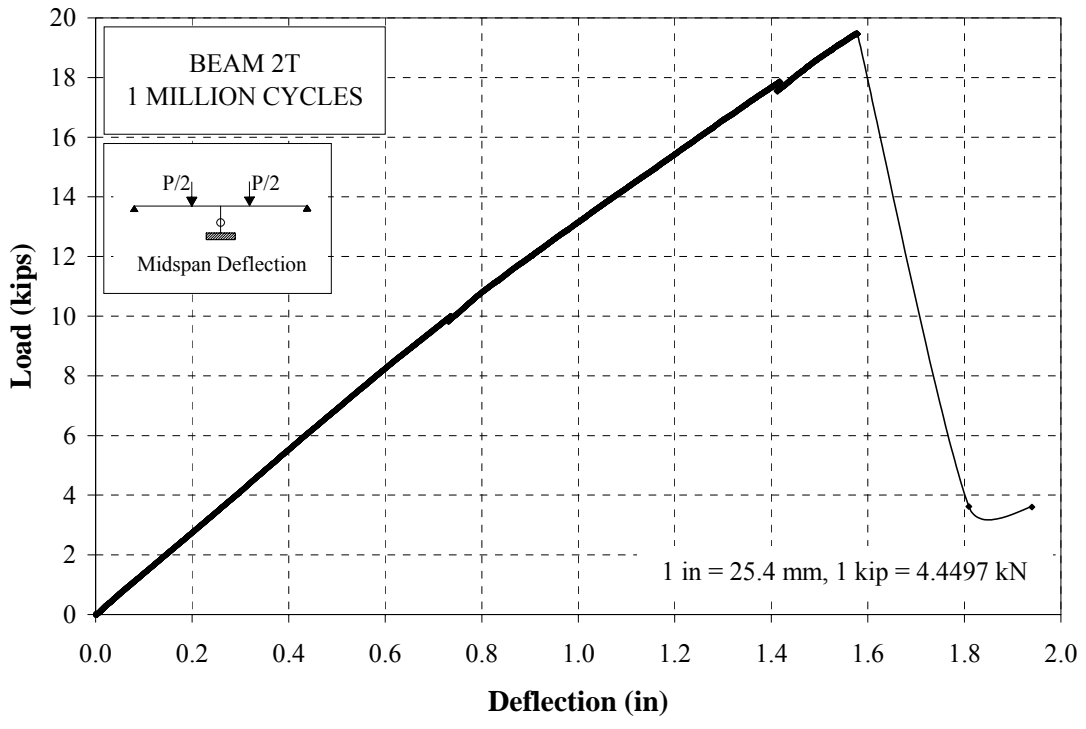


Figure D 27 Load vs. Midspan Deflection - Beam 2T - Fatigue Test

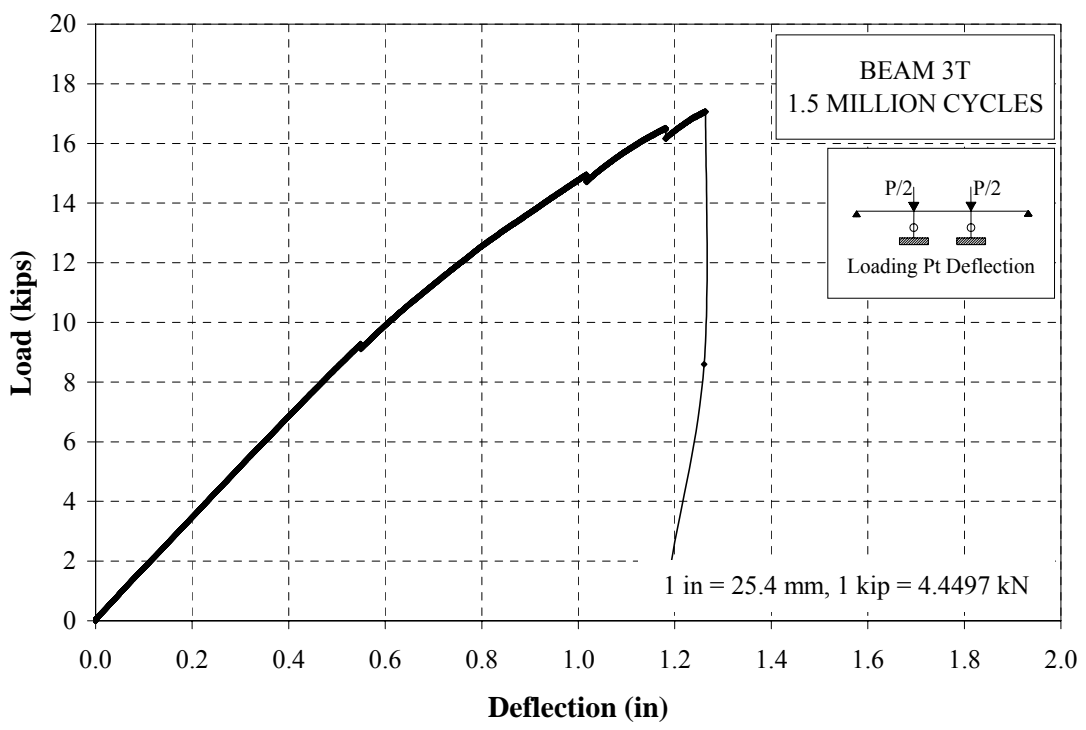


Figure D 28 Load vs. Loading Pt. Deflection - Beam 3T - Fatigue Test

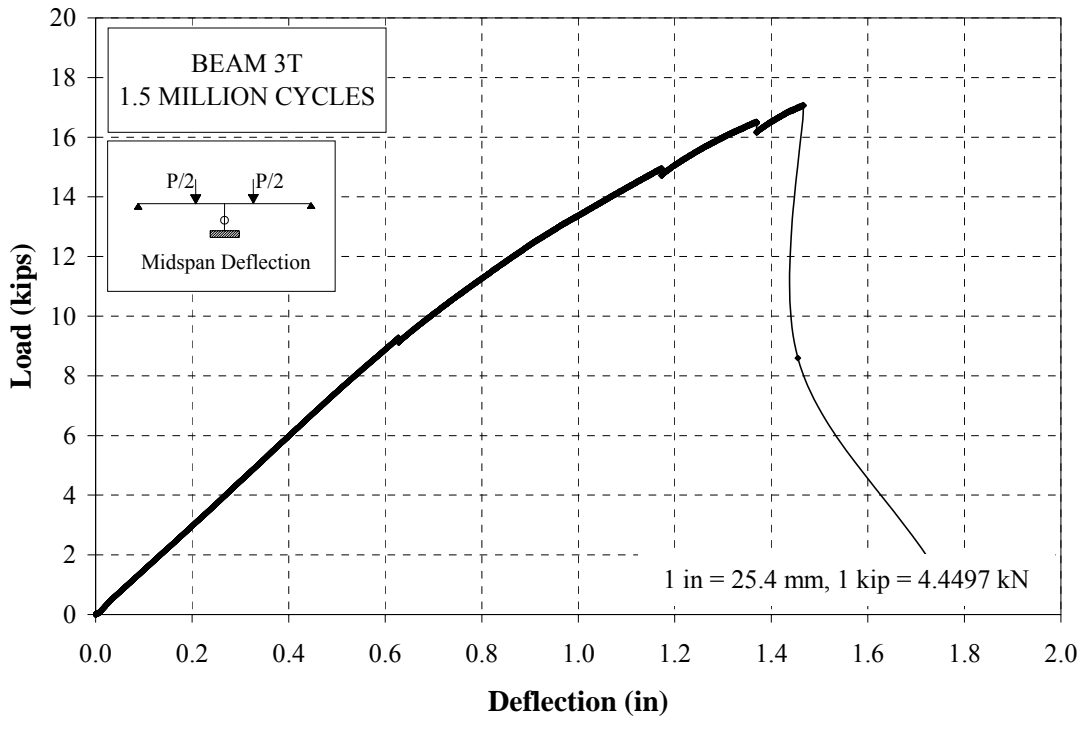


Figure D 29 Load vs. Midspan Deflection - Beam 3T - Fatigue Test

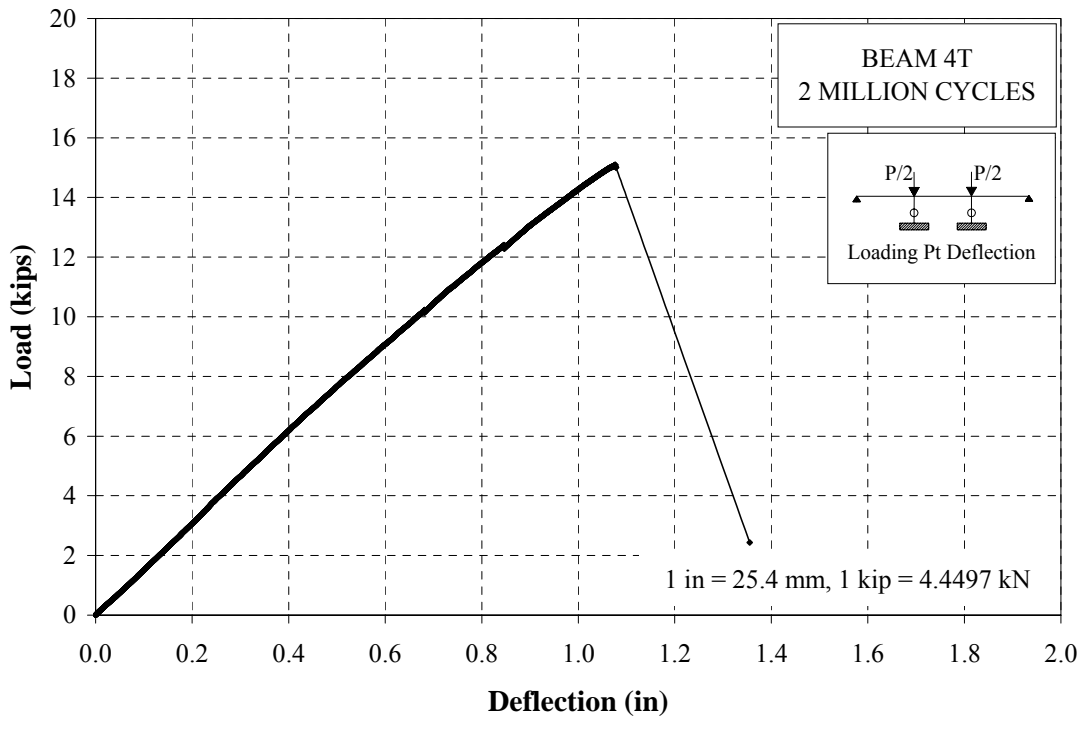


Figure D 30 Load vs. Loading Pt. Deflection - Beam 4T - Fatigue Test

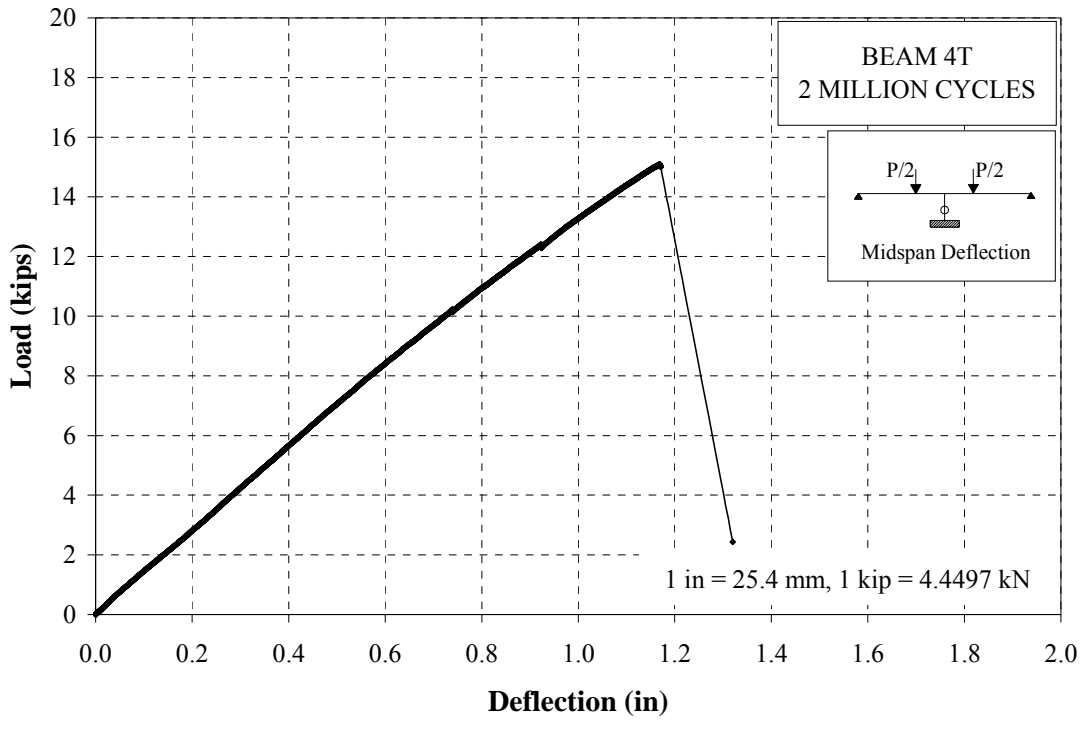


Figure D 31 Load vs. Midspan Deflection - Beam 4T - Fatigue Test

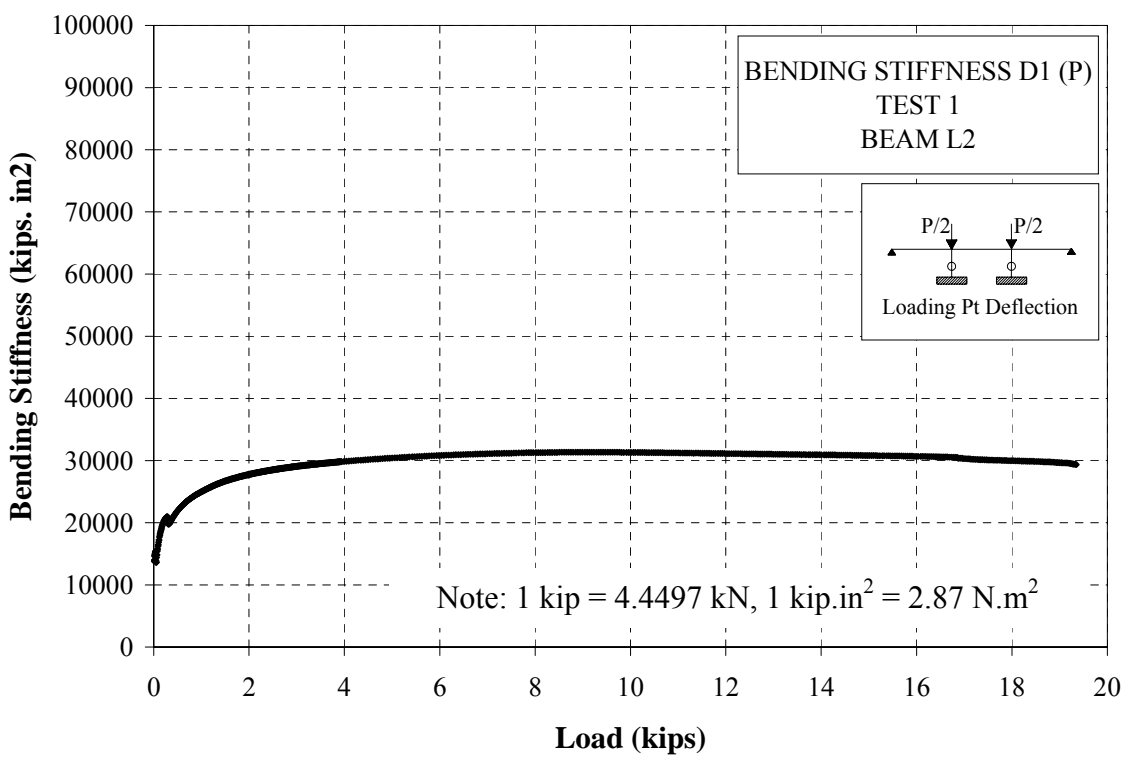


Figure D 32 Bending Stiffness D1 - Beam L2 - Static Test 1

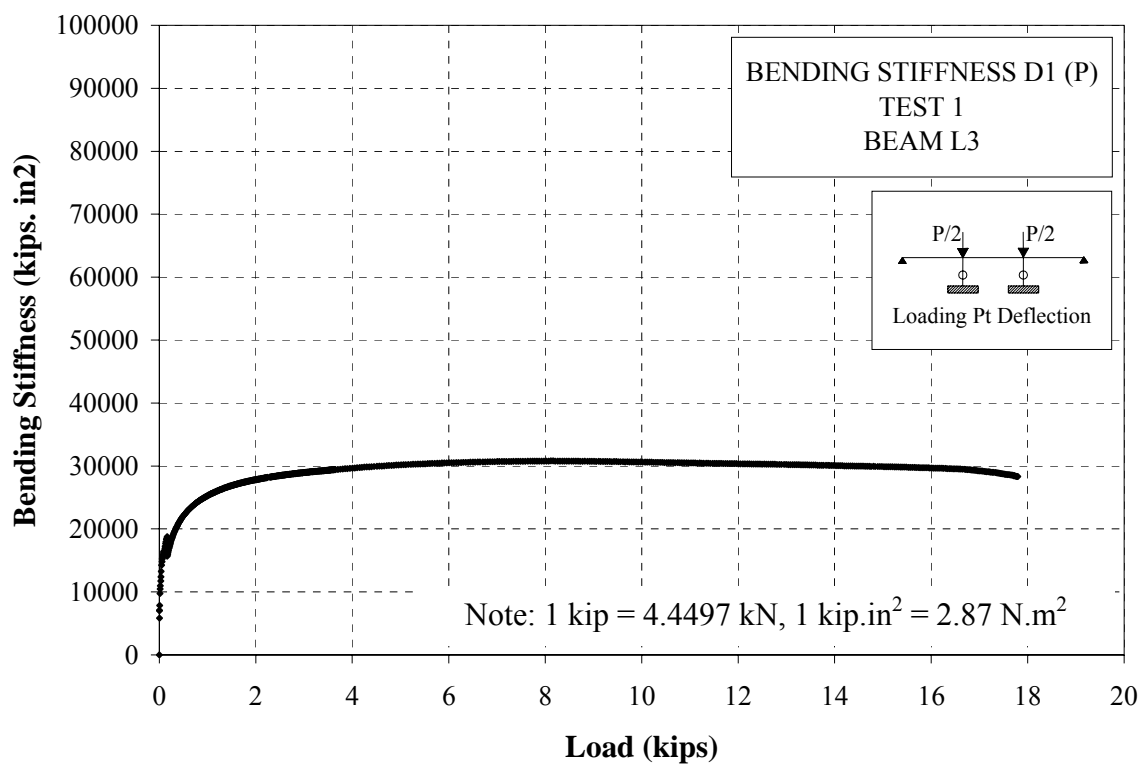


Figure D 33 Bending Stiffness D1 - Beam L3 - Static Test 1

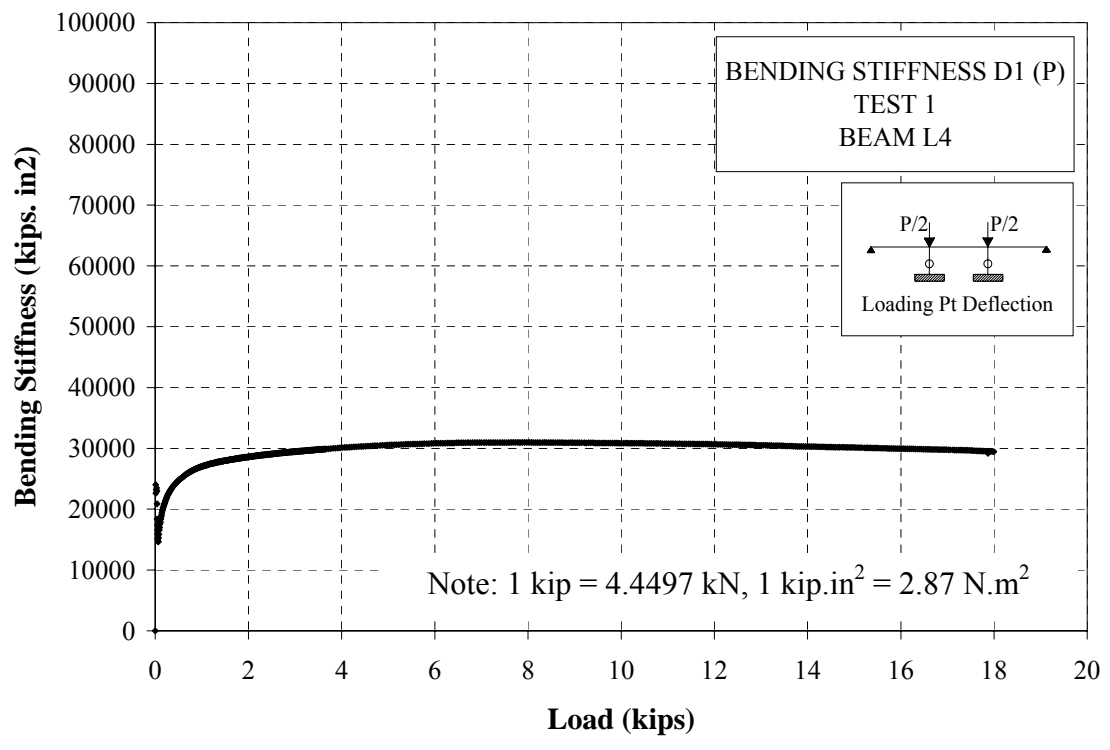


Figure D 34 Bending Stiffness D1 - Beam L4 - Static Test 1

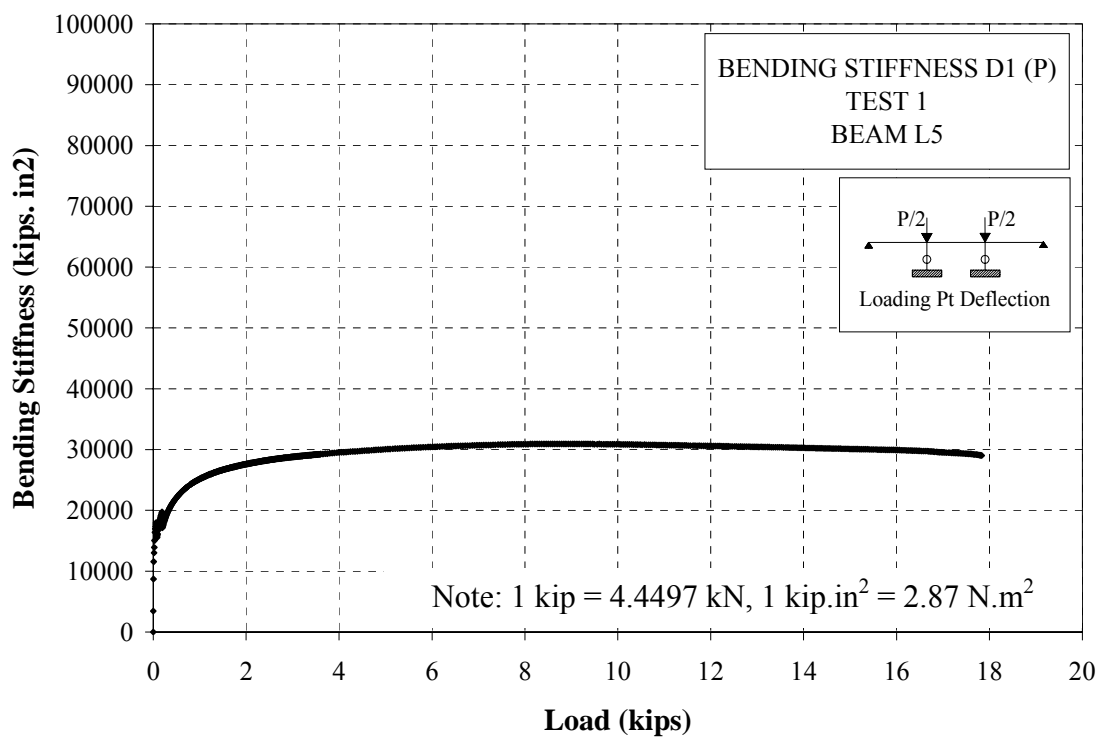


Figure D 35 Bending Stiffness D1 - Beam L5 - Static Test 1

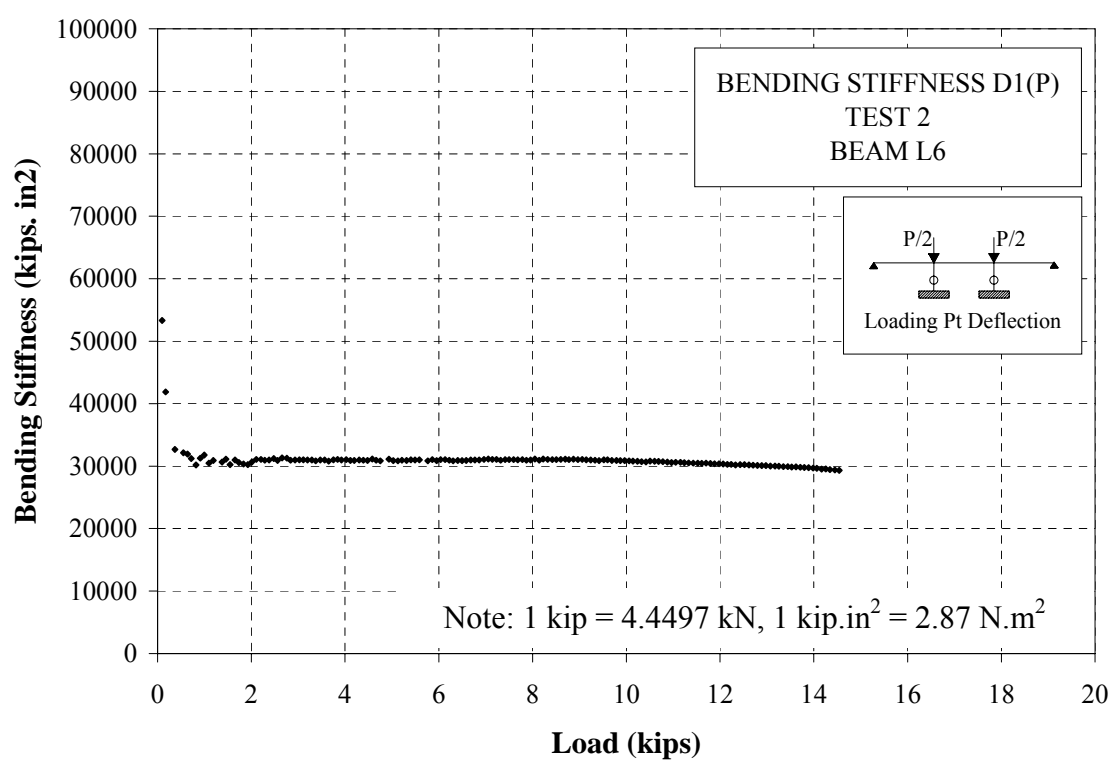


Figure D 36 Bending Stiffness D1 - Beam L6 - Static Test 2

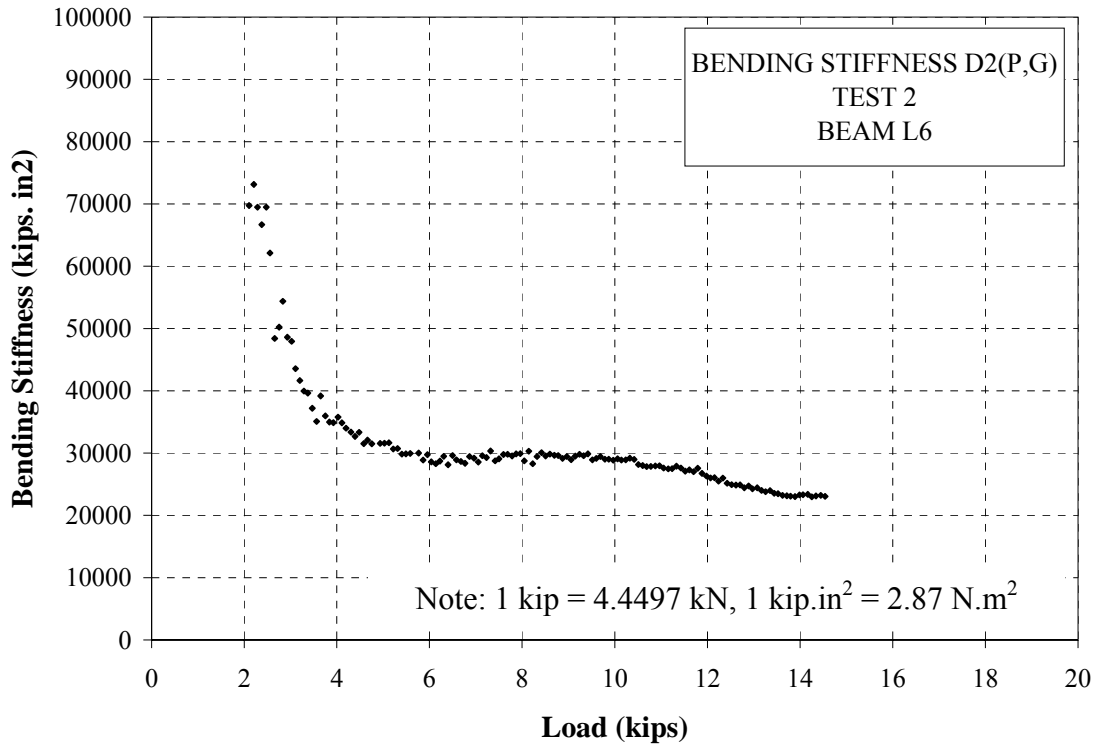


Figure D 37 Bending Stiffness D2 - Beam L6 - Static Test 2

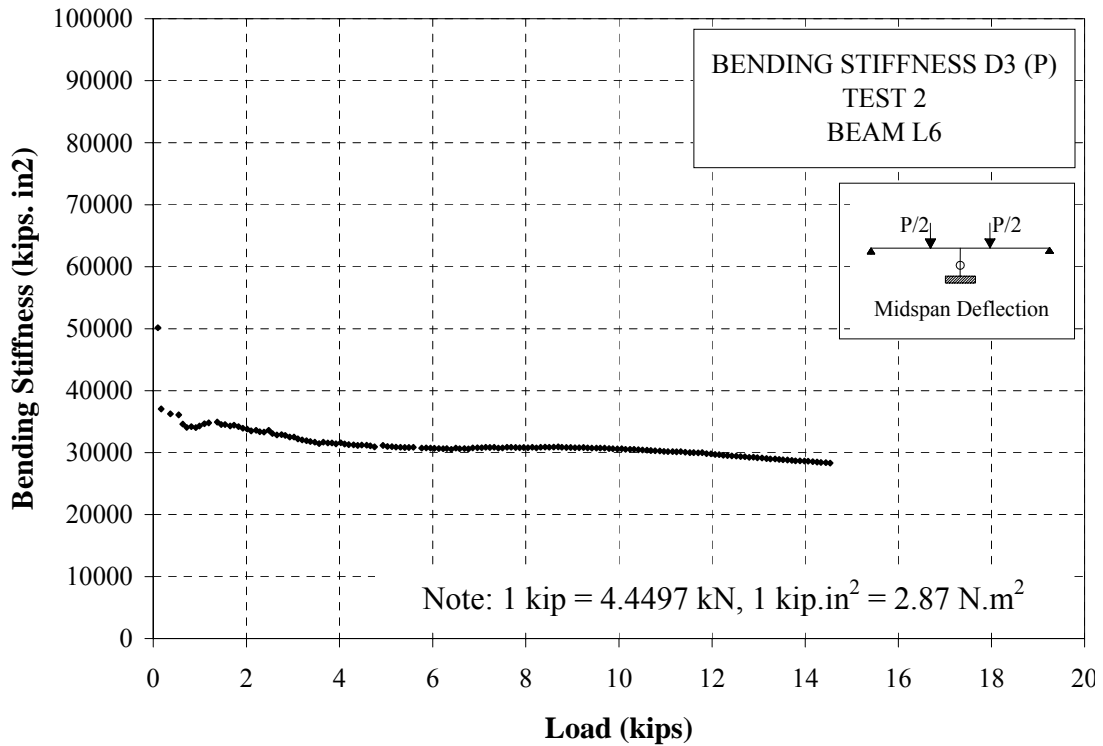


Figure D 38 Bending Stiffness D3 - Beam L6 - Static Test 2

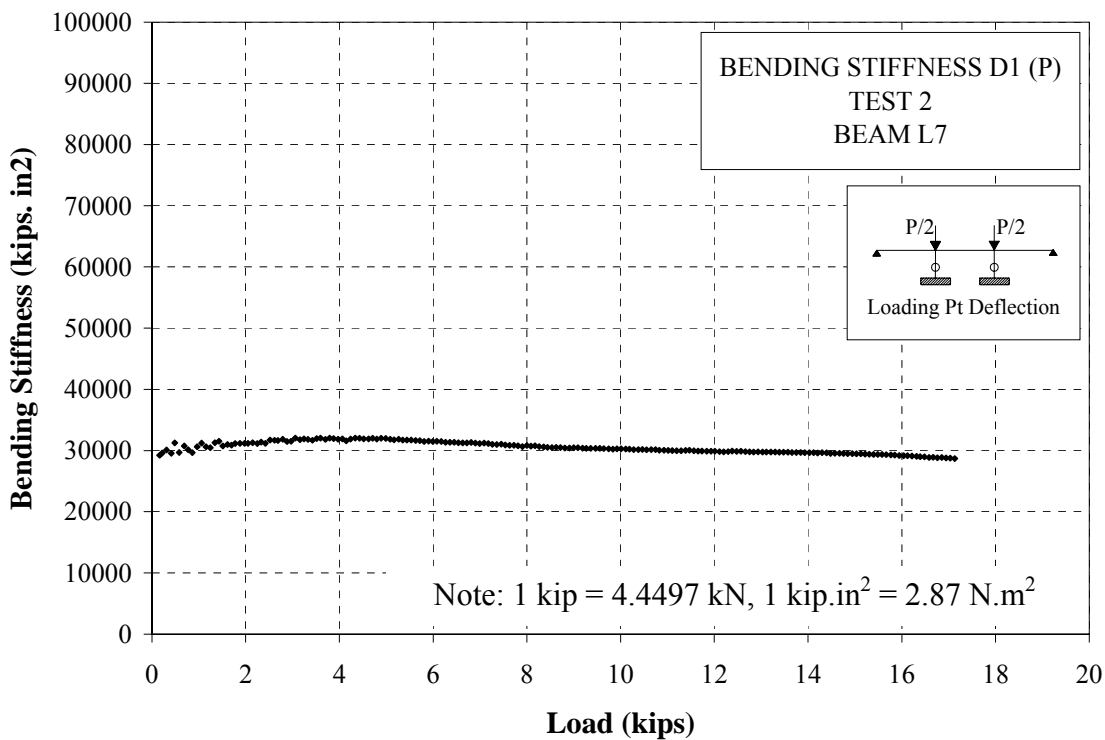


Figure D 39 Bending Stiffness D1 - Beam L7 - Static Test 2

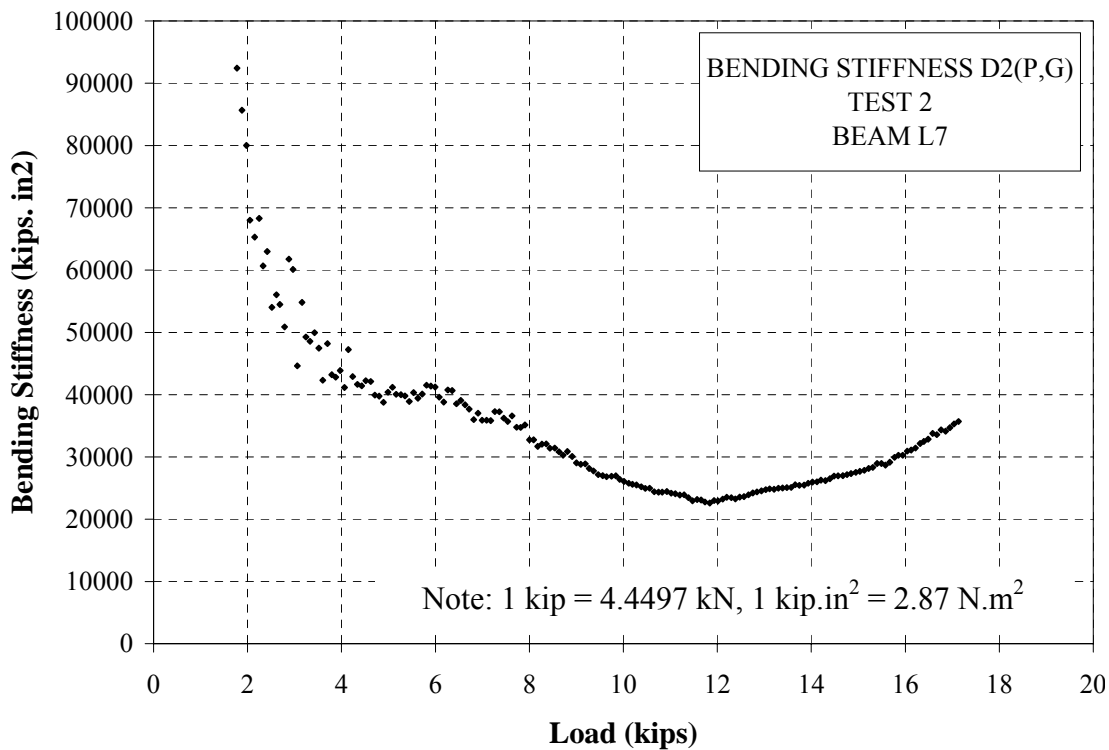


Figure D 40 Bending Stiffness D2 - Beam L7 - Static Test 2

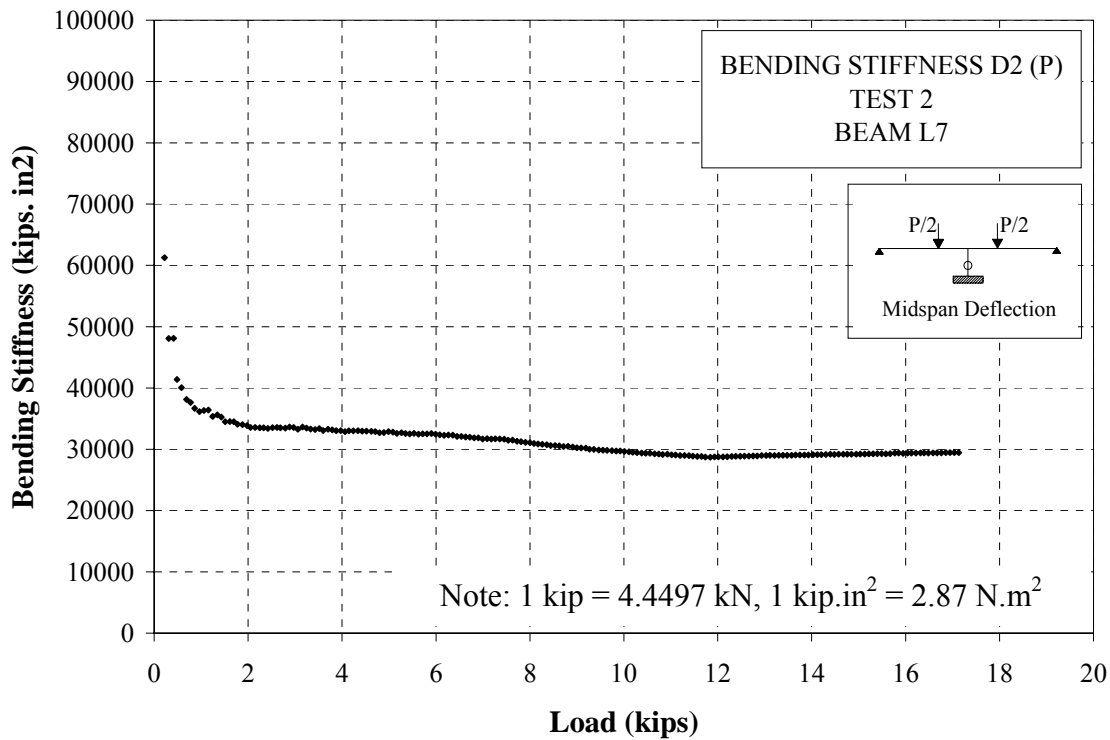


Figure D 41 Bending Stiffness D3 - Beam L7 - Static Test 2

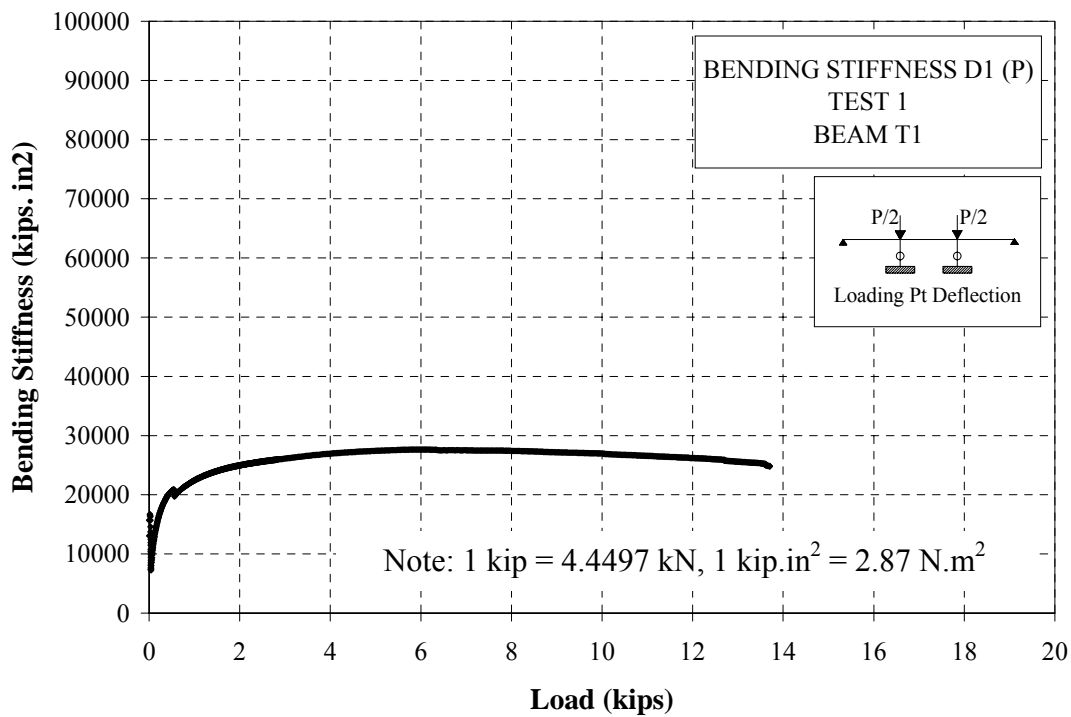


Figure D 42 Bending Stiffness D1 - Beam T1 - Static Test 1

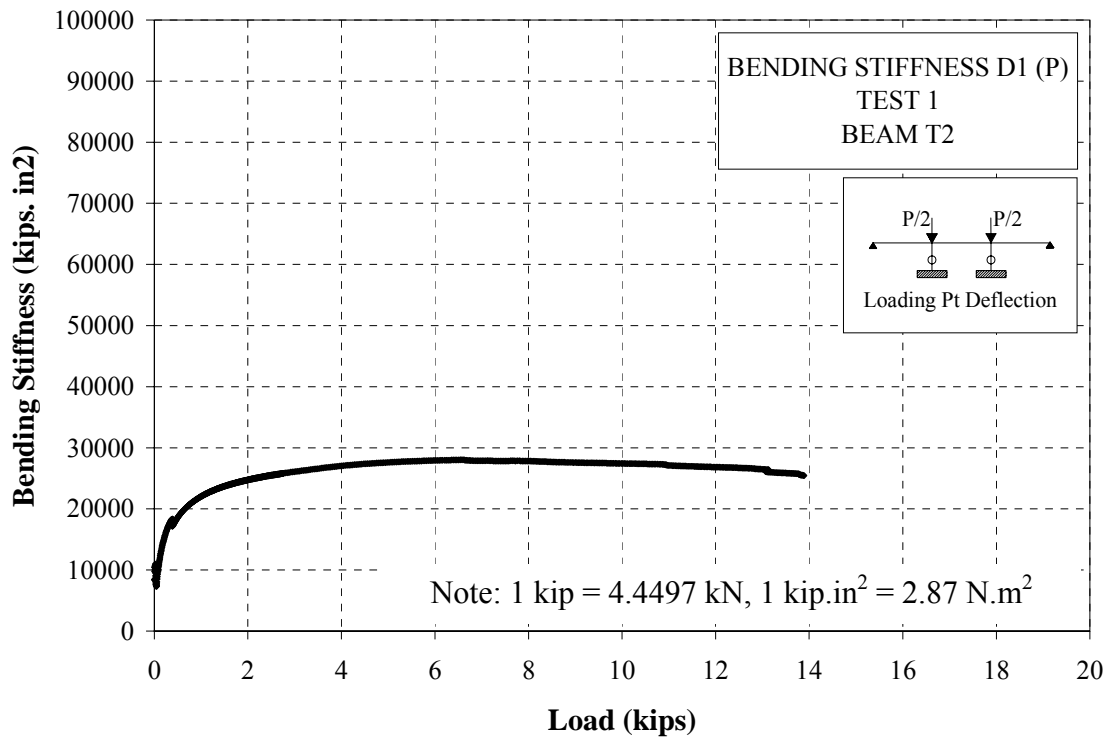


Figure D 43 Bending Stiffness D1 - Beam T2 - Static Test 1

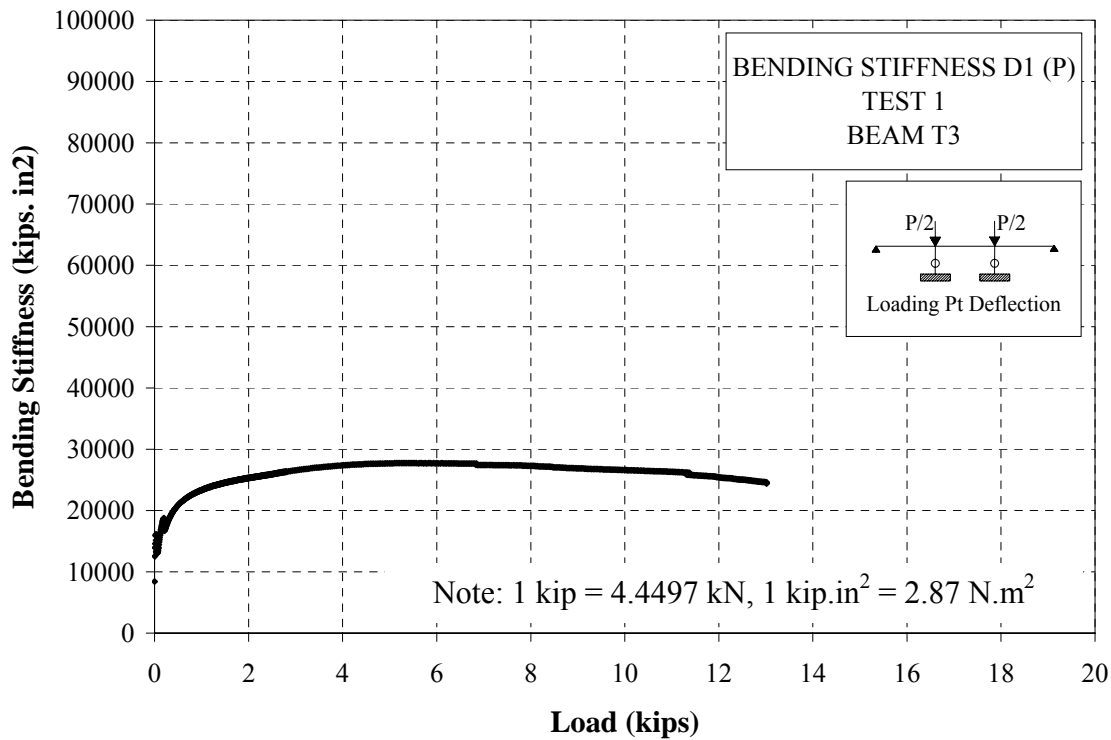


Figure D 44 Bending Stiffness D1 - Beam T3 - Static Test 1

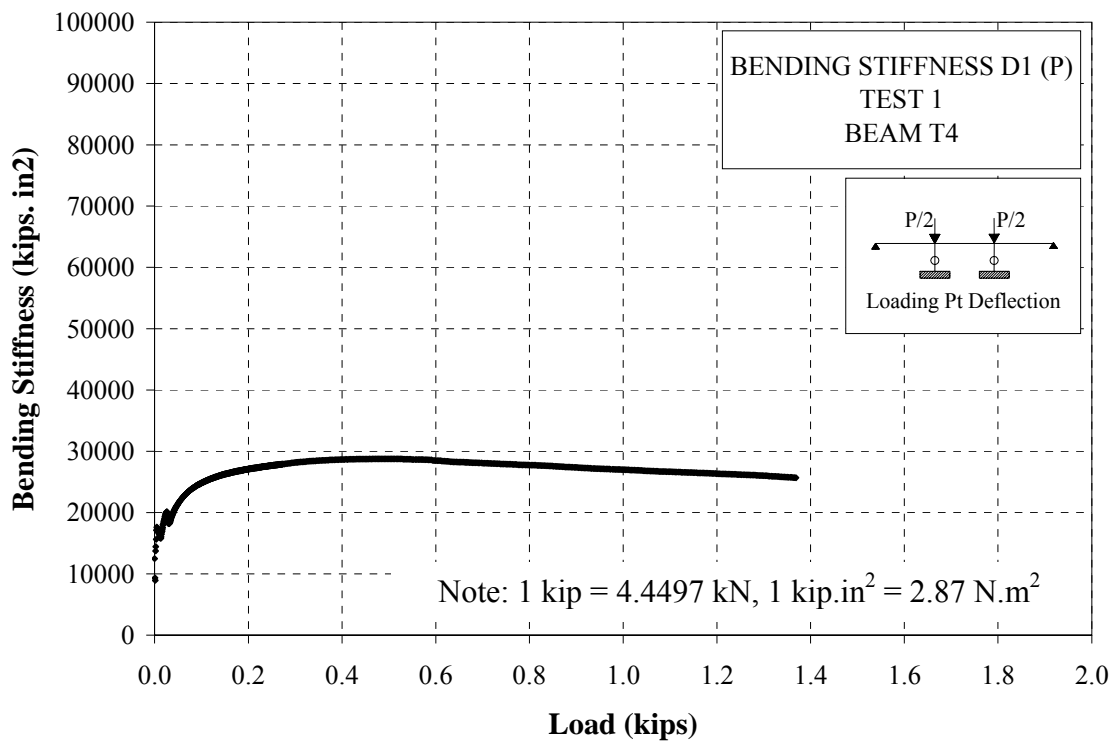


Figure D 45 Bending Stiffness D1 - Beam T4 - Static Test 1

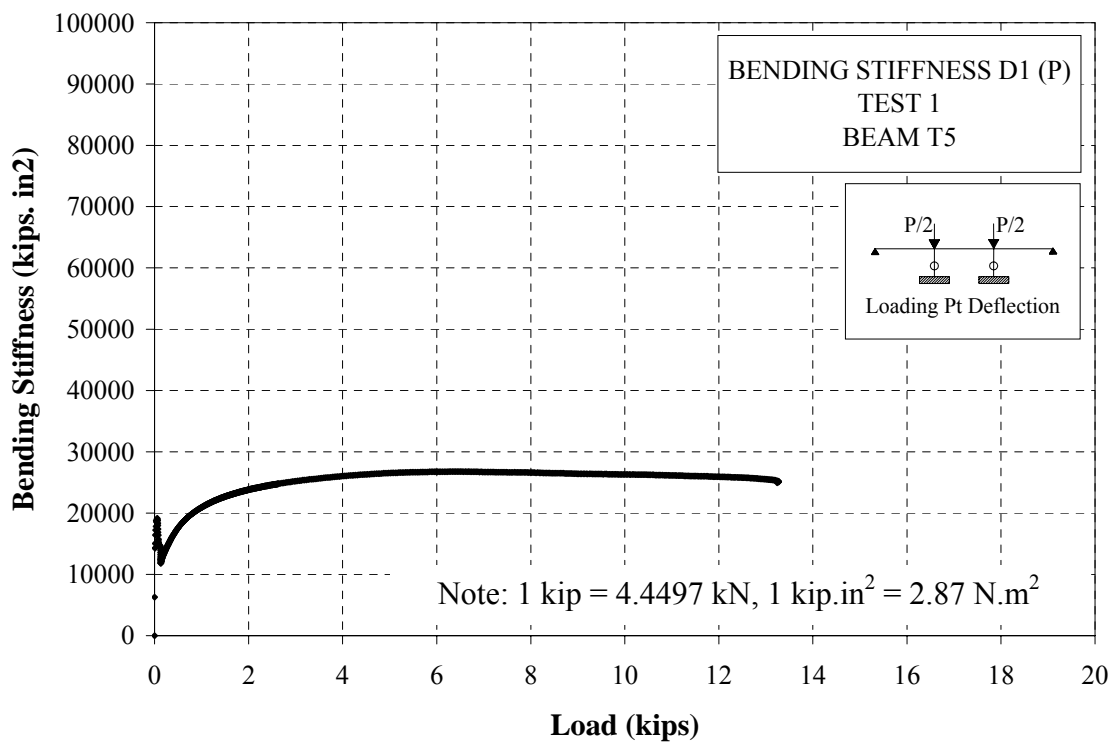


Figure D 46 Bending Stiffness D1 - Beam T5 - Static Test 1

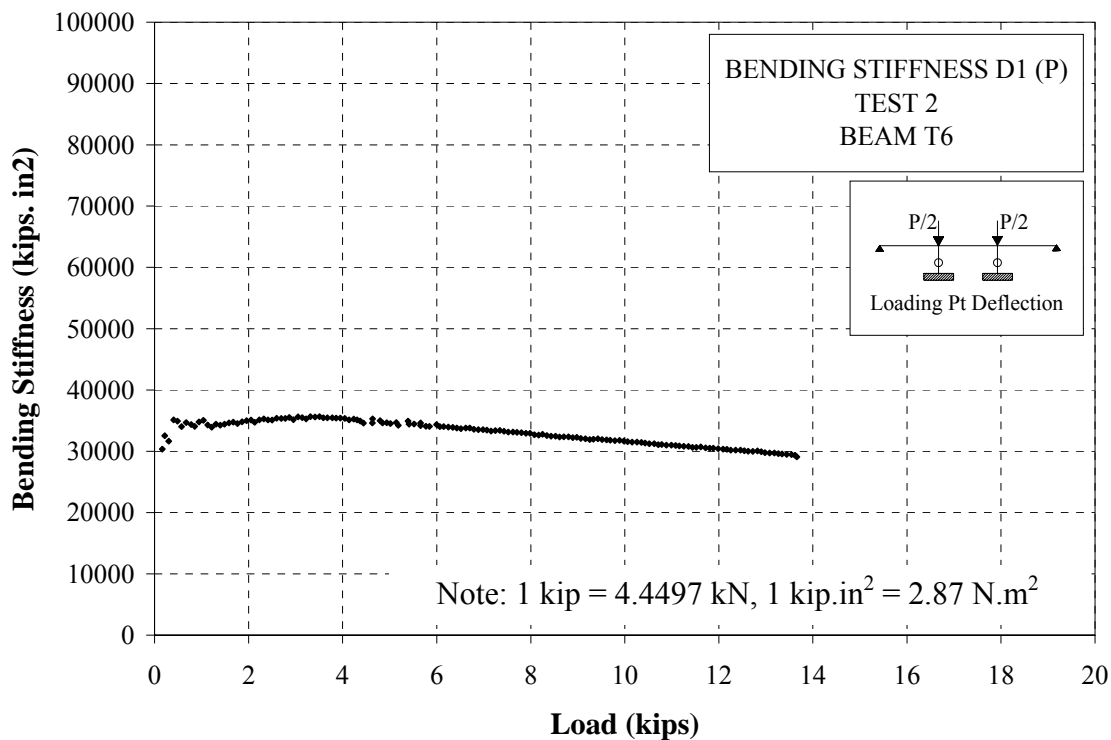


Figure D 47 Bending Stiffness D1 - Beam T6 - Static Test 2

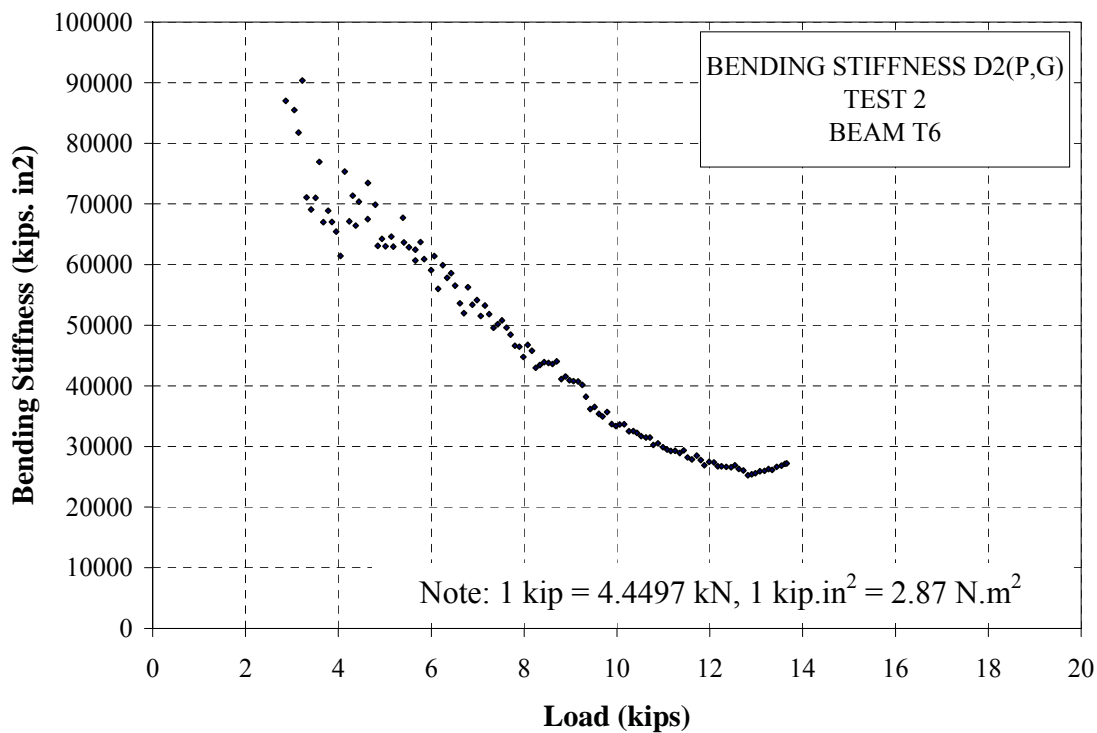


Figure D 48 Bending Stiffness D2 - Beam T6 - Static Test 2

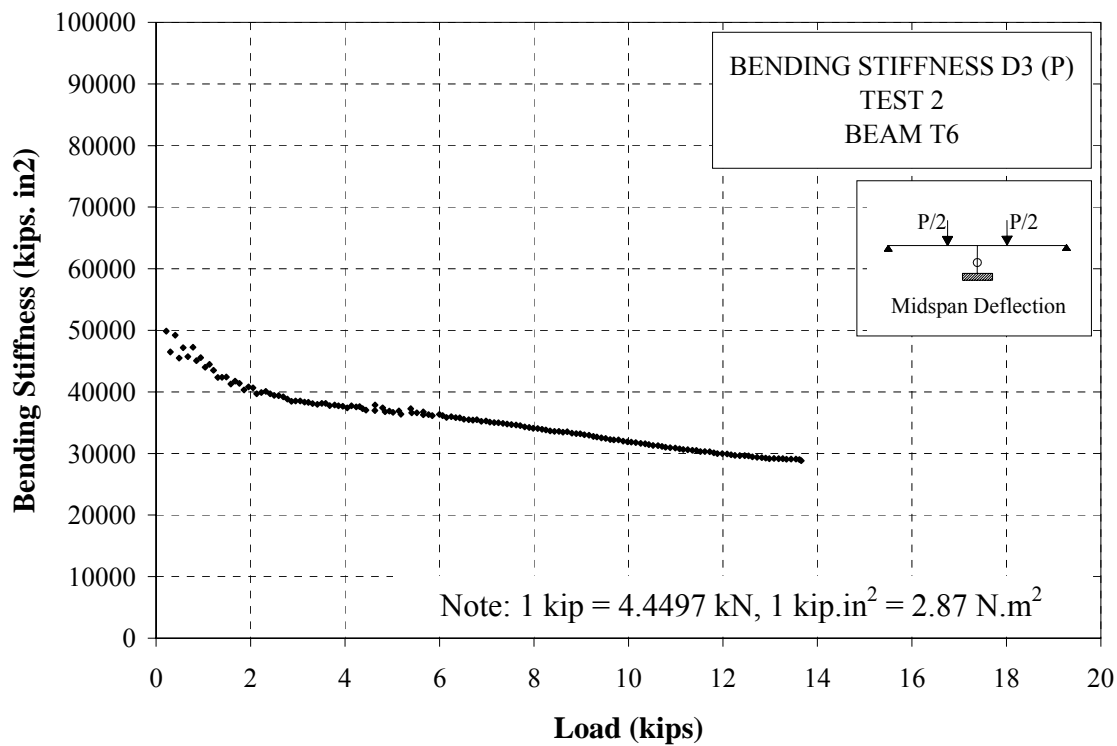


Figure D 49 Bending Stiffness D3 - Beam T6 - Static Test 2

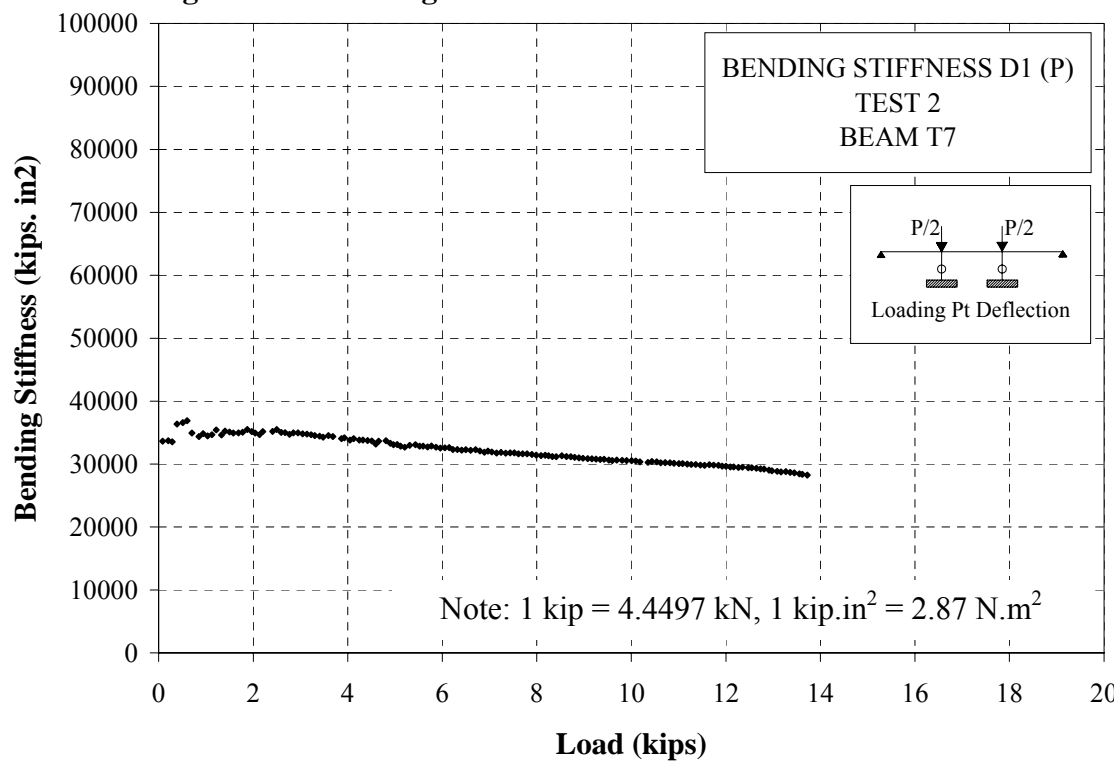


Figure D 50 Bending Stiffness D1 - Beam T7 - Static Test 2

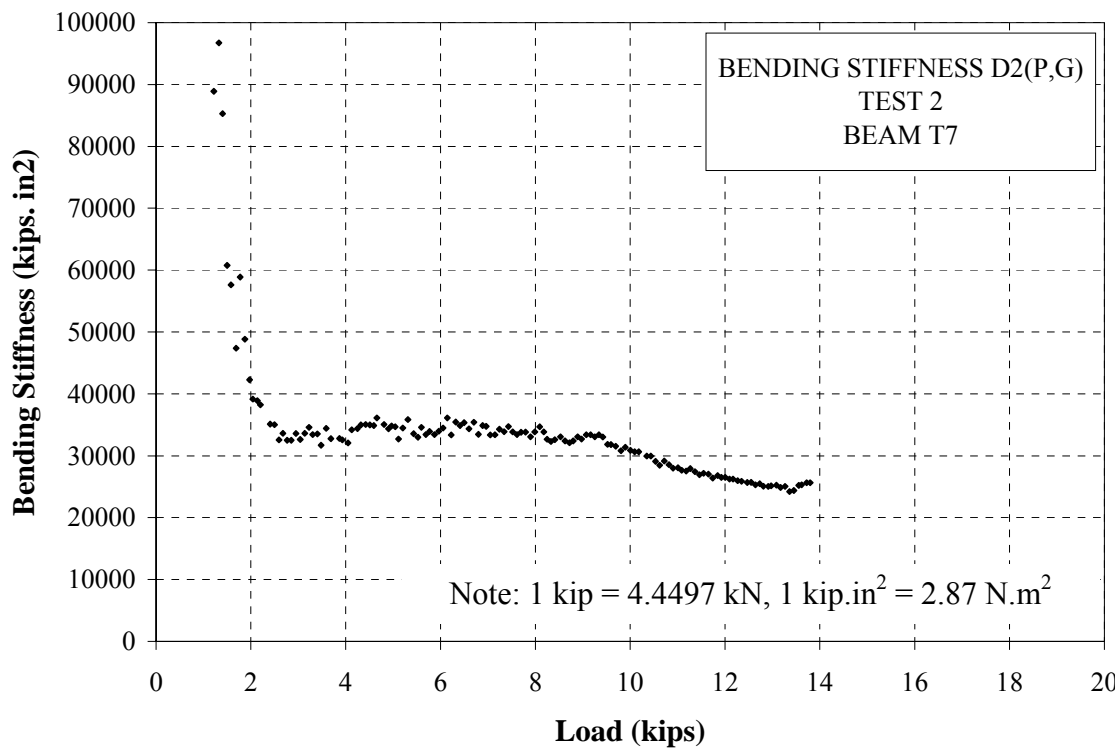


Figure D 51 Bending Stiffness D2 - Beam T7 - Static Test 2

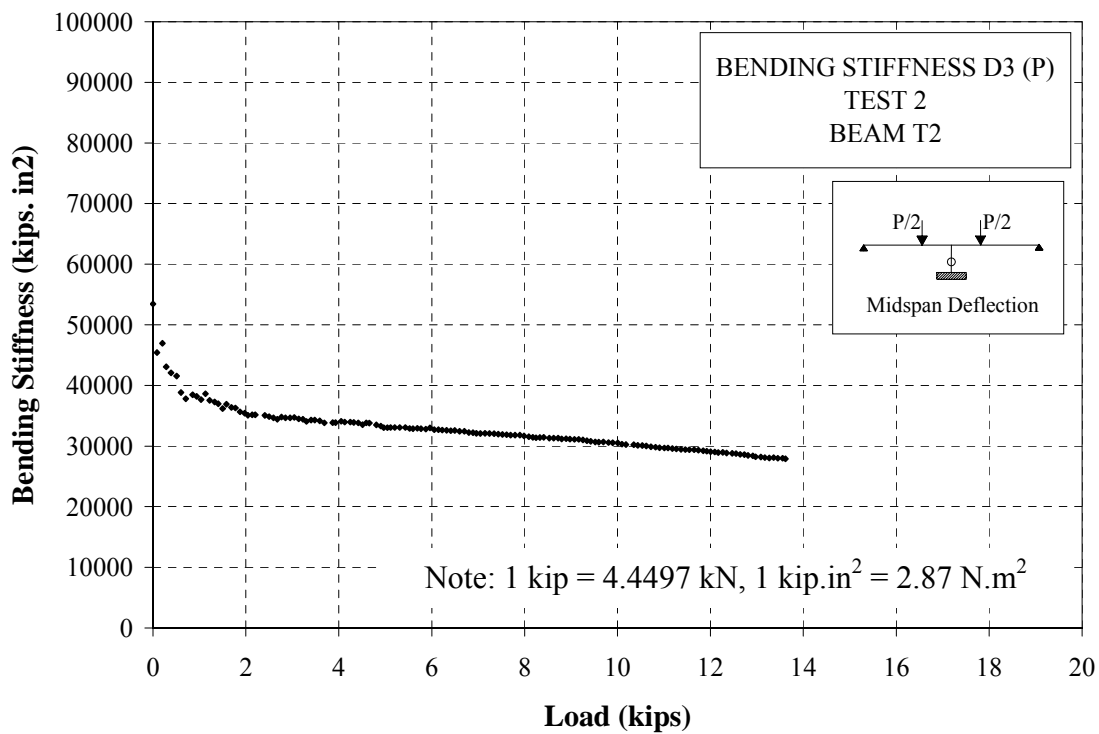


Figure D 52 Bending Stiffness D3 - Beam T7 - Static Test 2

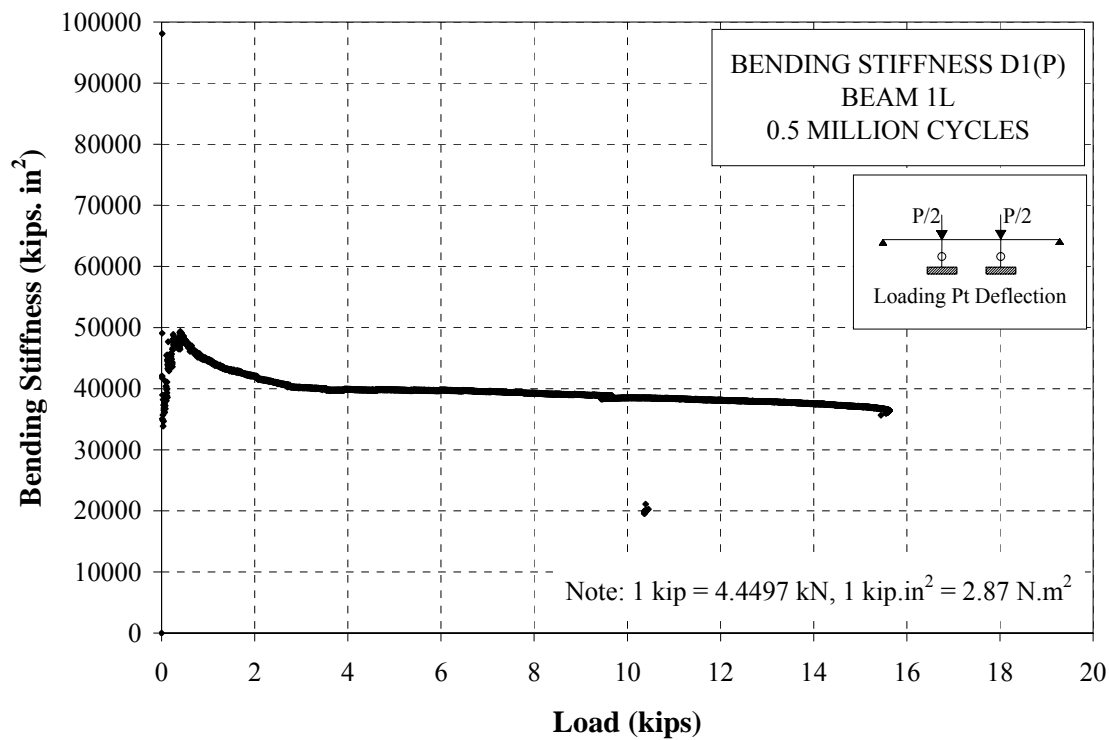


Figure D 53 Residual Bending Stiffness D1 - Beam 1L

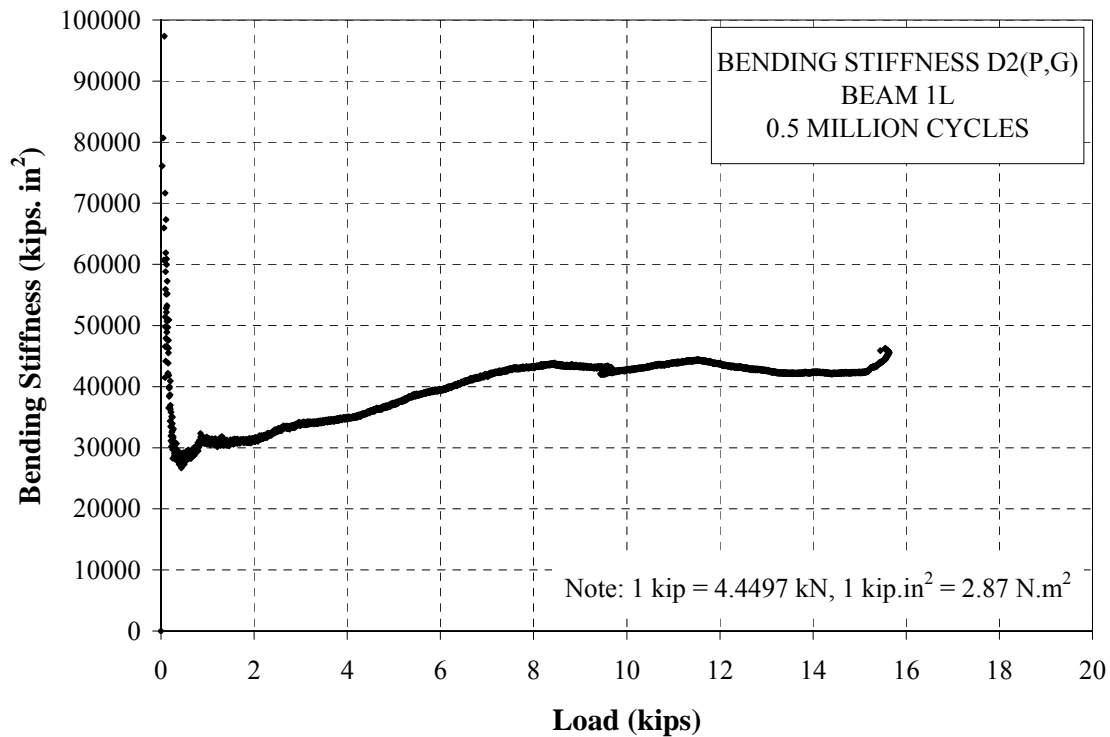


Figure D 54 Residual Bending Stiffness D2 - Beam 1L

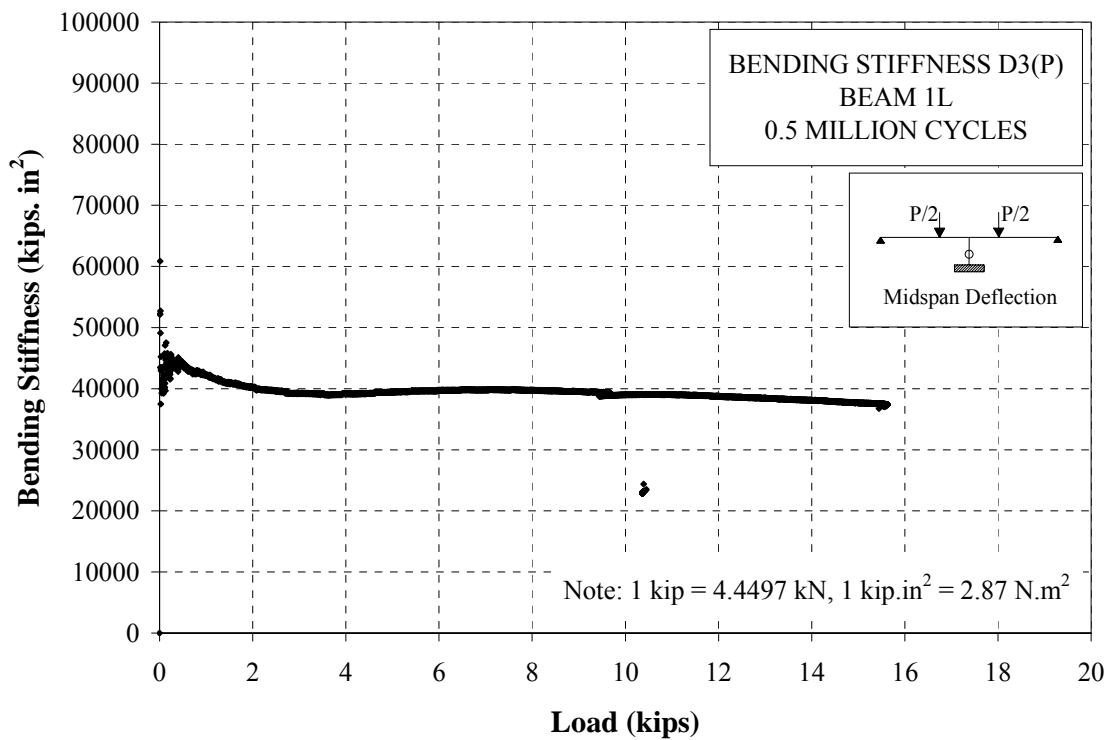


Figure D 55 Residual Bending Stiffness D3 - Beam 1L

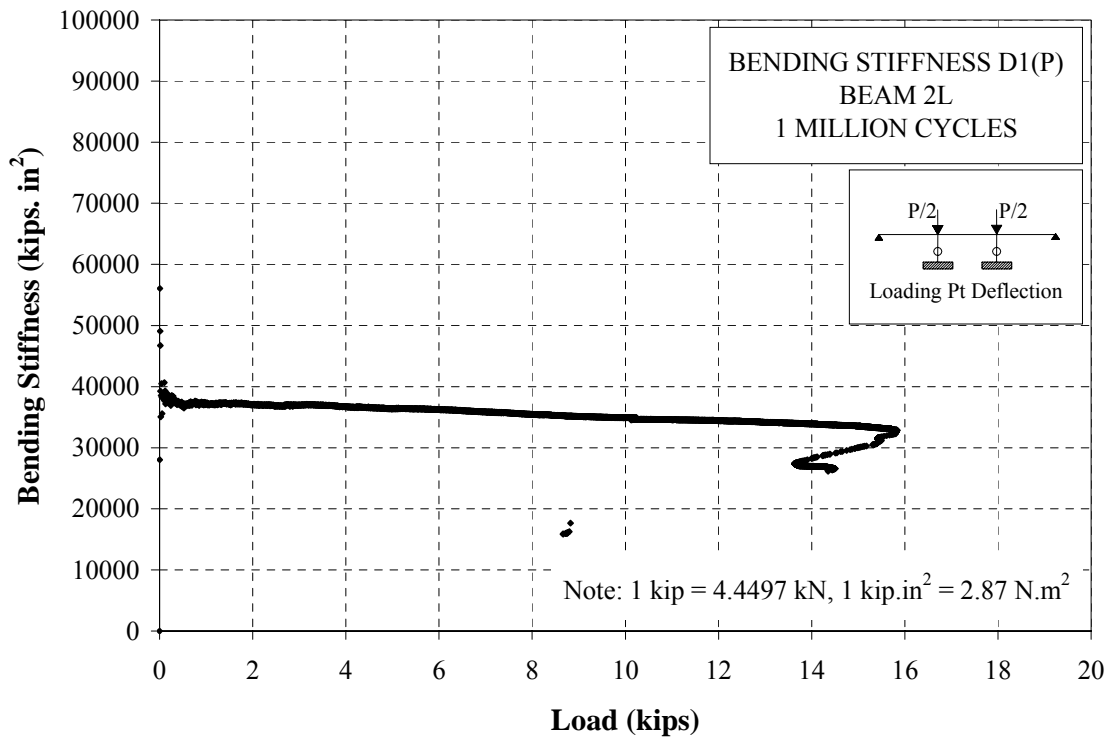


Figure D 56 Residual Bending Stiffness D1 - Beam 2L

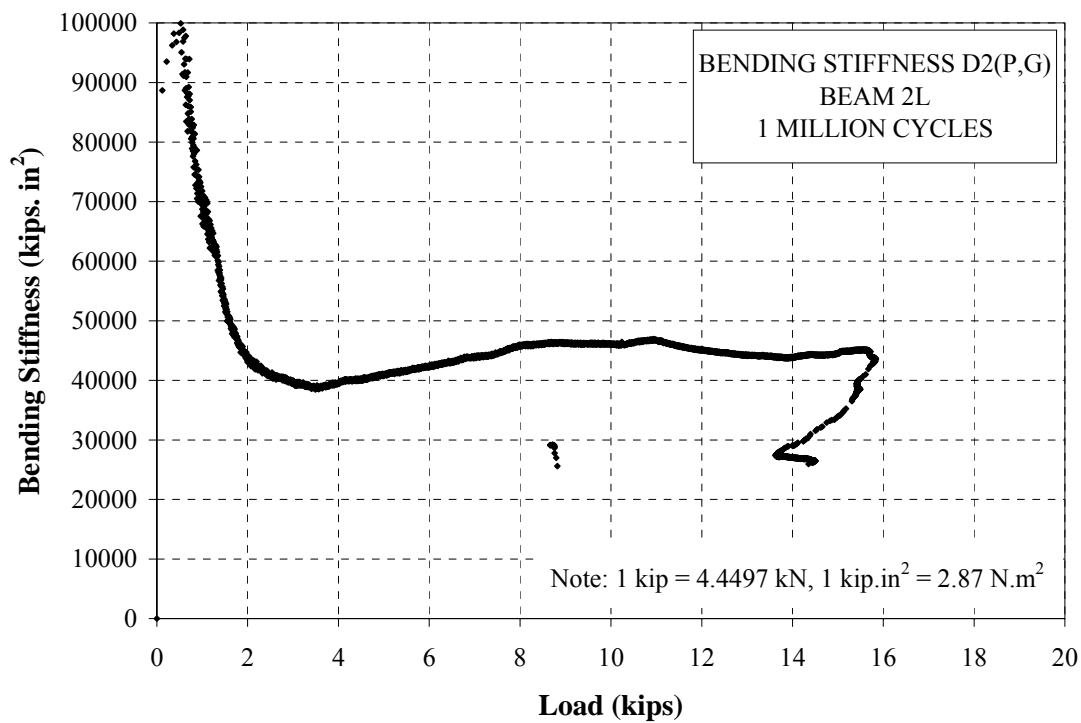


Figure D 57 Residual Bending Stiffness D2 - Beam 2L

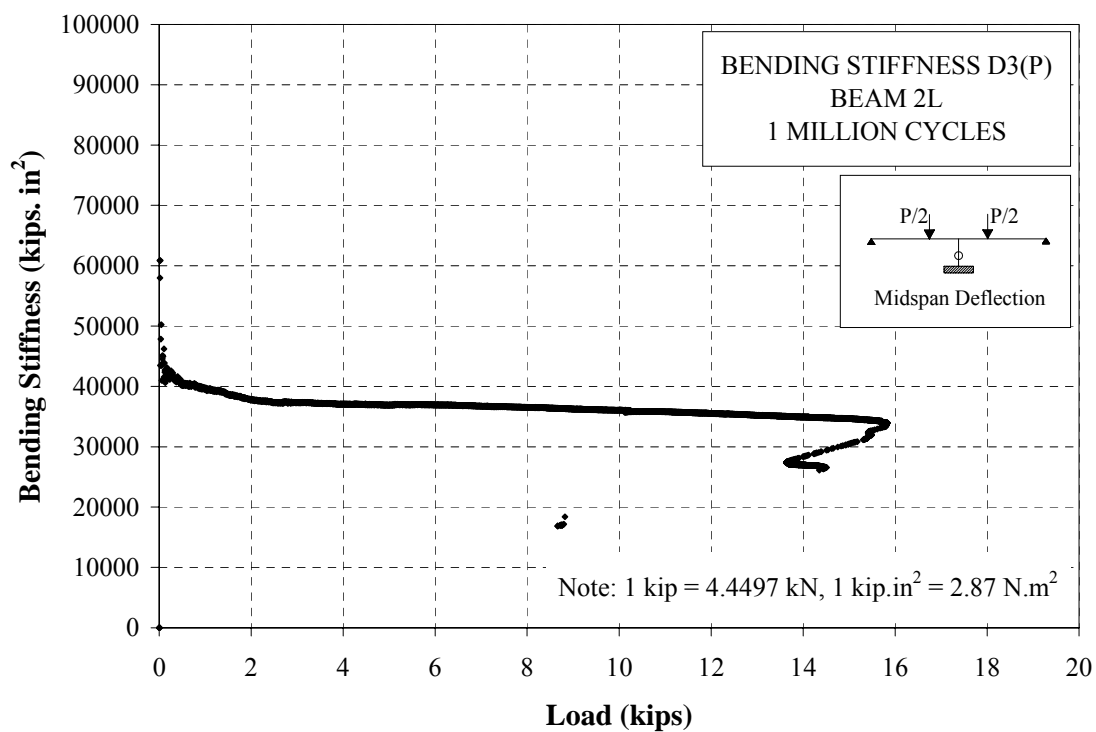


Figure D 58 Residual Bending Stiffness D3 - Beam 2L

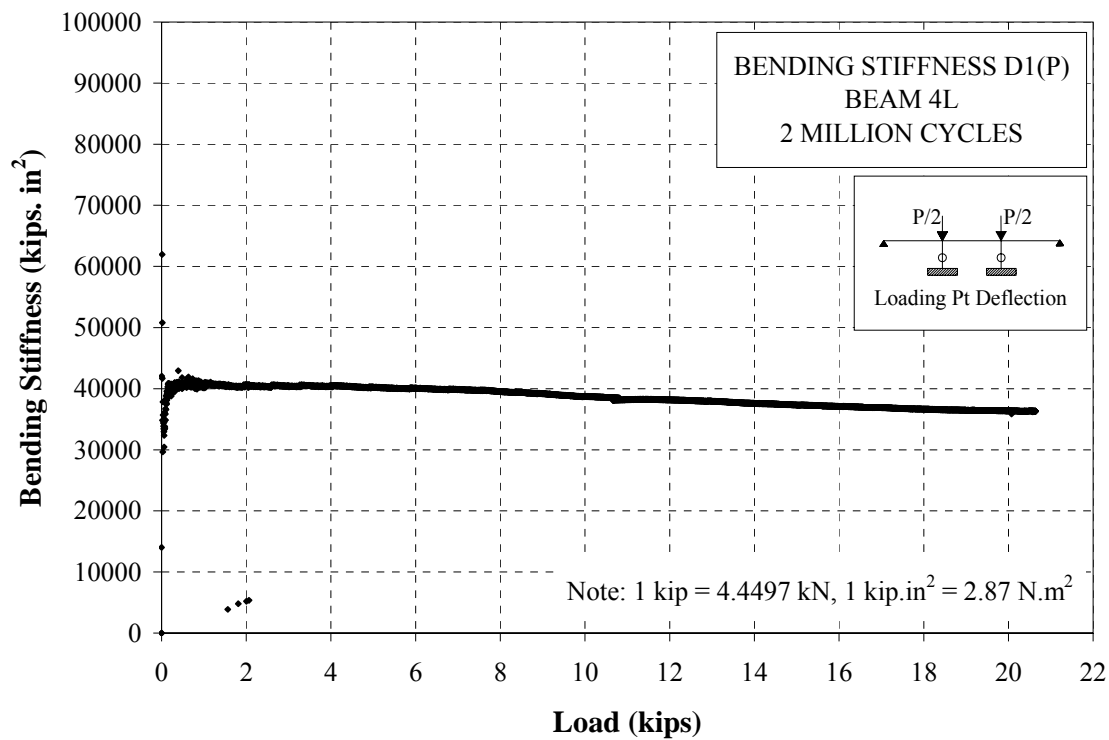


Figure D 59 Residual Bending Stiffness D1 - Beam 4L

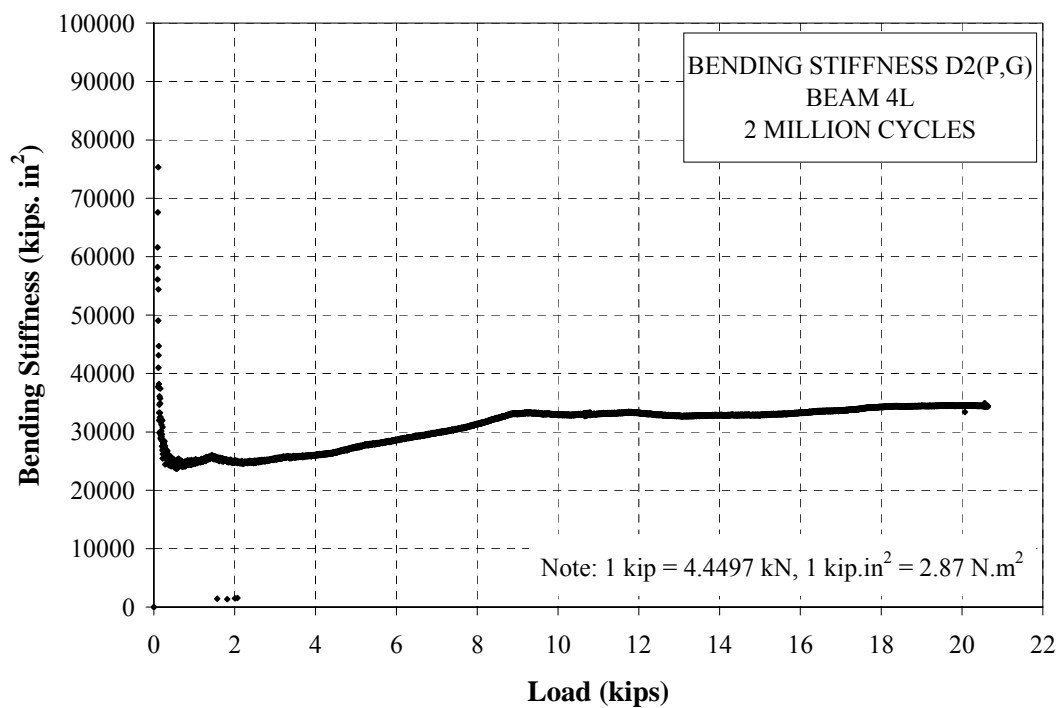


Figure D 60 Residual Bending Stiffness D2 - Beam 4L

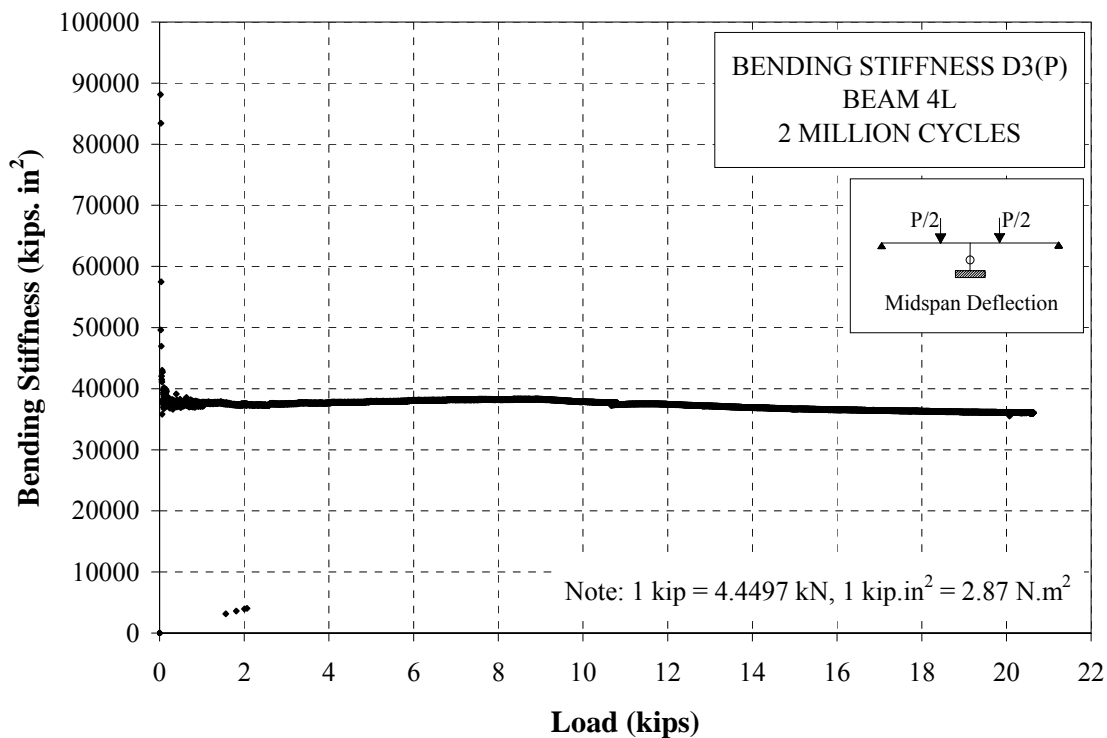


Figure D 61 Residual Bending Stiffness D3 - Beam 4L

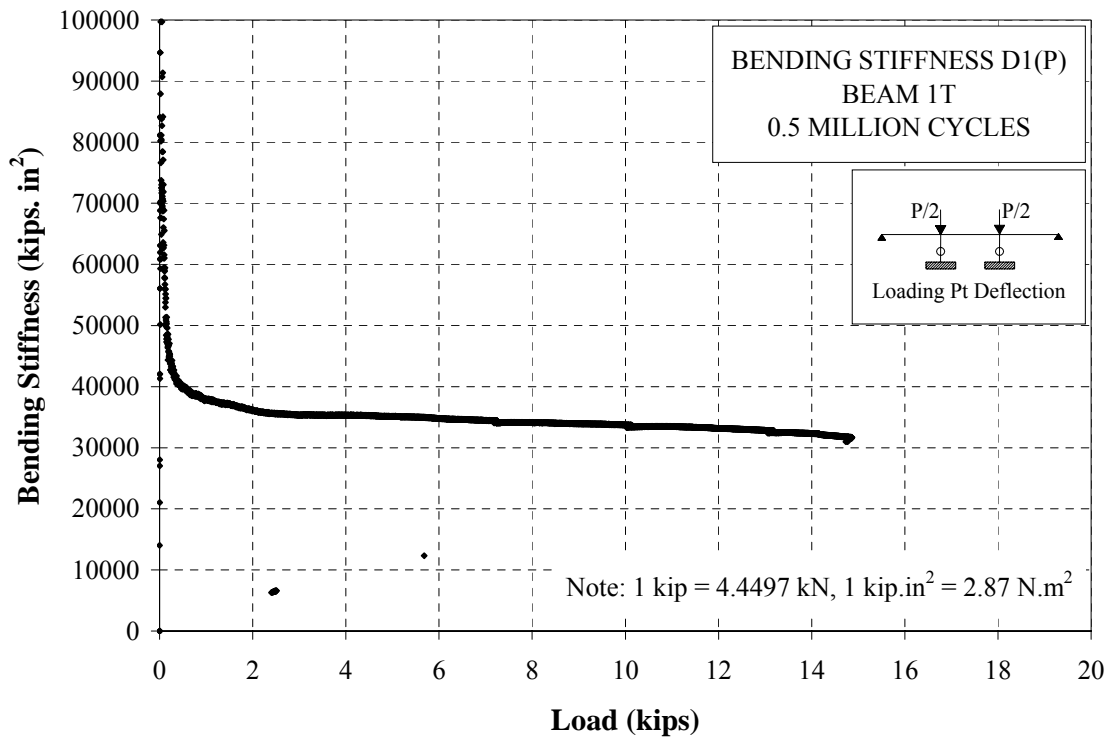


Figure D 62 Residual Bending Stiffness D1 - Beam 1T

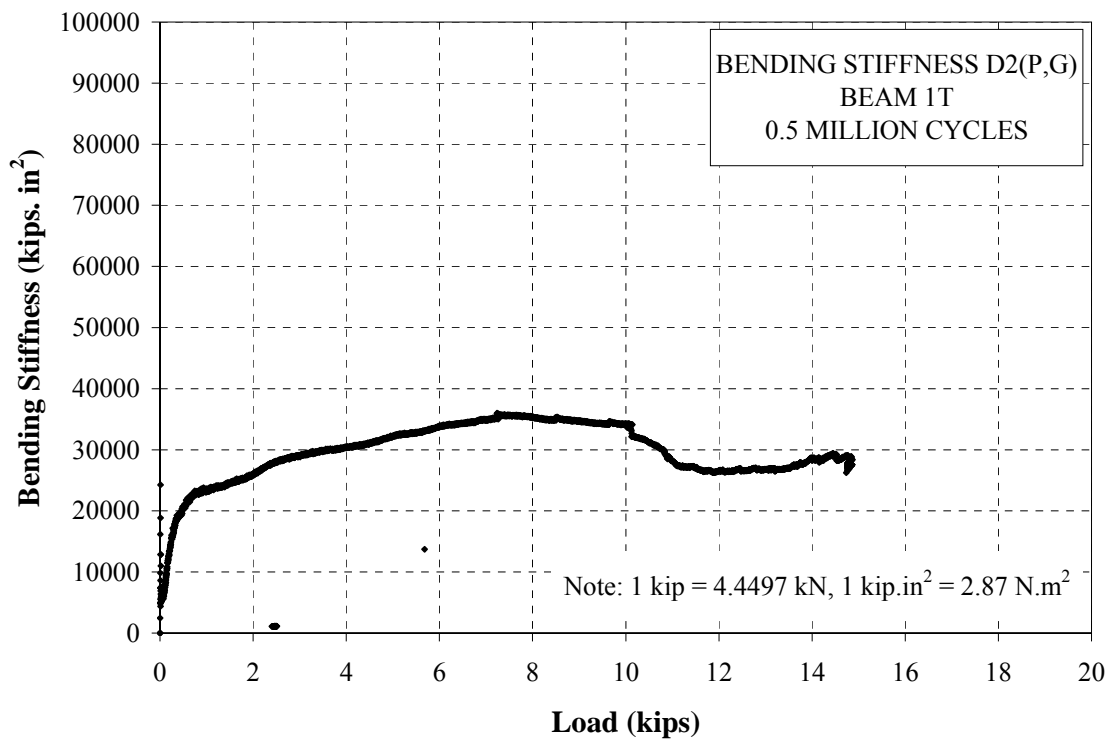


Figure D 63 Residual Bending Stiffness D2 - Beam 1T

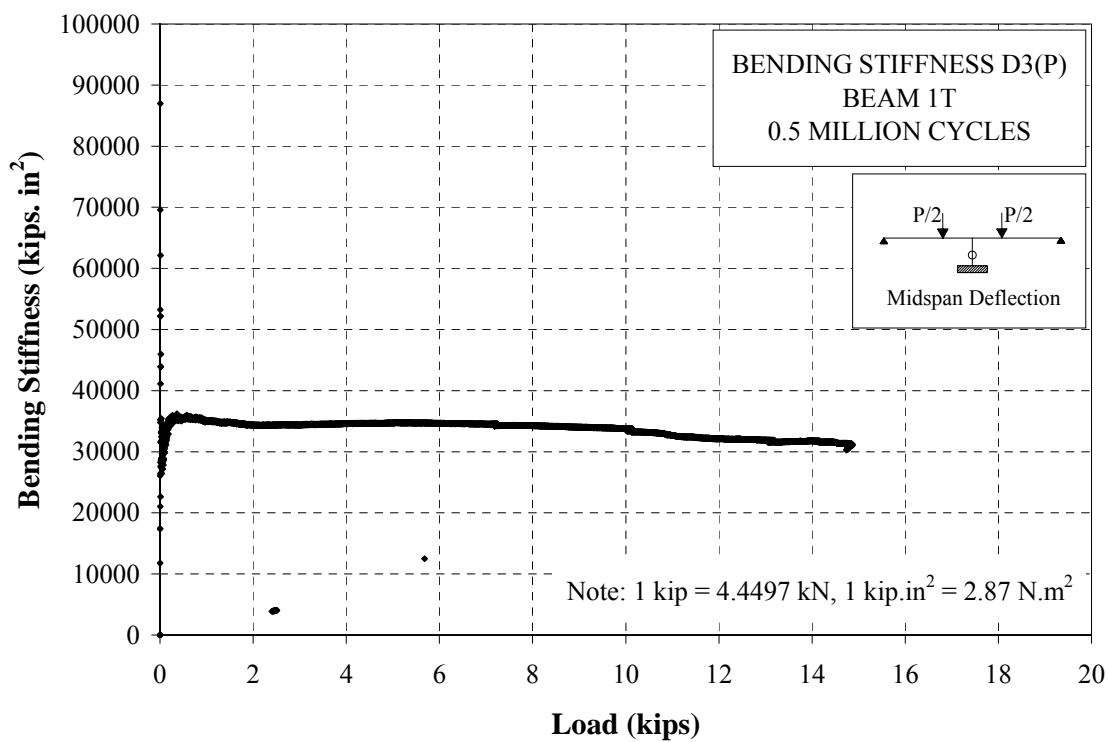


Figure D 64 Residual Bending Stiffness D3 - Beam 1T

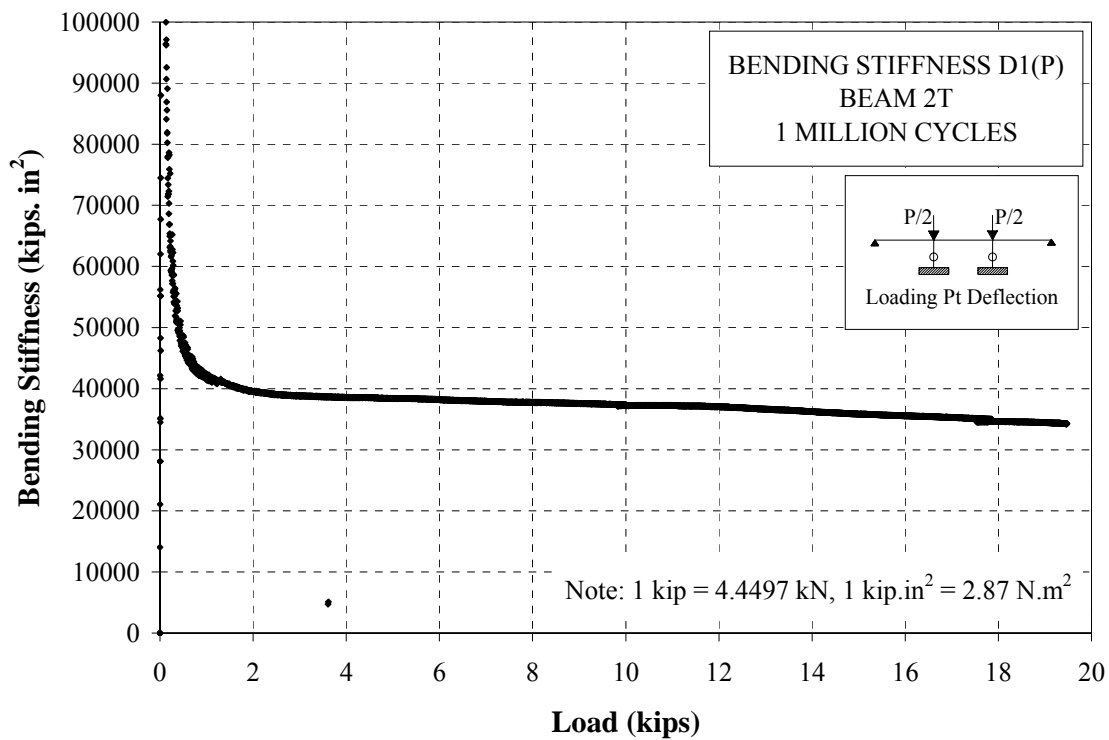


Figure D 65 Residual Bending Stiffness D1 - Beam 2T

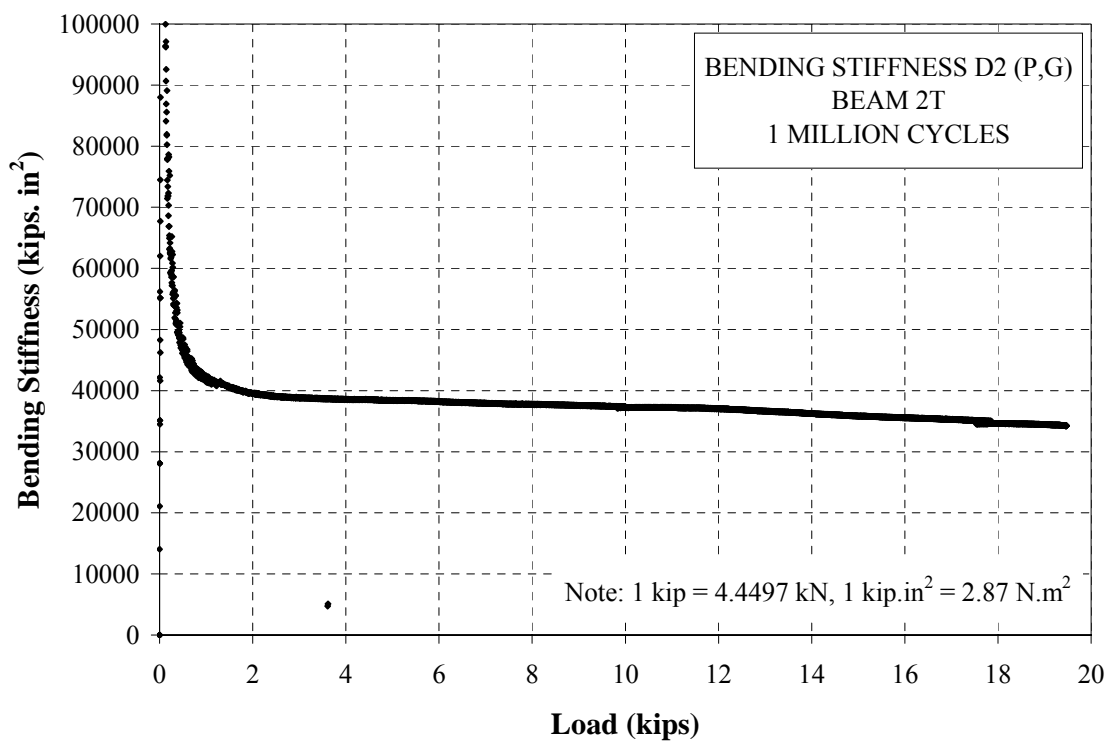


Figure D 66 Residual Bending Stiffness D2 - Beam 2T

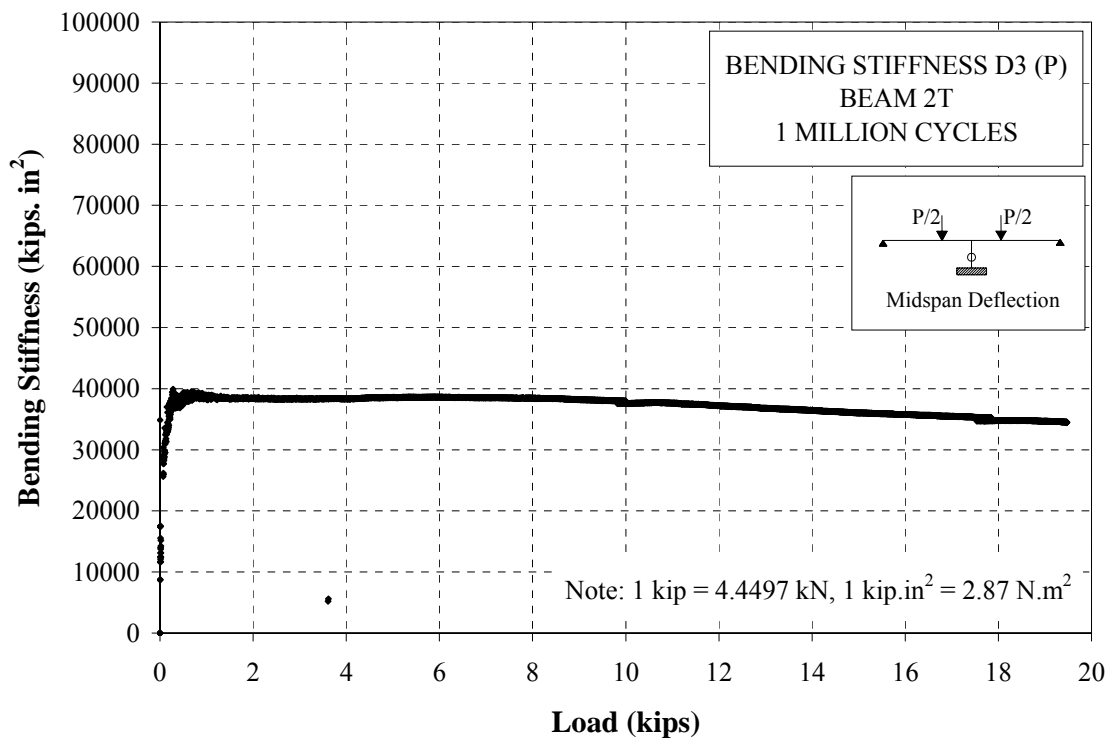


Figure D 67 Residual Bending Stiffness D3 - Beam 2T

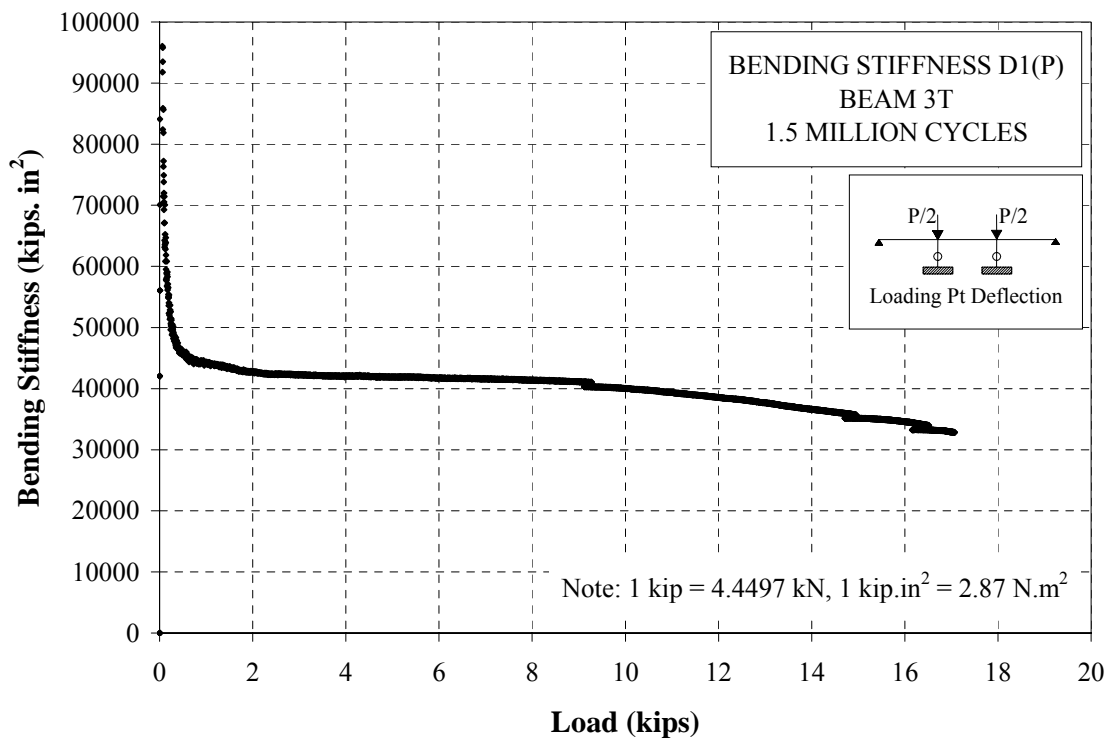


Figure D 68 Residual Bending Stiffness D1 - Beam 3T

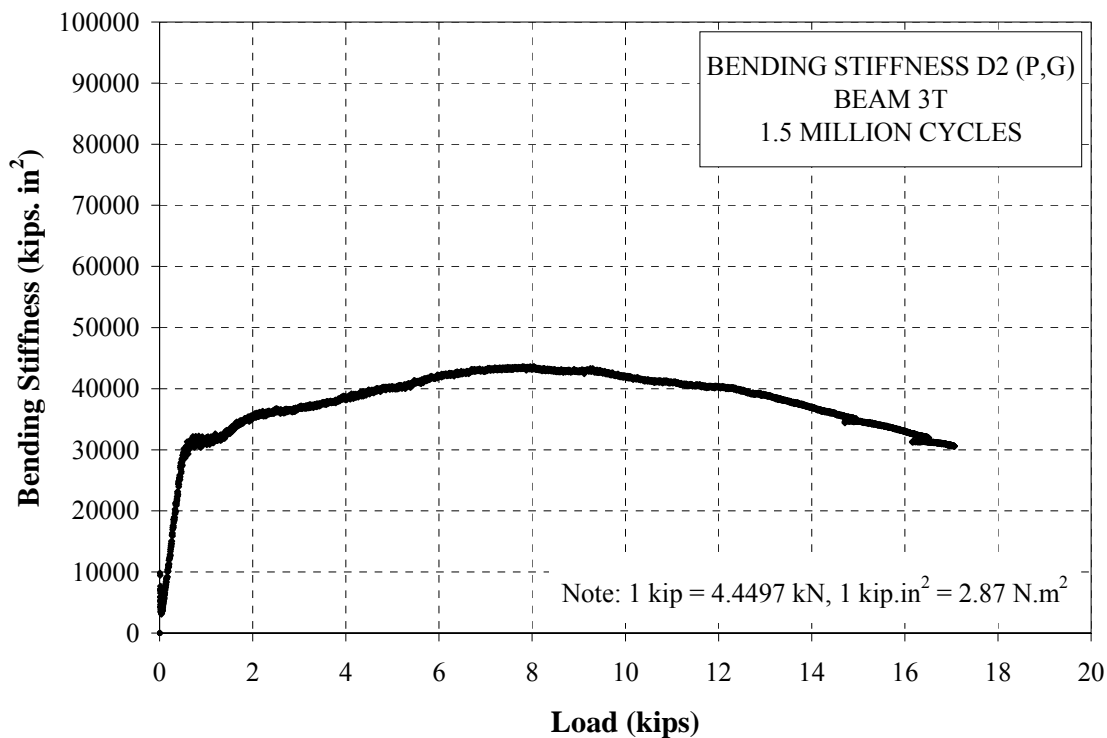


Figure D 69 Residual Bending Stiffness D2 - Beam 3T

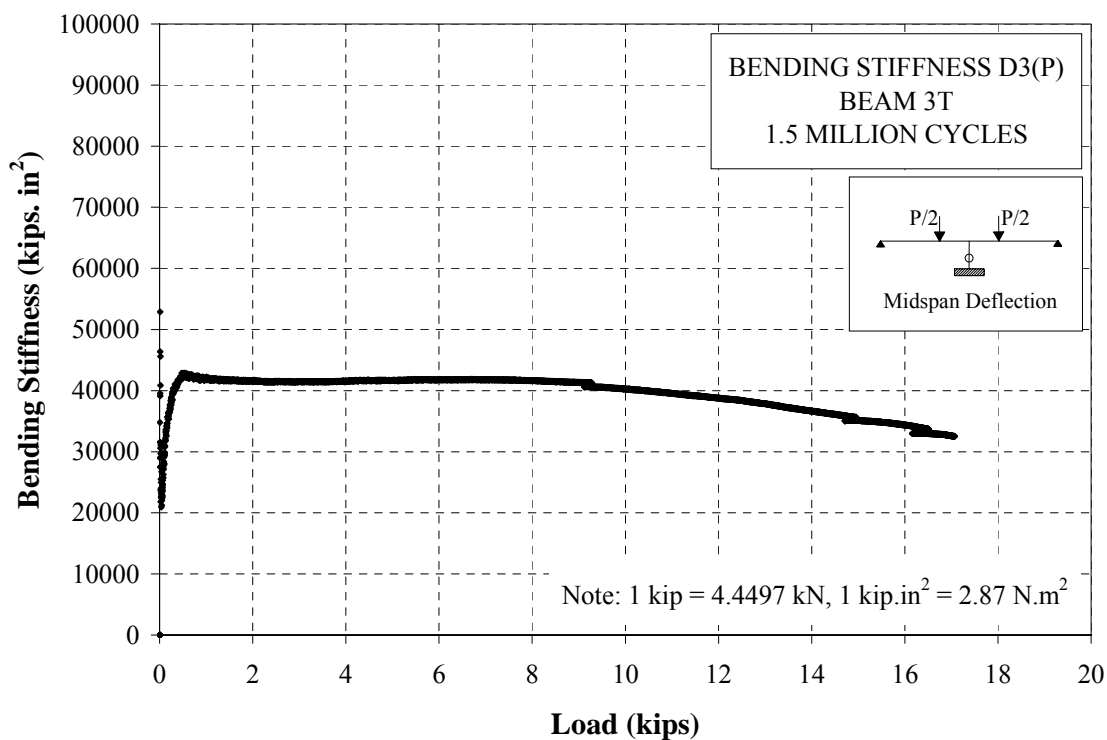


Figure D 70 Residual Bending Stiffness D3 - Beam 3T

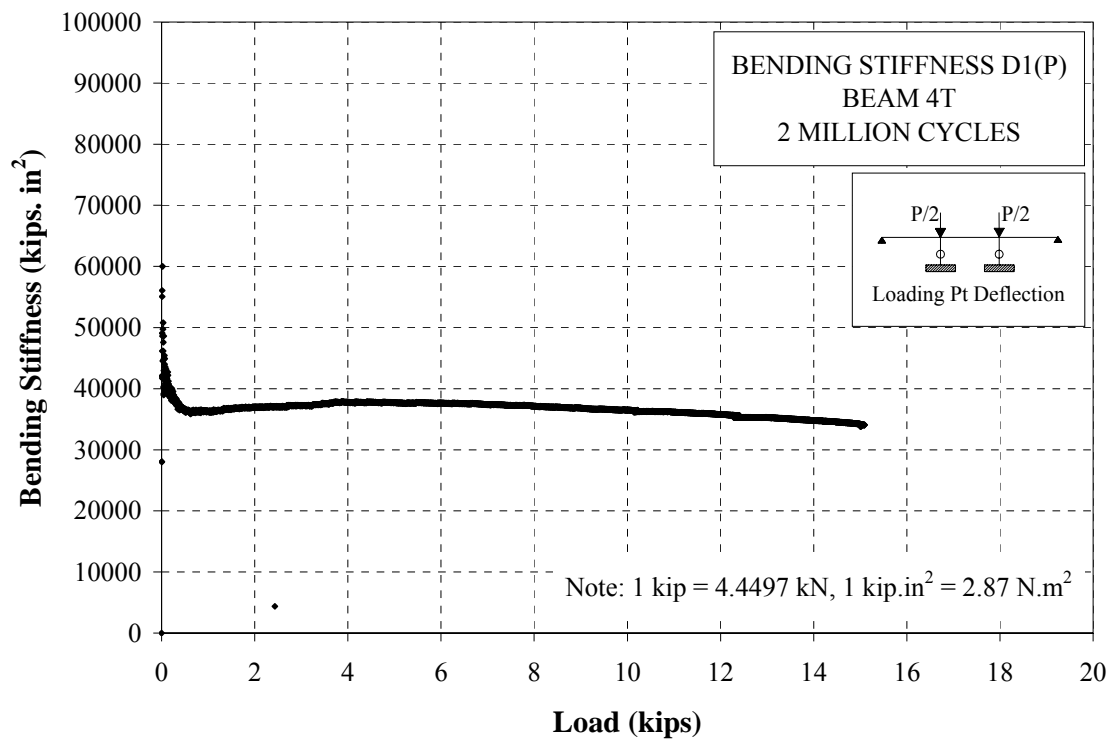


Figure D 71 Residual Bending Stiffness D1 - Beam 4T

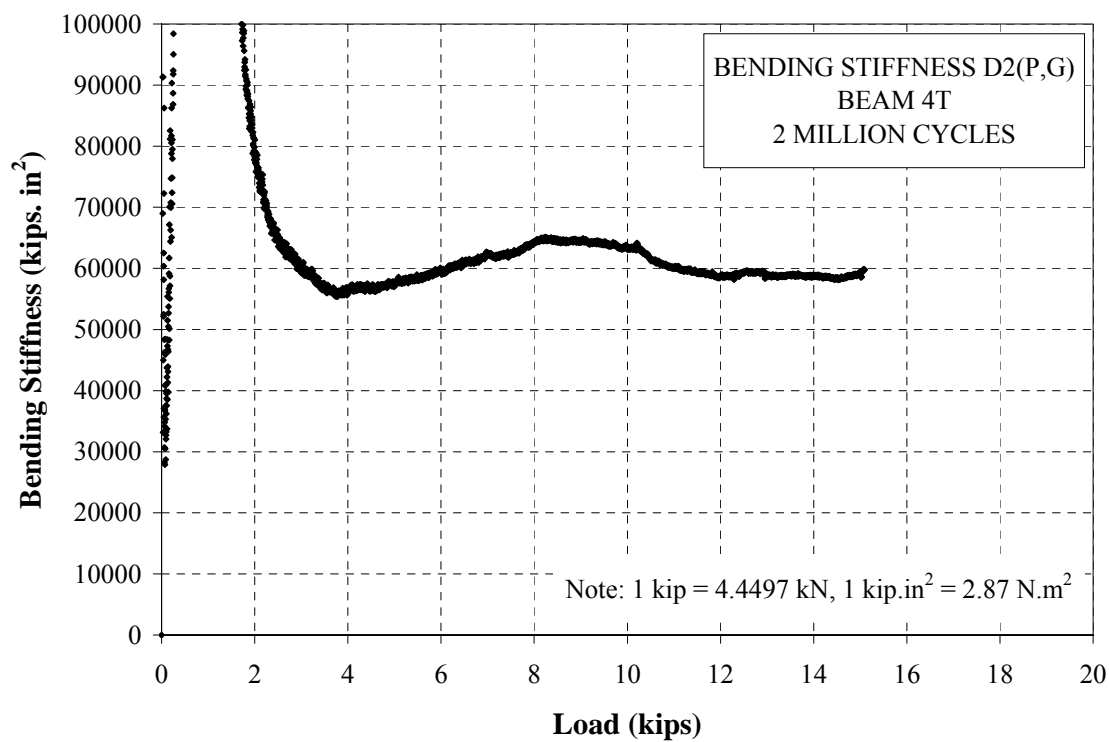


Figure D 72 Residual Bending Stiffness D2 - Beam 4T

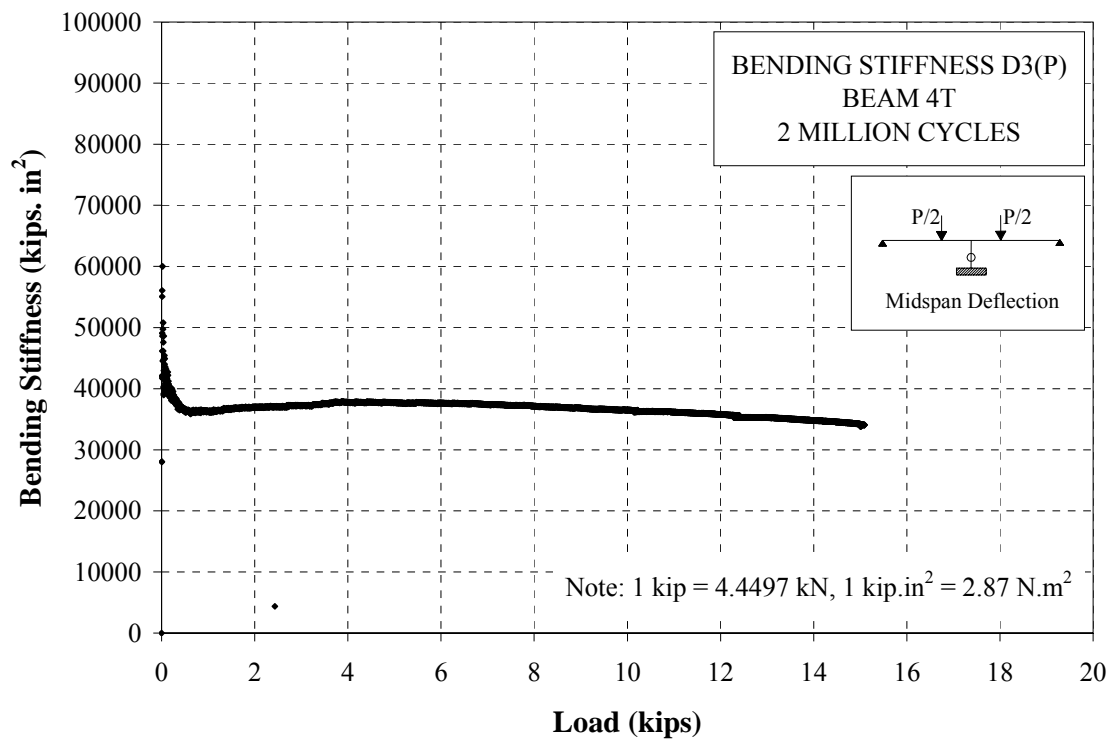


Figure D 73 Residual Bending Stiffness D3 - Beam 4T

APPENDIX E
NON DESTRUCTIVE EVALUATION

The need to increase the knowledge regarding the construction of low weight and low life-cycle cost sandwich panels has led to a development of different improved techniques, especially for quality control. The improved techniques are oriented to reduce the weight while maintaining or increasing the capacity to withstand load. Among these methods is the use of non-destructive test (NDT) or non-destructive evaluation (NDE).

Microwave method is one type of the numerous non-destructive techniques nowadays, and its applications started in 1948 when it showed to be suitable and proper to measure the moisture content in dielectric materials. But it is not until the 1960s, when papers linking the words “microwave” and non-destructive”, began to appear. In the very beginning, the technique was very specialized and limited due to instrumentation and systems by then developed.

Most of the applications since the fifties have been in aerospace but at the present time, the evaluation of dielectric materials such as composites is considered a new area of applications of microwave NDT.

The microwave NDT technique performs the inspection of the material through the use of high frequency electromagnetic energy. The frequency utilized in this method is generally taken between 3×10^8 and 3×10^{11} Hz. The proper operating frequency is selected in order to optimize the interaction of the electromagnetic energy with the dielectric layers, voids, inclusions, surface flaws, material vibrations and chemical components in the material under evaluation.

One of the principal advantages of the microwave NDT technique is that the transducer utilized to scan the surface of a certain material, does not need to be in contact with it, therefore, the inspection of areas that are difficult to reach is feasible. In addition to that, as part of the instrumentation, for NDT microwave inspection there is a variety of waveguides or probes (sensors), besides the electronic equipment such as oscillators, and network analyzers.

Since the FRP materials are manufactured involving a sequence of different process depending upon each type, they are susceptible of presenting some defects, therefore these imperfections will directly affect the overall performance. It is precisely the microwave type of non-destructive evaluation considered a very important device in the examination and inspection of material without affecting its usefulness. The objective is to provide consistent information regarding the structural integrity of the material.

There are applications in composites (demonstrated and potential) such as:

- Detection of delamination and voids in a layered media
- Detection and estimation of porosity in ceramics, glass, plastics, etc ...
- Detection and evaluation of corrosion in thick stratified composite-laminated coating
- Detection and measurement of moisture content in wood, textiles, etc...
- Impact damage detection and evaluation for reinforced composites structures
- Inspection of concrete for constituent determination as well as reinforcing location, chloride detection, safety evaluation, etc ...
- Detection and sizing of surface cracks in metals

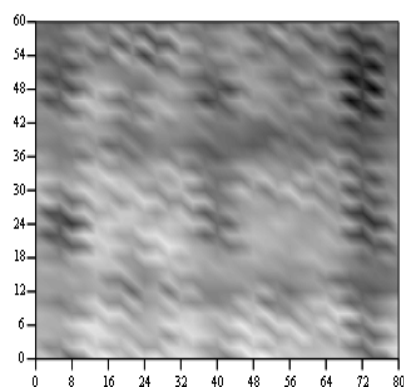
As part of the research conducted, the evaluation of the material through microwave NDT inspection was considered applicable. The intent to detect delamination in the interface foam-facing of the FRP sandwich panel or any other internal damage after conditioning of the cubic sandwich specimen, was the primary goal when applying this non-destructive evaluation technique.

The test took place in the Non-Destructive Test Laboratory at UMR. Same nominal cubic specimens as for the compressive test were provided. A sample of 4 in (102 mm) by 4 in

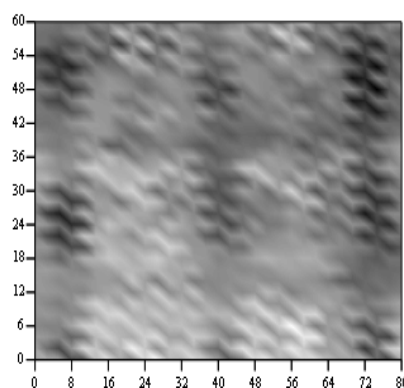
(102 mm) was scanned before subjected to any compressive load, and after conditioning to a certain level of load (fatigue compressive test). Later on, a larger portion of sandwich panel of 12 in (304.8 mm) by 12 in (304.8 mm) was also scanned, this was necessary in order to have a better understand of the configuration of the internal reinforcement of the core. In other words, the learning of how the structure was configured (x and y-direction features) was better comprehended in a larger specimen.

The scanning was carried out in a table properly prepared for the purpose, in addition to an open-ended rectangular waveguide probe and the network equipment for measuring the electromagnetic energy. In order to determine the best observations regarding possible internal flaws, defects or delamination, the scanning of the surface of the specimen was accomplished from multiple stand off distances (vertical distance between the probe and the material surface), varying from 0.04 in (1 mm) to 0.35 in (9mm). The stand off distance of 0.24 in (6 mm) showed to be the most adequate for the possible assessment of the defects within the structure.

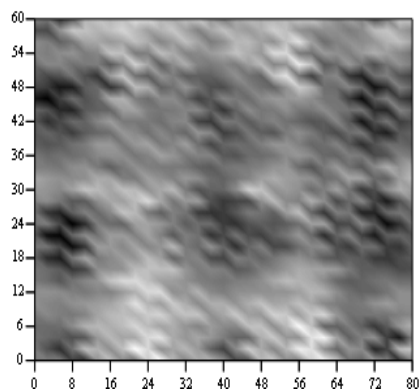
The following images were obtained at different stand off distances:



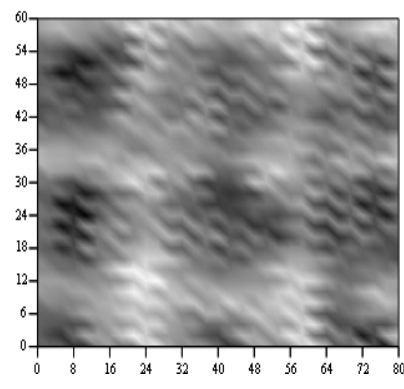
(a) Stand off: 1 mm.



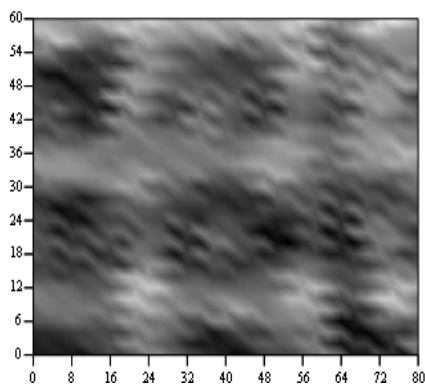
(b) Stand off: 2 mm.



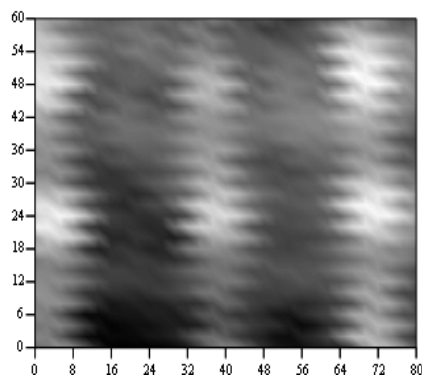
(a) Stand off: 3 mm.



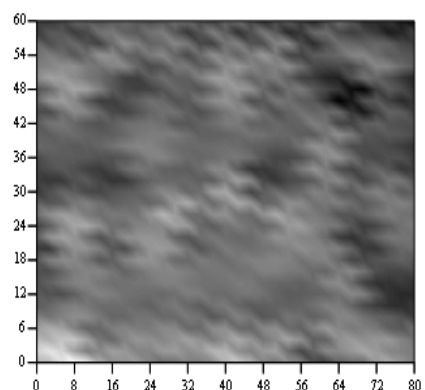
(b) Stand off: 4 mm.



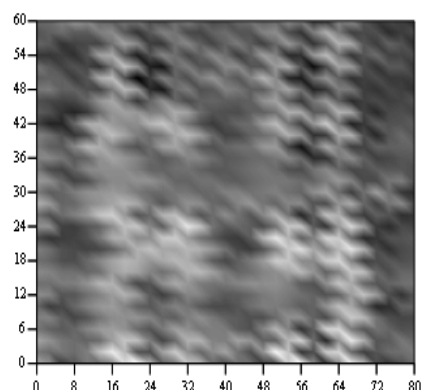
(a) Stand off: 5 mm.



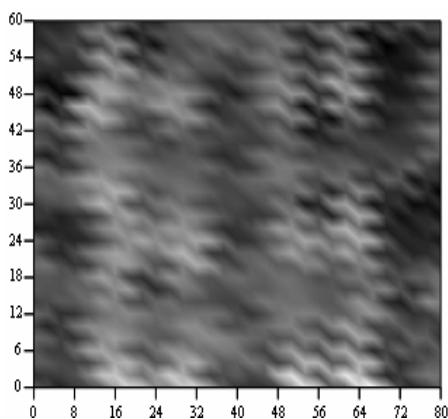
(b) Stand off: 6 mm.



(a) Stand off: 7 mm.



(b) Stand off: 8 mm.



(a) Stand off: 9 mm.

Note: 1 mm = 0.04 in

Figure E 1 Microwave Non-Destructive Technique Images

Even though the images did roughly reflect the layout of the internal sandwich structure, due to its high complexity and anisotropy (stitches in the longitudinal direction and continuous webs in the transverse direction), it was not possible to make a confident and accurate evaluation about the possible imperfections due either to manufacturing or to a loading

conditions. Additionally, the lack of a sample presenting a delamination or information of an initial or critical size flaw also was also an impediment for the proper development of this task.

Hence it can be concluded that the application of microwave non-destructive technique is not feasible for this type of sandwich construction.

APPENDIX F
SYSTEM PERFORMANCE SPECIFICATION FOR THE RAPID PARKING RAMP
EXPANSION (RPRE)

1. SCOPE

1.1 Background. The Air Force has identified a need to provide a faster, more transportable means for rapidly expanding parking aprons and taxiways at expeditionary airfields worldwide and provide a more expedient method to improve weak soils when appropriate. Deployed forces require a rapid means of expanding aircraft parking aprons and taxiways to increase capacity and traffic flow at airfields supporting contingency operations. The Rapid Parking Ramp Expansion (RPRE) program replaces the current AM-2 matting, used by DOD. This document addresses the requirements for developing and fielding a system that includes equipment, methods, and techniques to expedite taxiways and parking aprons by using the following:

- 1) rapid soil stabilization technology
- 2) development of a new lightweight airfield matting system
- 3) or a combination of both

1.2 Scope. This specification covers the requirements to achieve the following objectives:

a. Objective 1 (Above sub-grade) To develop a lightweight airfield matting system that is lighter, smaller, and requires less installation time than the current AM-2 mats (P/N615526).

b. Objective 2 (Sub-grade) To find the best methods and techniques to field recent developments in soil stabilization technology.

It is important to distinguish between the two objectives being “Above sub-grade” and “Sub-grade”. The user could have a potential worst-case situation where a desired location does not have an existing airfield with a natural sub-grade rated at least a California Bearing Ratio (CBR) of 4. For such a worst-case scenario, the main goal is to provide a surface that will be loaded to the requirements in Section 3. In order to achieve these requirements, the solution may be any combination of the above listed objectives.

1.3 System classification. Since the RPRE will be for various types of vehicles and aircraft with different landing gears, it is not classified as medium-duty or heavy-duty.

2. APPLICABLE DOCUMENTS

2.1 General. The documents listed in this section are those referenced in sections 3 and 4 of this specification.

2.2 Government Documents.

2.2.1 Specifications, Standards, and Handbooks. The following specifications and standards form a part of this document only to the extent specified herein. Unless otherwise specified, the issues of these documents are those listed in the Department of Defense Index of Specifications and Standards (DoDISS) and supplement thereto, cited in the solicitation

STANDARDS
MILITARY
TBD

FIELD AND TECHNICAL MANUALS
TBD

AIR FORCE MANUALS

AFMAN 32-4005, Personnel Protection and Attack Systems

2.2.2 Other Government Documents, Drawings, and Publications. The following Government documents, drawings, and publications form a part of this document to the extent specified herein. Unless otherwise specified, the issues are those cited in the solicitation.

2.3 Non-Government Publications. The following documents form a part of this document to the extent specified herein. Unless otherwise specified, the issues of the documents that are DoD adopted are those listed in the issue of the DoDISS cited in the solicitation.

AMERICAN WELDING SOCIETY, INC. (AWS)

(Application for copies should be addressed to the American Welding Society,
550 N.W. Lejeune Road, Miami, FL 33126)

ANSI/AWS D1.1 Structural Welding Code – Steel

ANSI/AWS D1.2 Structural Welding Code – Aluminum

ANSI/AIM BCI-1995, Uniform Symbology Specification –Code 39, 1995

AMERICAN SOCIETY FOR TESTING AND MATERIALS

ASTM-D975

2.4 Order of precedence. In the event of a conflict between the text of this document and the references cited herein, the text of this document takes precedence. Nothing in this document, however, supersedes applicable laws and regulations unless a specific exemption has been obtained.

3. REQUIREMENTS

3.1 Performance. The system shall be suitable for use as taxiways and parking aprons for heavy transport and tactical aircraft. Controlling aircraft for evaluation shall be C-17 and F-15E. The system shall be an improvement over the current system in the following areas: overall system weight; individual component weight; packed volume; installation time and degree of assembly difficulty.

3.2 Physical performance requirements.

3.2.1 Weight. The system, should it involve a light weight matting material, shall not weigh more than 2.9 pounds per square foot (threshold)

3.2.2 Shipping Volume. The system, including tools and equipment and/or materials when packaged for shipment shall have a volume of 25% (threshold) and 50% (objective) less than the current system. The baseline against which this will be measured is a 432 sq ft bundle of AM-2 matting, which occupies 76 cubic feet.

3.2.3 Vertical Loads

3.2.3.1 Cargo Aircraft. The system shall be able to withstand 1,000 coverages of a C-17 traveling at taxi speeds over an initial sub-grade with a CBR of 4 with soil rutting which does not exceed 2 inches.

3.2.3.2 Fighter Aircraft. The system shall be able to withstand 1,000 coverages of an F-15E traveling at taxi speeds over an initial sub-grade with a CBR of 4 with soil rutting which does not exceed 2 inches.

3.2.3.3 Helicopter/VTOL/VSTOL Aircraft. The system shall remain attached to the sub-grade during take-off and landing of helicopters, vertical take off and landing (VTOL), or vertical short take off and landing (VSTOL) aircraft. The system shall withstand landing loads and jet blast forces.

3.2.3.4 Material Handling and Support Equipment. The system shall be able to withstand movement of munitions handling units or forklifts including an adverse terrain forklift. The system shall also be capable of serving as facility flooring for aircraft hangers, warehouses or open storage yards and be able to withstand vertical pad loads not greater than 350 psi exerted by support equipment such as scaffolding and wheel stands.

3.2.4 Shear Loads. The system shall be able to withstand shear stresses caused by the braking and turning of F-15E and C-17 aircraft operating at maximum gross weight and traveling at taxi speeds. The system shall not exhibit a “bow wave” that will cause damage to the system, vehicles, or aircrafts.

3.2.5 Foreign Object Damage (FOD) Protection. The system shall not be a source of FOD and shall provide protection from FOD.

3.2.6 Aircraft Static Grounding. The system shall have provisions to accommodate aircraft static grounding requirements.

3.3 Environmental Performance Requirements.

3.3.1 Temperature range. The system shall be able to operate in ambient air temperatures ranging from -25 to +125 degrees F. The system shall also be able to withstand jet blast from conventional and VSTOL aircraft without damage that would prohibit operational use. Thermal expansion of the system shall be compensated to eliminate possible bow wave effect.

3.3.2 Ultraviolet rays. The system shall be able to withstand long durations of up to 10 years of exposure to sunshine and ultraviolet effects without degradation or failure.

3.3.3 Chemicals. The system shall not be damaged after exposure to vapors or direct contact for an extended amount of time with chemicals and liquids commonly used on a flight line such as, but not limited to, the following:

- a. Fuels per ASTM-D975 (commercial diesel No.1-D or No. 2-D, JP-4, JP-5, JP-8) or MIL-P-87107C (JP-10) or commercial grade Avgas
- b. Hydraulic fluids.
- c. Deicing fluids
- d. Cleaning agents
- e. Engine oils
- f. Liquid Oxygen (LOX)

3.3.4 Site Grade. The system shall be able to cover sub-grades crowned up to 1.5 percent.

3.3.5 All weather provisions. The system shall provide a non-skid surface and minimize slipping during any weather condition.

3.4 Logistics and Manpower.

3.4.1 Personnel. Operation and maintenance of the system shall not require, after minimal training, any new personnel characteristics such as grade, aptitude, skill level, and physical qualifications beyond that of the personnel who operate and maintain the current systems. Under all environmental conditions, the system shall be capable of being installed, assembled, operated, maintained, and repaired by personnel while dressed in all appropriate uniforms including mission-oriented protective posture (MOPP) LEVEL 2 to LEVEL 4, as described in AFMAN 32-4005, Appendix 4 and 5 (see Annex C), and arctic clothing. This includes lifting, transporting, and assembly.

3.4.2 System Safety Requirements. The system shall have no conditions, materials, operations, or functions that are hazardous to the operator and maintenance personnel. The system shall be safe to handle, transport, install, disassemble, and store by personnel using existing inventoried tools and equipment. Warning devices and safety labels shall be incorporated into the system to help prevent injury during system operations.

3.5 System Configuration and Installation. Specialized equipment needed for installation and maintenance shall be identified. The system shall allow the user to identify the components for proper installation. Installation rate shall be at least 309 sq ft per man-hour. The system shall be permanently marked on the outside of the containers with a bar coded national stock number, numeric national stock number, manufacturer's commercial and government entity (CAGE) code, manufacturer's part number, nomenclature, serial number, weight and cube, date of manufacture, and contract number. The first line shall be the bar coded national stock number with a bar code density of 3.0 to 9.4 characters per inch. Symbology for the bar code shall comply with ANSI/AIM BC1-1995, Uniform Symbology Specification-Code 39, 1995.

3.6 Maintenance and repair. Required preventive maintenance checks and services should not exceed a performance objective of 30 minutes. The repair time for the system should not exceed a performance objective of 1 hour. The system shall be capable of permitting the replacement of interior components within the 1-hour repair time. The system shall be able to be cleared of debris such as snow or dirt by standard methods like plowing and swiping without substantial damage or FOD. These methods shall use common tools to the maximum extent feasible. Any special tools require prior approval.

3.6.1 Panel Replacement. If part of the system, the panels in the assembled mat sub-system must be removable/replaceable in order to allow the replacement of damaged panels or to allow for maintenance of the sub-grade below groups of panels.

3.7 System Reuse and Storage. The system, if made of separate components, shall be recoverable for storage and suitable for reuse after being cleaned and repackaged. The system shall not degrade or cause a hazard to the environment, personnel, or equipment while being stored outdoors and uncovered for a period of 10 years.

3.8 Transportability requirements.

3.8.1 Material handling. All systems and equipment must be capable of being moved with standard military materiel handling equipment.

3.8.2 Air transport. The system shall be transportable worldwide in C-130 and larger military aircraft and shall fit the weight and volume limitations on C-130 aircraft. For planning purposes, C-130 sortie requirements are based on the weight & balance and volume criteria. All equipment

for mat installation must not exceed the current AM-2 matting installation equipment transportation footprint. Currently a C-130 can carry 4,300 ft² of AM-2 matting per mission. (see Annex B).

3.9 Recycled, Recovered, Disposal or Environmentally Preferable Materials. All material in the system shall be recyclable, environmentally safe, and easy to dispose of after use. The system shall be designed to eliminate or minimize environmental quality impacts. The system shall reduce or eliminate the use of hazardous materials and/or the generation of hazardous wastes during manufacture, use, and disposal of the system.

3.10 Training. Existing unit personnel shall be able to setup and maintain the RPRE after receiving computer based training using the technical manual provided

4. VERIFICATION. Performance verification shall be accomplished using this section along with a complete test plan documented under a separate cover. This section is being worked and will be added to this SPS at a later date.

5. PACKAGING

5.1 Packaging. The system shall be packaged in accordance with best commercial practices. The system shall be packaged for shipment via air (463L compatible), ship, rail and ground, using standard best commercial practices. Containerization may be used where practical. The system shall be capable of being packaged for intermodal transportability. MIL-STD-648 may be used as a reference.

6. Reliability. Availability and Maintainability. Contractual reliability is defined as mean-time-between-failures (MTBF) whereas operational reliability is defined as mean-time-between-maintenance (MTBM) for both scheduled and unscheduled maintenance. Operational availability (Ao) is the combination of reliability and maintainability. Operational Availability is equal to MTBM divided by the sum of MTBM plus mean downtime (MDT) that includes logistics delays. Based on these definitions, the operational availability for the RPRE system is 99%.

7. NOTES

(This section contains information of a general or explanatory nature that may be helpful, but is not mandatory.)

7.1 Definitions.

CBR – also known as California Bearing Ratio is a measure of the relative bearing capacity of soils and base materials and is expressed as a percentage of the unit load required to force a three square inch piston into the soil, divided by the unit load required to force the same size piston the same depth into a standard sample of compacted crushed rock.

Coverage – one application of the test wheel of the load cart over each point on the designated traffic lane. A coverage describes the number of times an aircraft's wheels traverse over the system using the same line of sight to test if the design withstands the loads without failure or excessive rutting, where one coverage is equal to one travel across the entire system's length.

Degradation of performance - Degradation of performance is defined as an event that results in degradation of the equipment to a degree such that the equipment cannot meet system performance requirements as specified in this document.

Damage - Damage is defined as any degradation or impairment of the performance of the system or any evidence of physical damage such as cracking, warping, bending, breaking, peeling, and flaking.

7.2 References.

7.2.1 Reference Documents.

MILITARY

MIL-STD-209	Slinging and Tiedown Provisions for Lifting and Tying Down Military Equipment
MIL-HDBK-310	Global Climate Data for Developing Military Products
MIL-STD-810	Environmental Test Methods
MIL-STD-1366	Transportability Requirements
MIL-STD-1472	Human Engineering Design Criteria for Military Systems, Equipment and Facilities
MIL-HDBK-1791	Design for Internal, Aerial Delivery in Fixed Wing Aircraft

(Unless otherwise indicated, copies of the above specifications, standards, and handbooks are available from Standardization Document Order Desk, 700 Robbins Avenue, Building 4D, Philadelphia, PA 19111-5094 or electronically in .pdf format from the following web address: <http://assist2.daps.dla.mil/quicksearch/>)

FIELD AND TECHNICAL MANUALS

FM 5-430-00-1/AFPAM 32-8013, VOL. I http://www.adtdl.army.mil/cgi-bin/atdl.dll/fm/5-430-00-1/toc.htm	Planning and Design of Roads, Airfields, and Heliports in the Theater of Operations – Airfield and Heliport Design
FM 5-430-00-2/AFPAM 32-8013, VOL.II http://www.adtdl.army.mil/cgi-bin/atdl.dll/fm/5-430-00-2/toc.htm	Planning and Design of Roads, Airfields, and Heliports in the Theater of Operations – Airfield and Heliport Design
FM 5-410 http://www.adtdl.army.mil/cgi-bin/atdl.dll/fm/5-410/toc.htm	Military Soils Engineering, Appendix A, California Bearing Ratio Design Methodology

(Unless otherwise indicated, copies of the above field and technical manuals are available electronically in .pdf format from the linked web address)

AIR FORCE MANUALS

AFMAN 32-4005

<http://www.e-publishing.af.mil/pubfiles/af/32/afman32-4005/afman32-4005.pdf>

Personnel Protection and Attack
Actions

7.2.2 Referenced load information. <http://www.ksu.edu/pavements/trb/A2B09/CS05-01.PDF> page 4, C-17 tire information, and <http://www.adtdl.army.mil/>, Field Manuals section, [FM 5-430-00-2](#), PLANNING AND DESIGN OF ROADS, AIRFIELDS, AND HELIPORTS IN THE THEATER OF OPERATIONS - AIRFIELD AND HELIPORT DESIGN, 29 SEP 1994, Chapter 11, Page 11-2, Table 11-1, Characteristics of certain Air Force aircraft, http://www.adtdl.army.mil/cgi-bin/atdl.dll/fm/5-430-00-2/Ch11.htm#tab11_2, and Chapter 12, Page 12-4, Table 12-1, Design aircraft, http://www.adtdl.army.mil/cgi-bin/atdl.dll/fm/5-430-00-2/Ch12.htm#tab12_1.

7.2.3 Referenced maintenance and repair. FM 5-430-00-2/AFJPAM 32-8013, Vol II, PLANNING AND DESIGN OF ROADS, AIRFIELDS, AND HELIPORTS IN THE THEATER OF OPERATIONS - AIRFIELD AND HELIPORT DESIGN, 29 SEP 1994, Appendix N, M19 MAT REPAIR, <http://www.adtdl.army.mil/cgi-bin/atdl.dll/fm/5-430-00-2/Appn.htm>,

7.2.4 Referenced CBR description. FM 5-410, Military Soils Engineering, Appendix A, California Bearing Ratio Design Methodology, <http://www.adtdl.army.mil/cgi-bin/atdl.dll/fm/5-410/Appa.htm>, and FM 5-430-00-1/AFJPAM 32-8013, Vol.1, [FM 5-430-00-1](#), PLANNING AND DESIGN OF ROADS, AIRFIELDS, AND HELIPORTS IN THE THEATER OF OPERATIONS - AIRFIELD AND HELIPORT DESIGN, [CHAPTER 5 - SUBGRADES AND BASE COURSES](#).

ANNEX A

THE 463L CARGO SYSTEM DESCRIPTION

The 463L system encompasses all phases of cargo loading, including material-handling equipment, cargo-loading platforms, restraint equipment, and in-aircraft systems. The 463L system is the USAF standard for moving concentrated cargo to be air landed. It is comprised of the following major components:

- Dual-rail system. The dual-rail system is installed in all airlift or 463L-capable military aircraft. This system consists of rows of rollers that allow the palletized cargo to easily move into the aircraft. Many of these rollers are stowable to convert the cargo deck to a flat, clear loading surface for wheeled or tracked cargo. The side rails guide the pallets into the aircraft and provide lateral and vertical restraint. These rails are equipped with detent locks that hold the pallet securely in place once inside the aircraft. The locks also prevent the forward and aft movement of pallets during flight. Cargo compartment floors also contain a series of tie-down fittings for securing wheeled or tracked cargo with chains.

- 463L pallet. The 463L pallet is made of corrosion-resistant aluminum with a soft wood core and is framed on all sides by aluminum rails. The rails have 22 attached tie-down rings with six rings on each long side and five rings on each short side. Each ring has a 7,500-pound restraint capacity. The rails also have indents (notches), which are designed to accept the detent locks located on numerous types of material-handling equipment on all airlift-capable aircraft. The overall dimensions of the 463L pallet are 88 inches long by 108 inches wide by 2-1/4 inches thick. The usable dimensions of the surface area are 84 inches wide by 104 inches long. This allows two inches around the periphery of the pallet to attach straps, nets, or other restraint devices. An empty pallet weighs 290 pounds (355 pounds with nets) and has a maximum load capacity of 10,000 pounds. Two or more pallets can be connected together for movement of cargo that exceeds the dimensions or weight limitations of a single pallet.

- 463L pallet nets. There are three nets to a set: one top net (yellow) and two side nets (green). The side nets attach to the rings of the 463L pallet. The top net attaches by hooks to the rings on the side nets. The nets have multiple adjustment points and can be tightened to conform to loads of almost any shape. A complete set of 463L nets provides adequate restraint for a maximum of 10,000 pounds when properly attached to a 463L pallet. A complete set of nets weighs 65 pounds.

- Other restraint devices. 10,000 and 25,000 pound (capacity) chains and locking devices are available to restrain large or heavy items such as containers, vehicles or tracked equipment. 5,000 pound straps are available for individual item restraint or to supplement 463L nets.

- Specialized 463L compatible containers with their own base or which incorporate an integral pallet base are available.

- Wheeled vehicles may be loaded directly on the cargo compartment floor and restrained with 10,000 and/or 25,000-pound capacity chains.

ANNEX B

Table F 1 C-130 COMPATIBILITY

Parameter	Applicable Aircraft	Requirement
Payload for planning purposes	C-130	25,000 pounds
Maximum individual axle weight	C-130	13000 pound each axle
Maximum tire pressure for wheeled equipment	C-130	100 psi
Cargo restraint criteria; load factors	C-130	2.0 G up, 4.5 G down, 3.0 G forward, 1.5 G aft, 1.5 G lateral Note: Criteria apply to cargo pallets, shipping containers and all equipment inside shipping containers.
Rapid decompression of aircraft	C-130	Sealed containers must provide for sufficient ventilation to safely relieve an 8.3-psi pressure differential within 0.5 seconds resulting from rapid decompression of the aircraft cabin.

Source: MIL-HDBK-1791

ANNEX C

MISSION-ORIENTED PROTECTIVE POSTURE (MOPP)

The personnel may be required to perform assembly and maintenance while wearing chemical and biological (CB) warfare protective gear. The primary use is for CB threats and pre-attack. Reference, AFM 32-4005, Personnel Protection and Attack Actions, <http://www.e-publishing.af.mil/search.asp?keyword=32-4014&Go.x=13&Go.y=9>. MOPP LEVEL 2 to 4 is the requirement for this system, which is:

MOPP LEVEL 2

- Worn by personnel
 - Overgarment
 - Mask carrier
 - Field gear
 - (Carry or keep at hand protective equipment such as M8/M9 paper, nerve agent antidotes, and decontamination kits)
 - Footwear covers

- Carried
 - Mask/Hood
 - Gloves

MOPP LEVEL 4

- Worn by personnel
 - Overgarment
 - Mask/Hood
 - Field gear
 - (Carry or keep at hand protective equipment such as M8/M9 paper, nerve agent antidotes, and decontamination kits)
 - Footwear covers
 - Gloves

- Nothing carried

LIST OF REFERENCES

ACI Committee 440. *Guide for the Design and Construction of Externally Bonded FRP Systems for Strengthening Concrete Structures*. (440. 2R – 02). Farmington Hills, MI: American Concrete Institute, 2002.

Allampalli, S., Yannotti, A., O'Connor, J., Norfolk, M., Schongar, G., and Greenberg, H. *In – service Monitoring of FRP Bridge in New York*. Structures Congress, Philadelphia, Pennsylvania, May 2000.

Allampalli, S., O'Connor, J., and Yannotti, A. *Fiber Reinforced Polymer Composites for Infrastructure of a Short – span Rural Bridge*. Transportation Research Board Annual Meeting, Washington, D.C., January 2001.

Allen, Howard G. *Analysis and Design of Structural Sandwich Panels*. New York: Pergamon Press, 1969.

American Society of Testing and Materials. *ASTM Standard Terminology of Structural Sandwich Constructions (C 274 – 99)*. West Conshohocken, PA: ASTM International 1999.

American Society of Testing and Materials. *ASTM Standard Test Method for Flexural Properties of Sandwich Constructions (C 393 – 00)*. West Conshohocken, PA: ASTM International 2000.

American Society of Testing and Materials. *ASTM Standard Test Method for Flatwise Compressive Properties of Sandwich Cores (C 365 – 00)*. West Conshohocken, PA: ASTM International 2002.

Chajes, M., Mertz, D., Shenton, H., and Eckel, D. *Delaware's First All Composite Bridge*. Structures Congress, Philadelphia, Pennsylvania, May 2000.

Chajes, M., Shenton, H., and Finch, W. *Performance of a GFRP Deck on Steel Girder Bridge*. Transportation Research Board Annual Meeting, Washington, D.C., January 2001.

Das, Braja. *Principles of Foundation Engineering*. Pacific Grove, Calif.: PWS Pub., 1999.

Ekenel, M. *Bending and Shear Stiffness of Single and Stacked Sandwich Beams*. April 2001.

Gill, S. and Plunkett, J. *Testing, Evaluation, and Installation of Fiber – Reinforced Polymer Honeycomb Composite Panels in Bridge Deck Applications*. Transportation Research Board Annual Meeting, Washington, D.C., 2000.

Gill, S. and Plunkett, J. *Testing, Evaluation, and Installation of Fiber – Reinforced Polymer Honeycomb Composite Panels in Bridge Deck Application*, Final Report, National Cooperative Highway Research Program, August 2000.

Henderson, M. *Evaluation of Salem Avenue Bridge Deck Replacement: Issues Regarding the Composite Materials Systems Used*, Final Report. Ohio Department of Transportation, December 2000.

Hetenyi, M. *Beams on Elastic Foundation. Theory with Applications in the Fields of Civil and Mechanical Engineering*. The University of Michigan Press, 1967.

Reising, R., Shahrooz, B., Hunt, V., Lenett, M., Christopher, S., Neumann, A., Helmicki, A., Miller, R., Konduri, S., and Morton, S. *Performance of a Five – Span Steel Bridge with Fiber Reinforced Polymer Composite Deck Panels*. Transportation Research Board Annual Meeting, Washington, D.C., January 2001.

Shekar, V., Petro, S., and GangaRao, H. *Construction of FRP Modular Decks for Highway Bridges*. Transportation Research Board Annual Meeting, Washington, D.C., January 2002.

Shull, P. *Non-Destructive Evaluation. Theory, Techniques, and Applications*, Altoona, Pennsylvania, 2002.

Stoll, F., Banerjee, R., Campbell, S., Day, S. *Manufacture of Fiber-Reinforced-Foam Composite Sandwich Structures*. Blacksburg, VA: ASC 16th Annual Technical Conference, September 2001.

Stoll, F., Klosterman D., Gregory M., Banerjee R., Campbell S., Day S. *Design, Fabrication, Testing and Installation of Low-Profile Composite Bridge Deck*. Long Beach, CA: SAMPE, May 2002.

Stone, D., Watkins, S., Nystrom, H., and Nanni, A. *Investigation of FRP Materials for Bridge Construction*. Proceedings of the Fifth National Workshop on Bridge Research in Progress, C.K. Shield and A.E. Schultz, Eds. University of Minnesota, Twin Cities, October 8 – 10, 2001, Minneapolis, Minnesota.

Taylor, J. *An Introduction to Error Analysis*. University Science Books. Mill Valley, CA. 1982.

Vinson, J. *The Behavior of Sandwich Structures of Isotropic and Composite Materials*. Pennsylvania: Technomic Publishing Company, Inc, 1999.

Wagh, V. *FRP Bridge Deck Design and Construction*, Structural Engineer, May 2001.

Zenkert D. *The Handbook of Sandwich Construction*. London, United Kingdom: Chameleon Press, 1997.

Zoghi, M., Fahrey, D., Foster, D. *Construction and Performance Evaluation of a Fiber – Reinforced Polymer Composite Bridge.* Transportation Research Board Annual Meeting, Washington, D.C., January 2002.